INVESTIGATING THE ONSHORE-TO-OFFSHORE STRUCTURE AND STRATIGRAPHY OF THE CARBONIFEROUS BAY ST. GEORGE SUBBASIN, WESTERN NEWFOUNDLAND

by © Miguel Shano

A Thesis submitted to the School of Graduate Studies in partial fulfillment of the requirements for the degree of

Master of Science

Department of Earth Sciences

Memorial University of Newfoundland

May, 2022

St. John's Newfoundland and Labrador

Abstract

The Bay St. George subbasin is a geologically complex onshore-to-offshore basin that has undergone significant deformation during Appalachian orogenesis. Despite this complex tectonic history, few studies have investigated the crustal inheritance and correlated the geology from the onshore-to-offshore. The main objective of this study is to use high-resolution geophysical data, including seismic, well log, and potential field data to investigate the structure and stratigraphy of the basin.

This study reveals significant subsurface compartmentalization reaching crustal-scale depths. A new 3-D gravity inversion and seismic interpretation provide evidence of juxtaposed lower crustal blocks caused by regional faults in the basin and broader Northern Appalachians. Based on the timing and structural characteristics of these regional faults, the Bay St. George subbasin has a history that involves both transtension and transpression.

General Summary

The Bay St. George subbasin is a relatively small sedimentary basin located in southwestern Newfoundland that extends across both onshore and offshore. This basin has a complex subsurface structure, including a significant number of faults that were active throughout geological time. There have been few studies correlating the geology between the onshore and offshore parts of the basin, including how it varies deeper into the Earth, which is the main motivation behind this project. Investigating the subsurface of the basin includes interpreting seismic, well log, gravity, and magnetic data. Earth models are produced from seismic interpretation and potential field modeling to infer how the basin evolved.

This study reveals the presence of significant faults reaching depths up to 30–40 km that likely continue to the south toward Nova Scotia. The timing and characteristics of faults suggest a fundamental change in the tectonic environment over time. The faults started as dominantly extensional and then transitioned to dominantly compressional, similar to basins of comparable settings elsewhere.

Acknowledgments

I would like to firstly thank my supervisor, Kim Welford, for providing me with this opportunity and for her support and guidance through the development of this project. Thank you to Alison Malcolm for being on my supervisory committee and for your constructive comments and suggestions. Erin Gillis is acknowledged for her critical suggestions, comments, and edits throughout this project.

I would like to thank the Memorial Applied Geophysics for Rift Tectonics (MAGRiT) research group for their constructive comments and feedback.

I would like to thank Peter Bruce for his help in preparing my seismic data for this project.

I would like to thank the Petroleum Exploration Enhancement Program (PEEP), funded by the Department of Industry, Energy and Technology, and the Oil and Gas Corporation of Newfoundland, for the financial support. The Canada-Newfoundland Offshore Petroleum Board (C-NLOPB) and the Department of Industry, Energy and Technology are appreciated for providing the seismic and well data.

Lastly, thank you to Jacob Newman, Steven Lethbridge, and Michael King for all their moral support and laughs throughout my degree.

Table of Contents

List of Tables

Table of Figures

List of Abbreviations

RIL	Red Indian Line
LBOT	Lushs Bight Oceanic Tract
LRF	Long Range Fault
RHT	Round Head Thrust
RBF	Romaines Brook Fault
SGBF	St. George Bay Fault
CBF	Central Bay Fault
SBF	Snakes Bight Fault
FBT	Flat Bay Thrust
C-NLOPB	Canada Newfoundland and Labrador Offshore Petroleum Board
VSP	Vertical Seismic Profile
QC	Quality Control/Quality Check
RC	Reflection Coefficient
TDR	Time–Depth Relationship
TWTT	Two-way travel time
PaP	Port au Port Peninsula

List of Appendices

Chapter 1 Introduction and Literature Review

This chapter provides an introduction to the study region and describes the main research objectives. Background of previous geophysical and geological work is also presented. The larger-scale regional geology is first described, followed by the local geology of the Bay St. George subbasin.

1.1 Purpose and Motivation

Western Newfoundland is an area with significant economic petroleum prospectivity as hydrocarbon seeps and staining have been naturally observed along some coastlines (Hogg & Enachescu, 2015). Specifically, the source rocks of the Snake's Bight Formation and the reservoir sandstones of the Anguille Group have significant petroleum potential (Hogg & Enachescu, 2015). This geophysical study uses a range of high-resolution geophysical data, including seismic, well log, and potential field data, to improve the subsurface geological knowledge that may be used to investigate this prospectivity. This project focuses on the southwesternmost part of Newfoundland, particularly the Bay St. George subbasin. The Carboniferous Bay St. George subbasin is situated south of the Port au Port Peninsula and extends onshore-to-offshore (Figure 1.1).

Western Newfoundland, part of the Appalachian orogen, has a complex geological history from the opening and closing of the late Precambrian to the early Paleozoic Iapetus Ocean (van Staal & Barr, 2012; Wilson, 1966). This resulted in significant deformation of the ancient passive margin and intervening oceanic rocks and sparked geological and geophysical interest in the area. Western Newfoundland has been a region of petroleum exploration from the 1800s to early 2010s. However, there has been little success from past petroleum exploration, partly due to the poor understanding of the complex subsurface. Multiple seismic surveys and exploration wells have been completed in Western Newfoundland to better understand the complex geology and to search for petroleum. The relationship between onshore and offshore geology in southwestern Newfoundland is poorly understood, as few studies have attempted to bridge the two. The crustal inheritance of the area is also not well understood since crustal-scale studies are limited in the Bay St.

George subbasin. In order to de-risk future hydrocarbon exploration, a better understanding of the tectonic evolution is required, which is part of the motivation behind this study. Reducing uncertainty in the onshore-to-offshore stratigraphic correlation and investigating the crustal structures within the Bay St. George subbasin are the motivation for this thesis project.

The main objective of this study is to investigate the onshore-to-offshore structure and stratigraphy of the Carboniferous Bay St. George subbasin using seismic data, well logs, and potential field studies. This involves a comprehensive seismic interpretation with well log correlation and potential field modeling to better constrain the deep and shallow structures. A 3-D gravity inversion of the basin and its surroundings, using improved shallow constraints, is also undertaken.

This research project aims to explain past uncertainties, including the faults of the Bay St. George subbasin and the changes in stratigraphy between the onshore and offshore geology. Salt-related structures are investigated using seismic data to determine how salt tectonics affected the structural evolution of the basin. The new gravity inversions in this study focus on the Bay St. George subbasin and use constraints from forward gravity modeling and seismic data interpretation. The depth to Moho and crustal thickness are determined from the gravity inversion using newer, higher resolution gravity data. From the 3-D density model, cross-sections are generated for regions lacking seismic coverage to inspire future exploration. The updated 3-D density model and seismic interpretations offer new insights into the complex tectonic history of the Bay St. George subbasin and the broader Northern Appalachians. Understanding the structure and stratigraphy of the Bay St. George subbasin may inspire future exploratory efforts.

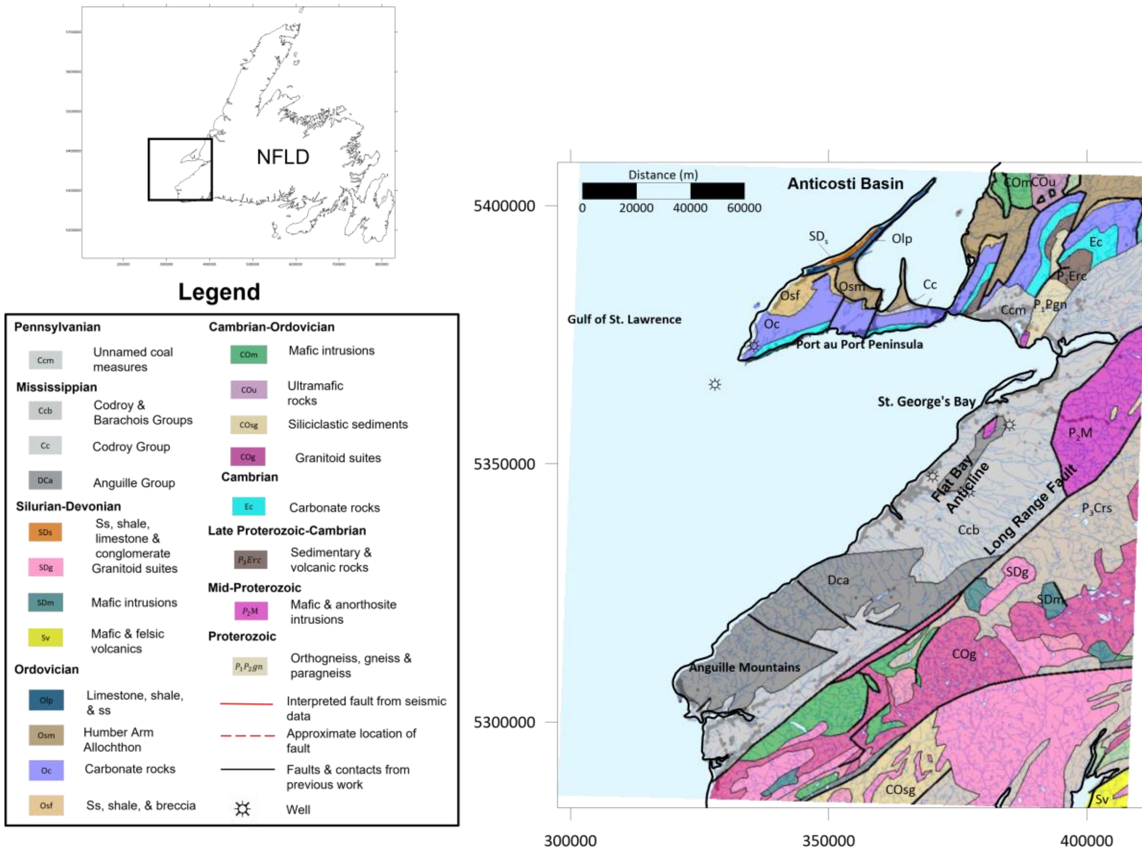

Figure 1.1: Geological map of the Bay St. George subbasin with the main stratigraphic units. The faults are interpreted from the seismic data in this study (red) and derived from previous work (black). The generalized onshore geology is from Coleman-Sadd et al. (2000), and the faults are from Knight (1983) and Langdon & Hall (1994).

1.2 Regional Geology

1.2.1 Tectonic Evolution

Newfoundland is separated into four major geological zones based on lithologic and tectonic characteristics. The four major zones are the Avalon, Gander, Dunnage, and Humber zones. The Laurentian margin is represented by the Humber and Dunnage zones (van Staal & Barr, 2012). The Gondwana margin is represented by the the Gander, Avalon, and Meguma zones (van Staal & Barr, 2012). Only three subdivisions are shown in Figure 1.2A, including the major geological terranes and sutures within Newfoundland and the surrounding area. The major sutures highlighted include the Red Indian Line (RIL) and the Dover Fault, which correspond to the sutures between Laurentia and peri-Gondwanan terranes and the boundary between Ganderia and Avalonia (two of those peri-Gondwanan terranes), respectively. The Humber Zone is the most important for this study since the Bay

St. George subbasin is part of the broader Maritimes Basin, which overlies rocks of the Humber Zone.

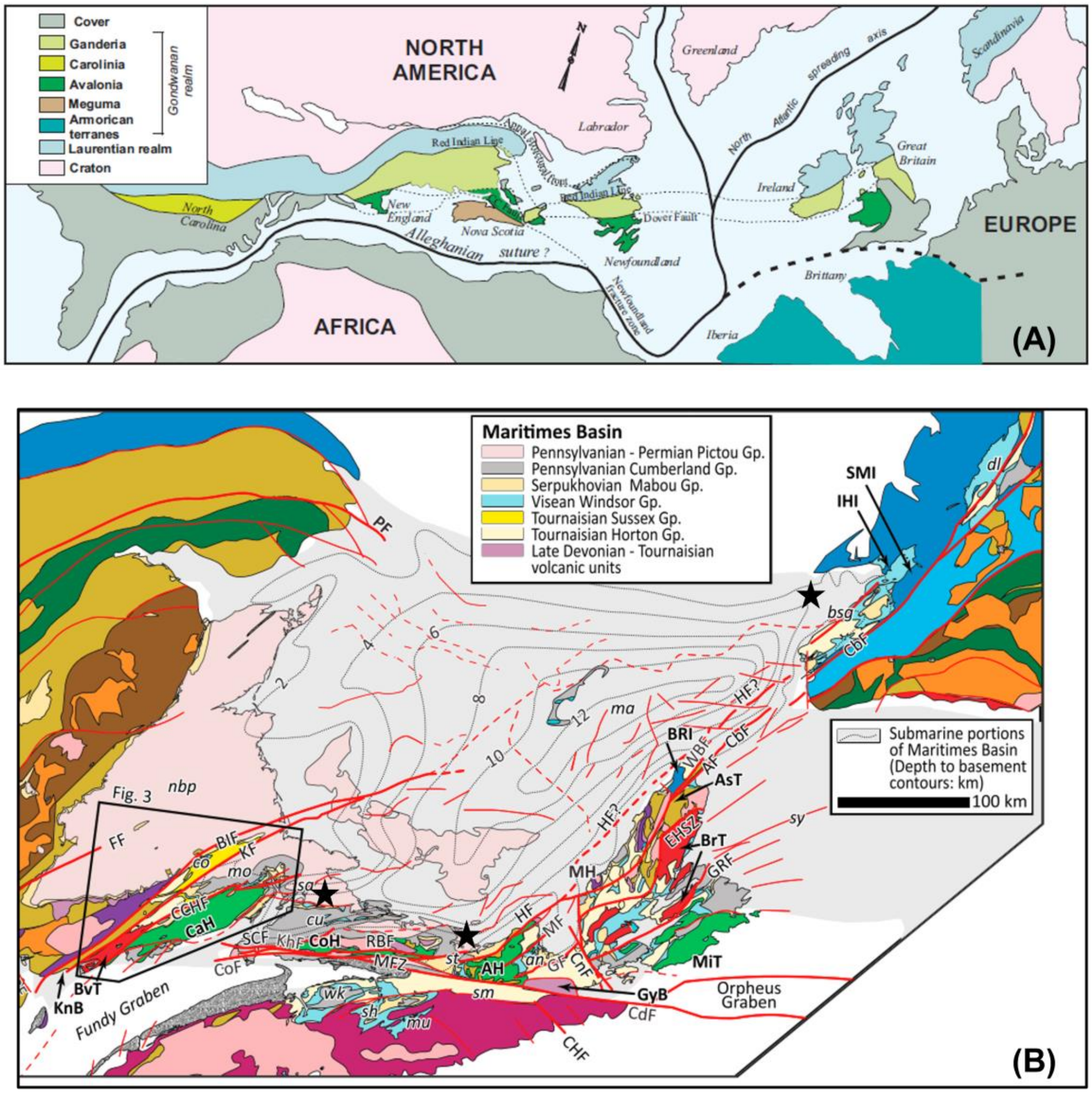

Figure 1.2: (A): Mesozoic restoration of Newfoundland and the surrounding area with labeled terranes and sutures. The Red Indian Line (RIL) represents the suture between Laurentia and Gondwana, while the Dover Fault represents the boundary between Ganderia and Avalonia. (B): The regional geology of Atlantic Canada with the Maritimes Basin and the smaller subbasins. The significant faults and structural features are annotated as red lines. The stars represent the Bay St. George subbasin (bsg), Cumberland subbasin (CU), and Stellarton subbasin (st). Figures from Waldron et al. (2015) and van Staal & Barr (2012).

The Paleozoic tectonic evolution of Western Newfoundland involved four main orogenic events (Figure 1.3), followed by Carboniferous faulting. Figure 1.3 displays a simplified sequence of the major tectonic events involving Western Newfoundland.

Western Newfoundland has a complex geological history beginning from the Precambrian Grenville Craton, which contains the intrusive igneous and metamorphic rocks that formed the foundation for the Laurentian margin (Stockmal et al., 1998; Waldron & Stockmal, 1994). These Mesoproterozoic rocks were amalgamated during the Supercontinent Rodinia construction before forming the Laurentian margin (Cawood et al., 2001; Waldron & Stockmal, 1994). The Laurentian margin formed from the rifting of the Supercontinent Rodinia during the Neoproterozoic to Early Ordovician (Cawood et al., 2001; Kamo et al., 1989). Continued rifting occurred leading to the opening of the Iapetus Ocran (van Staal & Barr, 2012). This resulted in Western Newfoundland representing the eastern passive continental margin of Laurentia (Waldron et al., 1998; Waldron & Stockmal, 1994).

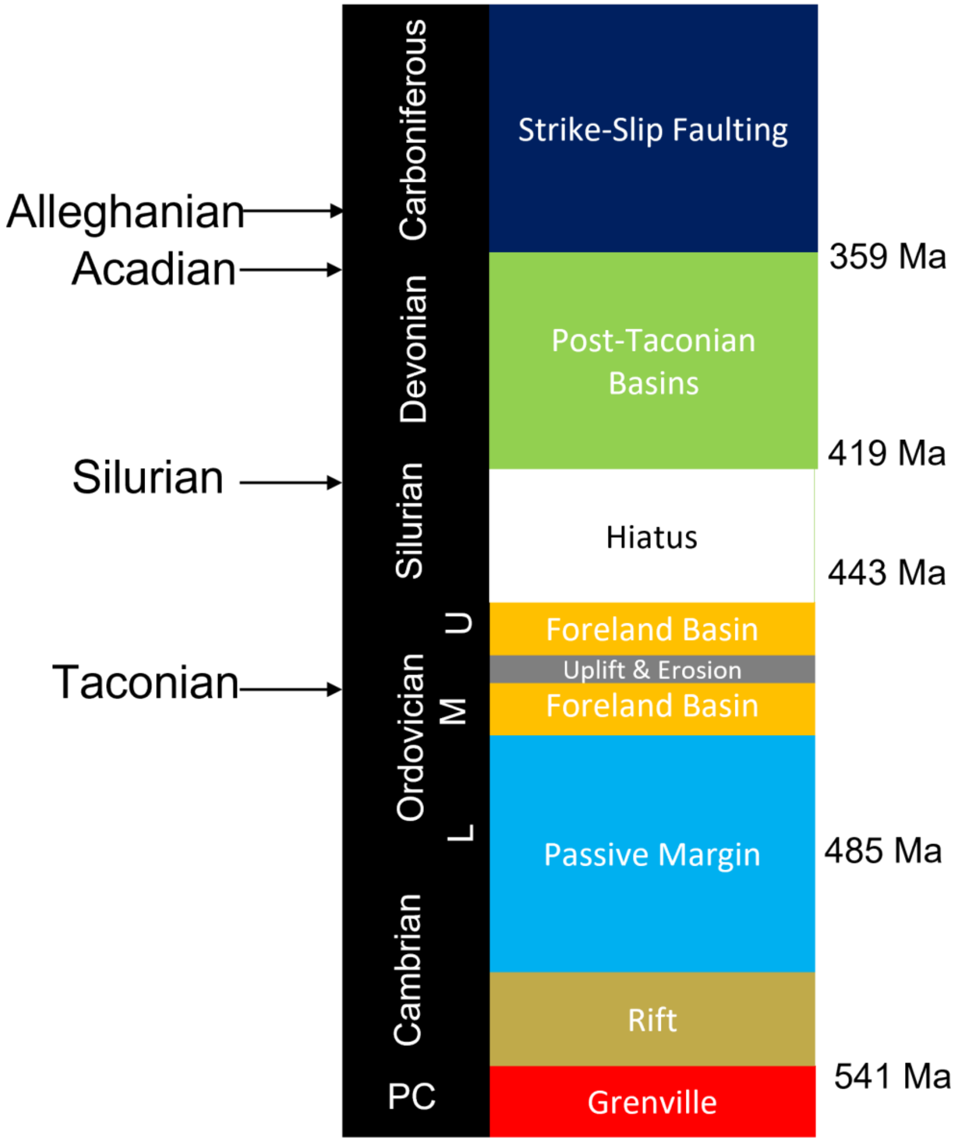

Figure 1.3: Simplified diagram of the orogenic events and subsequent strike-slip faulting associated with the tectonic evolution of the Newfoundland Appalachians. Figure modified after Lavoie et al. (2003).

The Ordovician Taconian Orogeny within Newfoundland marked the end of the eastern passive Laurentian margin and was the main driver of the Humber margin deformation (Figure 1.4) (Cawood, 1993). The Dashwoods microcontinent was a rifted fragment of Laurentia within the Iapetus Ocean, and it was the first block to be involved in the Taconian Orogeny (Figure 1.4) (Waldron & van Staal, 2001). The opening of the Humber Seaway, between the Laurentian margin and the Dashwoods microcontinent, generated the Lushs Bight Oceanic Tract (LBOT). This oceanic crust was later obducted onto the Dashwoods microcontinent, followed by the generation of the Notre Dame island arc (van Staal & Barr, 2012; Waldron & van Staal, 2001). As the Humber Seaway closed, the Dashwoods entered the oceanic trench, resulting in a subduction polarity flip (Figure 1.4) and the generation of the Bay of Islands Ophiolites, that formed within a backarc setting from transtensional rifting (Cawood & Suhr, 1992; Waldron & van Staal, 2001). The collision of the composite Dashwoods-LBOT block and the emplacement of the Humber Arm Allochthon, as deep-water sedimentary rocks (continental slope and rise sediments), involved obduction and deposition on the former shelf (Figure 1.5) (Cawood, 1993; Waldron et al., 1998). This emplacement and obduction created rapid subsidence and was recorded by a Taconian foreland basin succession (Figure 1.4) (Waldron & Stockmal, 1994).

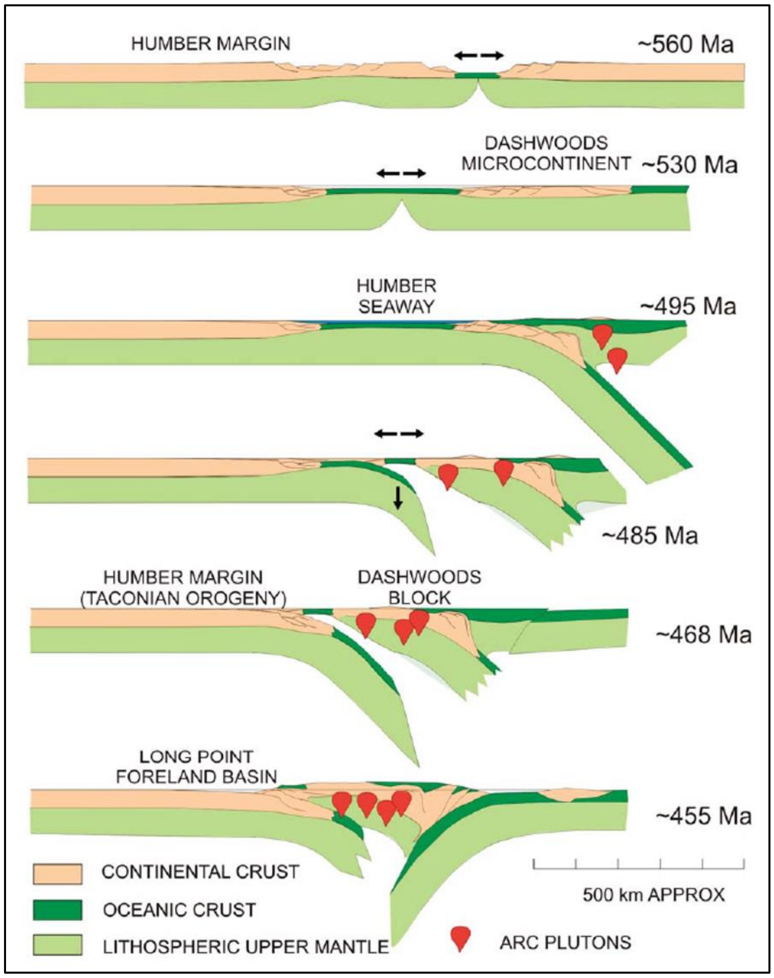

Figure 1.4: The Taconian continental collision and subduction involving the passive Laurentian margin with the eventual west-facing subduction zone and associated island arcs shaping the Humber Margin. The initial opening of the Humber Seaway involved the rifting of the Dashwoods from Laurentia. Subsequent closing of the Humber Seaway occurred as the Dashwoods block entered the oceanic trench resulting in slab break off. The Long Point Foreland Basin recorded the collision of the composite Dashwoods and the Humber Arm Allochthon emplacement. Figure from Waldron & van Staal (2001).

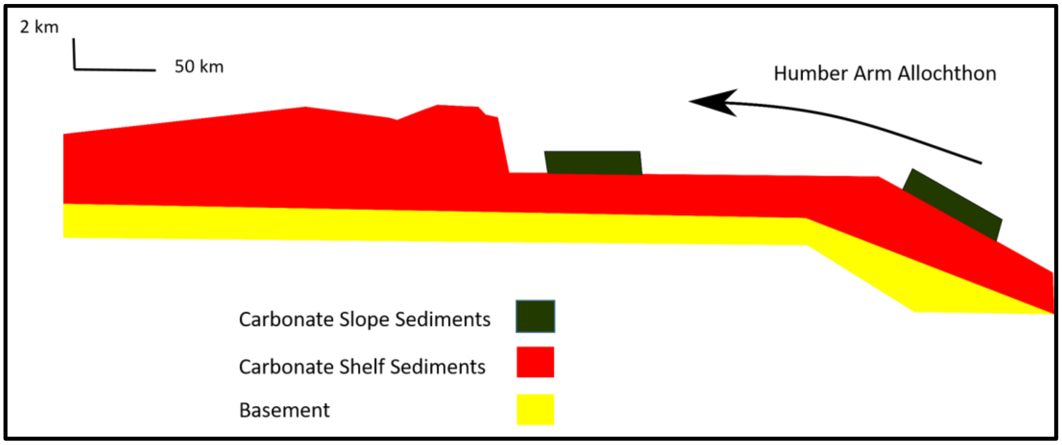

Figure 1.5: Schematic diagram showing the main stratigraphic units as the Humber Arm Allochthon consisting of the continental slope and rise sediments, is emplaced on top of the shelf sediments. The arrow represents the path of the slope sediment onto the shelf. Figure modified after Waldron et al. (1998).

Additional deformation occurred after the Taconian Orogeny during the Early Silurian, as evidenced by second-generation folds of the Taconian allochthon (van Staal & de Roo, 1996). Continued subduction and collision occurred to the east and below the continental margin involving Laurentia and Ganderia (van Staal et al., 1990). Furthermore, shear zones along the eastern part of the Humber Arm Allochthon preserve normal sense motion, followed by crustal shortening (Waldron & Milne, 1991).

The Devonian Acadian Orogeny involved a collision between composite Laurentia and Avalonia (van Staal, 2005; van Staal & Barr, 2012). During the Early Devonian, the Acadian Orogeny represented crustal shortening recorded from reactivation and inversion of brittle pre-existing normal faults, such as the Round Head Thrust Fault (RHT) (Stockmal et al., 1998). This fault is located near the Port au Port Peninsula and extends southwards in St. George Bay (Figure 1.1). The RHT initially formed from early rifting related to the opening of the Iapetus Ocean and became reactivated and inverted as thick-skinned deformation during the Devonian Acadian Orogeny (Stockmal et al., 2004).

The Alleghanian Orogeny began during the Early Carboniferous and continued into the Middle Permian (van Staal & Barr, 2012; Wilson, 1966). The Alleghanian Orogeny involved collision and amalgamation of the composite Laurentia and Gondwana, forming the supercontinent Pangea (van Staal & Barr, 2012; Wilson, 1966). The composite

Laurentia is suggested to form the upper plate, while the Gondwana mass forms the lower plate during the amalgamation (van Staal & Barr, 2012).

The Humber Zone contains a Grenvillian granitic basement, overlain by Cambrian–Ordovician age autochthonous and allochthonous shallow-water platform sequences, and a complex section of deeper water clastic and carbonate successions (Figures 1.1 and 1.3) (Hogg & Enachescu, 2015; Waldron et al., 1998; Williams, 1979). Overlying the rocks of the Humber Zone is the Maritimes Basin, which contains the smaller Bay St. George subbasin. The Maritimes Basin is a fairly large basin reaching 12 km depth that overprint older terranes associated with earlier orogenic events (Waldron et al., 2015). The Maritimes Basin contains smaller Carboniferous subbasins, such as the Bay St. George, Stellarton, and Cumberland subbasin (Figure 1.2B). These subbasins have similar tectonic histories with rocks of similar ages. The Bay St. George subbasin is the main focus in this thesis, however, correlations are drawn with these other subbasins in Chapter 5.

Carboniferous faulting during the Alleghanian Orogeny created significant deformation in southwestern Newfoundland. This event involved mainly dextral strike-slip faults, creating the deep Maritimes Basin, comprising multiple subbasins including the Bay St. George (Cawood, 1993). This deformation event is of prime importance since this thesis project focuses on the Carboniferous Bay St. George subbasin, located in southwestern Newfoundland, where significant dextral strike-slip faulting has been previously documented (Dafoe et al., 2016; Knight, 1983).

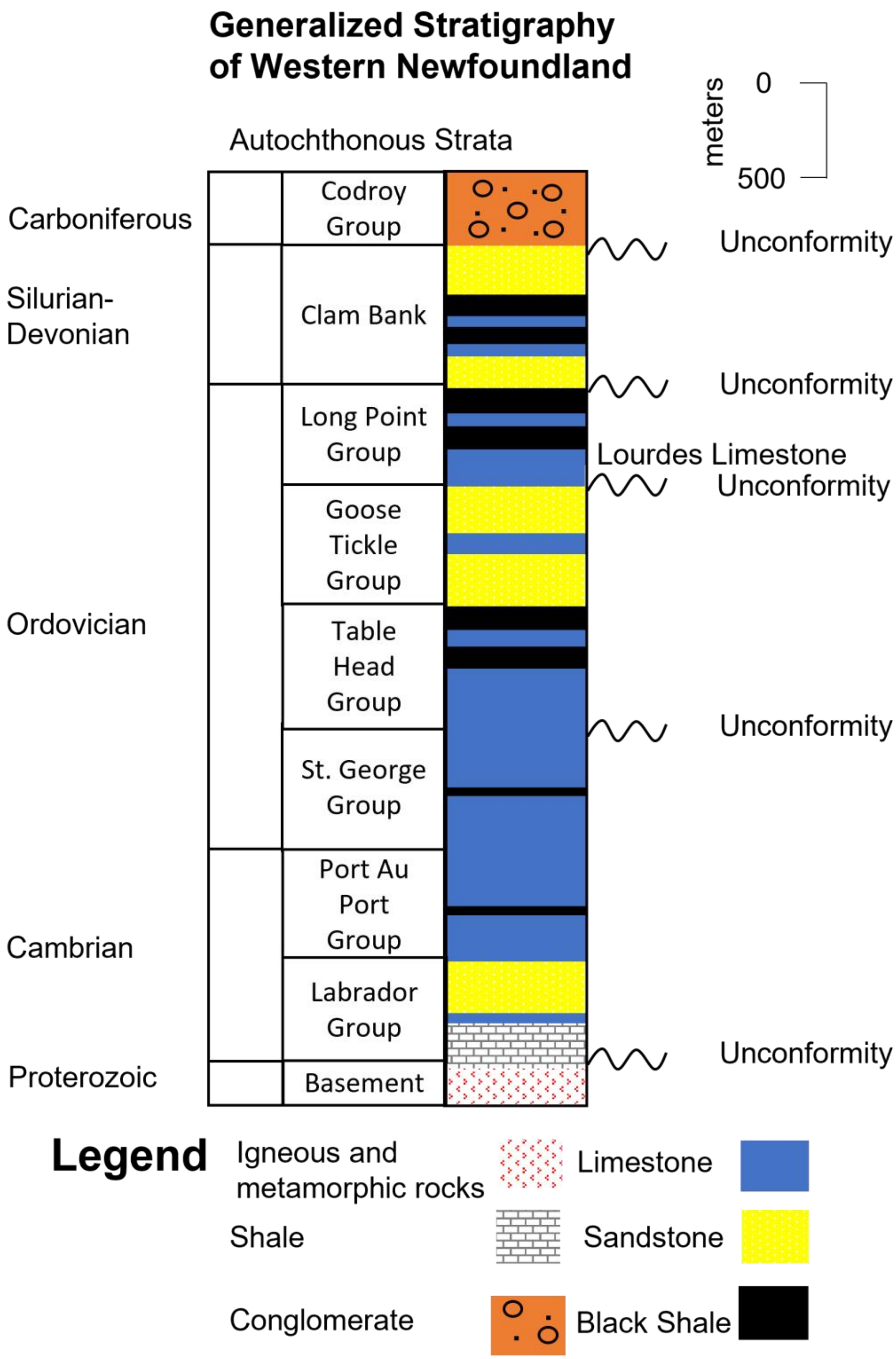

Figure 1.6: Simplified stratigraphic column for the major early Paleozoic geological units within western Newfoundland. Figure modified after Cooper et al. (2001).

1.2.2 *Western Newfoundland Stratigraphy*

The simplified stratigraphy of Western Newfoundland is displayed in Figure 1.6, containing a Precambrian Grenville basement and autochthonous Cambrian–Ordovician carbonate platform successions. Overlying the carbonate platform successions are the younger Carboniferous strata. The Carboniferous strata are abundant in the Bay St. George subbasin and are described in further detail in section 1.3.1.

The autochthonous Cambrian–Ordovician carbonate platform successions contain the Labrador, Port au Port, St. George, Table Head, Goose Tickle, and Long Point groups (Cooper et al., 2001) (Figure 1.6). The majority of the carbonate successions are preserved in the Port au Port, St. George, and Table Head groups, although there are still carbonate units present in the other groups. There are major unconformities presented in these groups, which are used as seismic markers in this study. The Base Cambrian–Ordovician carbonate platform succession corresponds to the Base Labrador Group unconformity. The Labrador Group formed during the rifting of the supercontinent Rodinia and contains siliciclastics and carbonates (Cawood et al., 2001; Waldron et al., 1998). This unconformity marks the base carbonate platform seismic horizon mapped in this study. The Top Cambrian–Ordovician carbonate platform is represented by the Lourdes Limestone in the Long Point Group and marks the top carbonate platform seismic horizon mapped in this study. The Long Point Group formed following the Taconian Orogeny and was recorded as foreland basin successions (Waldron & Stockmal, 1994).

1.3 Geology of the Bay St. George Subbasin

1.3.1 *Geological Setting and Stratigraphy*

The Carboniferous Bay St. George subbasin is located in southwestern Newfoundland, extending onshore-to-offshore. This basin is bounded to the north by the Port au Port Peninsula (Figure 1.1). It is a large (ca 2000 km^2) northeast-trending subbasin belonging to the larger Maritimes Basin.

The formation of the Bay St. George subbasin is interpreted to have involved multi-phase dextral strike-slip faulting during the Late Devonian and Carboniferous (Knight, 1983). Three main Carboniferous stratigraphic groups occur in the Bay St. George subbasin, including the Barachois, Codroy, and Anguille groups (Figure 1.7) (Knight, 1983). The detritus originated primarily from the mountains located to the northeast and southeast of the basin (Knight, 1983).

The oldest Anguille Group (Late Devonian to Early Mississippian) consists of non-marine siliciclastic rocks, mostly shale to coarse sandstone and localized conglomerate (Figure 1.7) (Knight, 1983). The Anguille Group contains the Kennels Brook, Snakes Bight, Friars Cove, and South Falls Formations (Knight, 1983). The Anguille Group is thickest in the southeast towards the Anguille Mountains (4.5 km thick) and thins drastically towards the northeast near the Flat Bay Anticline (Figure 1.1) (Knight, 1983). Although the Anguille Mountains are within the Bay St. George subbasin, structures and stratigraphy are not described from this area in this thesis since no seismic lines cover this region.

The underlying Codroy Group (Upper Mississippian) consists of marine and non-marine siliciclastic sandstone, shale, evaporites, and carbonate (Figure 1.7) (Knight, 1983). The base of this group represents a major marine transgression and deposition of the Ship Cove limestones. (Knight, 1983). This was followed by the deposition of the Codroy Road and Robinsons River Formations containing marine carbonate, evaporites, and siliciclastics (Knight, 1983).

The youngest Barachois Group (Lower Pennsylvanian) consists mainly of fluvial siltstone to sandstone sequences, with minor mudstone and coal (Figure 1.7) (Knight, 1983). This unit exists onshore, although it is poorly constrained offshore and suggested that these rocks are not broadly distributed (Dafoe et al., 2016).

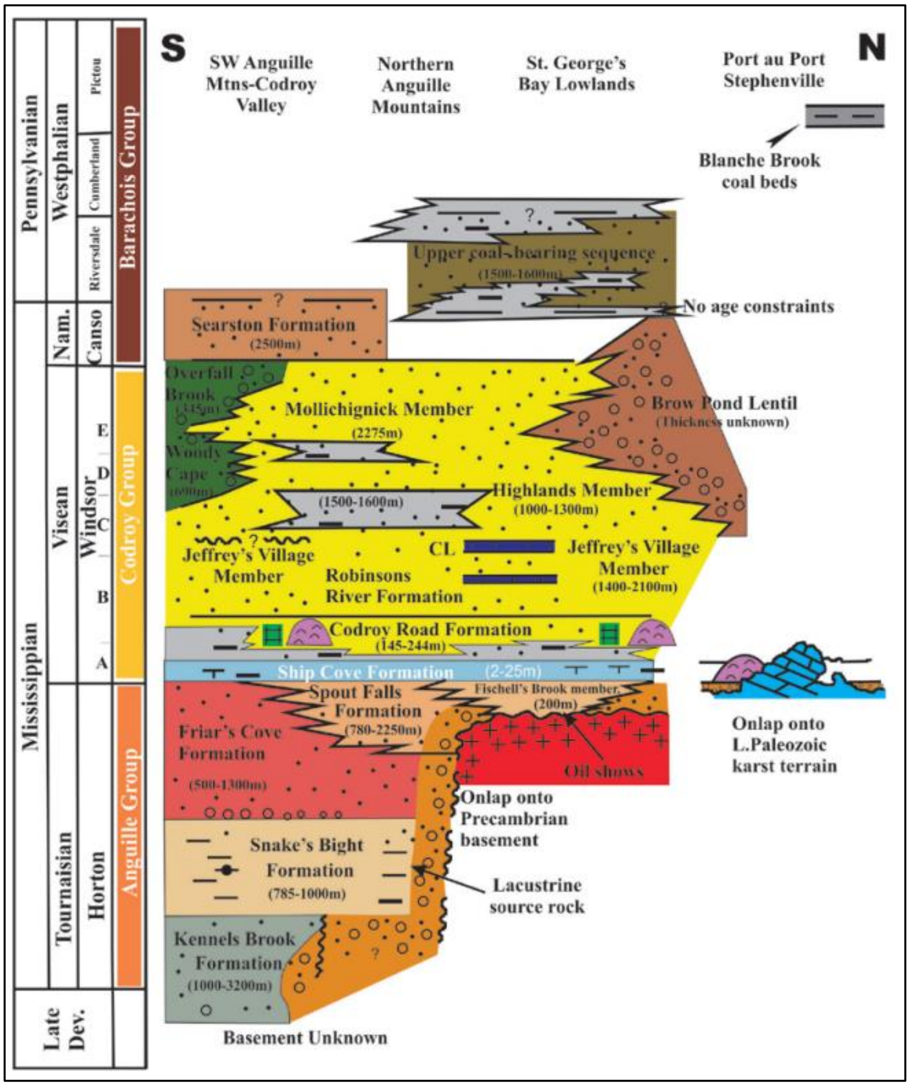

Figure 1.7: Stratigraphic column of Carboniferous units in Bay St. George subbasin, comprising three main groups, including the Anguille, Codroy, and Barachois groups. Figure from Knight (1983).

1.3.2 Structure of the Subbasin

The Bay St. George subbasin originated in the late Devonian to Carboniferous during multi-stage dextral strike-slip faulting along the Long Range Fault (LRF), often referred to as the Cabot Fault, and other associated NE–SW striking faults (Knight, 1983). Subsidence and deposition of sediments occurred within a transtensional environment in half-grabens (Knight, 1983). Subsequent deformation occurred during the Carboniferous from reactivation of northeast–southwest trending strike-slip faults resulting in present-day geometry (Knight, 1983; Stockmal et al., 2004).

The structure of the basin consists of two NE trending half-graben structures separated by a central basement high and the regional Central Bay Fault (CBF) (Robbins, 2000). The northern half-graben is characterized by northwest dipping faults. The southern half-graben structure is bounded to the south by the St. George Bay Fault (SGBF), and it is characterized as having complex salt pillows and diapirs (Robbins, 2000).

Most of the regional faults in the Bay St. George subbasin strike NE–SW, with additional E–W trending faults (Figure 1.1). The Round Head Thrust (RHT) and the Romaines Brook Fault (RBF) started as normal faults produced from early rifting related to the opening of the Iapetus Ocean (Stockmal et al., 2004). These faults later became reactivated and inverted as thick-skinned deformation during the Devonian Acadian Orogeny (Stockmal et al., 2004). The CBF is in the offshore bay, trending subparallel to the basin bounding LRF and St. George Bay Fault (SGBF). The CBF likely formed after the basin bounding faults within an environment of transtension and reactivated earlier pre-existing structures (RBF and the RHT) (Dafoe et al., 2016). The SGBF is an essential fault relating to the termination of carbonate platform succession offshore and strikes NE–SW near the coastline (Langdon & Hall, 1994). The onshore faulting is characterized by the dominant NE–SW trending Snakes Bight Fault (SBF) with associated E–W transtensional and compressional faults (Flat Bay Thrust) and is bounded to the east by the LRF (Knight, 1983; Miller et al., 1990). The FBT is a thrust fault onshore that strikes approximately E–W significantly offsetting Carboniferous strata.

1.3.3 Previous Geophysical Studies in the Bay St. George Subbasin

The majority of the geophysical studies within the Bay St. George subbasin were completed during the 1980s and 1990s (Hall et al., 1992; Langdon & Hall, 1994; Marillier & Verhoef, 1989; Miller et al., 1990). Additional work from Dafoe et al. (2016) provided new information about the bedrock and Quaternary features of St. George’s Bay. More recently, Snyder (2019) completed a study investigating the deformation of the Maritimes Basin, with work done specifically in the Bay St. George subbasin. Previous studies have involved analyses combining potential field data and either onshore or offshore seismic reflection datasets within the Bay St. George subbasin. However, no published literature has characterized the onshore-to-offshore stratigraphy and structures in the Bay St. George subbasin using both onshore and offshore seismic reflection datasets, in addition to potential field modeling.

Past geophysical studies from Langdon & Hall (1994), Hall et al. (1992), Miller et al. (1990), Marillier & Verhoef (1989), Dafoe et al. (2016), and Snyder (2019) provide a comprehensive foundation for regional studies as they each address aspects of the onshore-to-offshore structure and stratigraphy of the Bay St. George subbasin.

Langdon & Hall (1994) primarily investigated the Cabot Strait with additional work capturing the Bay St. George subbasin. The most important findings in their study regarding the Bay St. George subbasin are the mapped structural features. These structural features are displayed on the geological map in Figure 1.1. These structures were mapped using seismic data and are essential in understanding the structural relationships between the onshore-to-offshore Bay St. George subbasin. Langdon & Hall (1994) determined that the St. George Bay Fault marks the southern termination of the Cambrian–Ordovician autochthonous successions, with the Anguille successions present to the south of this regional fault.

Miller et al. (1990) contrasted the onshore-to-offshore structures using gravity field data and seismic data constraints. Forward modeling of gravity data was done along profile A–A' displayed in Figure 1.8 spanning onshore to offshore. They determined that the onshore and offshore have a similar general structure based on gravity data and sediment thicknesses ranging 3 km onshore to up to 6 km offshore (Miller et al., 1990). Miller et al. (1990) also modeled salt-related features, including salt-cored anticline structures corresponding to the large gravity lows (observed in Figures 1.8 and 1.9).

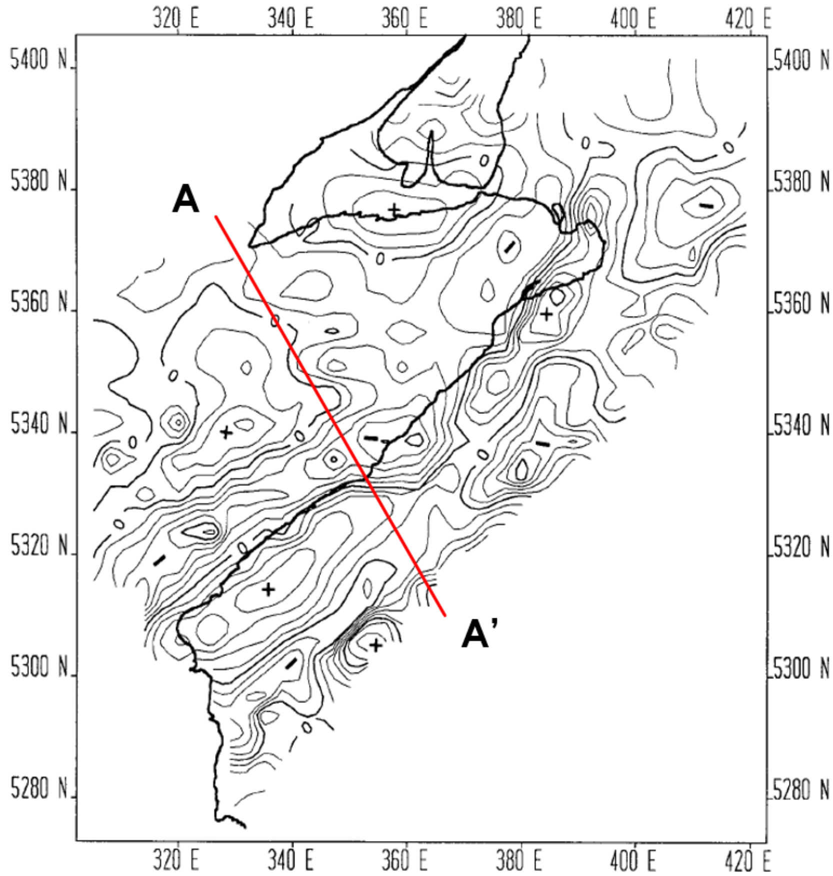

Figure 1.8: An onshore-to-offshore gravity transect (A–A') overlaying the residual gravity anomaly map used for forward modeling. The profile corresponds to the model in Figure 1.9. Figure modified after Miller et al. (1990).

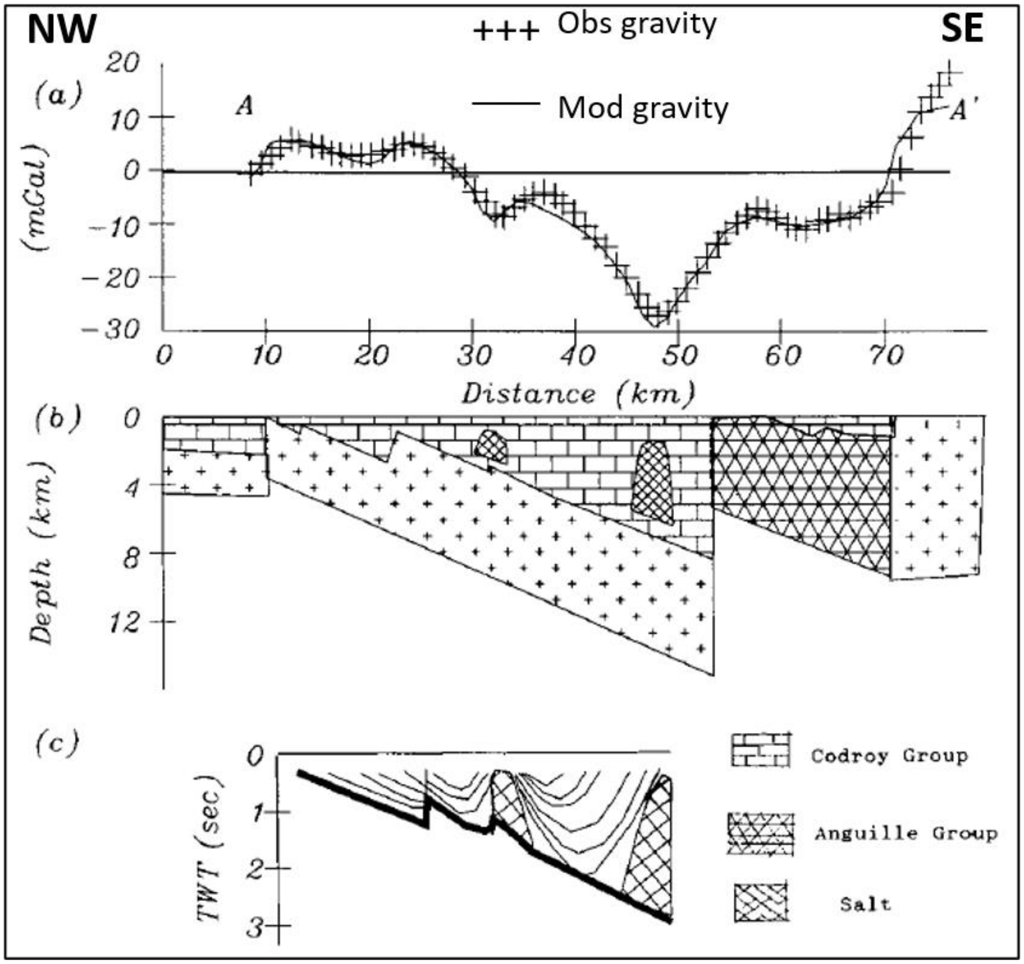

Figure 1.9: Gravity model of Miller et al. (1990), shown with a corresponding geological cross-section and seismic constraints. (A): The gravity responses show the solid line representing the modeled Bouguer gravity response, and the plus signs being the observed gravity. (B): Geological model from the A–A' gravity profile showing stratigraphy in half-grabens dipping towards the SE. (C): The line drawing from seismic data, where the solid black line represents the top of basement and the thin black lines are interpreted as intra-Carboniferous reflectors. The small crosses represent basement. The location of the A-A' profile is displayed in Figure 1.8.

Marillier & Verhoef (1989) provided crustal thickness estimates for the Gulf of St. Lawrence using complete Bouguer gravity anomaly and deep crustal seismic data. They performed a gravity inversion that resulted in a Moho depth of 42–44 km, assuming a constant crustal-mantle density contrast and an average depth to Moho of 43 km (Figure 1.10). They inferred high-density lower crustal layers beneath the Maritimes Basin and attributed them to many possible sources. Their preferred origin is the mafic underplating of the crust resulting from the tectonic evolution of the Maritimes Basin (Marillier & Verhoef, 1989).

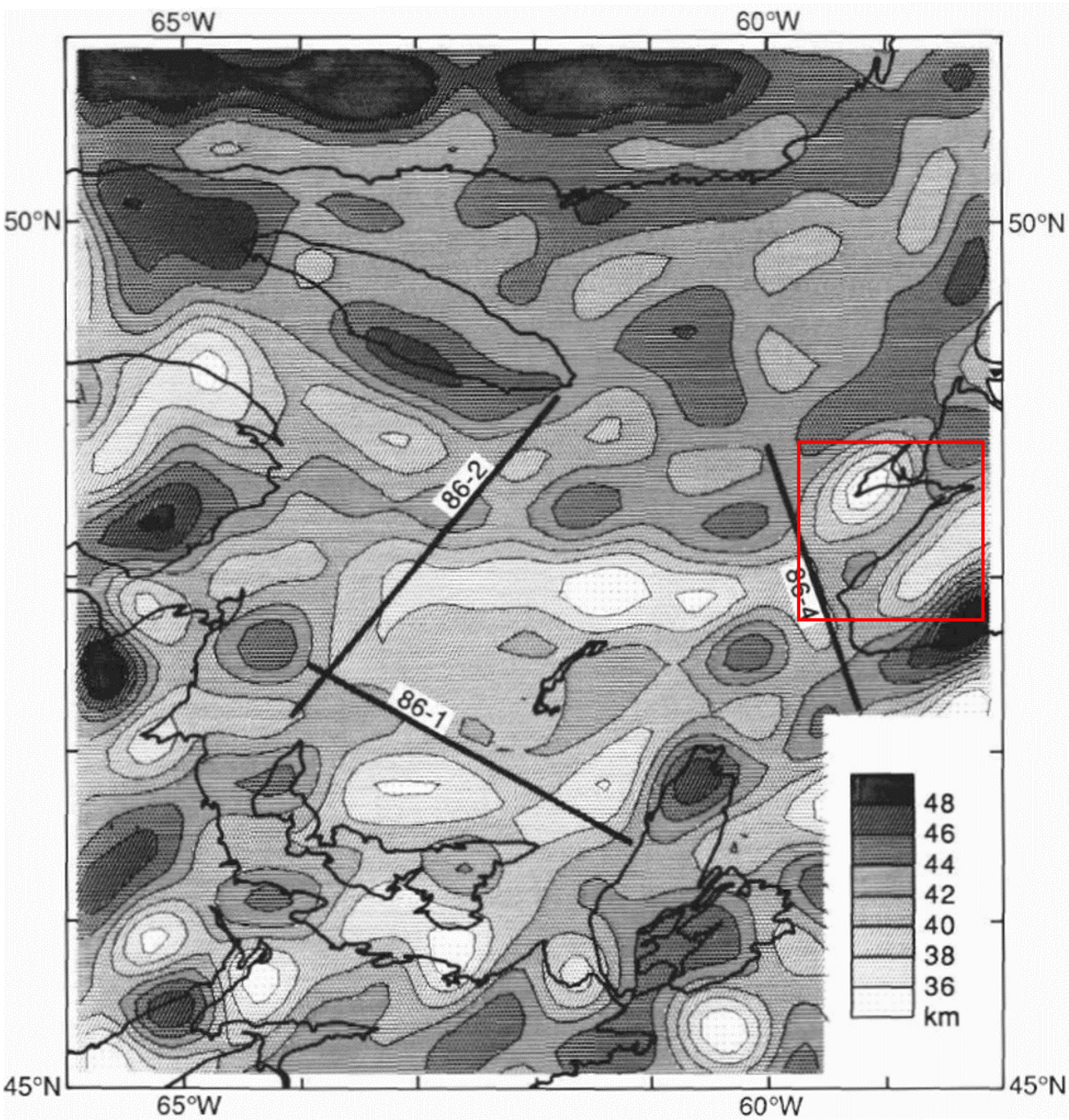

Figure 1.10: The depth to Moho map obtained from a complete Bouguer gravity inversion where assumptions included a constant crust-mantle boundary density of $0.6 g/cm^3$ (relative to $2.75\ g/cm^3$) and an average depth to Moho of 43 km. The red box is the location of the Bay St. George subbasin. Figure from Marillier & Verhoef (1989).

Hall et al. (1992) interpreted an onshore seismic reflection profile located at Robinson's River in the Bay St. George subbasin (blue line in Figure 1.11). They mapped a reflector (R) on this seismic profile corresponding to the contact between marine and overlying non-marine rocks in the Codroy Group (Hall et al., 1992) (Figure 1.12).

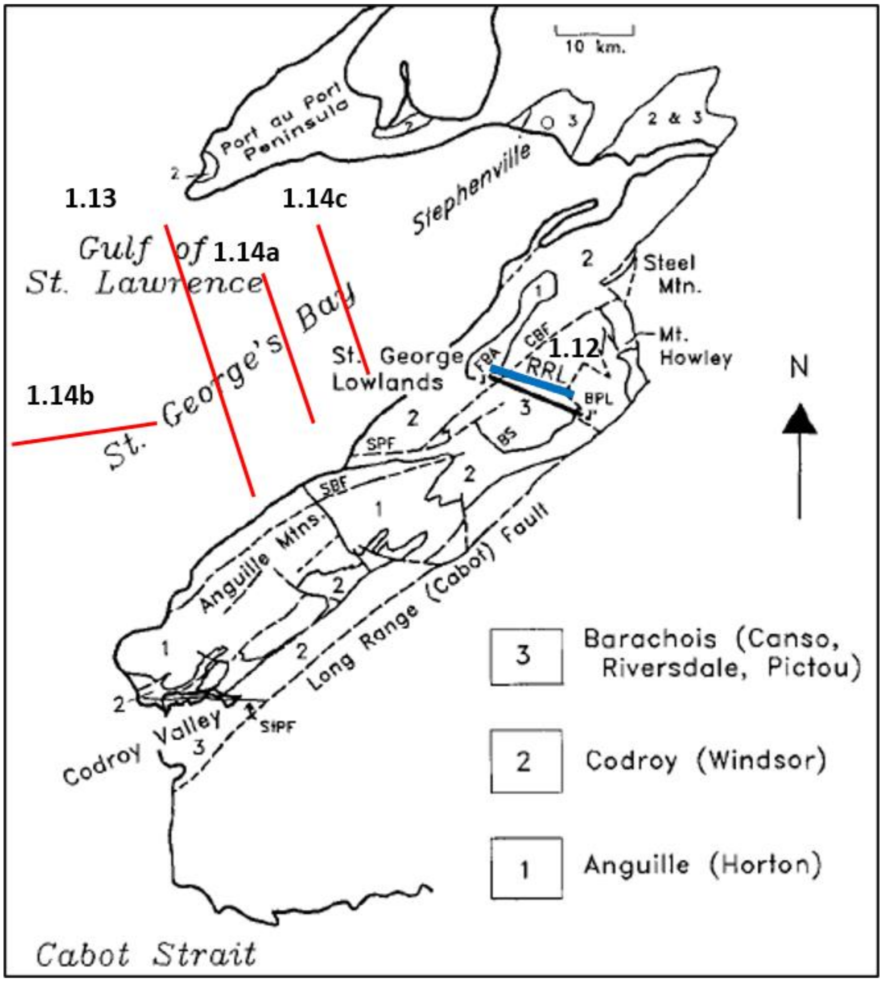

Figure 1.11: Geological map with the approximate location of seismic reflection profiles from past work, where the red lines correspond to Figures 1.13 and 1.14. The blue line corresponds to the seismic profile displayed in Figure 1.12. Figure modified after Hall et al. (1992).

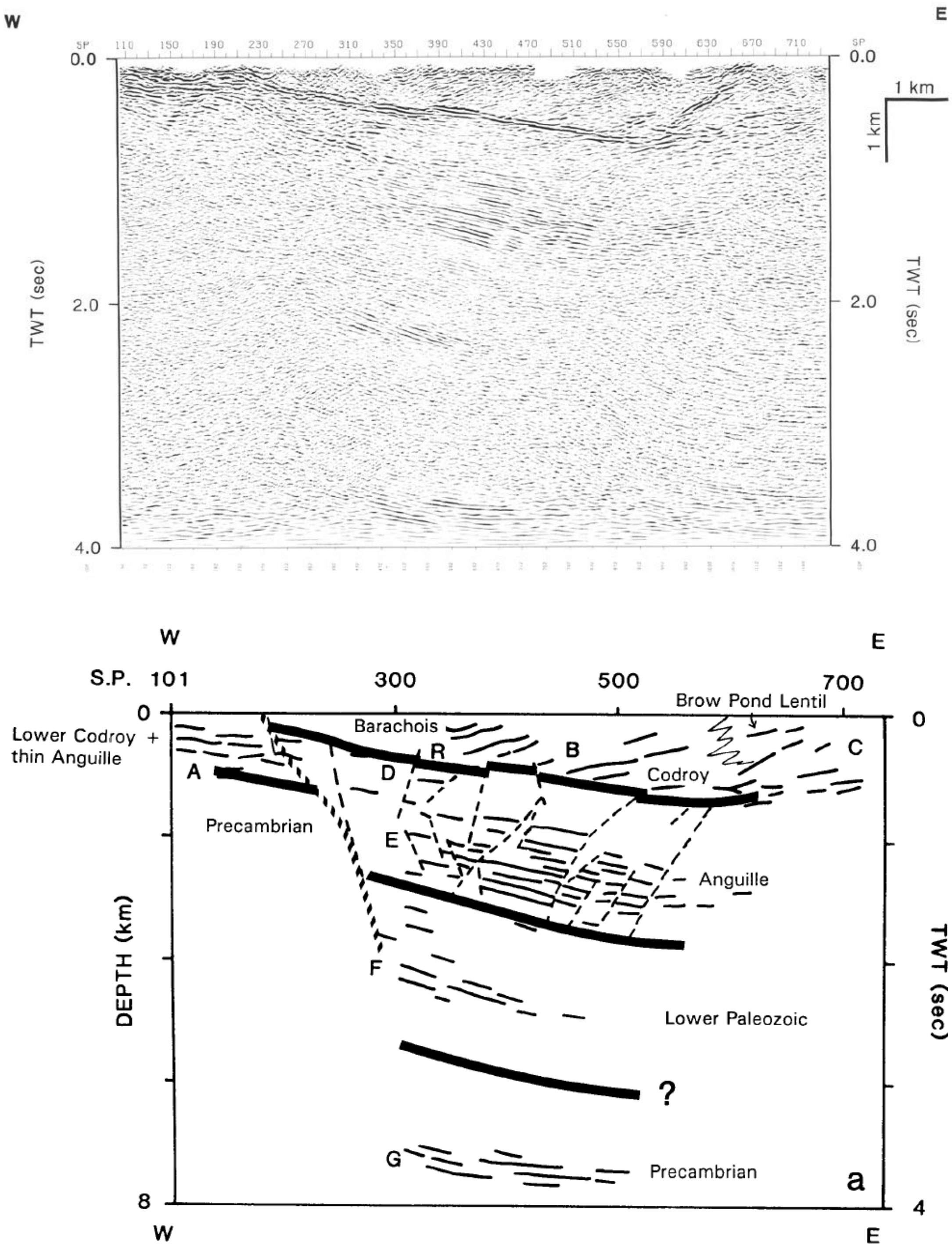

Figure 1.12: Top: The uninterpreted migrated seismic section. Bottom: The interpreted geological model from line drawings where reflector R corresponds to the Anguille and Codroy contact with a possible decollement. This is the seismic line shown in blue in Figure 1.11. Figure from Hall et al. (1992).

Newer peer-reviewed published geophysical work in the St. George Bay region has been done by Dafoe et al. (2016). They use an integration of datasets, including bathymetry, well and shallow drill core, seismic, and aeromagnetic data. Figures 1.13 and 1.14 display examples of their interpreted seismic data on which they map the Top Salt (green) and Base Codroy (orange) reflectors. The interpreted seismic section in Figure 1.13 shows a regional profile with salt-cored anticlines and adjacent salt expulsion minibasins. Faults appear to primarily offset the Base Codroy horizon dipping SE. The S1 syncline thickens to the SE, associated with the thickening of the salt. The seismic sections in Figure 1.14 show similar interpretations regarding brittle and salt deformation. Figure 1.14a shows a well-defined salt-cored anticline with intervening syncline. A dextral fault is observed in Figure 1.14b, associated with an offshore fault system. This fault is essential for the structural-to-stratigraphic relationship as the fault is interpreted to truncate salt deposition to the north. Figure 1.14c shows a similar fault truncating salt deposition to the north with an interpreted flower structure in the northern part of the seismic profile. The main relevant findings from Dafoe et al. (2016) include mapping a complex offshore fault system truncating salt deposition to the north, possibly related to pre-existing structures. They argue that this complex fault system formed in an environment of transtension and led to the reactivation of earlier structures such as the RHT and RBF. Dafoe et al. (2016) suggest that the halokinesis started during the deposition of overlying sediments in the deeper areas of the basin, with post-depositional halokinesis everywhere else. The work done by Langdon & Hall (1994) suggests the regional St. George Bay Fault marks the termination of carbonate platform successions offshore near the coastline. This regional fault observation is not confirmed by Dafoe et al. (2016) and further work is required to investigate this structure.

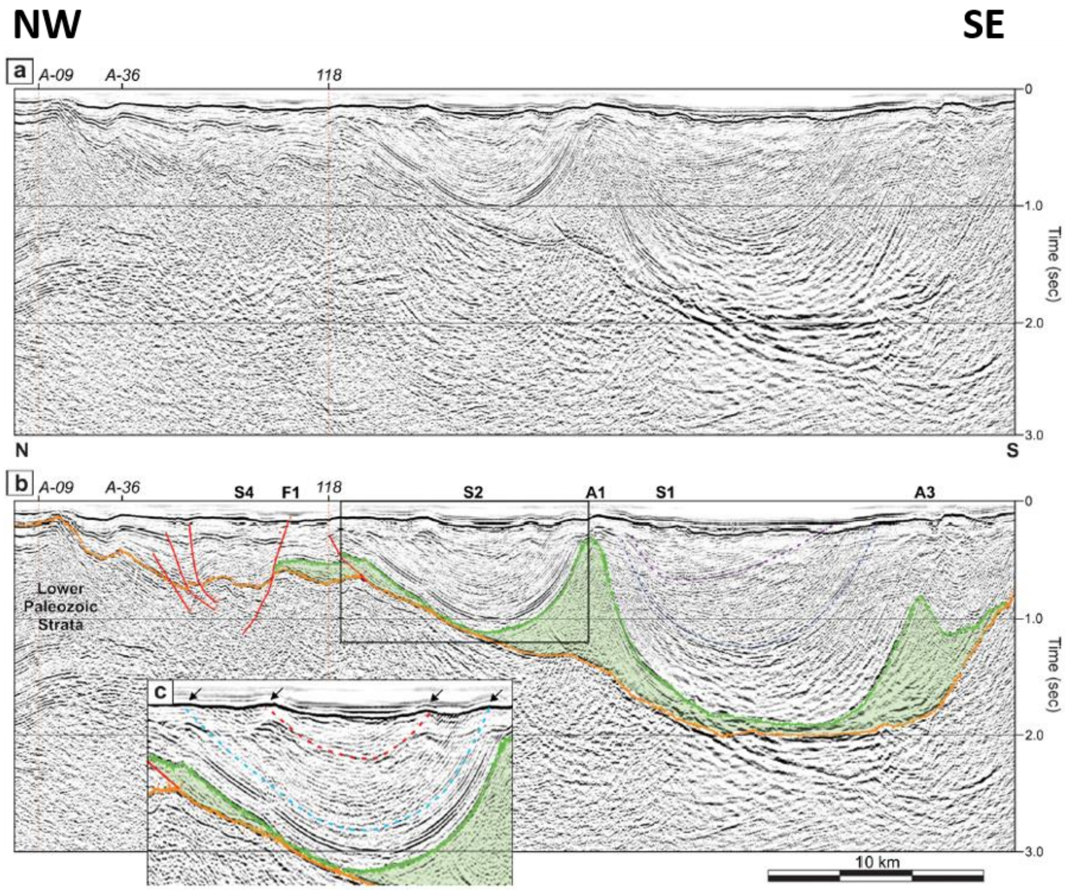

Figure 1.13: Regional seismic profiles across the St. George Bay from northwest to southeast. (A): Uninterpreted section. (B): Interpreted section where the green represents the Top Salt, orange corresponds to the Base Codroy Group, and solid red represents faults. Most of the faults offset the Base Codroy horizon and are primarily dipping SE. The S1 syncline appears to be thickening towards the SE. (C): Enlargement of (B), where red and blue dashed lines highlight synclines. The location of this seismic profile is displayed in Figure 1.11. Figure from Dafoe et al. (2016).

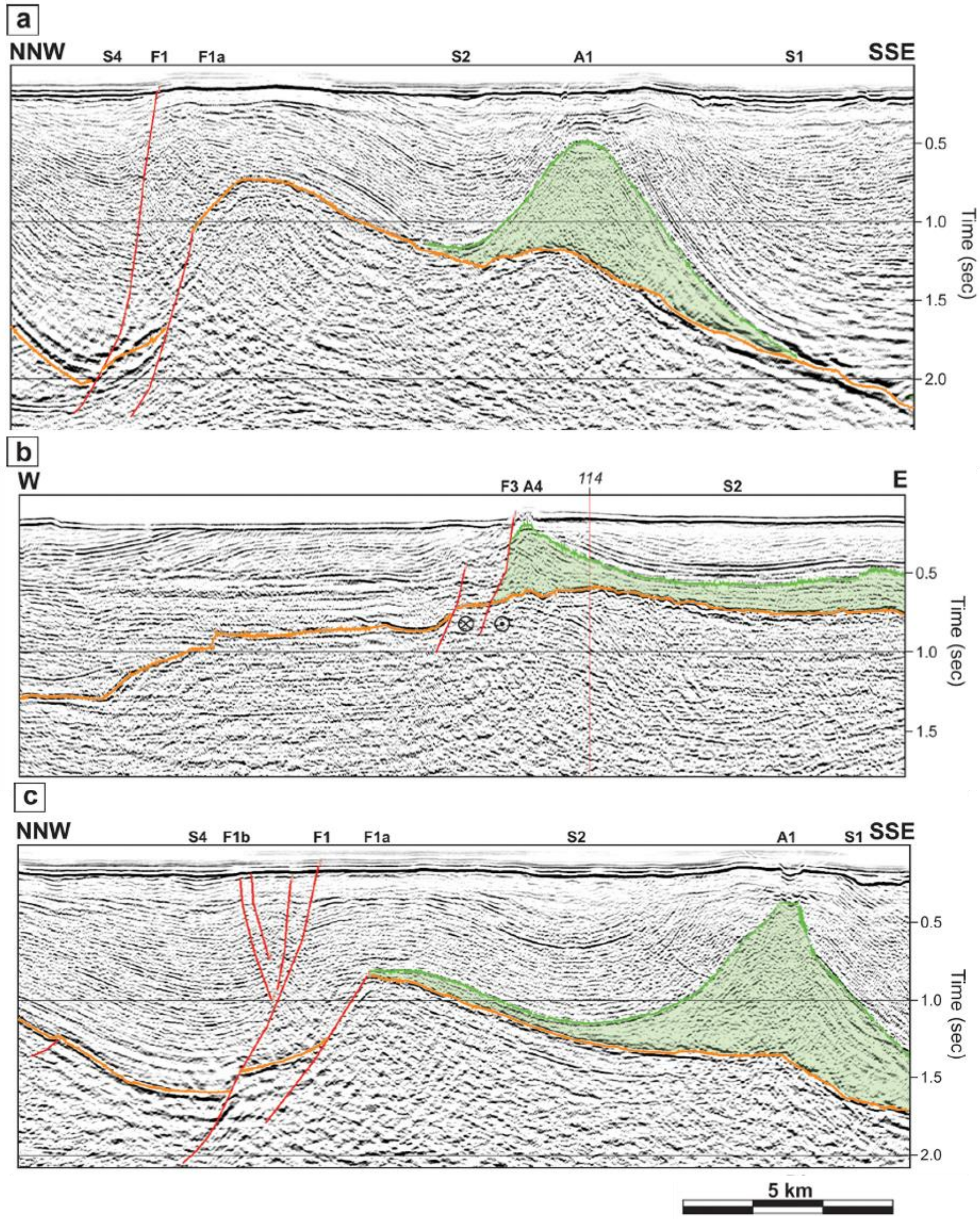

Figure 1.14: Three interpreted offshore seismic profiles. (a): Interpreted seismic section with an anticline structure, A1 and intervening synclines, S1 and S2. There are also synthetic NW dipping faults that offset the Base Codroy horizon. (b): Interpreted seismic section with an anticline, A4 truncated by a dextral fault, F3. This fault is interpreted to be part of the complex fault system (CBF). (c): Interpreted seismic section with a salt-cored anticline, A1, and associated synclines, S1 and S2. A possible interpreted flower structure is observed in the northern part of the seismic profile. This seismic profile has similar faults as previous sections that offset the Base Codroy Group, with additional antithetic faulting. The green and orange represent Top Salt and Base Codroy. The location of these seismic profiles is displayed in Figure 1.11. Figure from Dafoe et al. (2016).

The most up to date geological and geophysical work has been done by Snyder (2019), where she investigated the deformation history of the Maritimes Basin by doing a detailed analysis of two subbasins including the Bay St. George subbasin. A major takeaway from her work involved an interpreted tectonic wedge that correlates with the complex deformation history of the Bay St. George subbasin. Snyder (2019) traced trough points in salt-expelled minibasins to investigate salt movement (Figure 1.15) This technique involved mapping salt-expelled minibasins with the highest salt expulsion or dissolution (trough points). She determined a salt migration change from southeast to northwest due to the of a tectonic wedge. This implies that opposite verging thrusts are present creating this structure. Figure 1.15 displays traced surface troughs migrating towards the southeast on the seismic profiles without the interpreted wedge (E and W profiles in Figure 1.15), and migrating to the northwest on the seismic profile with the wedge (C profile in Figure 1.15).

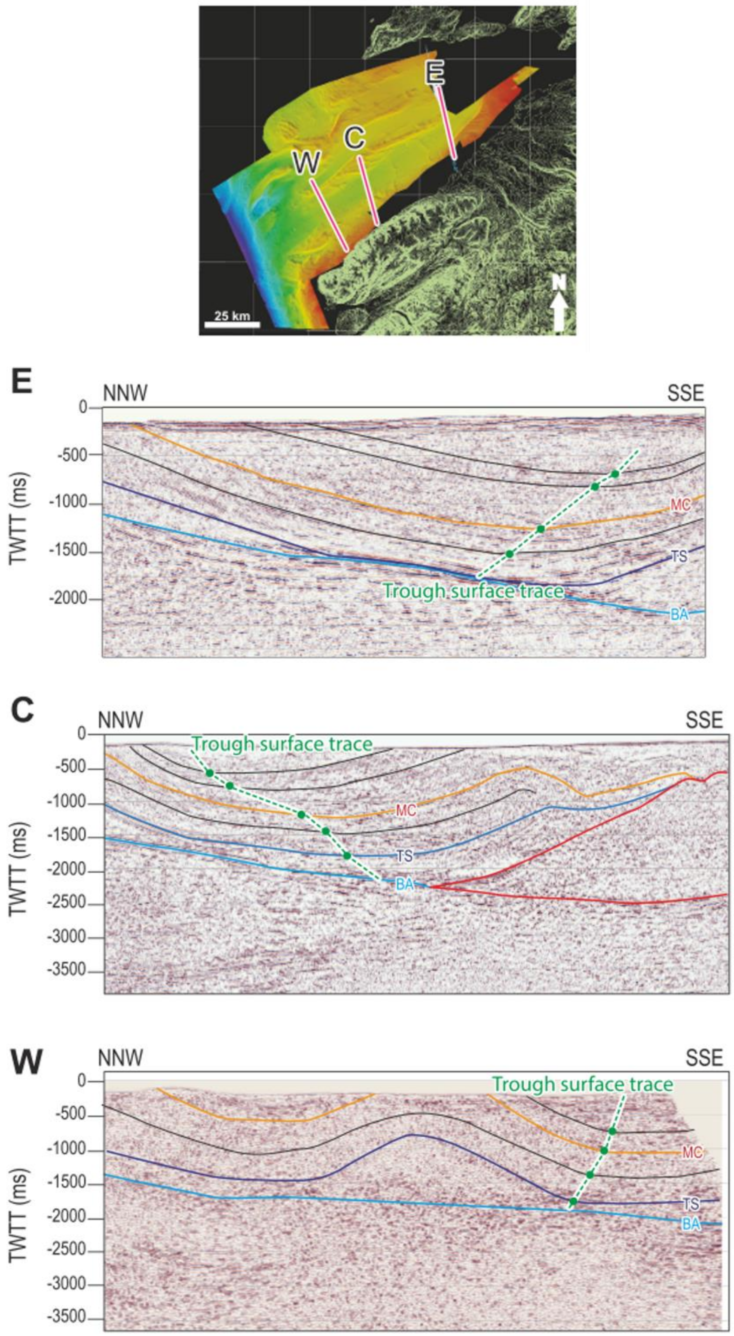

Figure 1.15: Trough surface traces interpreted on three seismic profiles corresponding to the bathymetric map location. The E and W seismic profiles indicate salt migration towards the southeast. The C seismic profile includes a tectonic wedge and shows salt migration towards the northwest. Figure from Snyder (2019).

Chapter 2 Dataset and Methodology

This chapter describes the datasets used in this project, including seismic, well logs, and potential field data. The methodology is explained for the seismic interpretation, well ties, time–depth conversion, and gravity modeling. Initial observations are also described from the potential field data.

2.1 Workflow

The general methodology workflow for this research project is displayed below in Figure 2.1. This workflow includes seismic interpretation, well log analysis, building a velocity model, potential field modeling, and correlating between the seismic and potential field datasets. These analysis techniques will be integrated to resolve the deep and shallow structures within the complex subsurface of the Bay St. George subbasin.

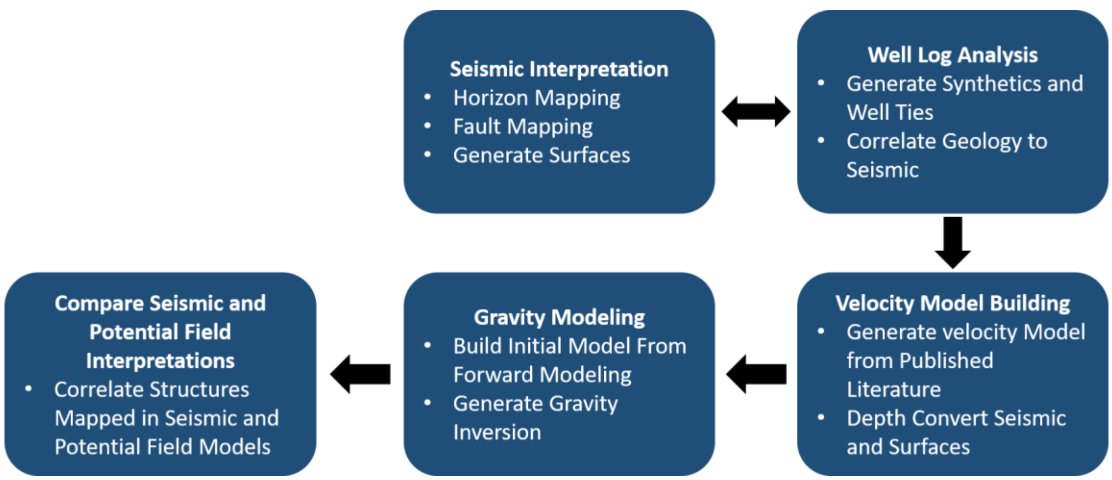

Figure 2.1: The general workflow of methods for this research project comprising seismic interpretation, well log analysis, velocity model building, potential field modeling, and comparing seismic and potential field interpretations.

2.2 Seismic Interpretation and Well Log Analysis

2.2.1 Seismic Dataset

The seismic reflection dataset for this thesis project is provided by the Canada Newfoundland and Labrador Offshore Petroleum Board (C-NLOPB) and the Department of Industry, Energy and Technology-Newfoundland and Labrador (Figure 2.2). It includes 60 onshore and offshore 2-D seismic reflection lines acquired in different years by different companies and, hence, with varying data quality and record lengths. Table 1 outlines the different seismic vintages and the operators that acquired the seismic data. The onshore seismic data are provided in standard SEGY format and directly imported into Petrel. Petrel is a geoscience software platform developed by Schlumberger that is utilized throughout this research project for seismic interpretation and well log analysis. The offshore seismic data are provided as PDF files and require digitization to SEGY files. Digitization of the seismic data to SEGY format is done by Peter Bruce from the CREAIT Network at the Memorial University of Newfoundland and imported in Petrel. Therefore, the amplitude range of the seismic data is limited, degrading the offshore seismic data quality.

Table 1: Seismic surveys acquired by different operators and various years used in this study.

Onshore/Offshore	Program Number	Operator	Year of Acquisition	SEGY or Scanned PDF
Offshore	CA-3000633-GOA	Marathon Petroleum Canada Ltd.	1992	Scanned PDF
Offshore	CA-3000719-GOA	Talisman Energy Inc.	1995	Scanned PDF
Onshore	EL-01-116-01-ES	Vulcan Minerals Inc.	2001	SEGY
Onshore	EL-04-116-01-ES	Vulcan Minerals Inc.	2004	SEGY
Onshore	EL-05-116-01-ES	Vulcan Minerals Inc.	2005	SEGY
Onshore	EL-07-116-01-ES	Vulcan Minerals Inc.	2007	SEGY

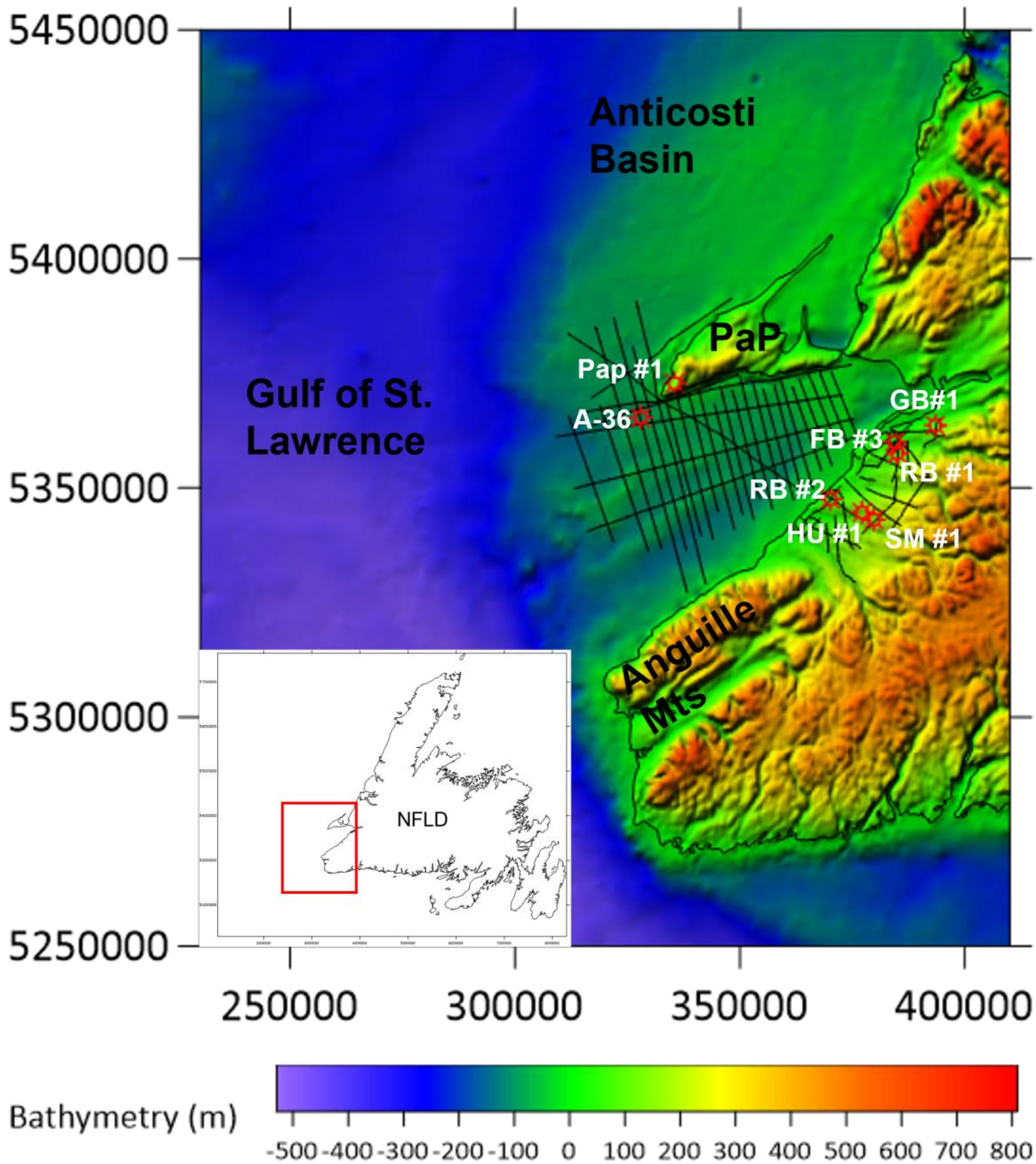

Figure 2.2 Bathymetry map of Western Newfoundland and the Bay St. George subbasin. The Bay St. George subbasin is located south of the Port au Port Peninsula (PaP). The black lines correspond to the seismic lines used in this project, and the red symbols represent the well locations. Pap #1: Port au Port #1 well. A-36: St. George Bay A-36 well. GB #1: Gobineau #1 well. FB #3: Flat Bay #3 well. RB #1: Robinsons #1 well. RB #2: Red Brook #2 well. HU #1: Huricane #1 well. SM #1: Storm #1 well. Bathymetry data downloaded from https://www.gebco.net/.

2.2.2 Seismic Interpretation

Seismic interpretation for this research project is completed using Schlumberger-Petrel E&P (Exploration and Production) Software to map the subsurface geology in SW

Newfoundland. The primary objective of the seismic interpretation is to map the main seismo-stratigraphic horizons and faults in the onshore-to-offshore Bay St. George subbasin. Seismic interpretation provides a geological and structural model of the basin that is integrated with the potential field modeling (Section 4). This thesis omits interpreting structures and stratigraphy in the southwestern part of the onshore basin near the Anguille Mountains since there are no seismic lines available.

There are six seismic horizons mapped including, the Seabed, Average-Top Salt, Base Codroy, Base Anguille, Top Cambrian–Ordovician Carbonate Platform, and Base Cambrian–Ordovician Carbonate Platform. (Table 2). These seismic horizons are tied with the picked well tops from the well logs and synthetics.

Table 2: The six seismic horizons mapped with their corresponding colors on the interpreted seismic sections. This table also indicates the region of the basin in which they are present.

Surface	Offshore/Onshore
Seabed	Offshore
Average-Top Salt	Both
Base Codroy	Both
Base Anguille	Onshore
Top Cambrian-Ordovician Carbonate Platform	Offshore
Base Cambrian-Ordovician Carbonate Platform	Offshore

Different colour bars are used to interpret the onshore and offshore seismic data because of the SEGY and digitized nature of the data for each line, along with the varying seismic vintages. The seismic interpretation of the onshore seismic data used a red–blue colour bar corresponding to a trough (red) and peak (blue), respectively (Figure 2.3). The offshore seismic data require a grey–red colour bar corresponding to a trough (grey) and peak (red), respectively (Figure 2.3). The grey–red colour bar is the only option that provides clear, interpretable views of the digitized data, and hence the peak is red for the offshore data and blue for the onshore data.

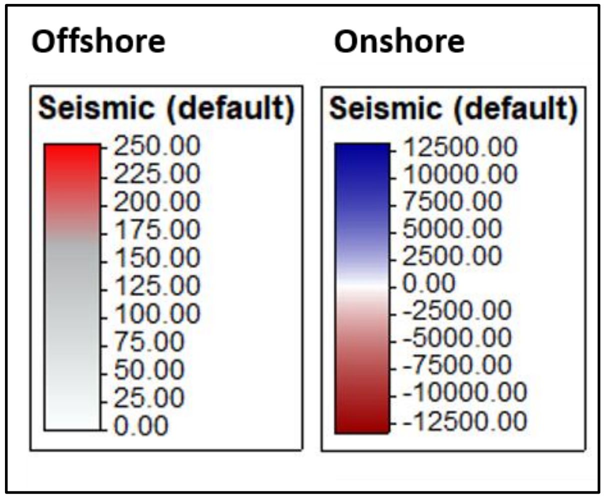

Figure 2.3: An example of the colour scale bars used for the offshore (left) and onshore (right) seismic data. Offshore: Red represents a peak, while all amplitudes below 125.00 are considered to represent troughs. Onshore: Blue represents a peak, and red represents a trough.

Both the Average-Top Salt and Base Codroy seismic horizons mapped in this basin are similar to observed seismic markers in other areas of the Maritimes Basin (Dafoe et al., 2016; Marillier et al., 1994; Marillier & Verhoef, 1989). These are the only two seismic horizons that are easily observed throughout the onshore-to-offshore basin. The majority of past studies that involve seismic interpretation of the Bay St. George subbasin do not attempt to map seismo-stratigraphic horizons beneath the Base Codroy Group (e.g., Dafoe et al., 2016). As such, this research investigates deeper surfaces and structures for a better understanding of the complex Bay St. George subbasin.

The Average-Top Salt reflector is identified as a peak due to a high seismic impedance contrast (Jackson & Hudec, 2017). The salt creates diapiric and pillow structures (e.g., red star in Figure 2.4A). The reflections lack internal reflectivity due to the salt structures (Dafoe et al., 2016). This unit is seismically distinct and mapped continuously onshore-to-offshore.

The Base Codroy reflector is the most seismically coherent and continuous horizon in the basin. This horizon appears as a strong seismic peak (Figure 2.4C and Figure 2.4D).

The base of the Anguille Group is poorly constrained in the Bay St. George subbasin, and can only be identified onshore (Figure 2.4E). Here, the Base Anguille reflector underlies the Base Codroy Group and appears as a peak (Figure 2.4E). This surface is an essential stratigraphic unit for defining the thickness of the Carboniferous sediments.

The autochthonous Cambrian–Ordovician carbonate successions are predominantly observed in the Port au Port Peninsula (Figures 2.2 and 1.6); however, seismic interpretation evidence indicates that these successions also extend into the offshore region of the Bay St. George subbasin. This is a controversial topic, as Dafoe et al. (2016) determined that these successions are not observed from the seismic and magnetic data that they interpreted. Langdon & Hall (1994) argue that these units can be identified using seismic data. Only a top and a base Carbonate Platform seismic horizon are mapped in this study, despite there being coherent reflections observed between these two seismic horizons. These reflections correspond to other stratigraphic contrasts in the Cambrian–Ordovician carbonate succession. Mapping a top and base Carbonate Platform seismic horizon is adequate as they act as seismic markers to aid in offshore seismic interpretation, by constraining the overall structure of the Cambrian–Ordovician succession. The carbonate successions are described as a band of high-amplitude, undulating reflections of relatively uniform thickness (Figure 2.4G). (Langdon & Hall, 1994; Waldron & van Staal, 2001). Geological correlations with well data support the idea that these surfaces exist under the Carboniferous strata in parts of the Bay St. George subbasin.

The other significant aspect of the seismic interpretation involves mapping faults. Faults are identified as breaks in reflectivity and acoustic blanking, indicating a fault trace. The offset of seismic horizons is also an important indicator of separation across faults.

Fault mapping defines much of the Bay St. George subbasin structure, increasing our geological understanding of the region.

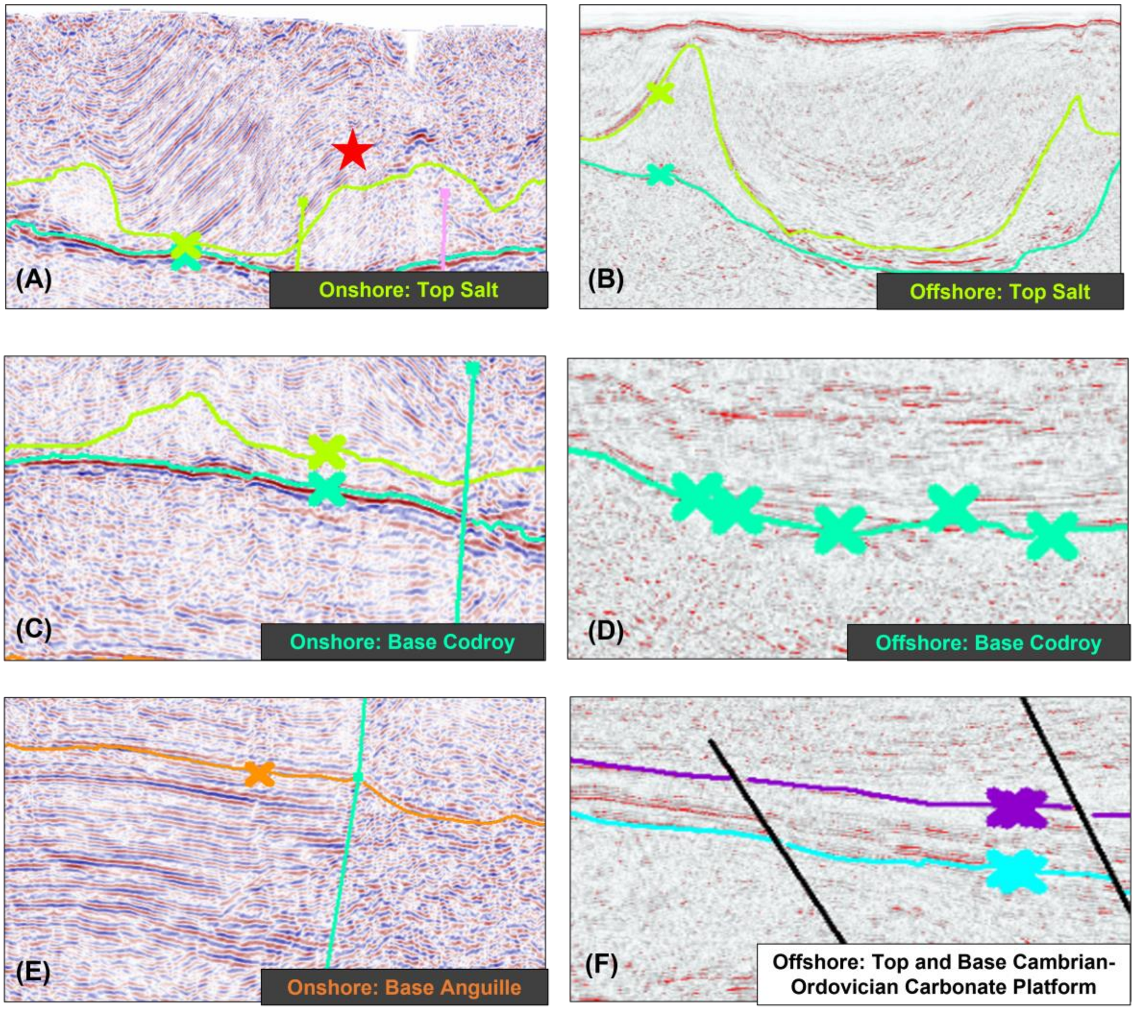

Figure 2.4: Examples from onshore and offshore seismic profiles of the mapped seismo-stratigraphic horizons defined by different seismic characteristics. The horizons are color coded according to Table 2. The subvertical lines crossing the horizons represent faults. The crosses represent intersecting seismic profiles. (A) and (B): Average-Top Salt. The red star highlights a diapiric salt structure. (C) and (D): Base Codroy. (E): Base Anguille. (G): Top and Base Carbonate Platform.

2.2.3 *Time Surface Maps*

Gridding of seismic surfaces is performed using interpreted seismic horizons to visualize the three dimensional structure of a stratigraphic unit. Seismic surfaces are also required for the calculation of isochron maps. The seismic horizons are gridded using 650 by 650 cell size within Petrel and displayed in a consistent manner using Petrosys Pro. Time surface maps are produced for the Average-Top Salt, Base Codroy, Base Anguille, Top Carbonate Platform, and Base Carbonate Platform seismic horizons (Figures 3.8–3.12).

2.2.4 Thickness Maps

Time thickness (isochron) maps are created by subtracting a lower surface from an overlying surface to determine the thickness between two horizons. Thickness maps help reveal stratigraphic changes and maximum sediment thicknesses. Time thickness maps are generated for the salt (Base Codroy–Average-Top Salt), Anguille Group (Base Codroy–Base Anguille), Middle Carboniferous (seabed–Base Codroy), Long Point Group (Base Codroy–Top Carbonate Platform), and Carbonate Platform Group (Top–Base Carbonate Platform).

2.2.5 Well Log Data

A total of eight onshore and offshore wells are available to correlate the geological information with the seismic data for the seismic interpretation (Table 3). Five wells are used in this study (given in Table 3), while the Storm #1, Flat Bay #3, and Robinsons #1 wells are not. This is because the logs for these wells are too shallow or lack critical log information. The five wells used are distributed throughout the basin (Figure 2.2), providing enough lateral coverage for well log correlation and well ties, despite the omission of three wells.

Table 3: The different Well names and log data used. CALI: caliper. GR: gamma-ray. RHO: density. PHI: porosity. RES: resistivity. The rows in green are the wells used and the rows in red are not used in this study due to limited depth penetration or missing log sections.

Well Name	Onshore/Offshore	CALI	GR	RHO	Slowness	PHI	RES
St. George Bay A-36	Offshore	✓	✓	✓	✓	✘	✘
Port au Port #1	Onshore	✓	✓	✓	✓	✓	✘
Storm #1	Onshore	✓	✓	✓	✓	✓	✘
Red Brook #2	Onshore	✓	✓	✓	✓	✘	✓
Flat Bay #3	Onshore	✓	✓	✓	✘	✘	✘
Hurricane #1	Onshore	✓	✓	✘	✓	✘	✘
Gobineau #1	Onshore	✓	✓	✓	✓	✘	✘
Robinsons #1	Onshore	✓	✓	✓	✓	✓	✓

2.2.6 Well Ties and Log Analysis

Well logs are the geological ground truth, and generating synthetics is essential for robust seismic interpretation as it ties the seismic events directly to the well. These seismic events correspond to the interpreted seismic horizons carried outward from the wells. These seismic events are represented by well tops picked by looking at the different logs (e.g., GR) and using the well reports (Allison, 1996; Forcinal, 2013; Halley, 2010; Smith, 2006). Synthetic traces are created for the St. George's Bay A-36, Red Brook #2, Hurricane #1, and Gobineau #1 wells to tie the lithological information from the wells with the seismic data. A synthetic trace is not generated for the Port au Port #1 well as no seismic data in this study extend to the Port au Port Peninsula. However, the Port au Port #1 well logs are used to correlate with the A-36 well (Appendix B).

The initial step in producing synthetic traces is to compute the acoustic impedance (AI), which is the seismic velocity and density product. The reflection coefficient (RC) is defined by how much energy is reflected, and it is determined using the AI of contrasting layers. The synthetic seismogram is finally generated by convolving the RC with a representative wavelet. The wavelets used in this study are either an extracted statistical wavelet from the zone of interest or an analytical wavelet (e.g., Ricker and Butterworth). Missing density logs are accounted for by using Gardner's equation (Gardner et al., 1974),

$$\rho = \alpha V p^{\beta}$$

where α and β are empirically derived constants corresponding to 309.545 and 0.25, respectively, and V_p is the P-wave velocity. Post-synthetic generation may require additional processing, including applying a bulk shift and stretching and squeezing to better match the estimated synthetic and real seismic data.

Two examples of well ties are displayed; an offshore well (St. George Bay A-36) (Figure 2.5) and an onshore well (Red Brook #2) (Figure 2.6). The quality of the well ties is dependent on the quality of the seismic and well data. As the offshore seismic data are digitized from PDF format, the quality is poor and the resulting tie is a consequence of this.

The St. George Bay A-36 synthetic trace (Figure 2.5) is generated using a zero-phase analytical Ricker wavelet with a central frequency of 25 Hz. A bulk shift of -26.0 ms is applied to match the synthetic and seismic data better. Finally, a Time–Depth Relationship (TDR) is applied using an assumed offshore velocity model built in this study.

A similar process is performed for the onshore Red Brook #2 well tie (Figure 2.6); however, a statistical wavelet is extracted from the zone of interest. Different wavelets are used between the A-36 and Red Brook #2 wells based on the data quality of the well logs. The A-36 well logs are noisy with many spikes (Figure 2.5), and hence an analytical wavelet is used. Moreover, the Red Brook #2 well logs are less noisy (Figure 2.6), allowing for a robust extracted wavelet. This extracted wavelet provides a representation of the source wavelet of the onshore seismic data. Once the synthetic is generated, a bulk shift of -27.0 ms is applied with additional stretching/squeezing. Finally, a TDR is applied using an assumed onshore velocity model.

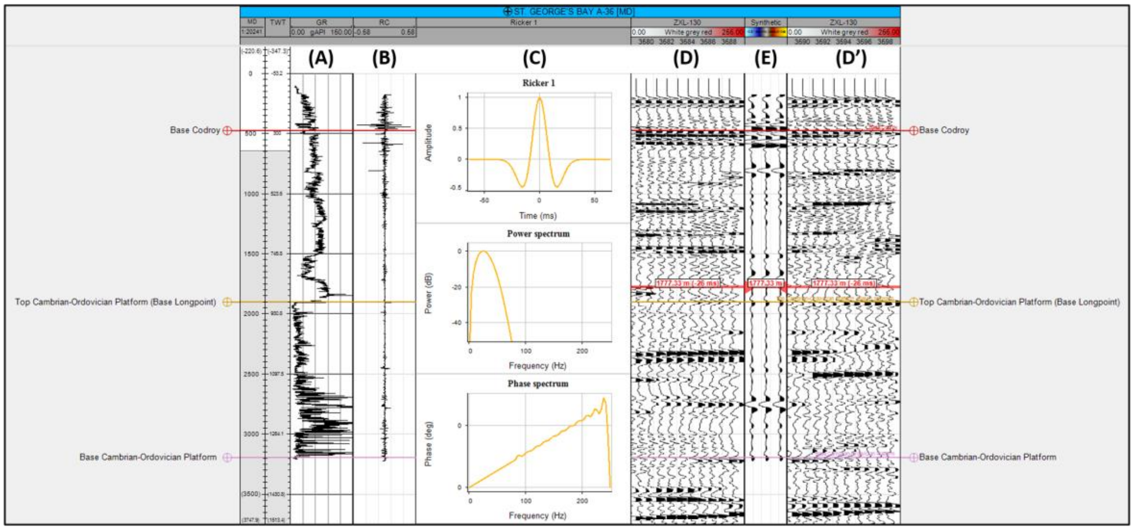

Figure 2.5: The St. George's Bay A-36 well tie. (A): Gamma Ray log (GR). (B): Reflection Coefficient (RC) series. (C): Analytical zero phase Ricker wavelet with a 25 Hz central peak. (D) and (D'): Traces from the 2-D seismic line. (E): Synthetic seismic trace.

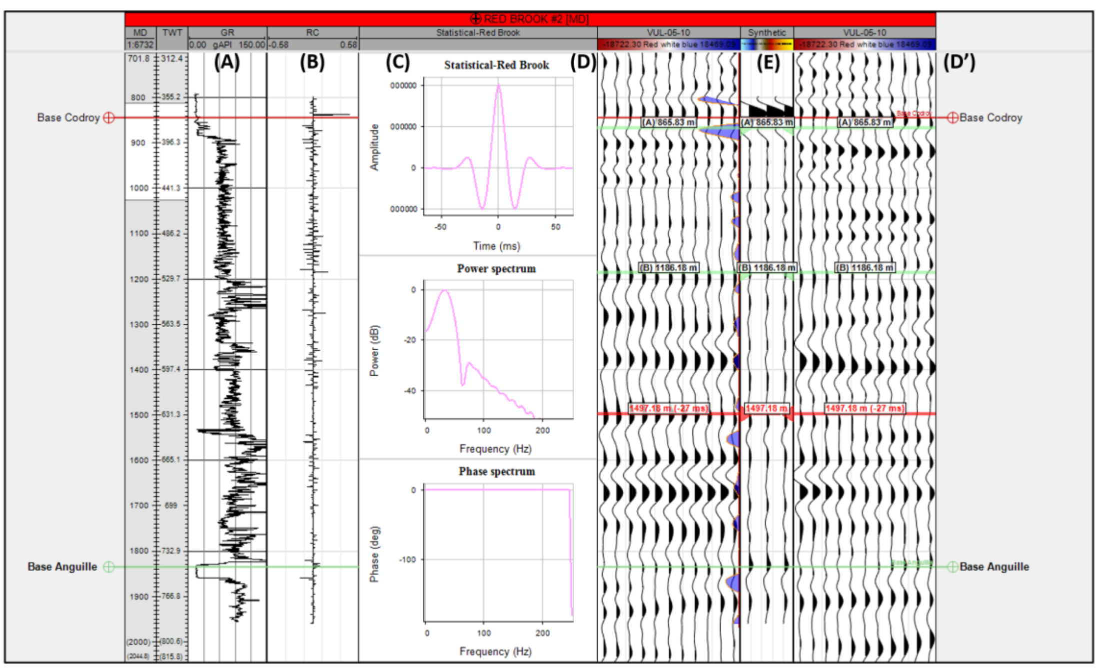

Figure 2.6: The Red Brook #2 well tie. (A): Gamma Ray log (GR). (B): Reflection Coefficient (RC) series. (C): Statistical wavelet extracted from the zone of interest. (D) and (D'): Traces from the 2-D seismic line. (E): Synthetic seismic trace.

2.3 Time–Depth Conversion

A time–depth conversion is important when interpreting seismic data as it gives you the ability to interpret structures and stratigraphy in depth and this is required to constrain potential field modeling. The generated velocity models allow for this domain conversion from time to depth. Two individual velocity models are built within Petrel to account for the different seismo-stratigraphic horizons between onshore and offshore. The two separate velocity models are required since there are differences in geology onshore and offshore.

An onshore velocity model is created using a processing velocity report from the northeast region of the onshore study area (Figure 2.7) (LeDrew, 2011). Since this velocity model does not use a discrete color bar, the approximate velocities are estimated and constrained with the discrete velocities obtained from the offshore velocity model (Figure 2.8).

An offshore velocity model used in the time–depth conversion is built using constraints from an offshore seismic refraction study located primarily in the Port au Port Peninsula (Figure 2.8) (Michel et al., 1992). An additional velocity layer is required in the offshore velocity model to consider the Cambrian–Ordovician strata. The offshore velocity model from Michel et al. (1992) contains Cambrian–Ordovician strata. However, the model does not contain Carboniferous strata since there is little to no Carboniferous strata in the Port au Port. Therefore, the Carboniferous strata velocity is constrained based on the onshore velocity model (Figure 2.7). It is noted and emphasized that the offshore velocity model used by Michel et al. (1992) does not represent a detailed complex model, and therefore, a relatively simple velocity model is used. Although the offshore seismic refraction study is north of the study area, it is still a geologically reasonable representation for parts of the offshore St. George Bay geology.

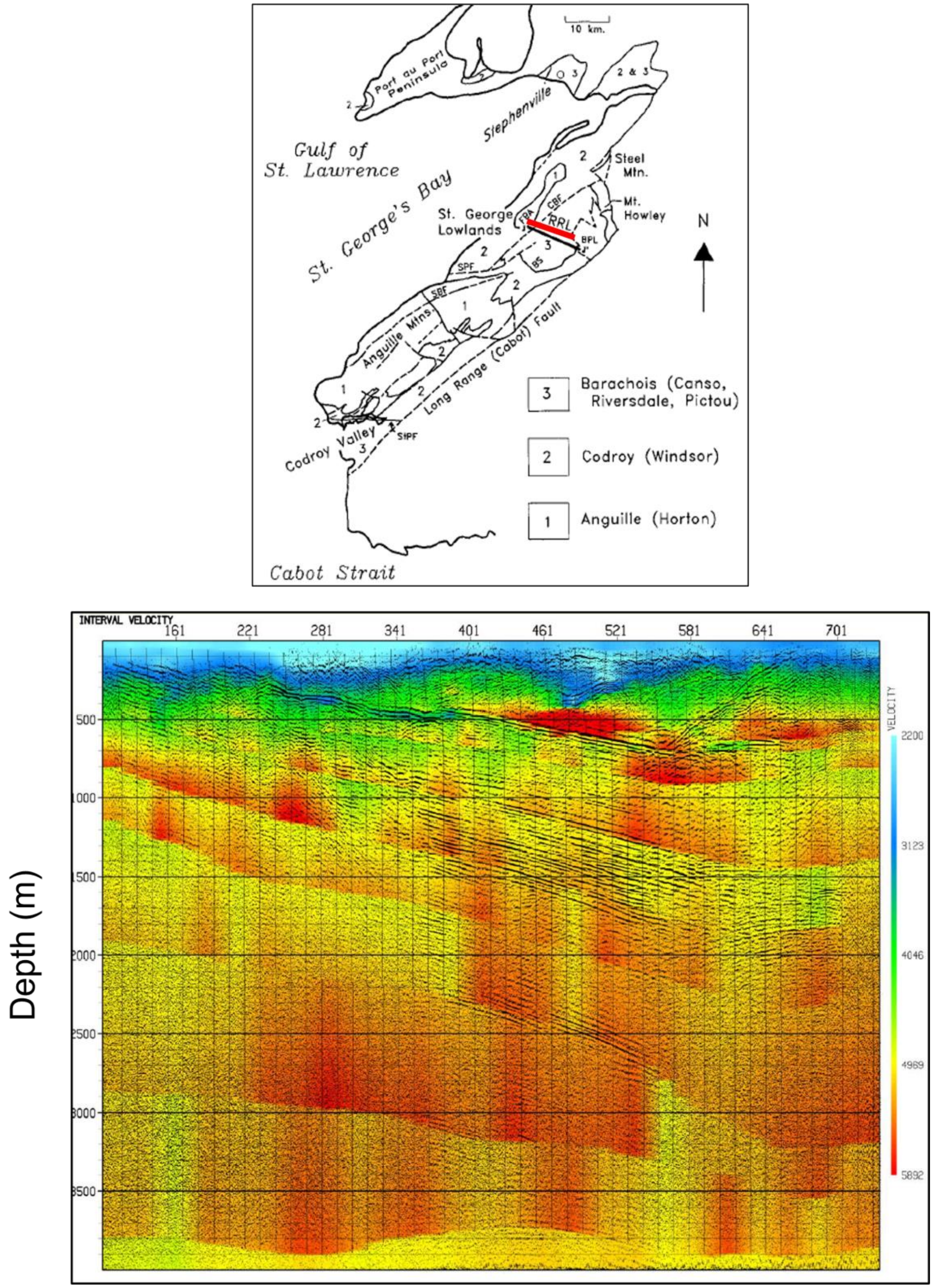

Figure 2.7: The interval velocity model used in the seismic processing by Triumph Atlantic of an onshore seismic line in the Bay St. George subbasin and used to constrain the velocity model built in this study. This is the same seismic profile as seen in Figure 1.12. Figure modified after LeDrew (2011).

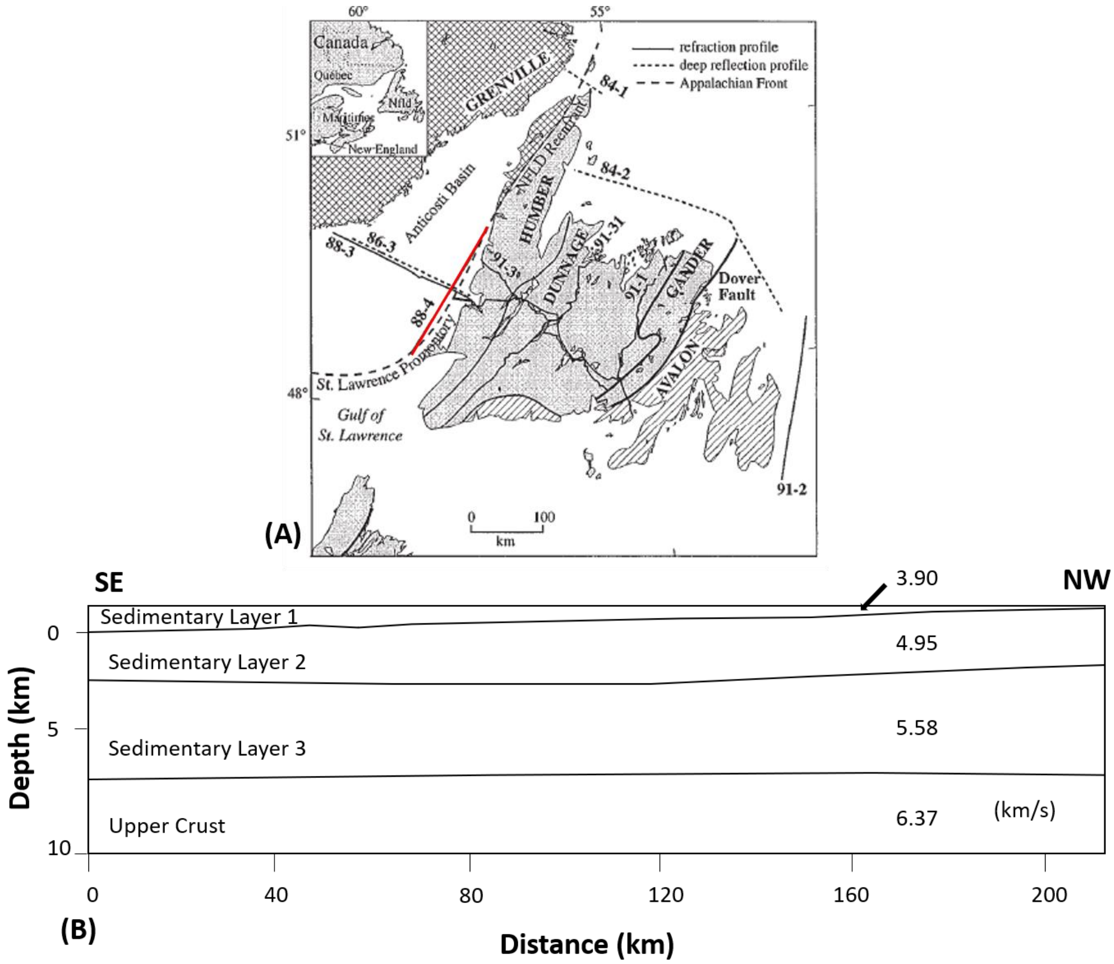

Figure 2.8: (A): The location of seismic refraction line 88-4 north of the Bay St. George subbasin. (B): The structural velocity model of 88-4 is determined from seismic refraction data. These velocities were used as a guide for the velocity model in this study. Figure modified after Jackson et al. (1998) and Michel et al. (1992).

Velocity intervals are defined using interpreted seismic horizons in this study, including the Seabed, Average-Top Salt, Base Codroy, Base Anguille, Top Carbonate Platform, and Base Carbonate Platform. The offshore velocity model (Table 4) contains six layers, including three sedimentary layers, a water column layer, a salt layer, and crystalline basement. The Barachois and Upper to Middle Codroy Groups are defined as the sediment package between the Seabed and the Average-Top Salt surfaces. The salt layer is defined by the package between the Average-Top Salt and Base Codroy surfaces. The Long Point Group is defined as the sediment package between the Base Codroy and Top Platform surfaces. The Carbonate Platform Groups are defined as the sediment package between the Top and Base Carbonate Platform surfaces. The remaining crystalline basement is defined as everything below the Base Carbonate Platform surface.

Table 4: The assigned interval velocities used for the offshore time–depth conversion. Velocities from Michel et al. (1992).

Water Column: 1500 m/s
Barachois and Upper to Mid Codroy Groups: 3900 m/s
Salt: 4500 m/s
Long Point Group: 5000 m/s
Carbonate Platform Groups: 5600 m/s
Basement: 6400 m/s

A similar process is performed for the onshore velocity model (Table 5); however, fewer layers are defined as there are fewer interpreted seismic horizons. The only different velocity layer onshore is the Anguille Group. This velocity layer is defined as the sediment package between the Base Codroy and Base Anguille surfaces.

Table 5: The assigned interval velocities used for the onshore time–depth conversion. Velocities from LeDrew (2011) and Michel et al. (1992).

Barachois and Upper to Mid Codroy Groups: 3900 m/s
Salt: 4500 m/s
Anguille Group: 5000 m/s
Basement: 6400 m/s

Quality Control (QC) is performed during the depth conversion to ensure that artifacts are not generated and faults are converted appropriately. The QC process includes looking for geologically unrealistic structures (e.g., pull-ups) and comparing the depths of those converted seismic profiles with previously depth-converted seismic data in the region (Hogg & Enachescu, 2015). Uncertainty in the time–depth conversion is emphasized, where the depth uncertainty in this study is estimated to be 500 m. This depth uncertainty is estimated by comparing the thickness maps with previous literature to investigate if the thicknesses agree based on the uncertainties. Sedimentary basin thickness maps generated by Miller et al. (1990) produce comparable results such that the depth uncertainty determined by them is 1 km. They used older seismic data acquired in 1971 and 1973, which must be considered. They obtained a maximum thickness of Carboniferous sediments reaching 6 km offshore and 3 km onshore, while this study found thicknesses reaching 5 km and 4 km, respectively. The results from this study agree with theirs considering these depth uncertainties.

2.4 Potential Field Dataset and Modeling

2.4.1 Gravity Field Dataset

Both free-air gravity and Bouguer gravity field data are compiled from global free sources. The free-air gravity data are downloaded from the DTU Space-National Space Institute and are mapped from Satellite Altimetry (Figure 2.9) (https://www.space.dtu.dk/english/research/scientific_data_and_models/global_marine_gravity_field). Bouguer gravity data are downloaded from the International Gravimetric Bureau website (http://bgi.obs-mip.fr/), and are derived from the Earth Gravitational Model (EGM 2008) (Figure 2.10). The data were released by the National Geospatial-Intelligence Agency (NGA) (Pavlis et al., 2008).

Since the Bay St. George subbasin extends onshore-to-offshore, a combination of free-air and Bouguer gravity datasets with a smooth transition from onshore to offshore is required for the gravity inversion to work appropriately. This is needed because the free-air gravity data are only corrected for elevation, and hence these data can only be used for the offshore part of the Bay St. George subbasin. Since the Bouguer gravity data are corrected for the elevation and the terrain, they are only used for the onshore part of the basin. Processing the gravity data to integrate both datasets is achieved by masking data using Oasis Montaj. A polygon is created around the Newfoundland coastline for the masking of data. All the free-air gravity data are masked inside this polygon, resulting in the free-air data being constrained to offshore. Similarly, the Bouguer gravity data are masked outside the polygon, resulting in the Bouguer data being constrained to onshore. Finally, both masked datasets are merged into one file for gravity modeling moving forward (Figure 2.11).

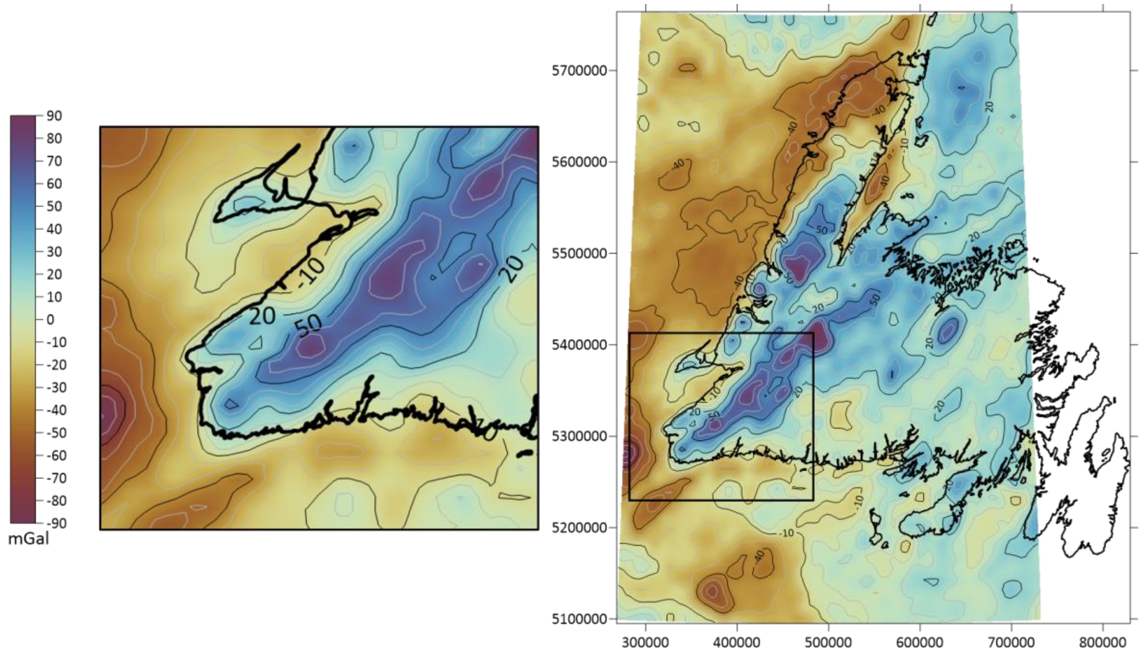

Figure 2.9: The free-air gravity anomaly map. The black box is an enlargement of the Bay St. George subbasin and surrounding area.

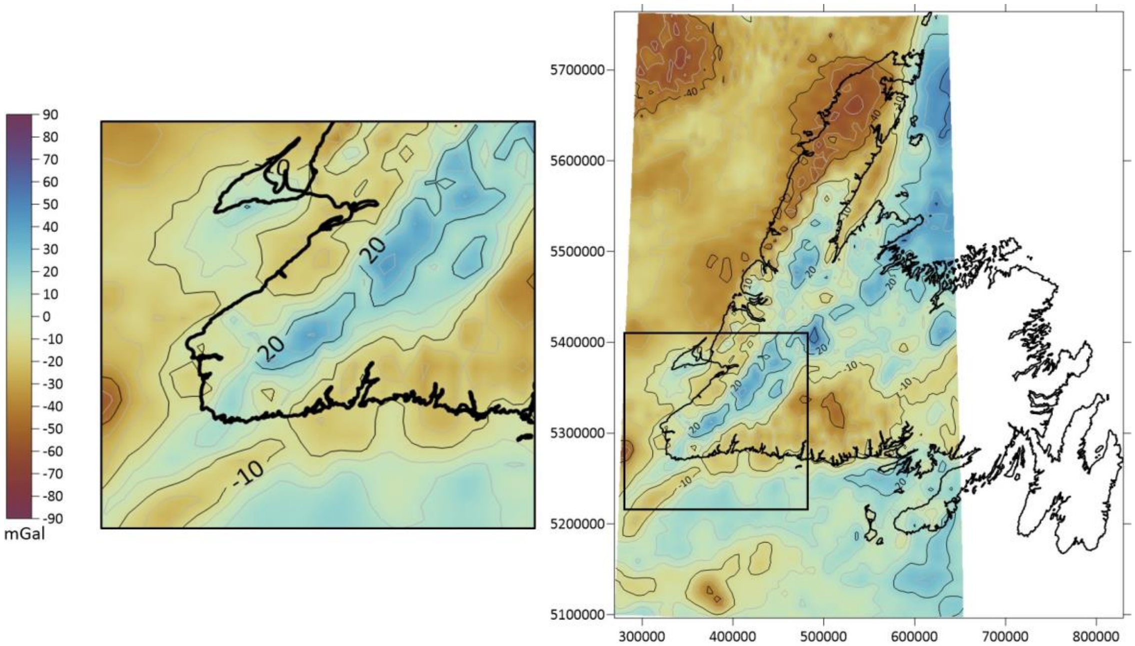

Figure 2.10: The Bouguer gravity anomaly map. The black box is an enlargement of the Bay St. George subbasin and surrounding area.

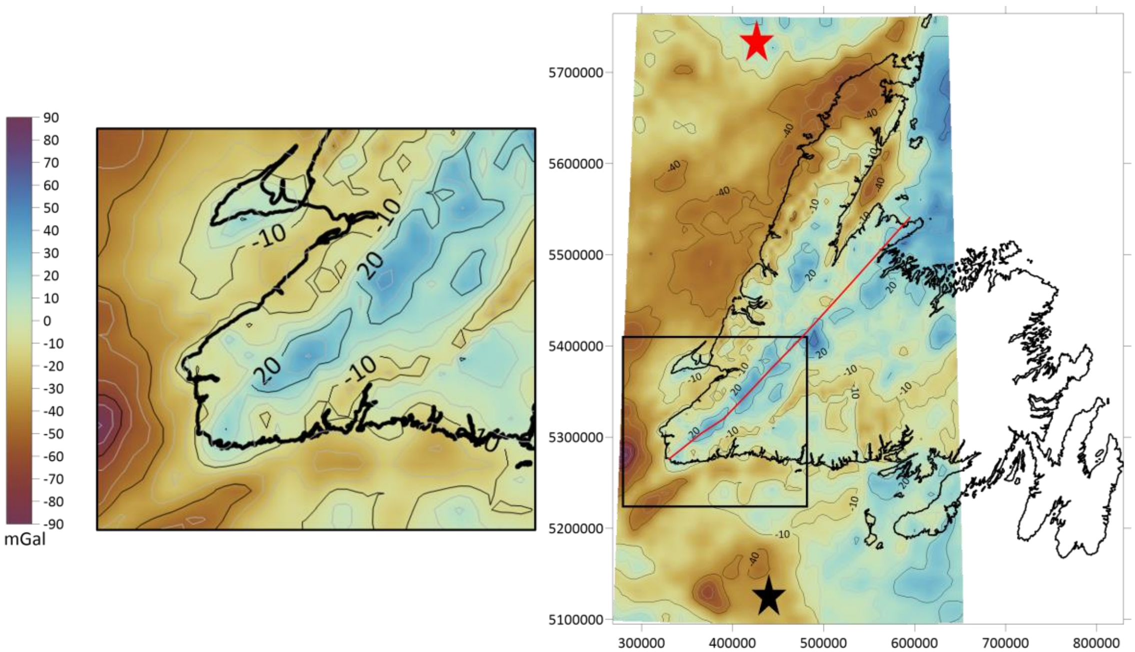

Figure 2.11: The integrated free-air and Bouguer gravity anomaly map. The black box is an enlargement of the Bay St. George subbasin and surrounding area. The red line indicates the trend of the Long Range Fault. The black star indicates the gravity low associated with the location of the Magdalen Basin. The red star indicates the high gravity associated with the Grenville Front.

2.4.2 *Gravity Field Data Observations*

Initial observations of the integrated free-air and Bouguer gravity anomaly map (Figure 2.11) include anomalous gravity lows and highs highlighted by a black and red stars, respectively. The gravity low is associated with the thick sediments of the Magdalen Basin. The high gravity anomaly northwest of Newfoundland highlighted by a red star is associated with the Grenville Front. A NE–SW trending gravity anomaly is observed and annotated as the red line and is likely associated with the Long Range Fault. Minor gravity variations are observed in the offshore Bay St. George subbasin due to differences in sediment thickness.

2.4.3 *Gravity Forward Modeling*

The gravity modeling in this study involves forward and inverse modeling to determine a 3-D density Earth model of the Bay St. George subbasin. The inverse models are highly non-unique such that there are infinitely many equivalent density models that can reproduce the observations. The non-uniqueness is mitigated using forward modeling with constraints from seismic data.

The forward modeling is completed prior to inversion because it gives the starting model for the gravity inversion. An initial model is constructed by minimizing the misfit between the observed and predicted gravity anomaly response. Forward modeling is done using ModelVision, a user-interactive potential field software package that allows users to apply filters and model potential field data. ModelVision also enables the output of files compatible with the GRAV3D inversion software. The GRAV3D modeling algorithm was developed by Li & Oldenburg (1996; 1998) and allows for the inclusion of a priori information. The same inversion algorithm was used for similar satellite altimetry datasets by Welford et al. (2010) and Welford & Hall (2007). The algorithm is further described in section 2.4.6

The forward modeling of gravity data completed in this study uses Free-Air and Bouguer gravity data for the offshore and onshore parts of the basin, respectively. Preliminary gravity data processing includes applying a low pass filter to remove near surface high frequencies to aid in modeling deeper regionally relevant structures. Arbitrary lines are created across the basin and sampled using the low pass gravity data (Figure 2.12). In this case, ten parallel lines are selected that are 74520 m long and have 150 sampled data points per line. The lines are modeled using density polygons constrained from seismically interpreted depth surfaces in this study and previous seismic refraction studies in Western Newfoundland. The seismic interpretation only constrains the shallow structures since the deeper crustal features are not imaged on the seismic data available for this research. Therefore, past seismic refraction studies from further north in the Humber Zone (Jackson et al., 1998; Marillier & Verhoef, 1989) provide the broad constraints for deeper crustal structures such as the Moho.

The forward modeling began at the northernmost line, with subsequent modeling performed southwards. Each line is modeled through an iterative process to reduce the misfit between the calculated and observed gravity data. Quality Control (QC) during the forward modeling ensures that geologically reasonable densities are assigned to the bodies.

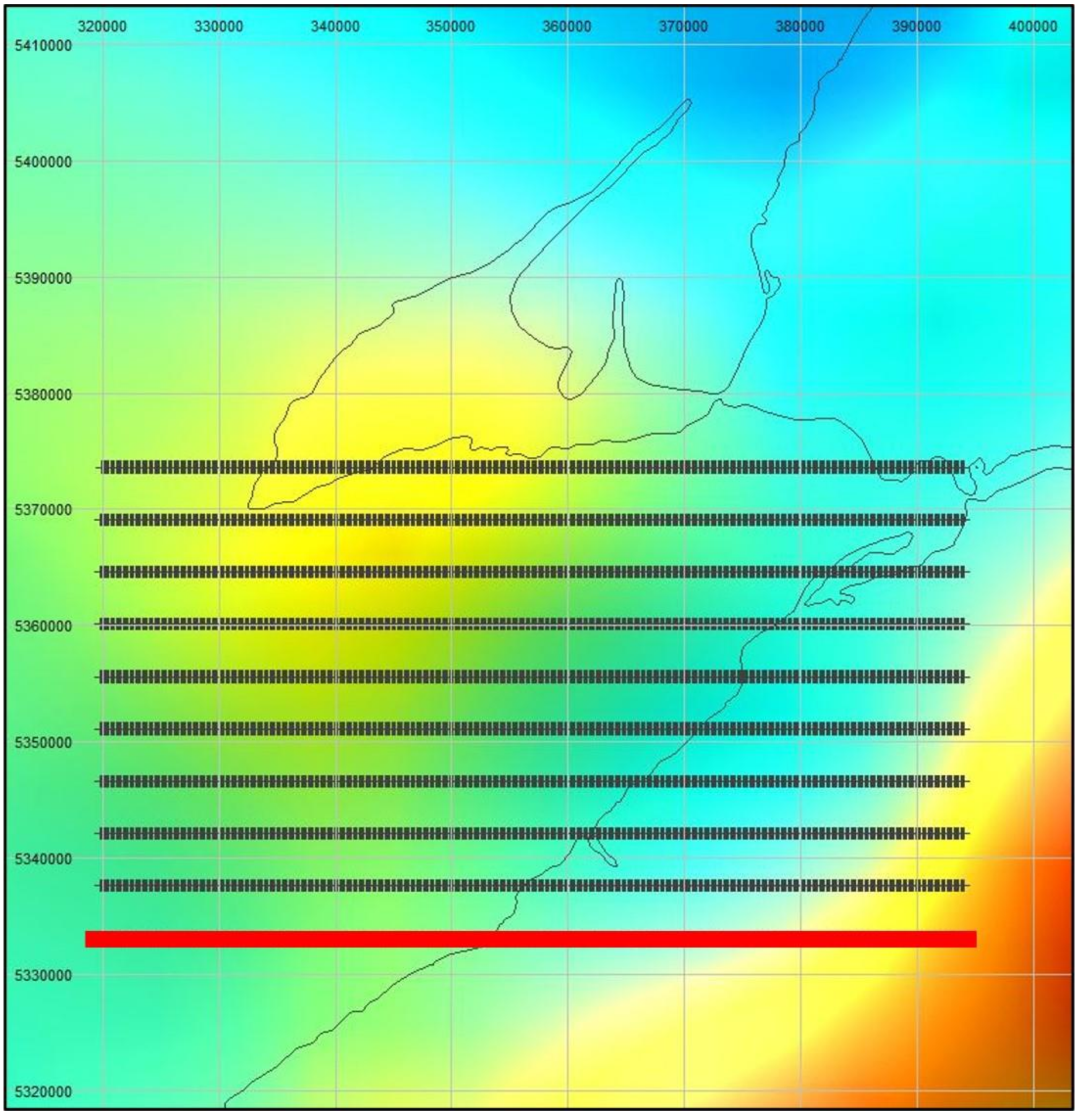

Figure 2.12: The filtered (low pass) gravity anomaly data with the ten gravity profiles. The red line corresponds to the cross-section displayed in Figure 4.1.

2.4.4 Gravity Inverse Modeling

The gravity inversion in this research is completed using the GRAV3D algorithm developed by Li & Oldenburg (1996; 1998). The GRAV3D algorithm generates a 3-D density anomaly Earth model by inverting observed gravity anomaly field data. This is achieved by minimizing the model objective function by fitting the observed data within a specified error bound. Two computations are done before running the inversion and constructing a density anomaly model. These computations include calculating the depth weighting function with the PFWEIGHT executable and calculating the sensitivity matrix with the GZSEN3D executable (Figure 2.13). A structured mesh with padding cells is also required to discretize the inverse problem using rectangular cells.

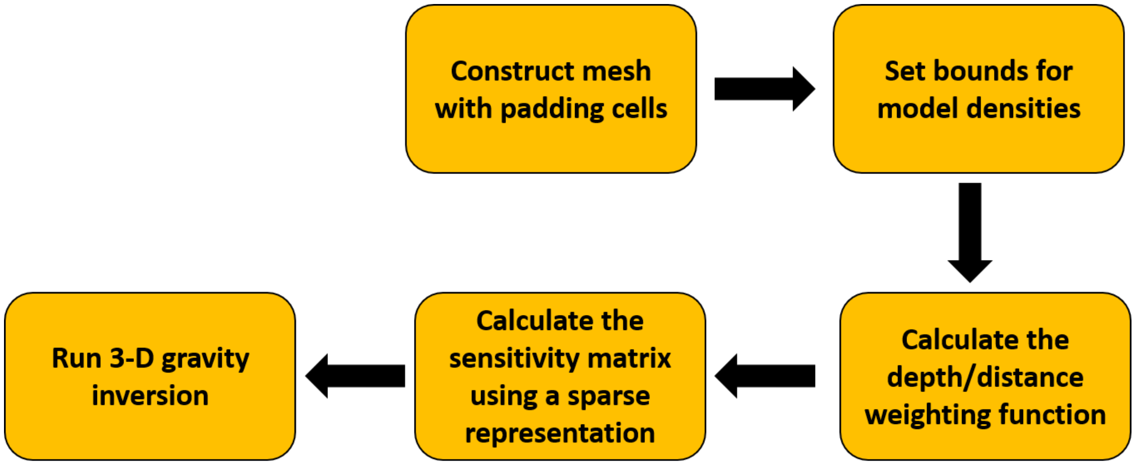

Figure 2.13: The simplified gravity inversion workflow used in this study. A mesh is required with padding cells to surround the region of interest and to discretize the density anomalies. Setting the bounds for the initial model densities is to ensure that the inversion restricts the densities to the specified bounds within each model cell. The depth/distance weighting function is calculated to resolve depth resolution issues with the gravity data. The calculation of the sensitivity matrix is used as one of the inputs for the subsequent inversion.

The structured mesh is built encompassing the region of interest and contains rectangular prisms assuming a constant density contrast in each cell. Additional padding cells are included in the mesh to reduce edge effects during the inversion. Various mesh dimensions are tested to find the optimal parameters. The cell sizes and the number of cells are also varied in the inversion runs to find the best matching combination.

The depth weighting function is required prior to running an inversion using the GRAV3D algorithm since it is used as the sensitivity calculation input. The depth weighting function accounts for the depth resolution uncertainties with gravity data, preventing the concentration of density anomalies near the observation locations when the objective function is minimized by fitting the predicted data. In other words, the lack of gravity data kernels that are further away from the observation locations needs to be accommodated. The depth weighting function accounts for the natural decay of kernels by taking the inverse of the geometrical decay, providing all cells an equal probability of being assigned a non-zero density contrast. The depth weighting function used during the gravity inversion for GRAV3D is defined as:

$$w(r_j) = \frac{1}{\sqrt{\Delta V_j}} \left\{ \sum_{i=1}^{N} \int_{\Delta v_j} \left[\frac{dv}{(R_{ij} + R_o)^\alpha} \right]^2 \right\}^{1/4} \quad , \mathrm{j} \ = \ 1, \dots, \mathrm{M}$$

where α=2.0, V_j is the volume of j^{th} cell, R_{ij} is the distance between a point within the source volume and the i^{th} observation, and R_o is a small constant used to ensure that the integral is well-defined.

A sparse representation of the sensitivity matrix is required to compensate for the large memory storage and long computation time requirements for calculating the model vectors and the sensitivity matrix. Forming the sparse representation of the sensitivity matrix is done using a wavelet transform, resulting in most coefficients being approximately zero. These small transform coefficients are removed (thresholding) from the sensitivity matrix, leaving only large values. This gives enough coefficients for calculating the wavelet domain, reducing the computation time and memory capacity needs (Li & Oldenburg, 2003; 2010).

Running the gravity inversion involves incorporating the initial density model obtained from forward modeling and the lower and upper density anomaly bounds for each cell in the model. The density contrast and the bounds are relative to the assigned background density of 2.67 g/cm^3. The bounds are set to restrict the acceptable density contrast values within a cell, allowing for a geologically reasonable result. Multiple test inversions are run using different density bounds and with and without a density contrast as the base of the crust (Moho).

2.4.5 Magnetic Field Dataset

Magnetic field data are compiled from the Department of Industry, Energy and Technology-Newfoundland and Labrador and were recently acquired (2009–2012), giving high-resolution coverage (Figure 2.14). Three different datasets are downloaded, including the Western Newfoundland residual magnetic data, the Indian Head residual magnetic data, and the Flat Bay regional magnetic data. A regional–residual magnetic separation is done for the Flat Bay magnetic data. This is done by determining the International Geomagnetic

Reference Field (IGRF) for the data acquisition date and subtracting that from the regional field. The resulting IGRF is calculated to be 52938 nT and separated from the Flat Bay regional field. The resulting Flat Bay residual gravity data are combined with the other two residual datasets (Figure 2.14). The regional–residual separation and subsequent merging of the datasets did not give a smooth transition from the onshore-to-offshore. Therefore, data masking is required for the rough transition in the Flat Bay residual magnetic data. This is achieved by creating a polygon around the artifact and nulling the data.

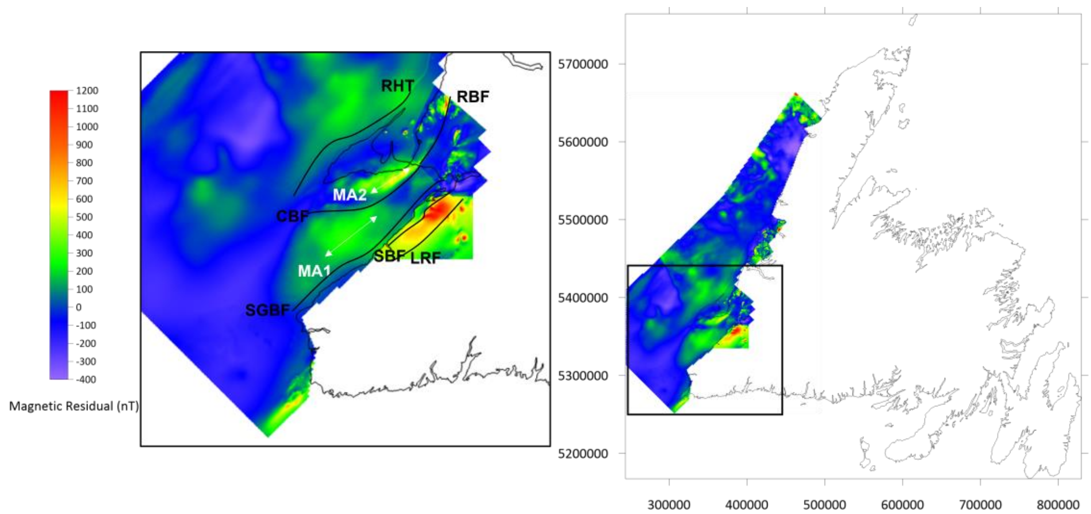

Figure 2.14: Magnetic residual anomaly map of Western Newfoundland. This magnetic map includes three different datasets merged into one. The black box is an enlargement of the Bay St. George subbasin with fault lineations and magnetic anomaly interpretations. MA1 is an offshore magnetic anomaly associated with the plunge direction of a salt-cored anticline. MA2 is an offshore magnetic anomaly associated with the RBF and CBF. The regional faults (CBF, RHT, RBF, SBF, SGBF, and LRF) are trending approximately NE–SW.

2.4.6 Magnetic Field Data Observations

The residual magnetic data in the offshore Bay St. George subbasin enhance fault lineations and regional trends associated with the opening of the basin (Figure 2.14). The onshore southeastern part of the basin has a relatively high magnetic residual reaching 1200 nT, representing anorthosite and mafic rocks (Dafoe et al., 2016). These basement rocks were likely uplifted due to the Flat Bay anticline structure (Figure 1.1) (Dafoe et al., 2016). Two offshore magnetic anomalies (MA1 and MA2) are observed corresponding to the doubly plunging direction of salt-cored anticlines and faults (Dafoe et al., 2016)

Regional fault trends are evident in the residual magnetic data and are interpreted in Figure 2.14 as the Round Head Thrust (RHT), Romaines Brook Fault (RBF), Central

Bay Fault (CBF), Snakes Bight Fault (SBF), St. George Bay Fault (SGBF), and Long Range Fault (LRF). These faults are trending approximately NE–SW, paralleling the magnetic anomalies, and are related to basin formation.

Chapter 3 Seismic Interpretation Results

This chapter describes the seismic interpretation results and observations with examples of seismic profiles and surface and thickness maps. Additional seismic profiles are displayed in Appendix A as both uninterpreted and interpreted seismic sections to provide further insight into the seismic interpretation results. The seismic interpretation is completed in two-way travel time (TWTT) and involves mapping faults and the main seismo-stratigraphic horizons using well control. The onshore and offshore seismic interpretations are performed separately and then correlated by creating composite onshore-to-offshore seismic lines and generating gridded surfaces.

3.1 Offshore Seismic Interpretation

The offshore seismic data were acquired in a grid, and therefore they are easier to interpret than the onshore data (Figure 2.2). Three different offshore seismic profiles are chosen in different orientations, including composite lines crossing most of the St. George Bay offshore. There are five major seismic horizons mapped offshore, including the Seabed, Average-Top Salt, Base Codroy, Top Cambrian–Ordovician Carbonate Platform, and Base Cambrian–Ordovician Carbonate Platform (Table 2).

3.1.1 Average-Top Salt

The Average-Top Salt horizon is mapped throughout most of the offshore region of the basin, and it is represented by evaporites in the Codroy Group. This seismo-stratigraphic horizon is characterized as a peak with obscured underlying reflectivity and associated anticline structures. The offshore salt dominates in the southern offshore and is truncated to the north by the Central Bay Fault (CBF) (Figures 3.1 and 3.2). The CBF highlighted in Figures 3.1 and 3.2 cuts off salt deposition offshore and is related to a complex offshore fault system.

The salt-cored anticlines have corresponding synclines in the offshore data that may indicate salt growth timing. The S1 and S2 synclines in Figure 3.2 show parallelism and progressive deformation, respectively. The S1 synclines show relatively uniform shape and structures, while the S2 synclines reveal unparallel structures and deformation towards the southeast (Figure 3.2). The salt-cored anticline structures and diapirs often have associated adjacent salt expelled minibasins (Figure 3.1C). Salt expelled minibasins form syn-kinematically as overlying sediment is deposited, and salt is removed laterally, increasing subsidence rates and producing accommodation space for younger sediments (Callot et al., 2016; Jackson & Talbot, 1991). These salt expelled minibasins are relatively small compared to sedimentary basins and are often underlain by salt welds created when salt expels from beneath the minibasins and wells up to either side (Callot et al., 2016). Primary salt welds are sub-horizontal, forming at the base of minibasins produced from the evacuation of autochthonous salt (Figure 3.1C) (Jackson et al., 2014).

3.1.2 Base Codroy

The Base Codroy horizon is mapped continuously in the offshore Bay St. George subbasin, and it is the most seismically coherent and distinguishable surface (Figures 3.1–3.3). This seismo-stratigraphic hoziron is characterized as a strong peak underlying the Average-Top Salt horizons. The Base Codroy seismic horizon is represented by marine carbonates and sandstones of the Codroy Group. The Base Codroy surface is defined as an unconformity overlying Devonian autochthonous strata offshore.

The Base Codroy surface is susceptible to faulting as most faults mapped offshore offset the Base Codroy Group (Figures 3.1–3.3). Figure 3.2 displays an antithetic fault (CBF) with a significant offset associated with an opposite dipping listric fault. The CBF is interpreted to have experienced some oblique motion, complicating attempts to image and map this faults. The oblique motion is interpreted based on the significant offset of the Base Codroy compared with the offset of underlying Cambrian–Ordovician successions. The Bay St. George subbasin architecture is primarily constrained by using this horizon since it is the most seismically clear and continuous feature throughout the study area.

3.1.3 Top and Base Cambrian–Ordovician Carbonate Platform

The Top and Base Cambrian–Ordovician Carbonate Platform successions are only distributed offshore. The Top Cambrian–Ordovician Carbonate Platform succession unconformably underlies the Base Codroy strata offshore and is characterized as a peak. This is represented by the Lourdes Limestone of the Long Point Group. This basal limestone is a prominent reflector used to characterize the autochthonous successions (Waldron et al., 1998). The Base Cambrian–Ordovician Carbonate Platform succession is also described as a peak and is represented by the Labrador Group. The Labrador Group contains siliciclastics in addition to carbonate successions. Coherent reflectors between the Top and Base Carbonate Platform seismic horizons are observed that represent the Port au Port, St. George, Table Head, and Goose Tickle groups. These reflections are not interpreted since the base and top seismic horizons provide an adequate representation for the structure of the carbonate successions. The thickness of the carbonate platform successions is relatively uniform throughout the offshore, and they are interpreted to be terminated in the south by the regional St. George Bay Fault (SGBF) (Figure 3.1c). Although this fault is not interpreted on the seismic profiles, it is suggested to exist along the coastline striking NE–SW. Figures 3.1–3.3 illustrate a possible interpretation such that the SGBF cuts off the carbonate platform groups. The SGBF is a key structure constraining the carbonate platform successions offshore and explains the lack of carbonate strata observed onshore. The Round Head Thrust (RHT) is another significant fault identified in the offshore seismic data (Figures 3.1 and 3.2). This fault shows reactivation and inversion, as evident from the adjacent synthetic faults, which are showing normal movement.

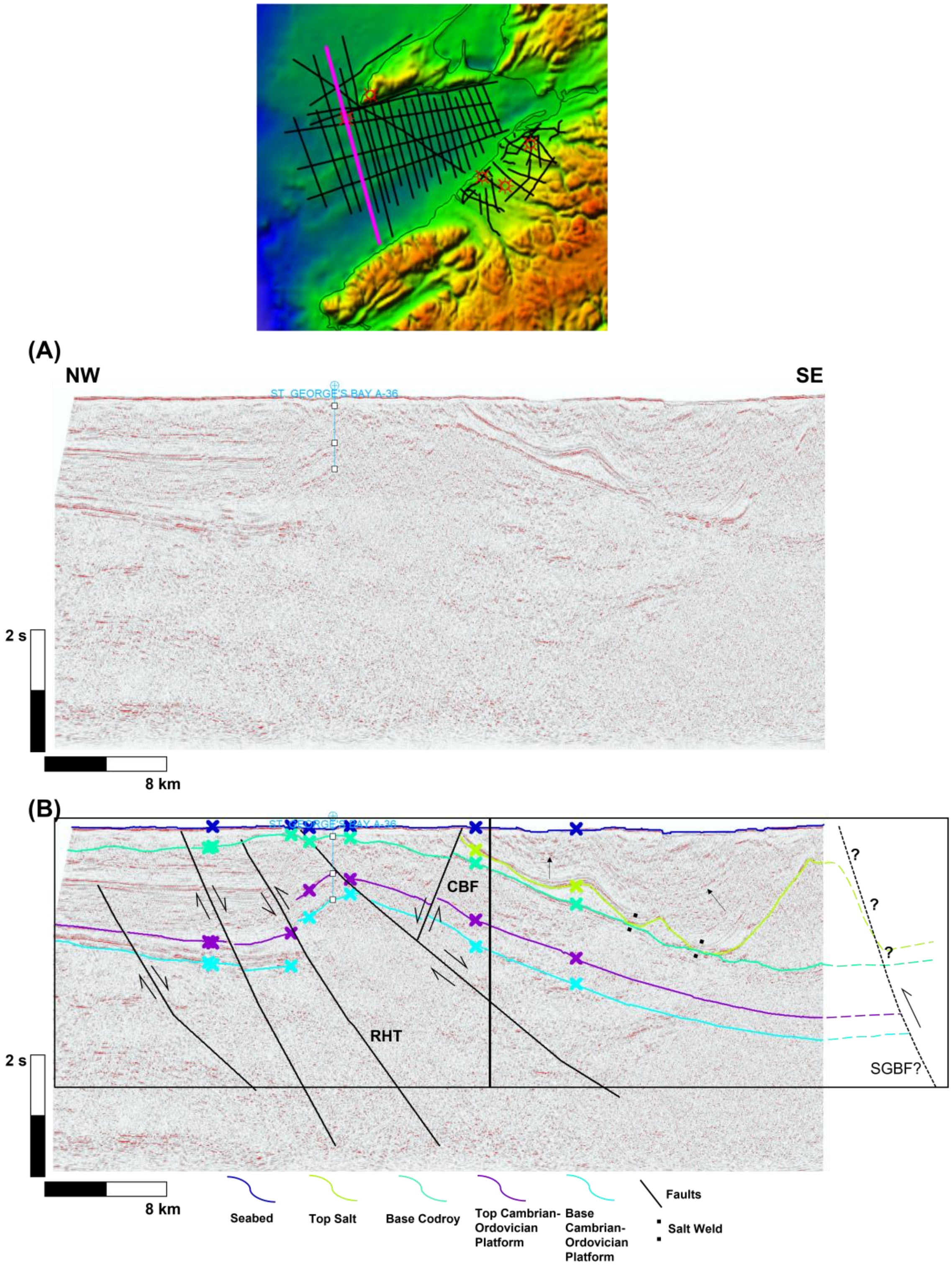
(A)
NW
SE
ST. GEORGE'S BAY A-36
2 s
8 km
(B)
CBF
RHT
SGBF?
?
2 s
8 km
Seabed
Top Salt
Base Codroy
Top Cambrian-Ordovician Platform
Base Cambrian-Ordovician Platform
Faults
Salt Weld

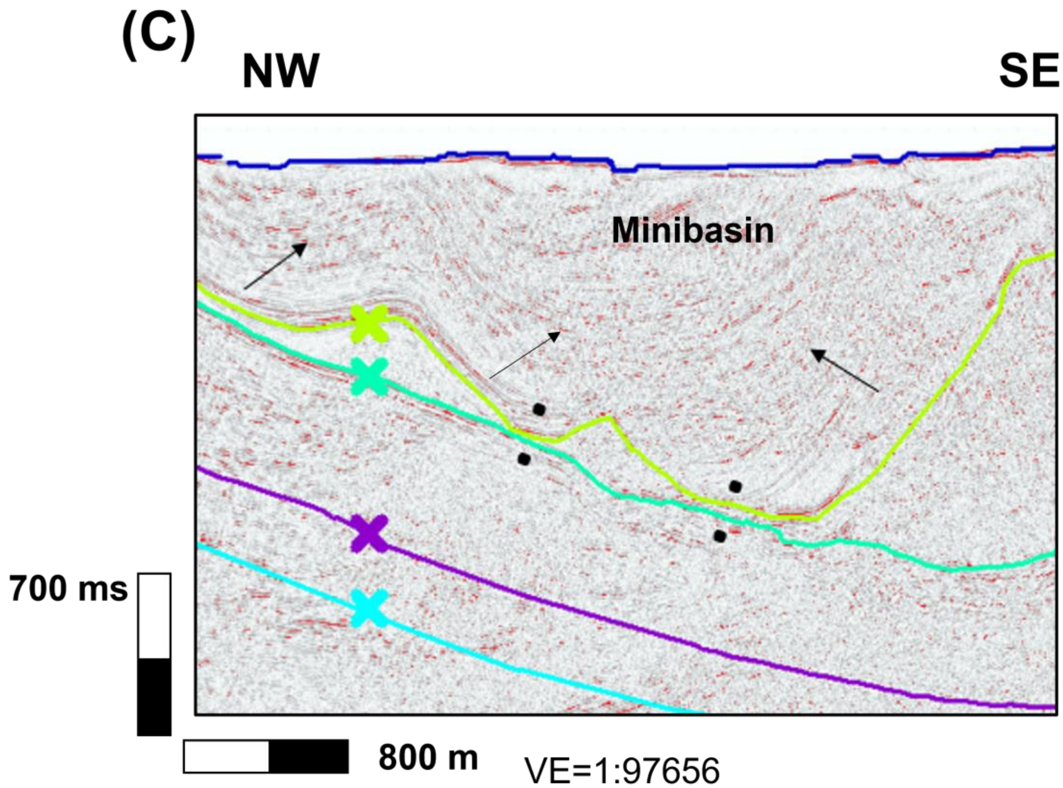

Figure 3.1: Seismic section of a NW–SE offshore profile showing the different mapped features, where (A) is uninterpreted, (B) is the interpreted section, and (C) is an enlargement of an interpreted salt expelled minibasin. The black arrows point out synclines. The St. George's Bay A-36 synthetic seismic trace is used to correlate the seismic features with the geology from the well logs. The small squares along the well path represent the different seismo-stratigraphic horizons picked from the synthetic. The black box is the extent extracted in Figure 5.4B and C. CBF is the Central Bay Fault, and RHT is the Round Head Thrust.

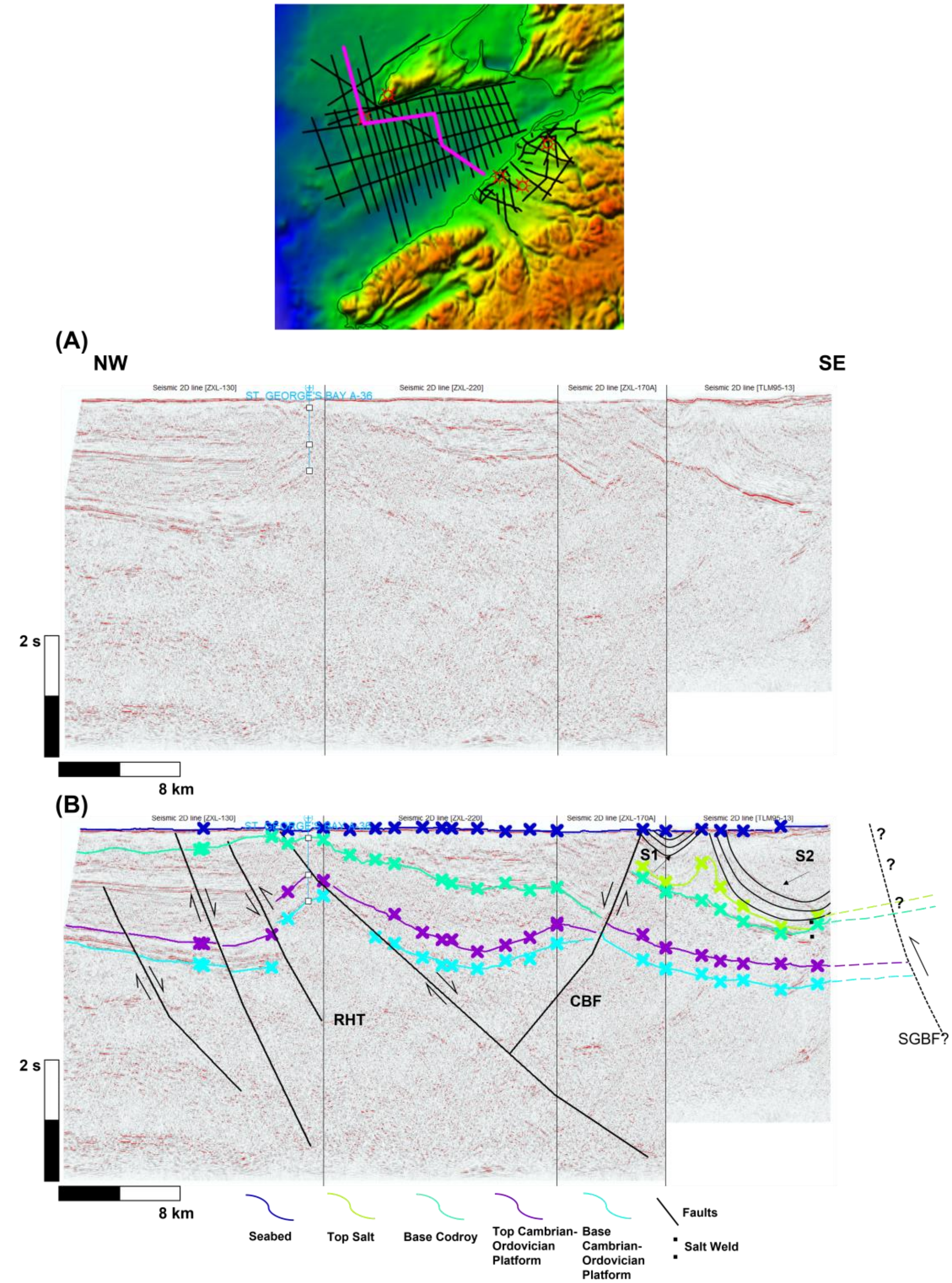

Figure 3.2: Seismic section of a composite NW–SE offshore profile showing the different mapped features, where (A) is uninterpreted and (B) is interpreted. The arrows indicate synclines, where S1 shows parallelism and S2 shows progressive deformation. The St. George’s Bay A-36 synthetic seismic trace is used to correlate the seismic features with the geology from the well logs. The small squares along the well path represent the different seismo-stratigraphic horizons picked from the synthetic. CBF is the Central Bay Fault, and RHT is the Round Head Thrust.

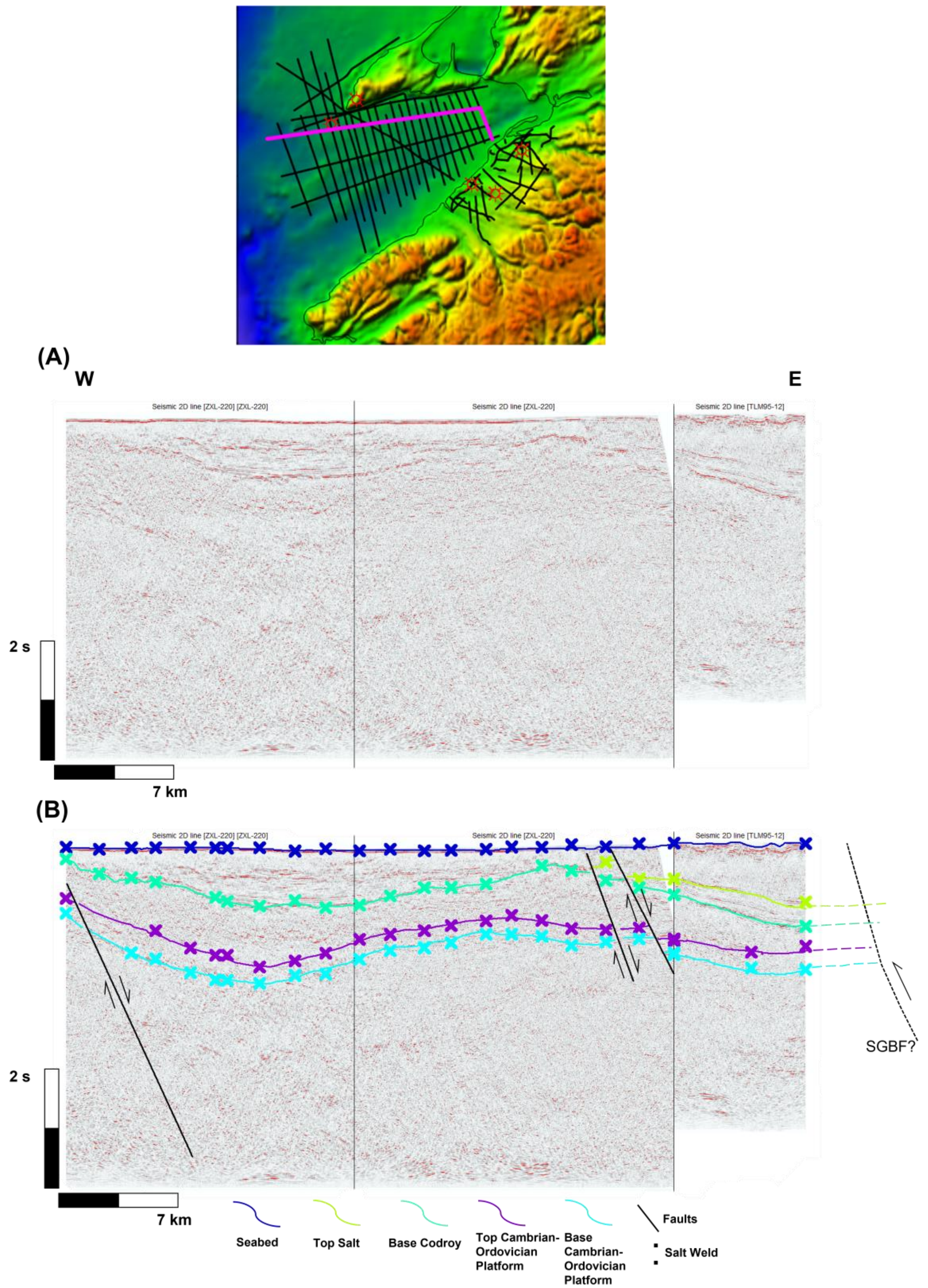

Figure 3.3: Seismic section of a composite W–E offshore profile showing the different mapped features, where (A) is uninterpreted and (B) is interpreted.

3.2 Onshore Seismic Interpretation

The onshore seismic data were acquired along irregularly spaced and oriented lines (Figure 2.2). Three different onshore seismic profiles are displayed, capturing similar structures to the offshore data. Only three seismic horizons are mapped for the onshore data, including Average-Top Salt, Base Codroy, and Base Anguille (Table 2), and these are tied with the available onshore wells. The other surfaces observed offshore, such as the Seabed, Top Carbonate Platform, and Base Carbonate Platform, are not observed onshore.

3.2.1 Average-Top Salt

The Average-Top Salt horizon is mapped in the onshore seismic data as a peak, often with a lack of reflectivity beneath it. The salt horizon is relatively thin compared to offshore and is related to onshore structures like the Flat Bay Anticline.

Similar to offshore, salt-related structures are interpreted onshore, such as salt-cored anticlines with intervening synclines, salt welds, and salt expulsion minibasins. Figure 3.6C displays an example of a salt expelled minibasin that forms when salt is expelled and wells up, creating salt welds and salt walls surrounding the minibasin (Callot et al., 2016). The faults are observed to offset the Average-Top Salt horizon (Figures 3.4–3.6); however, no fault systems truncate the salt deposition as they do offshore.

3.2.2 Base Codroy

The Base Codroy unconformity continues onshore as a seismically coherent, distinct seismic peak underlying the Average-Top Salt horizon (Figures 3.4–3.6). The Base Codroy seismic horizon refers to the R reflector described by Hall et al. (1992) as the contact between the Codroy and Anguille groups. Similar seismic patterns are observed onshore, and this surface corresponds to clastics and carbonates of the Codroy Group. As observed for the offshore data, faults are interpreted to cut through the Base Codroy horizon (Figures 3.4–3.6).

3.2.3 Base Anguille

The Base Anguille surface is mapped as a peak and is only identified onshore. The Base Anguille is suggested to thin out and terminate against a fault (Figure 3.7) and is further described in section 3.3. This seismic horizon has moderate–strong reflectivity and marks the end of Carboniferous sedimentation. The Base Anguille surface is susceptible to faulting, with some areas showing significant offset (Figure 3.5).

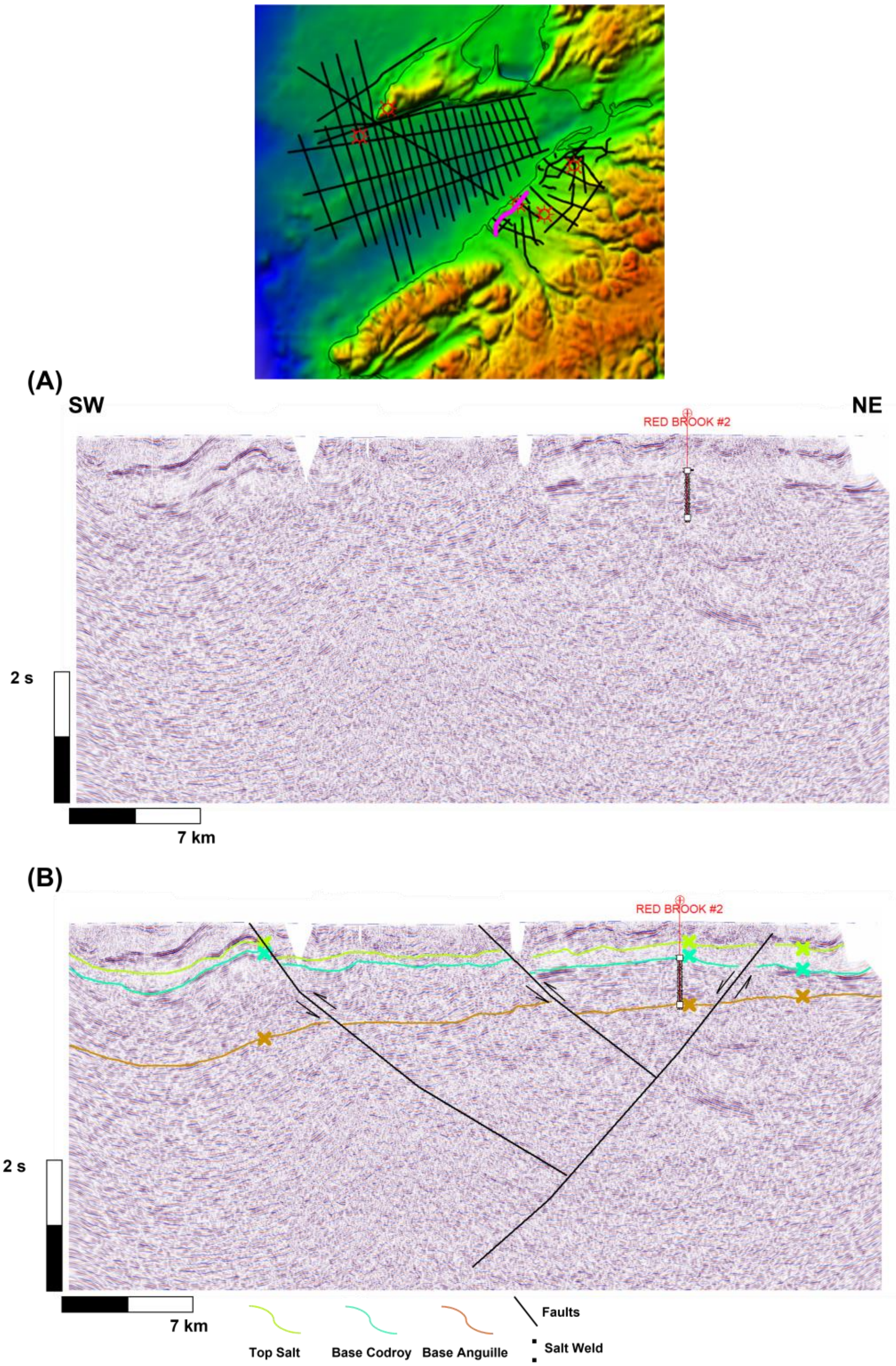

Figure 3.4: Seismic section of a SW–NE onshore profile showing the different mapped features, where (A) is uninterpreted and (B) is interpreted. The Red Brook #2 synthetic seismic trace is used to correlate the seismic features with the geology from the well logs. The small squares along the well path represent the different seismo-stratigraphic horizons picked from the synthetic.

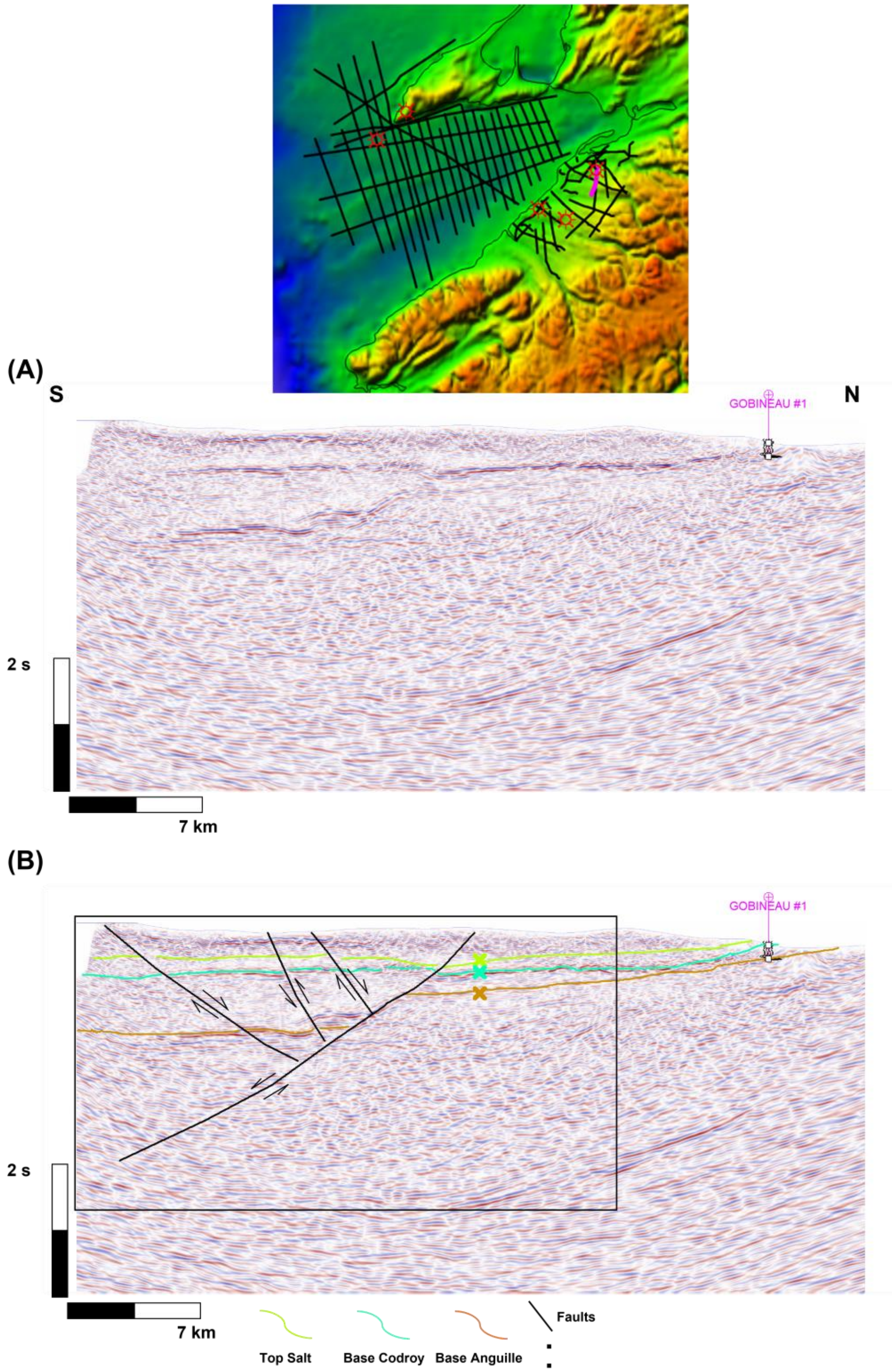

Figure 3.5: Seismic section of a S-N onshore profile showing the different mapped features, where (A) is uninterpreted and (B) is interpreted. The Gobineau #1 synthetic seismic trace is used to correlate the seismic features with the geology from the well logs. The small squares along the well path represent the different seismo-stratigraphic horizons picked from the synthetic. The black box is the extent extracted in Figure 5.4E.

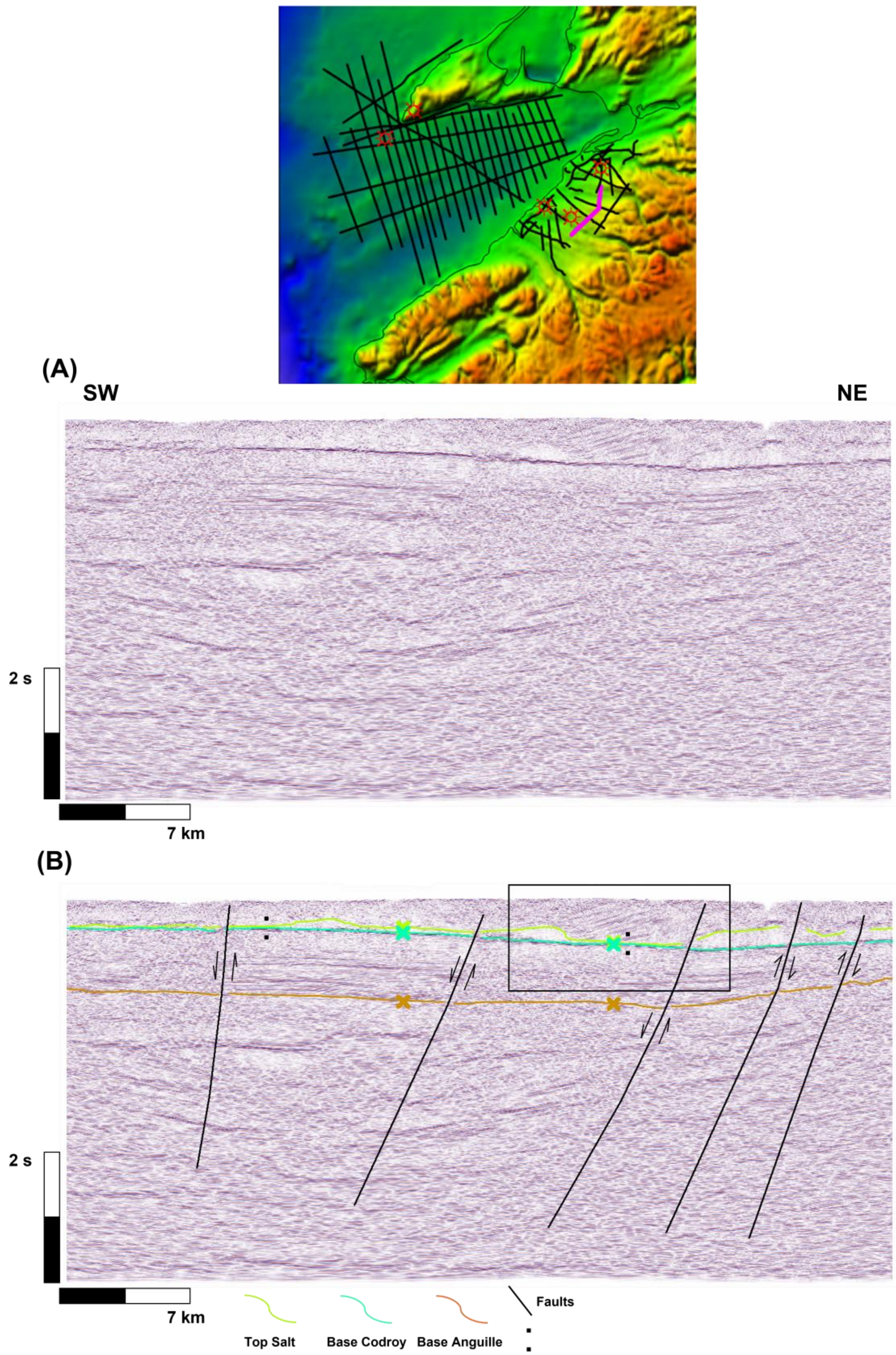
(A)
SW
NE
2 s
7 km
(B)
2 s
7 km
Top Salt
Base Codroy
Base Anguille
Faults

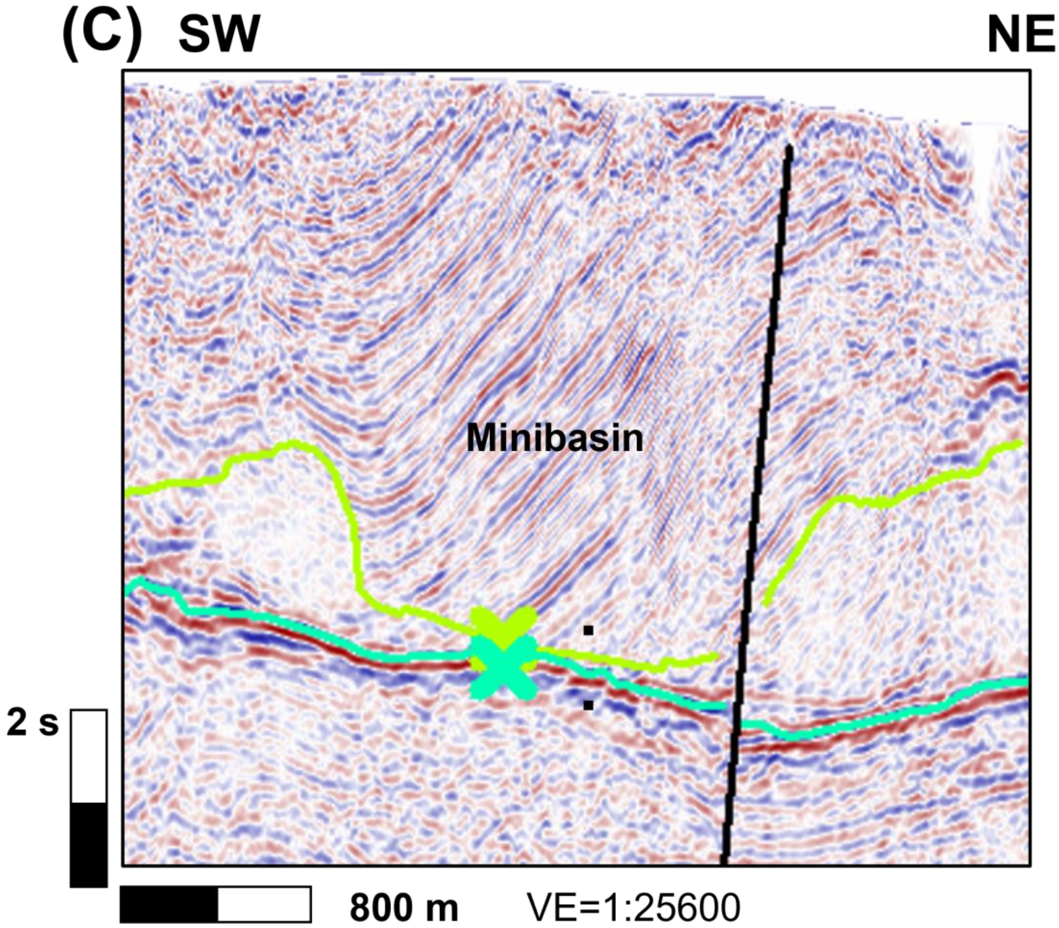

Figure 3.6: Seismic section of a SW–NE onshore profile showing the different mapped features, where (A) is uninterpreted and (B) is the interpreted section. (C): An enlargement of an interpreted salt expelled minibasin with a primary salt weld and salt-cored anticline.

3.3 Onshore-to-Offshore Seismic Interpretation

A composite onshore-to-offshore seismic line (Figure 3.7) is created in the northeast part of the basin. Figure 3.7 shows a composite seismic line consisting of three seismic profiles, where the white space corresponds to a gap in seismic coverage. This composite line is a critical seismic profile for investigating the onshore-to-offshore stratigraphic changes and constraining potential field modeling.

Different seismic horizons are interpreted onshore and offshore, with the Average-Top Salt and Base Codroy surfaces mapped on both. Overall, there is a deepening of Carboniferous sediments towards the offshore, and there are similar seismic reflectivity patterns on all profiles. The fault in the offshore segment of Figure 3.7 corresponds with the Central Bay Fault (CBF) and marks the sharp truncation of salt deposition offshore. The offshore profile shows the Carbonate Platform package, which does not appear on the onshore data. The Carbonate Platform package corresponds with the regional St. George Bay Fault, suggesting that this fault is the southern termination of platform deposition (Figure 3.7).

In contrast, the onshore profiles show the Base Anguille surface, which does not appear on the offshore data. Therefore, the Base Anguille surface is suggested to have pinched out against a splay fault synthetic with the SGBF (Figure 3.7). Faulting is abundant on the composite seismic profile (Figure 3.7), particularly on the onshore segments where significant offsets are observed. The Flat Bay Thrust (FBT) is a large reverse fault that significantly offsets the entire Carboniferous sequence. Additional minor reverse faults are interpreted in the onshore section, primarily synthetic to the FBT. The reflectors are not horizontally continuous in the onshore seismic profiles and appear to be tilted.

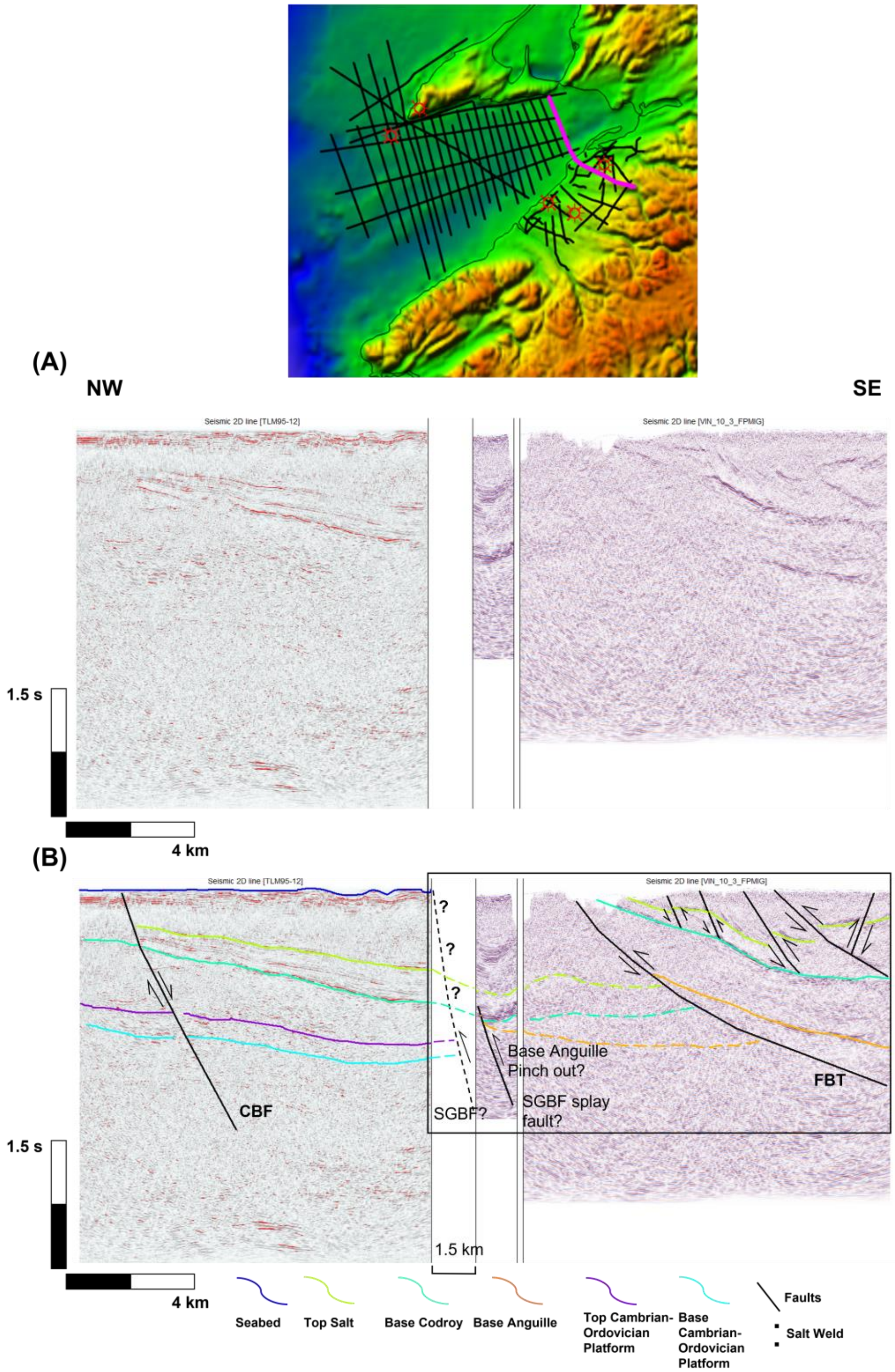

Figure 3.7: Seismic section of a NW–SE composite onshore-to-offshore profile showing three different seismic profiles with the various mapped features, where (A) is the uninterpreted and (B) is the interpreted section. The white space in between the three sections represents a gap in seismic coverage. The black box is the extent extracted in Figure 5.4A. CBF is the Central Bay Fault, and FBT is the Flat Bay Thrust.

3.4 Time Surface Maps

Time surfaces are generated by gridding the interpreted seismic horizons to better visualize the structure. Time surface maps are produced for the Average-Top Salt, Base Codroy, Base Anguille, Top Carbonate Platform, and Base Carbonate Platform seismic horizons. The time surface maps are displayed within Petrosys Pro using 300 ms contour levels, providing a clean and consistent display.

3.4.1 Average-Top Salt Surface

The Average-Top Salt time surface is displayed in Figure 3.8, and it is not distributed throughout the entire basin compared to the Base Codroy surface (Figure 3.9). The Salt surface distribution is limited because of an interpreted central offshore fault system that cuts off the deposition of salt in the north. The Average-Top Salt is observed to be shallow onshore and offshore near the middle of the basin due to anticline structures. The Average-Top Salt surface also deepens offshore near the edge of the coastline.

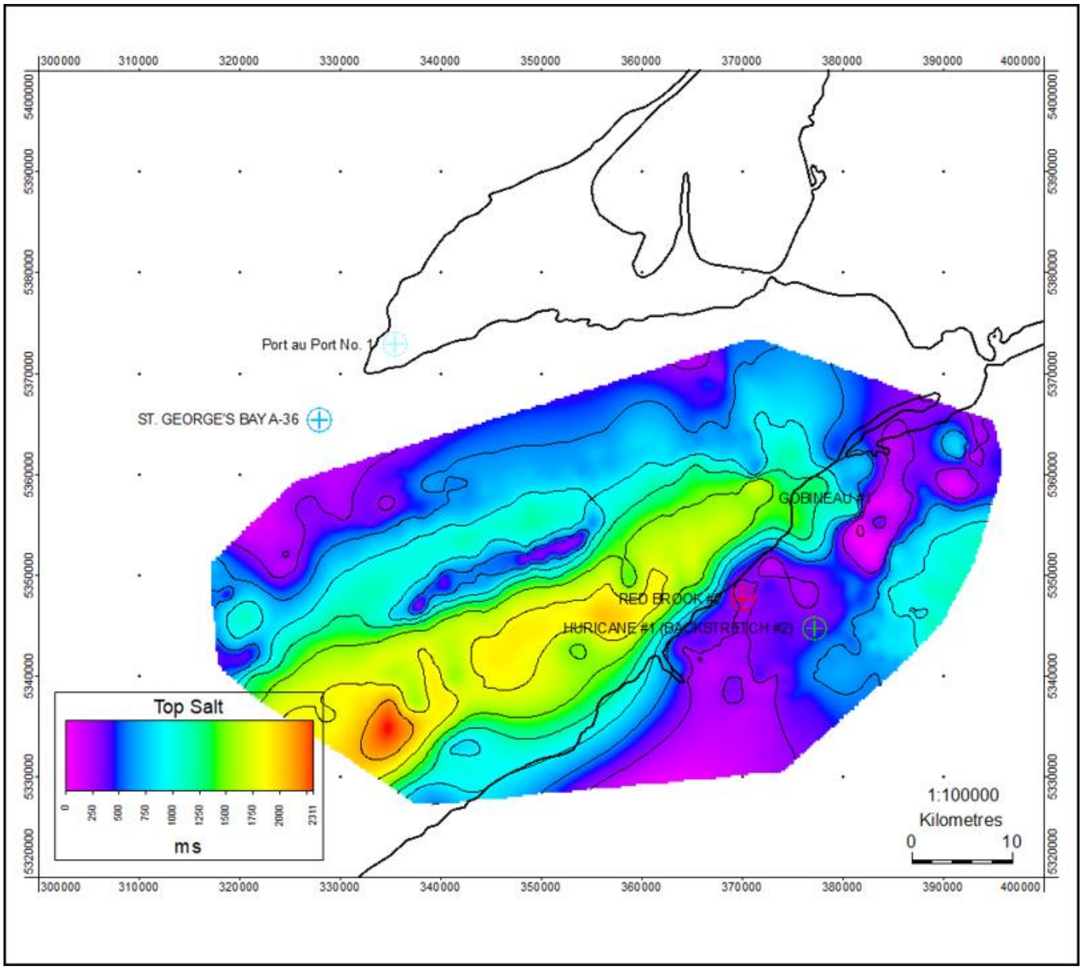

Figure 3.8: The Average-Top Salt time surface. Contour intervals are plotted every 300 ms. This surface shallows onshore, corresponding to anticline structures, and generally deepens offshore.

3.4.2 Base Codroy Surface

Figure 3.9 displays the Base Codroy time surface as it extends throughout the entire basin and is mapped on all the seismic lines in this study. The Base Codroy surface deepens offshore near the coastline. An interpreted small sedimentary basin offshore is labeled as a white star in Figure 3.9 near the Port au Port Peninsula. This basin is associated with the same central offshore fault system (CBF) observed in the salt surface map. The Base Codroy surface shallows onshore due to nearby anticline structures.

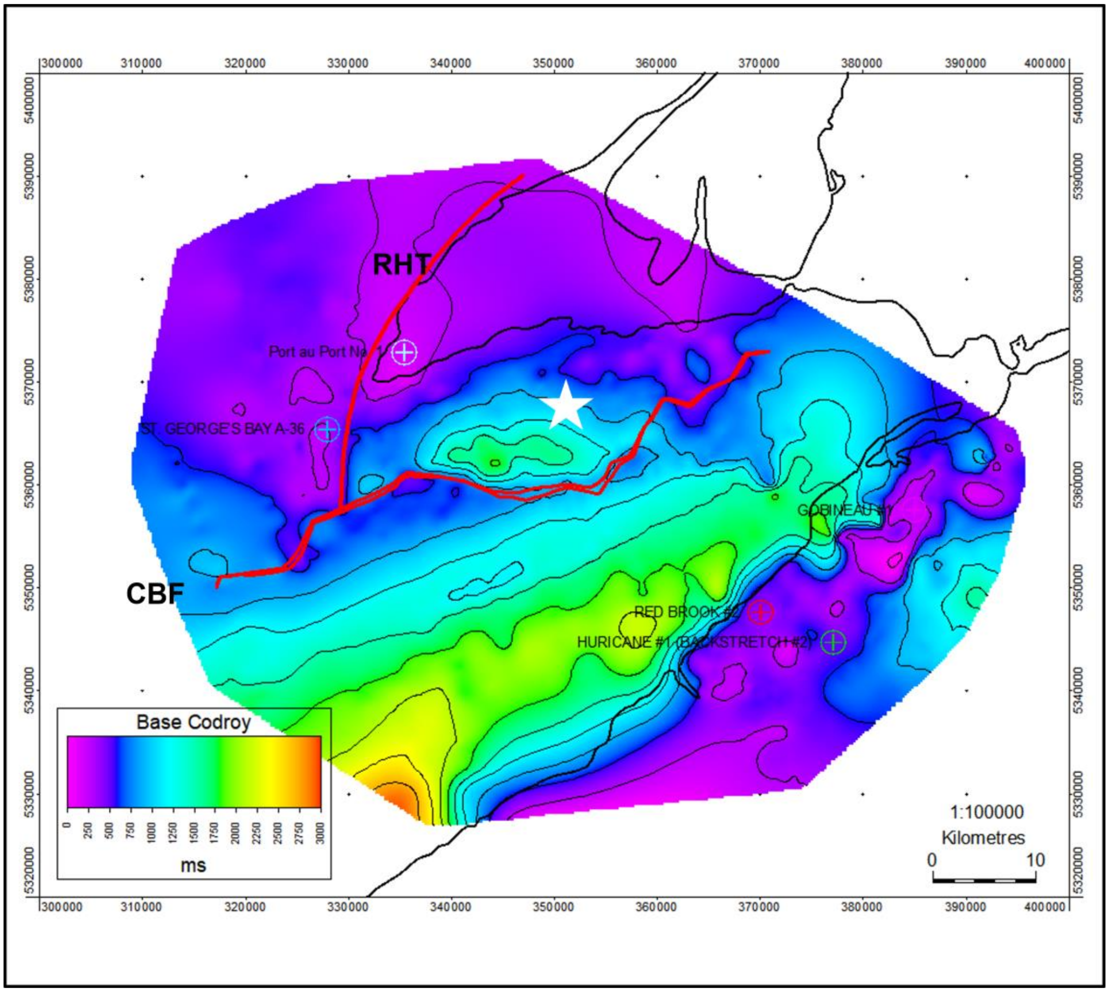

Figure 3.9: The Base Codroy time surface. Contour intervals are plotted every 300 ms. The Base Codroy surface has an interpreted small sedimentary basin labeled as a white star in the northern offshore near the Port au Port Peninsula associated with the central offshore fault system. Regional faults, including the Round Head Thrust (RHT) and Central Bay Fault (CBF), are displayed for structural context.

3.4.3 Base Anguille Surface

The Base Anguille time surface (Figure 3.10) is only distributed onshore and not present offshore. The St. George Bay Fault is argued to exist along the coastline striking NE–SW and plays an essential role in the pinch out of Anguille sediments. This pinch-out event is illustrated on the onshore-to-offshore seismic profile in Figure 3.7. The Anguille surface generally deepens towards the south/southeast, correlating with the provenance of the strata (Knight, 1983). The structural highs are associated with structures such as the Flat Bay Anticline.

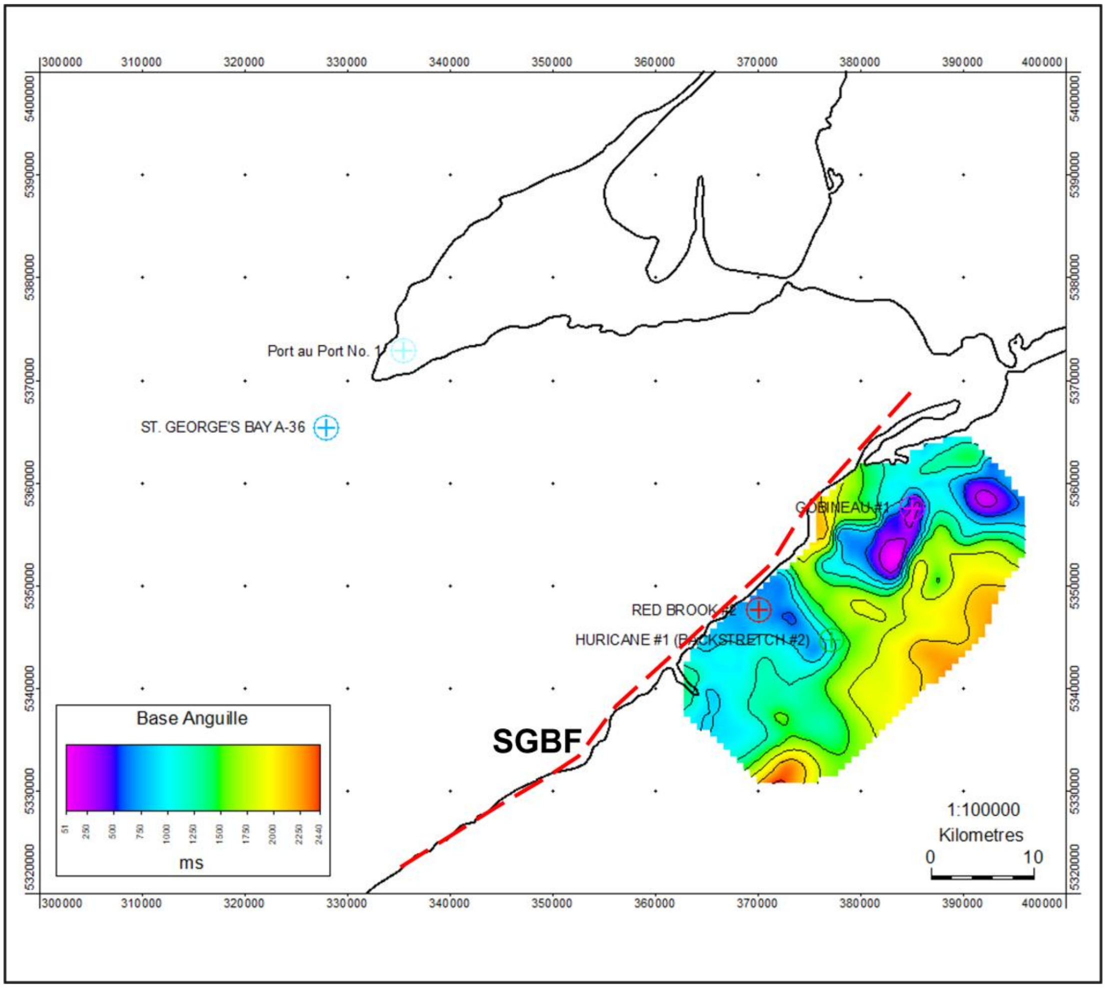

Figure 3.10: The Base Anguille time surface is only distributed onshore. Contour intervals are plotted every 300 ms. This surface deepens towards the southeast/east and has shallow elements related to anticline structures. The St. George Bay Fault (SGBF) is displayed since it represents an interpreted truncation for the onshore Anguille sediments.

3.4.4 Top and Base Cambrian–Ordovician Carbonate Platform Surfaces

The Top and Base Cambrian–Ordovician Carbonate Platform time surfaces (Figures 3.11 and 3.12) show similar structural features. The Carbonate Platform time surfaces have structural highs northwards and structural lows southward. The structural highs correspond with the shallowing of the autochthonous strata, and the structural lows are due to sediment deepening southward. Both surfaces are limited to offshore as the St. George Bay Fault (SGBF) is suggested to mark the southern termination of platform successions.

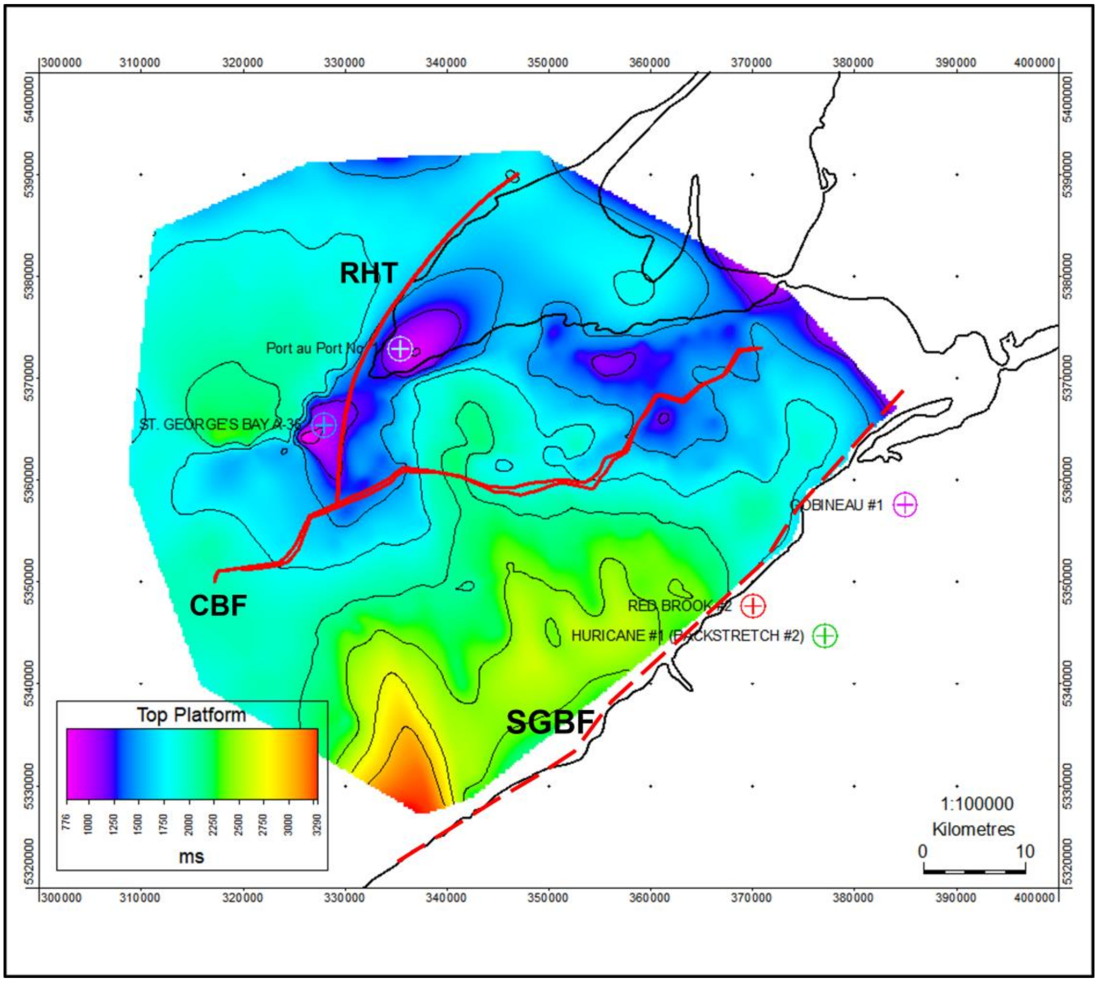

Figure 3.11: The Top Cambrian–Ordovician Carbonate Platform time surface. Contour intervals are plotted every 300 ms. This surface has some structural highs in the northern parts of the offshore. Regional faults, including the Round Head Thrust (RHT), Central Bay Fault (CBF), and the St. George Bay Fault (SGBF), are displayed as they provide structural context.

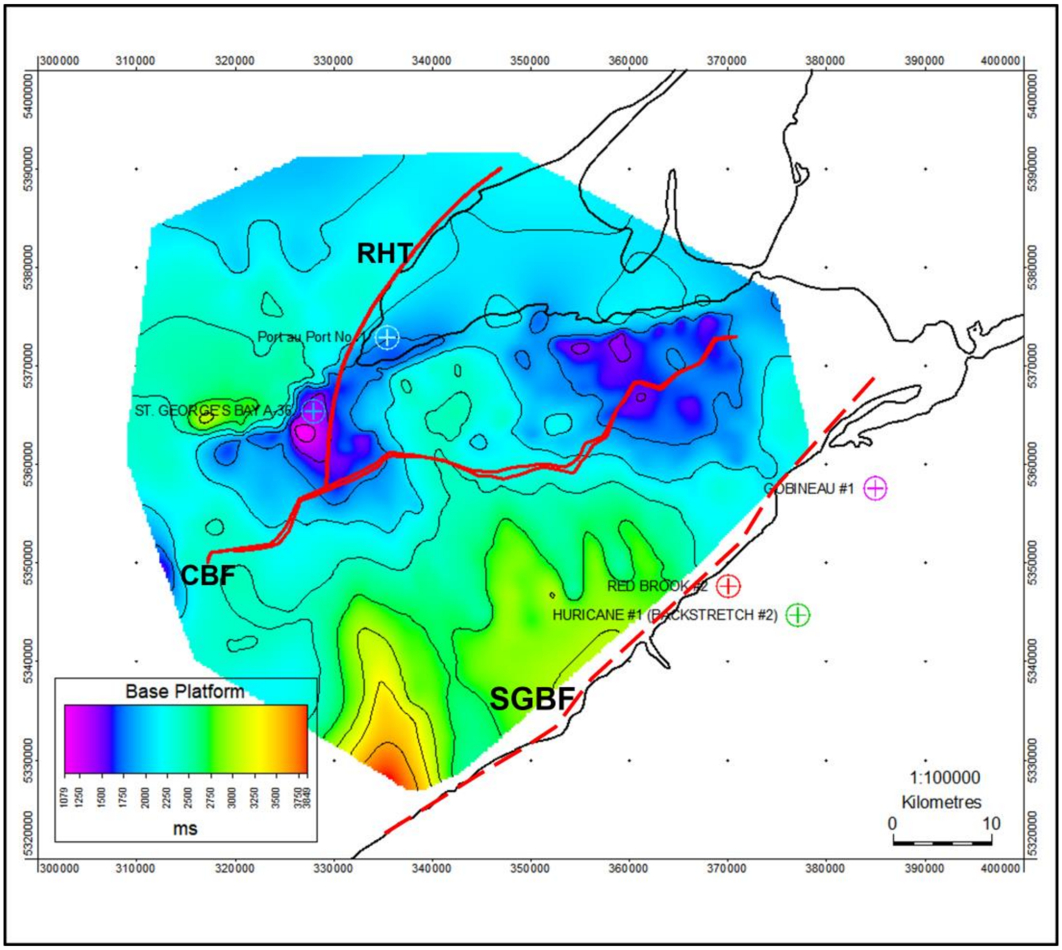

Figure 3.12: The Base Cambrian–Ordovician Carbonate Platform time surface. Contour intervals are plotted every 300 ms. This surface has some structural highs in the northern parts of the offshore. Regional faults, including the Round Head Thrust (RHT), Central Bay Fault (CBF), and the St. George Bay Fault (SGBF), are displayed as they provide structural context.

3.5 Thickness Maps

Time thickness (isochron) maps are calculated by subtracting the base surface from the overlying surface to determine the thickness between layers. Thickness maps are useful for investigating stratigraphic changes and are an essential aspect of mapping hydrocarbon prospects. The following isochron maps are displayed using 300 ms contour levels, except for the Middle Carboniferous thickness map. The 300 ms contour levels allow for an easier visualization since a denser contour level gives a busy display. However, the Middle Carboniferous isochron map displays 150 ms contour levels to interpret the regional faults crossing this surface more effectively.

3.5.1 Carboniferous Thickness Maps

Three isochron maps are calculated to determine Carboniferous sediment thicknesses, including the Salt (Figure 3.13), Anguille (Figure 3.14), and Middle Carboniferous strata (Figure 3.15) thicknesses.

The salt thickness map (Figure 3.13) is calculated using the Average-Top Salt and Base Codroy time surfaces. The salt thickness is generally around 0–300 ms, with anomalous highs reaching up to 900 ms offshore. These high salt thicknesses correspond with the plunging direction of the salt-cored anticline structures defined from the seismic and magnetic data. The thick salt packages created from the doubly plunging salt-cored anticlines show *en echelon* character and are parallel to the basin-bounding faults. Figure 3.13 shows a well-defined example of a thick salt package created from the salt-cored anticlines. This example is annotated in Figure 3.13, showing the doubly plunging direction (black arrows) and the strike-slip motion (orange arrows) of this salt structure. Additional thick salt packages are identified in the southwestern extent of the isochron map; however, they are not as well-defined due to the limit of seismic data coverage.

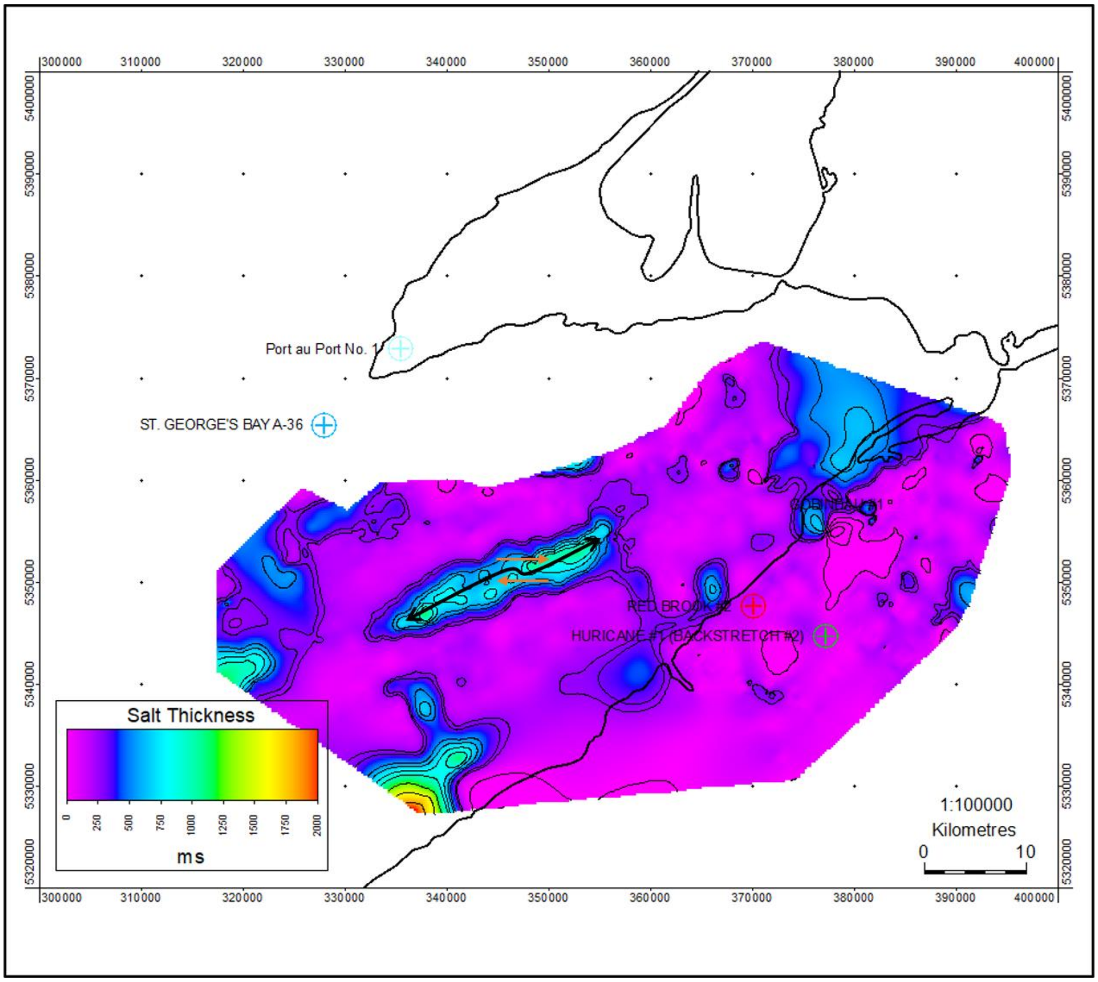

Figure 3.13: The salt time thickness map, generated by subtracting the Average-Top Salt and the Base Codroy time surface maps. The anomalous highs are associated with the plunging direction of salt-cored anticline structures. The black annotated arrows indicate the doubly plunging direction of the salt-cored anticlines. The orange arrows indicate the dextral strike-slip motion within the structure.

Figure 3.14 displays the Anguille thickness map, calculated using the Base Codroy (Top Anguille) and Base Anguille time surface maps. The Anguille thickness map is only constrained onshore since the Base Anguille surface is not observed offshore. This is due to the Base Anguille pinching out against a fault, as displayed in Figure 3.7. The Anguille thickness reaches up to around 1750 ms, with overall sediment thickening towards the south/southeast.

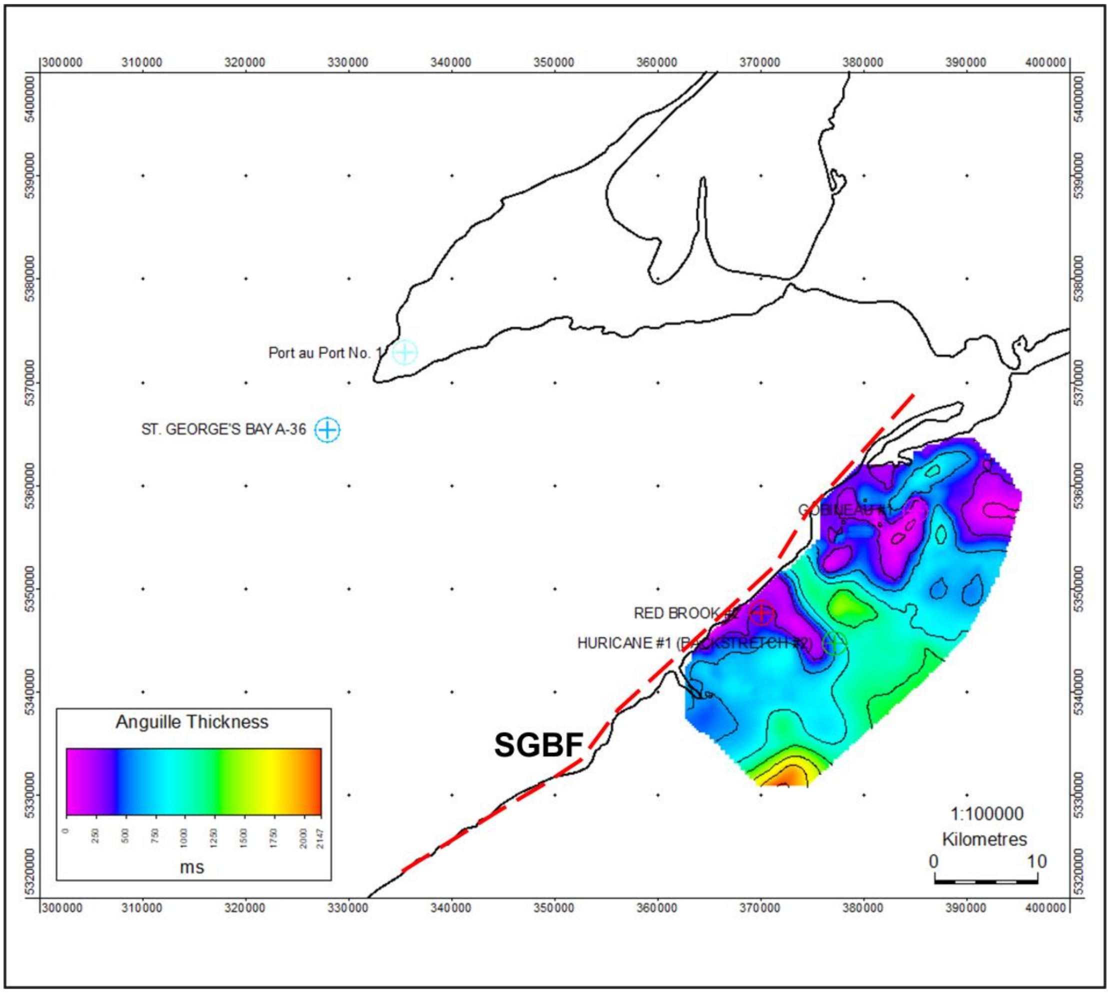

Figure 3.14: The Anguille time thickness map, generated by subtracting the Base Codroy and Base Anguille time surface maps. The surface is thickening towards the south/southeast. The St. George Bay Fault (SGBF) is displayed since it represents the termination of onshore Anguille sediments.

The Middle Carboniferous sediment thickness (Figure 3.15) is determined using the seabed and the Base Codroy surface. Figure 3.15 shows the thickening of sediments at the transition between onshore and offshore. There is also thickening observed in the northern part of the offshore and eastwards onshore. The maximum sediment thickness reaches approximately 2000 ms offshore and 1500 ms onshore. Regional faults such as the Round Head Thrust (RHT) and the Central Bay Fault (CBF) are easily observable on the Middle Carboniferous sediment thickness map. The white star north in Figure 3.15 represents a small sedimentary basin related to the movement of the CBF.

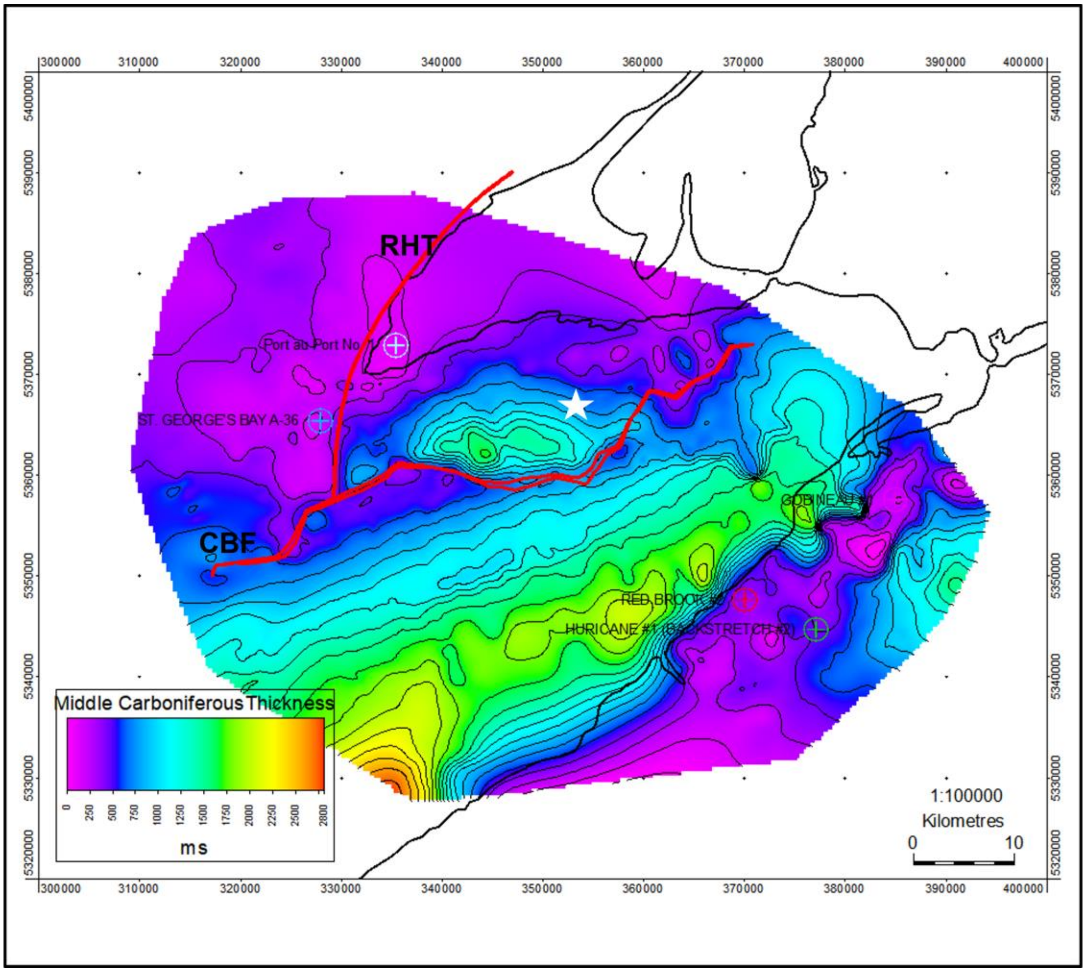

Figure 3.15: The Middle Carboniferous sediment time thickness map, generated from subtracting the seabed surface and the Base Codroy time surface. Sediment thickening is observed at the onshore-to-offshore transition and north of a complex fault system (red lines). The white star represents a small sedimentary basin related to the CBF. Regional faults, including the Round Head Thrust (RHT) and Central Bay Fault (CBF), are displayed as they provide structural context.

3.5.2 Autochthonous Strata Thickness Maps

Two thickness maps are calculated to represent autochthonous strata, including the Long Point Group (Figure 3.16) and the Carbonate Platform (Figure 3.17) successions. These strata are predominantly observed near the Port au Port Peninsula; however, they are also present in the offshore Bay St. George subbasin.

The Long Point thickness map (Figure 3.16) is calculated from the Base Codroy and Top Carbonate Platform time surface maps. This thickness map varies significantly throughout the offshore with generally thicker sediments near the Port au Port Peninsula.

There is also a thick package of Long Point strata near the middle of the offshore. The Long Point Group thickness map is restricted to the offshore since the SGBF cuts off the Top Carbonate Platform surface.

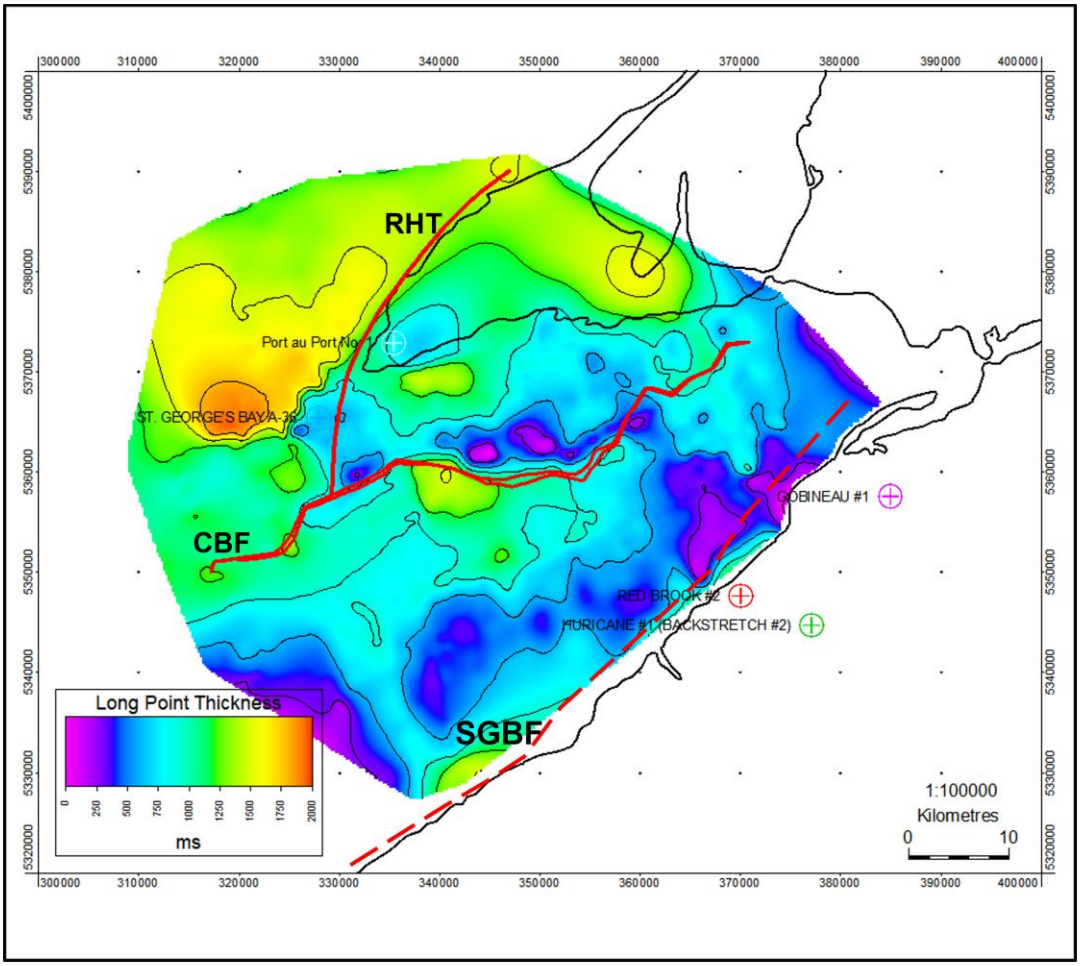

Figure 3.16: The Long Point time thickness map, generated from subtracting the Base Codroy and Top Platform time surface maps. Thickening is observed northward as expected since this surface is predominantly near the Port au Port Peninsula. Regional faults, including the Round Head Thrust (RHT), Central Bay Fault (CBF), and the St. George Bay Fault (SGBF), are displayed as they provide structural context.

The Carbonate Platform thickness map (Figure 3.17) is determined using the Top and Base Platform surface maps. The Platform thickness map shows relatively uniform thicknesses ranging from 200–400 ms. This time thickness map is also restricted offshore since the Carbonate Platform successions do not exist southeast onshore and are terminated by the SGBF.

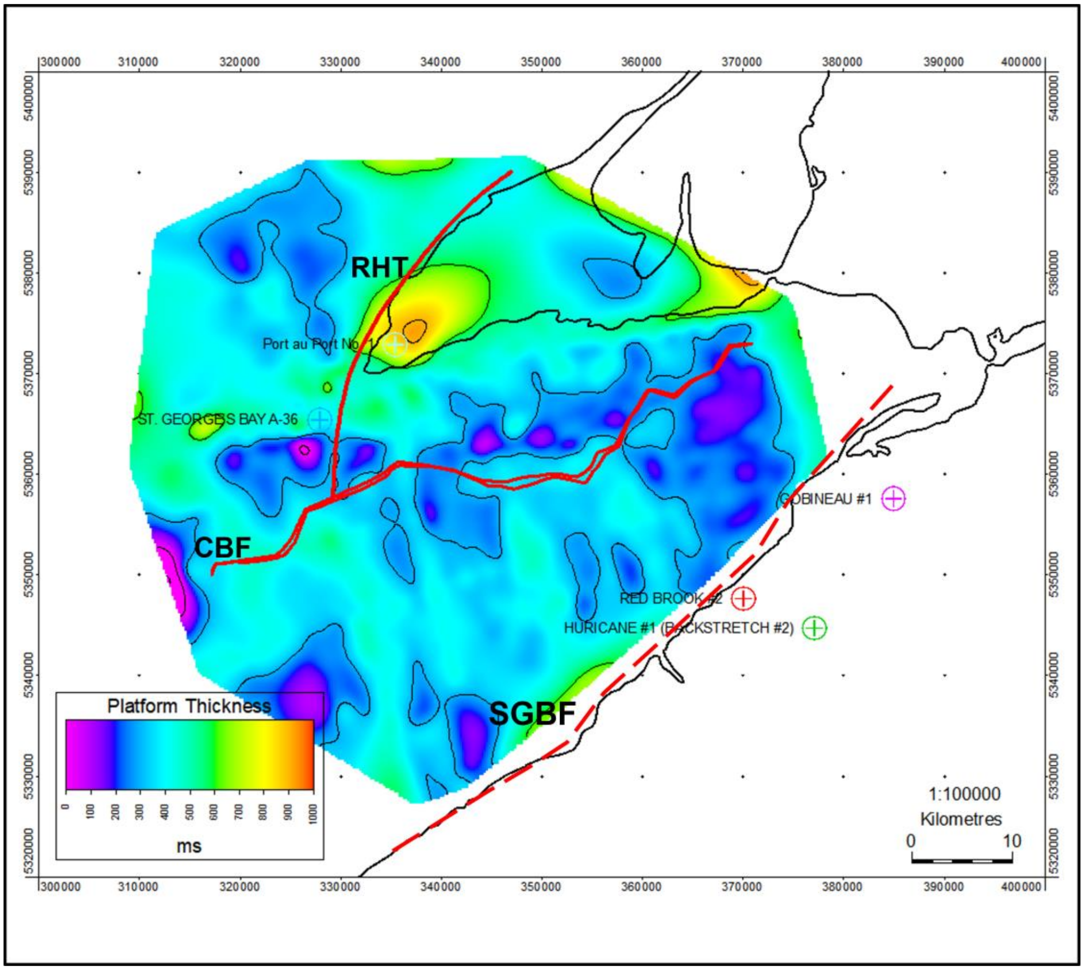

Figure 3.17: The Carbonate Platform time thickness map, generated from subtracting the Top and Base Platform time surfaces. There is generally an overall uniform thickness. Regional faults, including the Round Head Thrust (RHT), Central Bay Fault (CBF), and the St. George Bay Fault (SGBF), are displayed as they provide structural context.

3.6 Fault Framework

Faulting is a significant part of the seismic interpretation as it describes the compartmentalization of structures in the subsurface. Similar fault patterns are observed onshore and offshore. Synthetic (e.g., Figure 3.2) and antithetic faults (e.g., Figure 3.5) are identified throughout the study area. Thrust faults are also abundant throughout the basin, such as the Flat Bay Thrust (FBT) in Figure 3.7 and the Round Head Thrust (RHT) in Figures 3.1 and 3.2. Additionally, a complex fault system involving the Central Bay Fault (CBF) (e.g., Figures 3.1 and 3.2) cuts across the central offshore consisting of numerous faults. This complex fault system is interpreted to have experienced some oblique motion, as evident from the offset of strata in Figure 3.2. The CBF in Figure 3.2 shows a significant offset in the Base Codroy surface; however, minimal offset is observed for the deeper platform successions.

Figure 3.18 displays the fault framework of the basin with the overlying onshore geology and significant isochron maps. The faults interpreted from the seismic data in this study are displayed along with faults derived from previous work (Coleman-Sadd et al., 2000; Knight, 1983; Langdon & Hall, 1994). There are several significant fault systems interpreted offshore and onshore that also correlate with past interpretations. These main faults are striking approximately NE–SW and E–W and are related to the opening of this basin.

The offshore regional basin bounding faults are displayed in Figure 3.18. The northernmost fault system is identified as the Round Head Thrust (RHT), and it extends southwestward from the Port au Port Peninsula. The RHT is observed in the offshore seismic profiles and creates structural highs (Figures. 3.1 and 3.2). Near the central offshore is a complex fault system involving numerous faults defined collectively as the Central Bay Fault (CBF). The CBF is inferred to reactivate and invert pre-existing faults such as the Romaines Brook Fault (RBF) and the RHT as thick-skinned deformation (Stockmal et al., 2004). Inversion is evident from Figures 3.1 and 3.2, where the RHT appears to initiate as a synthetic fault parallel with the other adjacent SE dipping faults; however, the RHT is now showing reverse motion. The NE–SW trending CBF marks the northern cut-off of the salt deposition (Figures. 3.1 and 3.2). This fault system is also observed on the isochron maps (e.g., Figure 3.15). The southernmost offshore fault is identified as the St. George Bay Fault (SGBF). Although this fault is not imaged on the seismic data, it is suggested to exist along the coastline and represents an essential divide between the onshore and offshore sediments (Langdon & Hall, 1994). The SGBF marks a significant stratigraphic change as the cut-off of carbonate platform deposition offshore. The Anguille sediments are deposited to the south of the SGBF (Langdon & Hall, 1994).

The onshore faults are harder to map and correlate between seismic lines than the offshore data due to sparser seismic coverage. Several onshore faults are mapped on the seismic data and highlighted in Figure 3.18, trending approximately E–W and NNE–SSW.

The NE–SW trending onshore fault is defined as the Snakes Bight Fault (SBF) (Figure 3.18). The SBF is interpreted to splay from the main LRF. The northernmost E–W trending onshore fault is defined as the Flat Bay Thrust (FBT), and it displays large displacement in Carboniferous sediments (Figure 3.7).

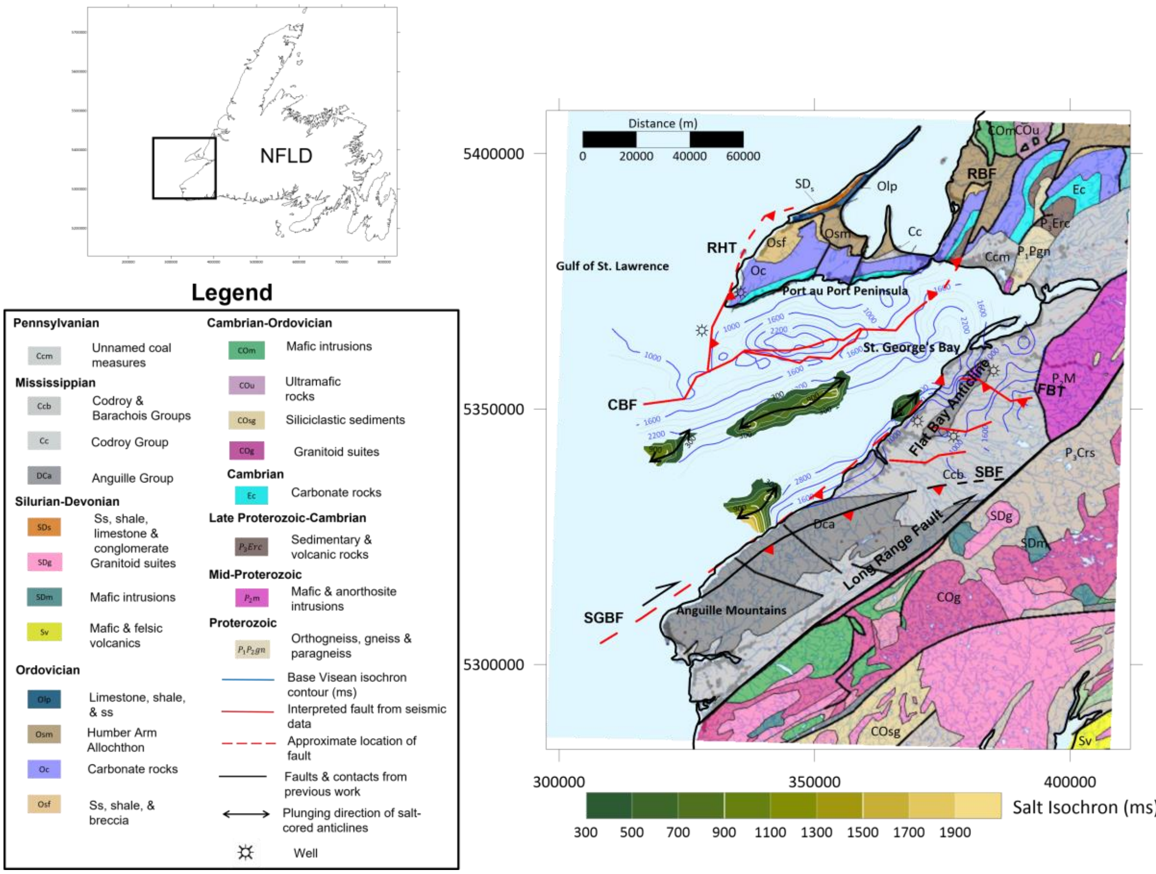

Figure 3.18: The structure map of the Bay St. George subbasin with overlying onshore geology. The faults are interpreted from the seismic data in this study (red) and derived from previous work (black). This map also displays important isochron maps. The Middle Carboniferous (blue) and salt isochron (green–yellow) contours are displayed as they correlate with major bounding faults. The onshore geology and interpolated faults are from Coleman-Sadd et al. (2000), Knight (1983), and Langdon & Hall (1994).

Chapter 4 Gravity Modeling Results

This chapter describes the 3-D gravity modeling results and observations from density slices. The 3-D gravity modeling in this research comprises forward and inverse modeling to determine a subsurface representation of the Bay St. George subbasin's densities. The resulting Earth model generated from this chapter may inspire future gravity work to better determine the subsurface structure and reduce previous uncertainties. This chapter also describes the geological information extracted from the gravity inversion, including depth to Moho and crustal thickness results.

4.1 Forward Modeling Results

Forward modeling is completed along ten arbitrary parallel lines throughout the Bay St. George subbasin (Figure 2.1). Each line is modeled using density bodies generated from this study's seismic interpretation (sedimentary layers) and previous seismic refraction work (crustal structures). The bodies along each line have comparable densities, depths, and shapes since there is only a slight variation in the gravity data from line to line.

The densities used in the forward modeling are derived from previous drill core, seismic refraction, and gravity work (Bell, 2005; Jackson et al., 1998; Marillier & Verhoef, 1989; Peavy, 1985) (Table 6). The sedimentary layers range from 2.33 to 2.52 g/cm^3 and are determined from testing of drill core samples and basement rocks (Bell, 2005; Peavy, 1985). The densities of the samples have a wide range of values due to differences in mineralogy and different geological formations. There is also an evaporite layer identified from the seismic data, and it is given a density of 2.18 g/cm^3 (Peavy, 1985).

The crust is subdivided into an upper and lower crust with densities varying from 2.56 to 3.00 g/cm^3 (Table 6). The differences in density may be due to the old Laurentian crust and the complex Cambrian–Carboniferous tectonic history. High density lower crustal bodies reaching up to 3.00 g/cm^3 are necessary during forward modeling to fit the observed gravity anomaly data. Since the seismic data used in this study do not image deep crustal features, previous studies must be used to constrain these structures. The crustal densities used are derived from a velocity model of a seismic refraction profile north of the

Bay St. George subbasin (Jackson et al., 1998). The upper mantle is given a density of 3.40 g/cm^3 with Moho constraints from Marillier & Verhoef (1989).

Table 6: The densities assigned for each body where each row's color corresponds to the body's color seen in the forward model result (Figure 4.1). Density ranges indicate that the layer required additional polygons with differing densities and is not homogenous

Body	Density (g/cm^3)
Datum-Seabed	1.00
Datum-Overburden	1.30
Seabed-Salt	2.33
Salt-Codroy	2.18
Codroy-Top Carbonate	2.42
Codroy-Anguille	2.46
Top-Base Carbonate	2.52
Upper Crust	2.56-2.88
Lower Crust	2.86-3.00
Mantle	3.40

Figure 4.1 displays an example of a forward model result with a reduced misfit between the observed and modeled gravity data. According to the seismic interpretation, layers such as the Codroy–Anguille body are only observed onshore and do not extend throughout the entire profile. Crustal features like the upper and lower crust are generally not homogeneous throughout the study region and must be subdivided into sub-bodies to fit the observed gravity.

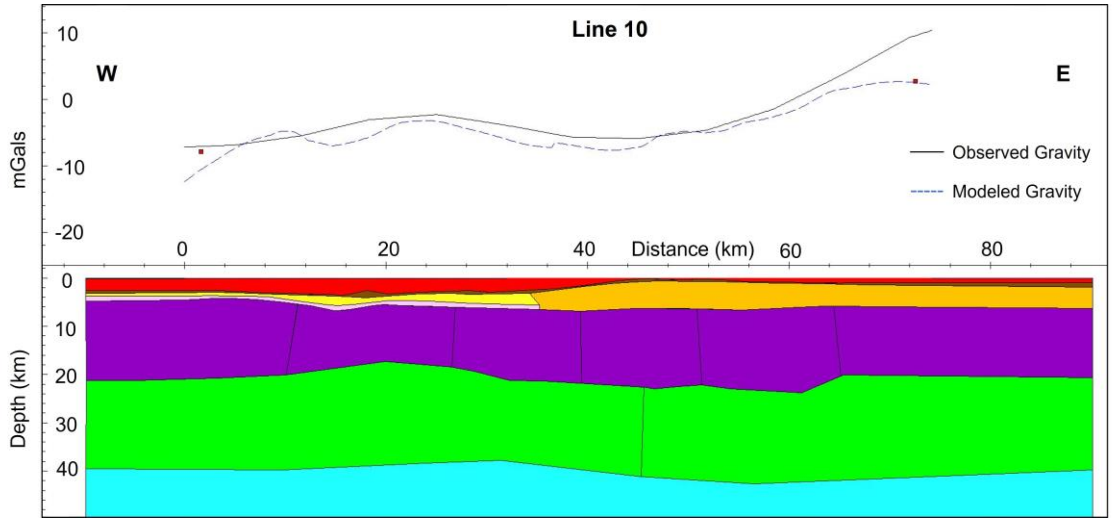

Figure 4.1: An example of a cross-section from a forward model result, where the corresponding body densities are seen in Table 6. The location of this gravity profile is highlighted in Figure 2.12.

A 3-D representation of the subsurface density model obtained from forward modeling is presented in Figure 4.2, and it includes all of the modeled gravity profiles. This model is used as the input for the inversion modeling in GRAV3D. The 3-D subsurface model looks relatively blocky; however, this is resolved after the model is discretized using a mesh with GRAV3D.

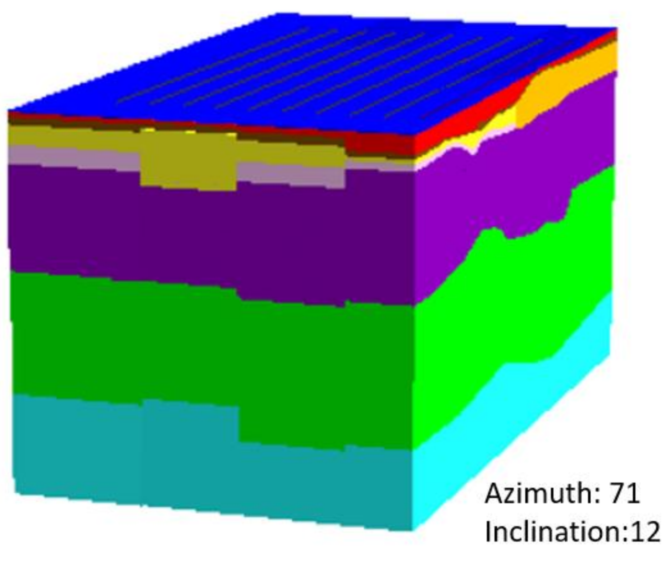

Figure 4.2: The 3-D forward model result generated using ModelVision. The lines on top of the blue layer represent the ten gravity profiles that were modeled. The densities outlined in Table 6 correspond to the colors of each layer.

The forward modeled gravity data are a gauge to determine the performance of the forward modeling. Figure 4.3 shows the observed and predicted gravity derived from the forward modeling, along with the difference between the two. The modeled gravity data do a reasonable job of reproducing the observed gravity data (Figure 4.3B). The same general shape and gravity anomaly values are generated from the modeled data with some minor variations. Overall, the differences between the observed and predicted data are relatively small throughout the region (Figure 4.3C). The correlation between the true and predicted gravity is deemed sufficient for the inversion modeling process.

4.2 Inversion Results

A total of fifteen inversions are run with varying mesh parameters and density bounds. Manually adjusting the forward model was also done to continuously improve the initial model prior to successive inversions (Table 7). Gravity modeling is highly non-unique, with an infinite number of equivalent recovered models. All the gravity inversions are performed using the filtered combined free-air and Bouguer gravity data with GRAV3D. The densities for the initial model are displayed in Table 6, with the corresponding bounds in Table 7. During the ModelVision output process, problems were encountered with the shallow water column and overburden layers since these shallow layers are thinner than the height of the mesh cells. Consequently, their densities are averaged with densities of underlying strata.

The first six inversions have the same density bounds with relatively tight bounds assigned for the crustal layers. The poor inversion results are primarily a consequence of these tight bounds. The significant differences between these six inversions are the mesh parameters. Inversion one uses a smaller subset of the entire dataset for QC purposes and confirms the correct execution of the algorithm. The mesh does not enclose the whole region of interest like the other inversion iterations. Inversion two includes an appropriate mesh encompassing the area of interest; however, it produces a poor result. This poor result is due to the tight density bounds assigned to each cell. Inversion three does not have padding cells and is run to test the inversion algorithm performance without padding cells. The result is poor, and therefore padding cells are included for the remaining iterations.

Inversions four and five have the same density bounds and mesh parameters, with the only difference being an improved starting model for inversion five. The sixth inversion uses a slightly shallower mesh (61.2 km), improving the inversion result.

The seventh inversion does not include any Moho constraints, and it is done to assess the quality of the inversion result without this prior knowledge. The seventh inversion successfully reproduces the observed gravity considering there are no Moho constraints provided to the inversion algorithm (Figure 4.3F). The crustal layers are all assigned the same broad bounds (2.50–3.60 g/cm^3). The predicted gravity data and the observed data are compared by plotting a residual map, where the average is 2.844 mGals (Figure 4.3G). The residual plot is also compared with the best inversion result (inversion twelve), showing relatively minor discrepancies. Although this inversion provides reasonable results, efforts continue to generate additional models with different parameters to fit the data better.

Inversions eight and nine use the same mesh parameters, with the only differences being the density bounds of the mantle layer. The eighth inversion has tighter mantle bounds (3.00–3.60 g/cm^3) than the ninth inversion (2.70–3.60 g/cm^3) and results in a blocky crust–mantle boundary. Therefore, the bounds assigned for the remaining inversion attempts are 2.70–3.60g/cm^3.

The tenth and eleventh inversion attempts use various mesh dimensions and number of cells. Inversion ten uses much fewer cells than any other inversion with the consequence of larger cell sizes. The eleventh iteration involves a slightly shallower mesh depth (51 km) to evaluate how that would impact the inversion result. Both inversions generate reasonable results; however, they are not optimal at reproducing the structures and observed gravity data. The residual between the observed and predicted gravity is found to be 3.211 mGals, and as such further inversion attempts are required.

The twelfth inversion is considered the best result and includes the Moho constraint of a sharp density contrast boundary in the initial model (Figure 4.4). This inversion involves tight bounds on the sedimentary layers, assuming the seismic interpretations are correct, and looser bounds for the crustal layers. The crustal bounds have much more freedom than the sedimentary layers since there are fewer constraints for the crustal features. The model from the twelfth inversion (Figure 4.4) shows the density contrasts mainly increasing with depth. In some parts of the model, this is not the case due to the salt layer. The major boundaries, including the basement–upper crust, upper crust–lower crust, and lower crust–upper mantle, are recovered in the model with highly non-unique, geologically reasonable density values. The predicted gravity data from inversion twelve are displayed in Figure 4.3D. The observed and predicted gravity data fit is assessed using a residual plot (Figure 4.3E). Overall, the predicted data match the observed data well, with similar structures and gravity anomaly values. The average residual between the observed and predicted gravity data is 2.837 mGals compared to the average of 2.844 mGals from inversion seven.

The remaining inversion attempts are conducted to improve the inversion result by changing the mesh parameters and tightening the sedimentary layer bounds. The thirteenth inversion uses a smaller mesh surrounding the region of interest with less cells and the same density bounds. The fourteenth inversion uses the same mesh dimensions and density bounds as inversion twelve but an increased number of cells. Lastly, inversion fifteen has the same inversion parameters as twelve; however, tighter sedimentary bounds. These three inversion attempts do not yield a better result than inversion twelve. The remaining gravity inversions produce a larger residual between the observed and predicted data (2.865 mGals). Additionally, they do not mimic the structure of the observed gravity data better than inversion twelve. Therefore, inversion twelve is the preferred density model used moving forward.

Table 7: Summary of the 3-D gravity inversion parameters, including the density bounds and mesh parameters. Inversions seven and twelve are bolded since they produce the best results.

	Mesh Parameters		Density Bounds (g/cm^3)									
Inversion	**Mesh Dimensions (x y z)**	**Number of Cells (x y z)**	**Datum-Seabed**	**Datum-Overburden**	**Seabed-Salt**	**Salt-Codroy**	**Codroy-Top Carbonate**	**Codroy-Anguille**	**Top-Base Carbonate**	**Upper Crust**	**Lower Crust**	**Mantle**
1	147000 x 59000 x 73440	110 x 100 x 80	0.90-1.40	0.90-1.40	2.00-2.50	2.00-2.30	2.20-2.60	2.20-2.60	2.30-2.70	2.50-2.90	2.80-3.10	3.20-3.60
2	147000 x 84000 x 73440	110 x 100 x 80	0.90-1.40	0.90-1.40	2.00-2.50	2.00-2.30	2.20-2.60	2.20-2.60	2.30-2.70	2.50-2.90	2.80-3.10	3.20-3.60
3	75000 x 60000 x 60000	100 x 90 x 70	0.90-1.40	0.90-1.40	2.00-2.50	2.00-2.30	2.20-2.60	2.20-2.60	2.30-2.70	2.50-2.90	2.80-3.10	3.20-3.60
4	147000 x 84000 x 62640	110 x 100 x 80	0.90-1.40	0.90-1.40	2.00-2.50	2.00-2.30	2.20-2.60	2.20.60	2.30-2.70	2.50-2.90	2.80-3.10	3.20-3.60
5	147000 x 84000 x 62640	110 x 100 x 80	0.90-1.40	0.90-1.40	2.00-2.50	2.00-2.30	2.20-2.60	2.20-2.60	2.30-2.70	2.50-2.90	2.80-3.10	3.20-3.60
6	147000 x 84000 x 61200	110 x 100 x 85	0.90-1.40	0.90-1.40	2.00-2.50	2.00-2.30	2.20-2.60	2.20-2.60	2.30-2.70	2.50-2.90	2.80-3.10	3.20-3.60
7	**147000 x 84000 x 61200**	**110 x 100 x 85**	**0.90-1.40**	**0.90-1.40**	**2.00-2.50**	**2.00-2.30**	**2.20-2.60**	**2.20-2.60**	**2.30-2.70**	**2.50-3.60**	**2.50-3.60**	**2.50-3.60**
8	147000 x 84000 x 61200	110 x 100 x 85	0.90-1.40	0.90-1.40	2.00-2.50	2.00-2.30	2.20-2.60	2.20-2.60	2.30-2.70	2.50-3.00	2.70-3.20	3.00-3.60
9	147000 x 84000 x 61200	110 x 100 x 85	0.90-1.40	0.90-1.40	2.00-2.50	2.00-2.30	2.20-2.60	2.20-2.60	2.30-2.70	2.50-3.00	2.70-3.20	2.70-3.60
10	147000 x 84000 x 61200	20 x 20 x 85	0.90-1.40	0.90-1.40	2.00-2.50	2.00-2.30	2.20-2.60	2.20-2.60	2.30-2.70	2.50-3.00	2.70-3.20	2.70-3.60
11	147000 x 84000 x 51000	110 x 100 x 85	0.90-1.40	0.90-1.40	2.00-2.50	2.00-2.30	2.20-2.60	2.20-2.60	2.30-2.70	2.50-3.00	2.70-3.20	2.70-3.60
12	**147000 x 84000 x 61200**	**110 x 100 x 85**	**0.90-1.10**	**1.20-1.40**	**2.25-2.45**	**2.10-2.30**	**2.35-2.50**	**2.35-2.50**	**2.40-2.60**	**2.50-3.00**	**2.70-3.20**	**2.70-3.60**
13	116000 x 68000 x 61200	104 x 94 x 85	0.90-1.10	1.20-1.40	2.25-2.45	2.10-2.30	2.35-2.50	2.35-2.50	2.40-2.60	2.50-3.00	2.70-3.20	2.70-3.60
14	147000 x 84000 x 61200	154 x 124 x 105	0.90-1.10	1.20-1.40	2.25-2.45	2.10-2.30	2.35-2.50	2.35-2.50	2.40-2.60	2.50-3.00	2.70-3.20	2.70-3.60
15	147000 x 84000 x 61200	110 x 100 x 85	0.90-1.10	1.20-1.40	2.28-2.38	2.13-2.25	2.35-2.45	2.40-2.50	2.40-2.60	2.50-3.00	2.70-3.20	2.70-3.60

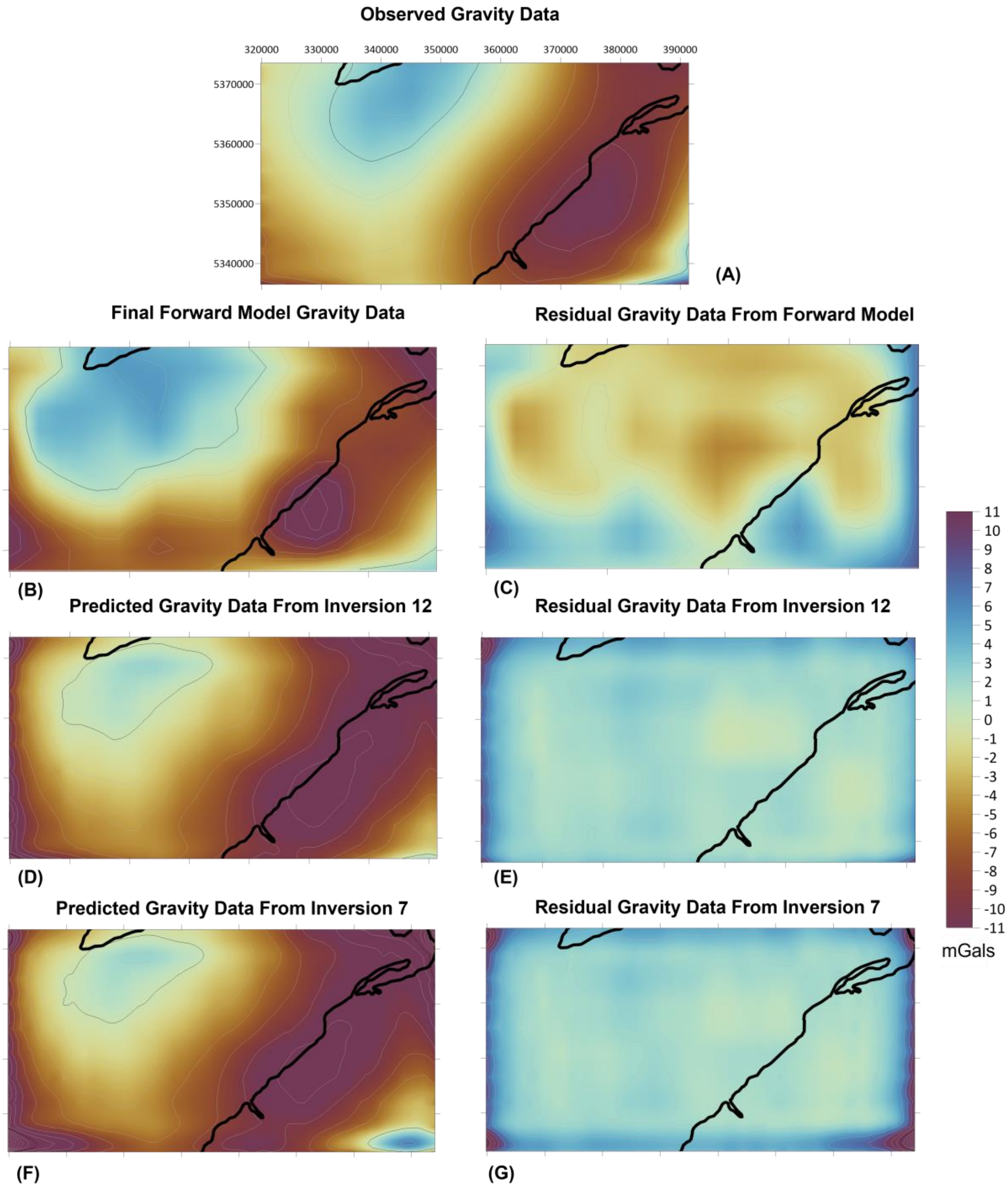

Figure 4.3: Gravity anomaly maps. (A): The observed gravity anomaly data with a low pass filter applied. (B): The modeled gravity data produced from the final forward model. (C): The residual map between plots (A) and (B). (D): The predicted gravity data using inversion twelve. (E): The residual map between plots (A) and (D), where the mean value is 2.837 mGals. (F): The predicted gravity data using inversion seven. (G): The residual map between plots (A) and (F), where the mean value is 2.844 mGals.

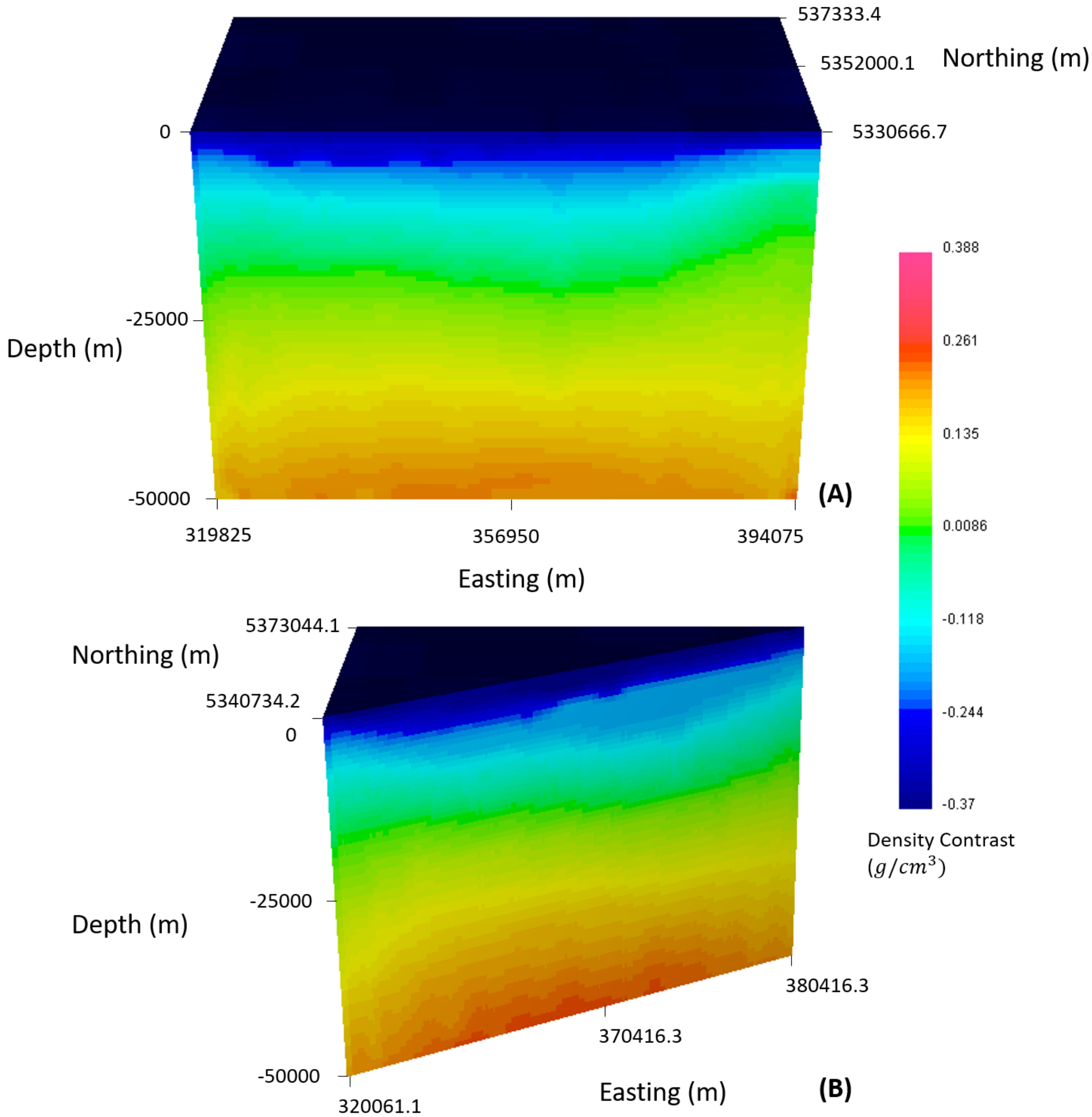

Figure 4.4: The twelfth inversion results, where (A) is the front view and (B) is the diagonal view. The density contrast is relative to the background density (2.67 g/cm^3).

4.2.1 Density Slices

Slices through the inverted density anomaly model provide 2-D visualizations of the model structure and can be used to compare with the seismic interpretation. Four slices taken throughout the basin are displayed in Figures 4.5–4.8, with three surfaces overlain. Additional density slices are provided in Appendix C for supplementary material. The density slices are displayed using two different color bars to emphasize shallow and deep crustal structures. The rainbow color bar is used to highlight the variations in the shallow sedimentary structures, while the red-white-blue color bar is used to emphasize the deep crustal variations. The top basement from the depth converted seismic interpretation represents the purple surface. The inferred mid-crustal boundary (green) and depth to Moho (black) are extracted from the gravity inversion using density anomaly proxies. The mid-crustal-boundary proxy corresponds to 0.0 g/cm^3 and the Moho-proxy corresponds to 0.23 g/cm^3 (both relative to 2.67 g/cm^3).

In general, these density slices show well-correlated correspondence between the gravity inversion and seismic interpretation. Figures 4.5–4.8 also show the plot between the observed and predicted gravity data, where the differences are minimal. The density profiles indicate juxtaposed contrasting densities associated with crustal-scale faults. These crustal-scale faults are interpreted on the density profiles as red dashed lines (Figures 4.5, 4.6, 4.8). The density slices reveal an overall high-density contrast trend to the north near the Port au Port Peninsula due to the Round Head Thrust (RHT) (Figure 4.8) and to the southeast near the Long Range Fault (LRF) (Figures 4.5 and 4.6). The inferred RHT is displayed on the density profile (Figure 4.8), where there are juxtaposed lower crustal blocks with contrasting densities. The RHT juxtaposes high-density lower crust to the northwest and low-density lower crust to the southeast. The inferred LRF is displayed on the density profiles (Figures 4.5 and 4.6), juxtaposing contrasting lower crustal blocks. High-density lower crust is observed in the southeast, and low-density lower crust is observed in the northwest due to the LRF. Figure 4.7 reveals high salt thicknesses recovered as low densities from the gravity inversion. The high salt thicknesses are observed at shallow depths and are particularly seen on the density slice with the red-white-blue color bar represented by a deep red layer near 5 km depth (Figure 4.7). These thick salt packages correlate with the salt-cored anticlines in Figures 3.13.

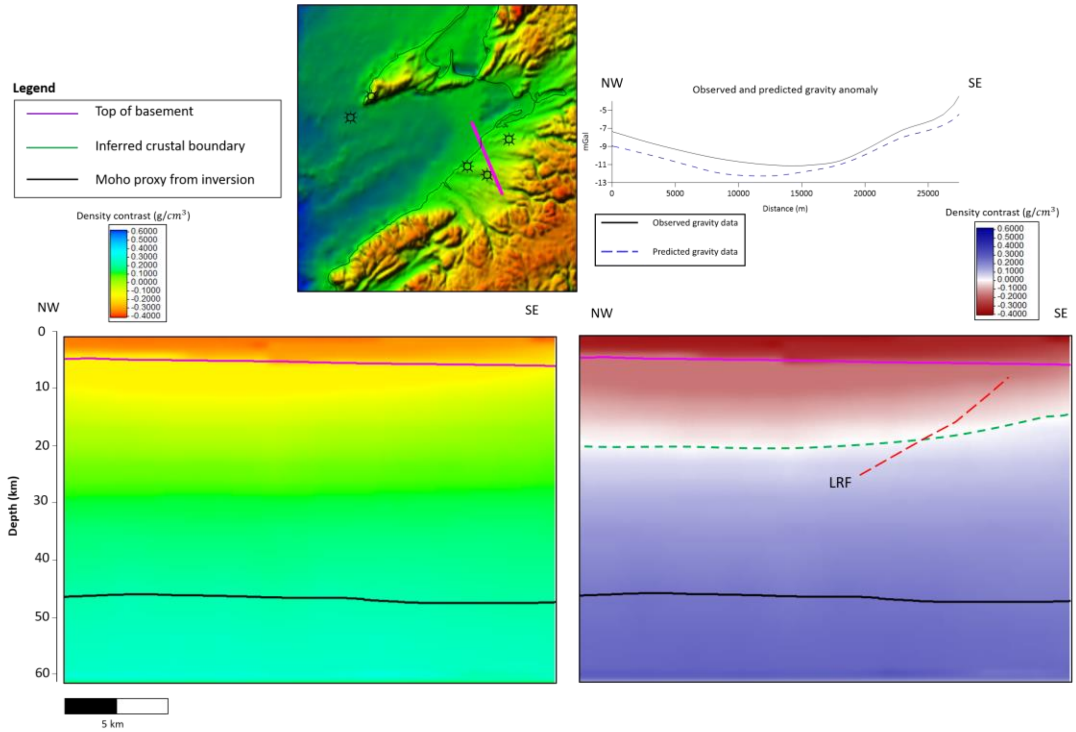

Figure 4.5: A slice through the inverted density model along an onshore-to-offshore NW–SE profile. The rainbow and red-white-blue color bars are displayed to emphasize shallow and deep structures, respectively. The top basement (purple), mid-crustal boundary (dashed green), and depth to Moho (black) are displayed. The red dashed line is the inferred crustal-scale LRF juxtaposing lower crustal blocks. The observed and predicted gravity data are also plotted to show how well correlated the gravity responses are.

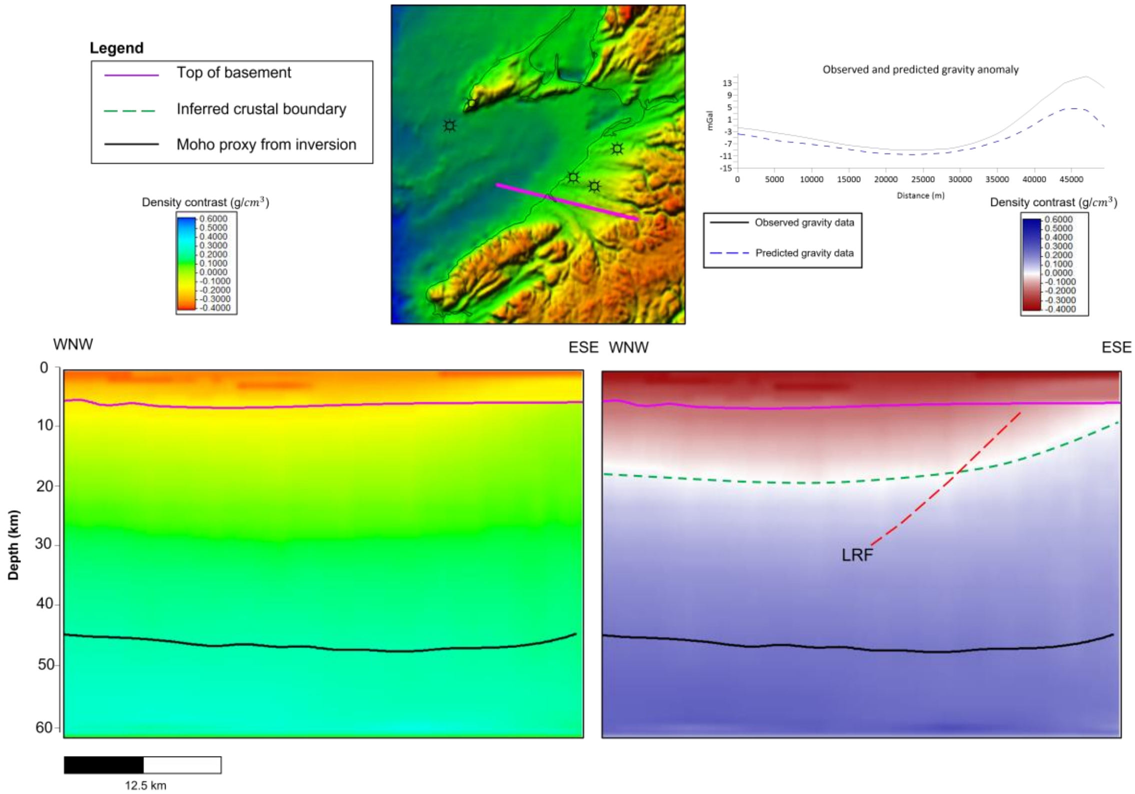

Figure 4.6: A slice through the inverted density model along an onshore-to-offshore WNW–ESE profile. The rainbow and red-white-blue color bars are displayed to emphasize shallow and deep structures, respectively. The top basement (purple), mid-crustal boundary (dashed green), and depth to Moho (black) are displayed. The red dashed line is the inferred crustal-scale LRF juxtaposing lower crustal blocks The observed and predicted gravity data are also plotted to show how well correlated the gravity responses are.

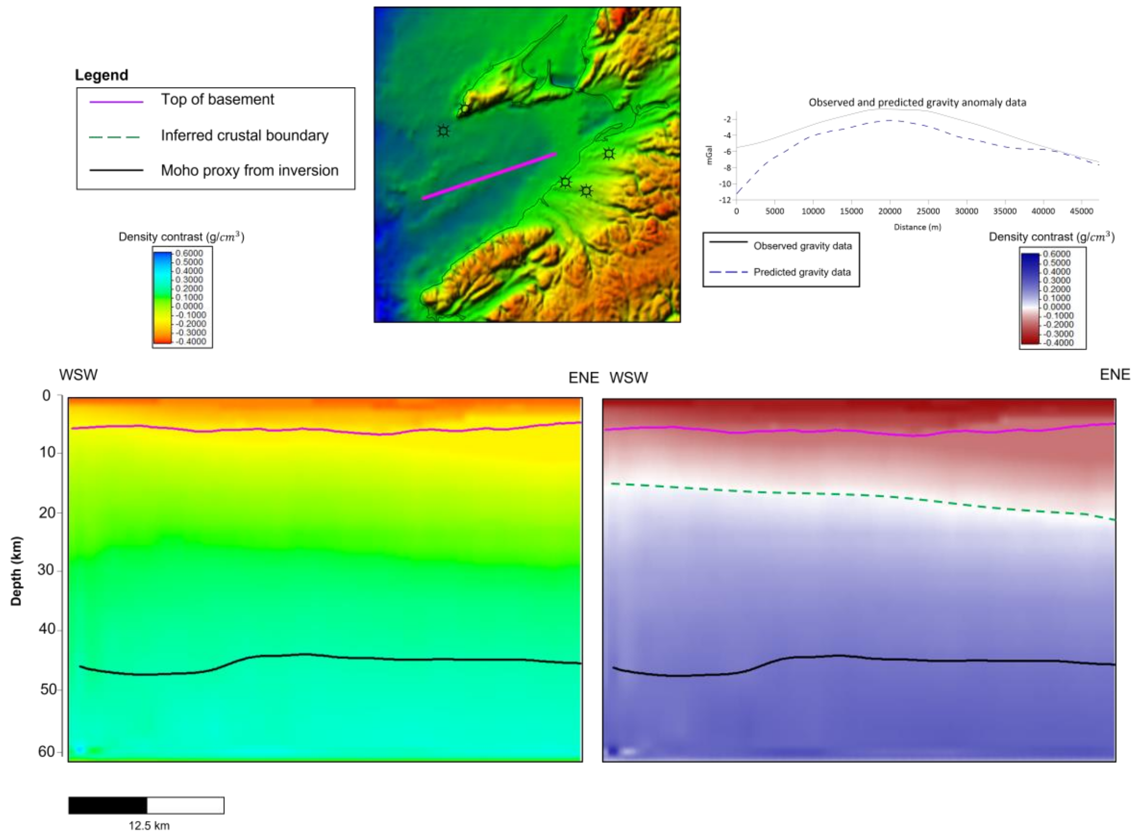

Figure 4.7: A slice through the inverted density model along an offshore WSW–ENE profile. The rainbow and red-white-blue color bars are displayed to emphasize shallow and deep structures, respectively. The top basement (purple), mid-crustal boundary (dashed green), and depth to Moho (black) are displayed. The observed and predicted gravity data are also plotted to show how well correlated the gravity responses are.

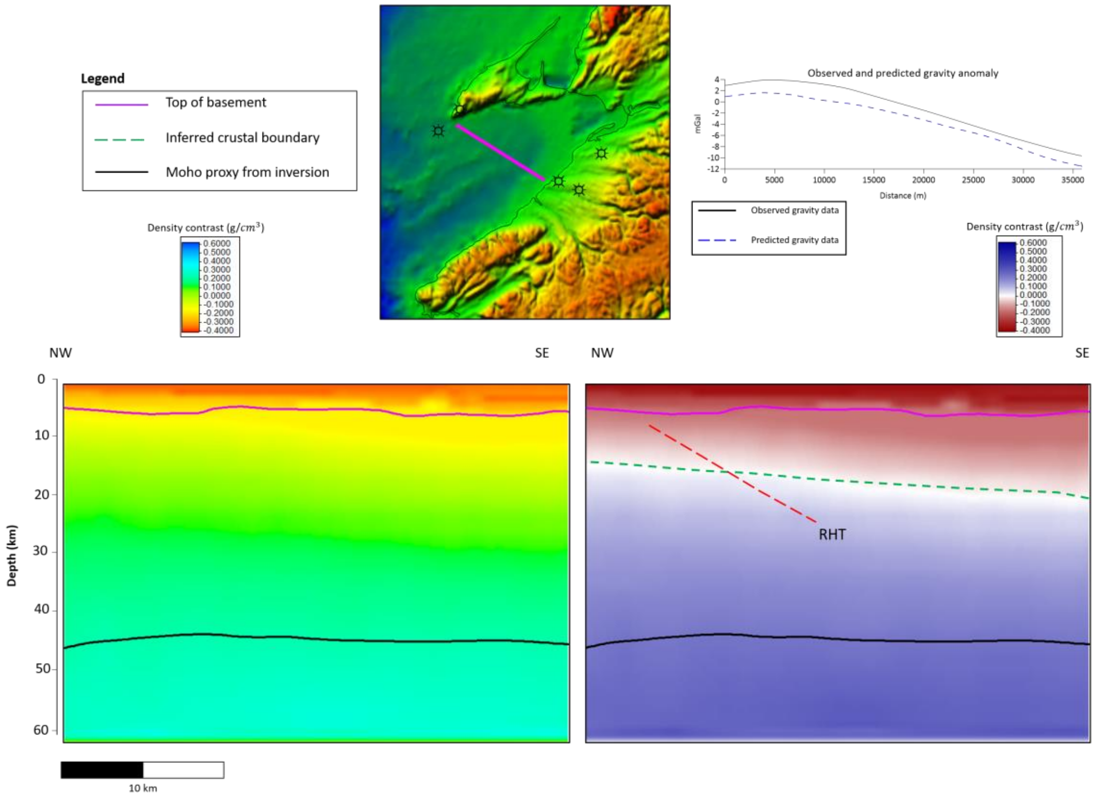

Figure 4.8: A slice through the inverted density model along an offshore NW–SE profile. The rainbow and red-white-blue color bars are displayed to emphasize shallow and deep structures, respectively. The top basement (purple), mid-crustal boundary (dashed green), and depth to Moho (black) are displayed. The red dashed line is the inferred crustal-scale RHT juxtaposing lower crustal blocks. The observed and predicted gravity data are also plotted to show how well correlated the gravity responses are.

4.2.2 Moho Results

The Moho discontinuity represents the seismic boundary between the lower crust and upper mantle. Although the Moho is not imaged on the seismic data used in this study, previous work has identified the Moho location and structure for the Bay St. George subbasin (Marillier & Verhoef, 1989). The depth to Moho determined by inversion of Bouguer gravity data from Marillier & Verhoef (1989) is shown in Figure 1.10, and the average Moho depth is found to be 43 km.

The extraction of the Moho structure is done from the inverted density anomaly model using a Moho-proxy that corresponds to 0.23 g/cm^3, relative to the background density (2.67 g/cm^3), which would represent the density at the base of the crust rather than mantle densities. Figure 4.9 displays a volume render of inversions twelve and seven, where the minimum cut-off density contrast is 0.23 g/cm^3. Figure 4.9 displays the differences in Moho structure between models twelve and seven. The difference between model twelve and seven is that model seven does not have Moho constraints included in the starting model for the inversion, while model twelve does.

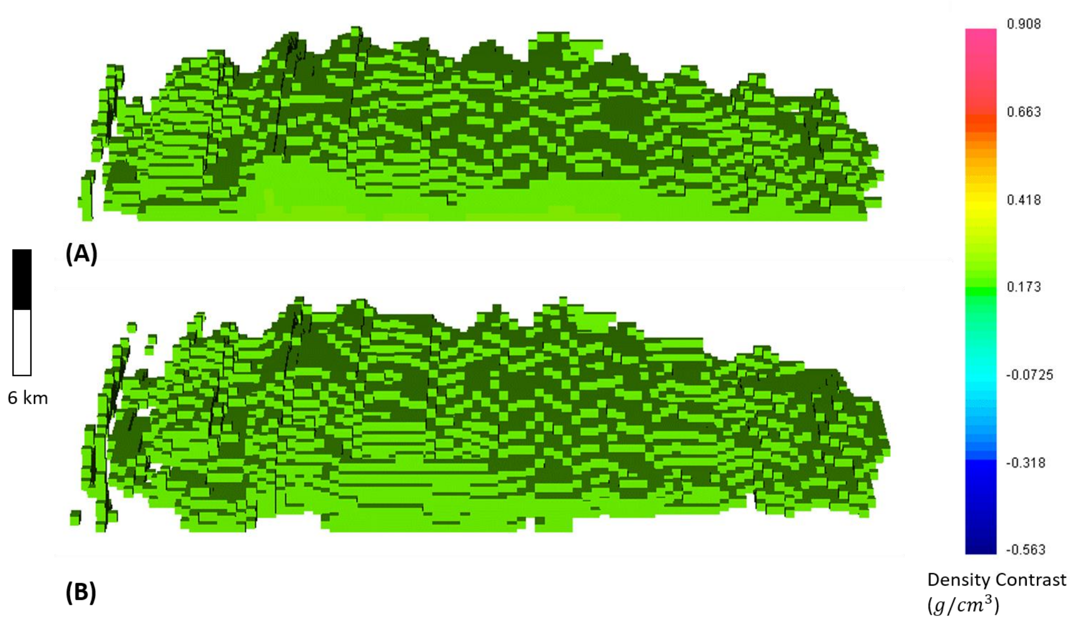

Figure 4.9: The 3-D inversion models visualized using a minimum cut-off density contrast of 0.23 g/cm^3, where (A) is inversion twelve and (B) is inversion seven. The scale bar is relative to the background density (2.67 g/cm^3).

The depth to Moho maps for the inversions and final forward model are displayed in Figure 4.10. The Moho depths derived from the gravity inversions vary from 39–49 km (Figures 4.10A and 4.10B), while the forward model Moho depths range from 36–44 km (Figure 4.10C). The Moho maps obtained from the gravity inversions give similar results with relatively minor differences (Figures 4.10A and 4.10B). The average depth to Moho determined from the inversions is 46 km, with the shallowest Moho near the central offshore. In contrast, the depth to Moho map obtained from forward modeling (Figure 4.10C) reveals the Moho is deepest in the central offshore in the Bay St. George subbasin. The average depth to Moho extracted from the final forward model is found to be 41 km (Figure 4.10C). These discrepancies could be explained because high-density lower-crustal blocks are included in the forward model but are interpreted as Moho variations by the inversion algorithm.

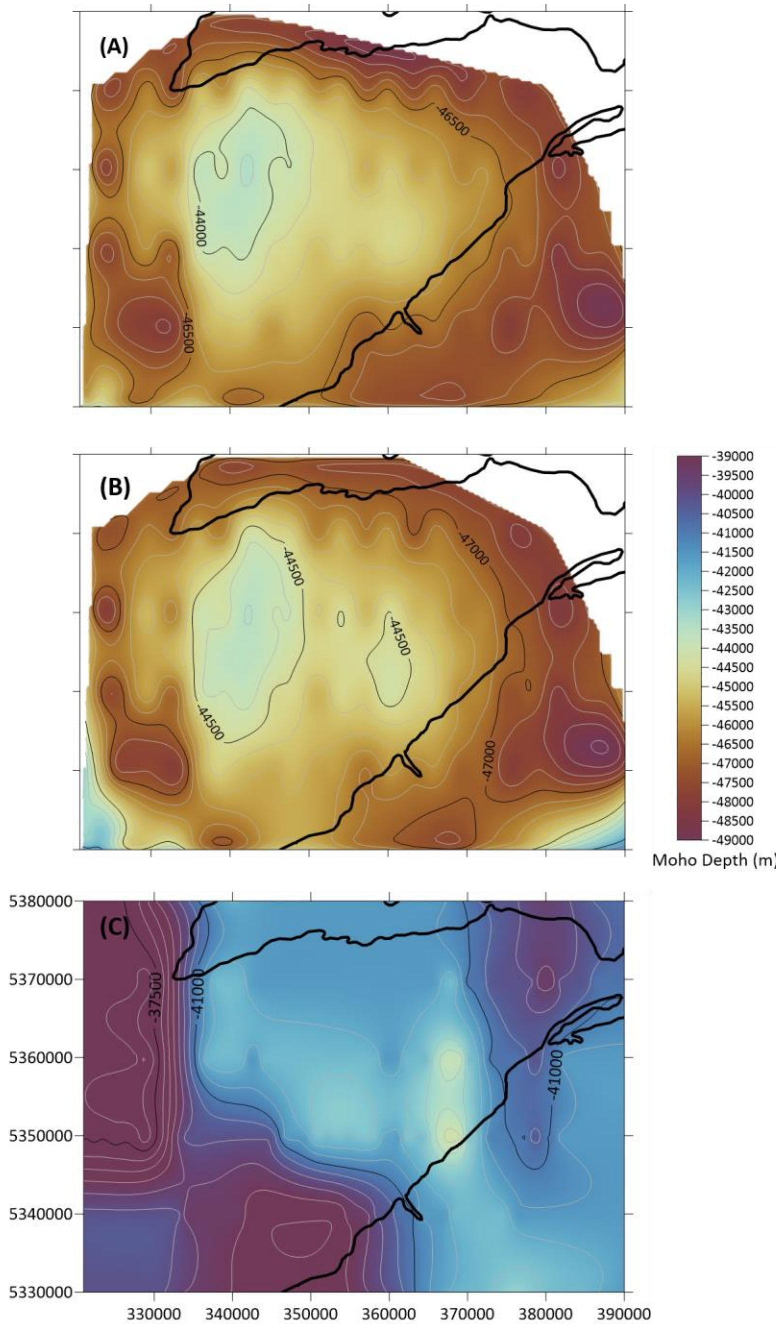

Figure 4.10: The depth to Moho maps where (A) is for inversion twelve, (B) is for inversion seven, and (C) is for the final forward model. The Moho maps determined from the inversions show similar structures where the depths are the shallowest in the center.

4.2.3 Crustal Thickness Results

The crustal thickness of the Bay St. George subbasin is obtained using the depth to basement seismic constraint and the inverted Moho depth model. The crustal thickness map derived from inversion twelve (Figure 4.11) varies between 32 and 46 km thick with an average crustal thickness of 41 km. Overall, the thinnest crust is observed in the central offshore and thickens radially. The crustal structure correlates with the Moho depth map, where the shallowest Moho is in the central offshore.

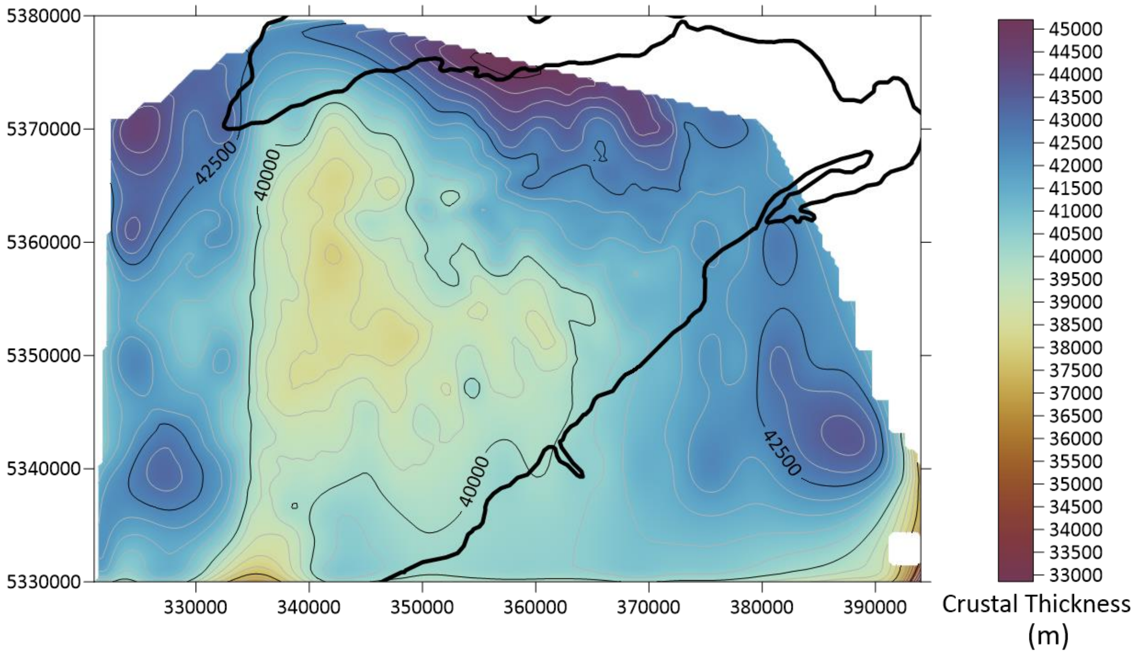

Figure 4.11: The crustal thickness map obtained using the depth to Moho from inversion twelve and the depth to top basement constrained from seismic data.

A mid-crustal boundary is interpreted on the density profiles using a density proxy of 0.0 g/cm^3, relative to 2.67 g/cm^3. This mid-crustal surface is used with the top basement to calculate the upper crustal thickness (Figure 4.12). The lower crustal thickness (Figure 4.13) is calculated using the mid-crustal surface and the depth to Moho from the gravity inversion. The upper and lower crustal thickness maps are used to analyze variations in thicknesses of individual layers and infer crustal significance.

The upper crust is characterized as having thicknesses ranging from 4–17 km with an average of 13 km (Figure 4.12). Overall, the upper crust is the thickest offshore, particularly in the east. In the southeasternmost region onshore, there are anomalously thin upper crustal thicknesses. This structure corresponds with the location of the Long Range Fault suggesting that this fault separates regions of different crustal thicknesses.

The lower crustal thicknesses range from 25–37 km with an average of 28 km (Figure 4.13). Several trends are observed throughout the basin, including thin lower crustal thicknesses in the southeastern region offshore. The thin lower crustal thickness correlates with the thick upper crustal thicknesses at a similar location. The lower crustal thickness is observed to be increasing towards the west/northwest. Additional thickening of the lower crust is observed in the southeast, corresponding to the Long Range Fault.

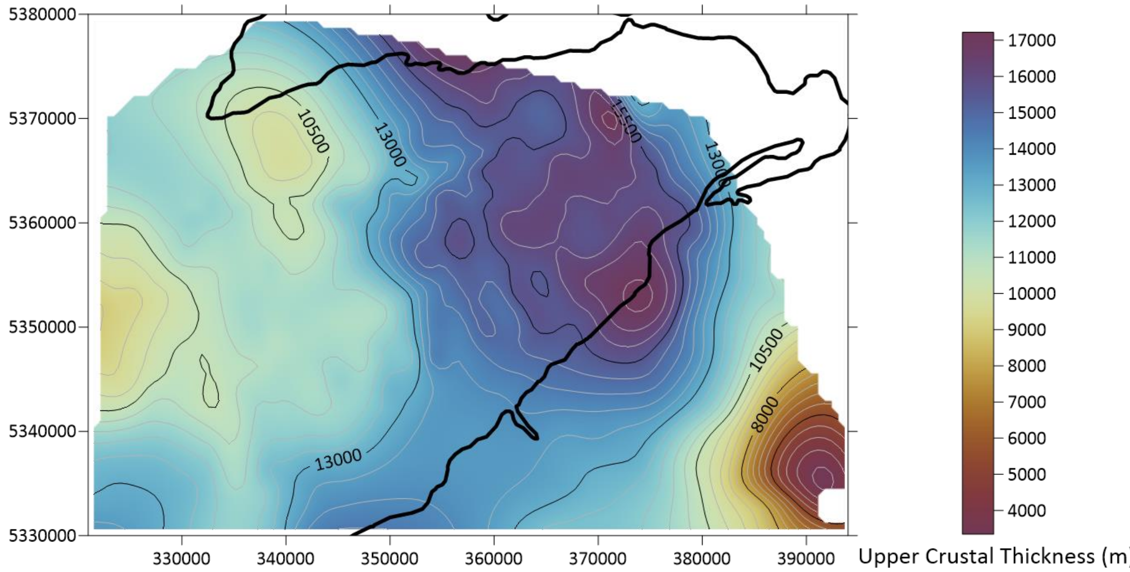

Figure 4.12: The upper crustal thickness map obtained using the depth to top basement and mid-crustal surfaces.

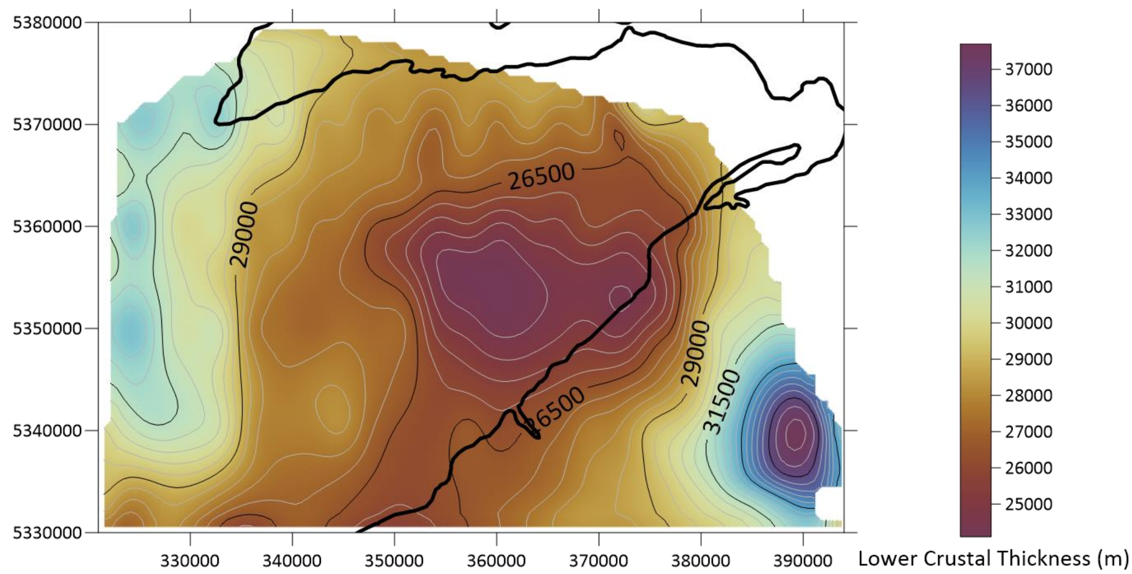

Figure 4.13: The lower crustal thickness map obtained using the mid-crustal and depth to Moho surfaces.

Chapter 5 Discussion

This chapter discusses the results obtained from this study and compares them with previous work where appropriate. The discussion is subdivided into several topics starting with the Bay St. George subbasin stratigraphy and structure, followed by the broader tectonic implications. The topics discussed include sedimentary basin thickness, brittle deformation, salt deformation, Moho and crustal variations, global analogs, and tectonic evolution. The tectonic evolution section provides the regional implications of this work for the deformation history of the Bay St. George subbasin and the broader Northern Appalachians.

5.1 Sedimentary Basin Thickness

The sediment thickness of the Bay St. George subbasin is determined using the interpreted seismic surfaces. The sediment thickness maps (isopachs) are calculated by subtracting two seismic depth surfaces. The depth surfaces are converted from the time domain using the velocity models discussed in section 2.3. Gravity anomaly data are also correlated with sediment thicknesses of the basin. Generally, negative gravity anomalies correlate with thicker sediments, and positive gravity values often relate to thinner sediment thickness. However, this is not always true and must be checked with other crustal maps such as the crustal thickness and depth to Moho maps.

The sediment thicknesses vary throughout the basin and particularly at the onshore-to-offshore transition. Figure 5.1 displays the overall sediment thickness map, which includes autochthonous strata and is calculated using the seabed and Base Carbonate Platform depth surfaces. The maximum overall sediment thickness offshore reaches about 7–8 km (black stars in Figure 5.1). The maximum thickness observed north near the Port au Port Peninsula in Figure 5.1 is a consequence of the deep Top Platform surface (Base Carboniferous) and was likely influenced by the nearby Round Head Thrust (RHT) footwall. The maximum Carboniferous sediment thickness offshore is approximately 5 km (black star in Figure 5.2). The similar maximum thicknesses observed near the onshore-to-offshore transition in Figures 5.1 and 5.2 are due to the steeply dipping Base Codroy, and Carbonate Platform surfaces towards the coastline. Moreover, the maximum sediment thickness onshore is approximately 4 km (black star in Figure 5.3). The onshore sediment thickness does not include autochthonous strata since they are not present and only contain Carboniferous sediments.

Additional localized pockets of high sediment thickness are observed in the northern offshore part of the basin (white star in Figure 5.2) and the central region onshore (labeled as FBA in Figure 5.3). Gravity anomaly data are integrated with sedimentary thickness maps to provide a first-order correlation. Strong negative gravity anomalies were observed near the onshore-to-offshore transition (Figure 2.11), correlating with thicker sediment cover and confirming the seismic interpretation results.

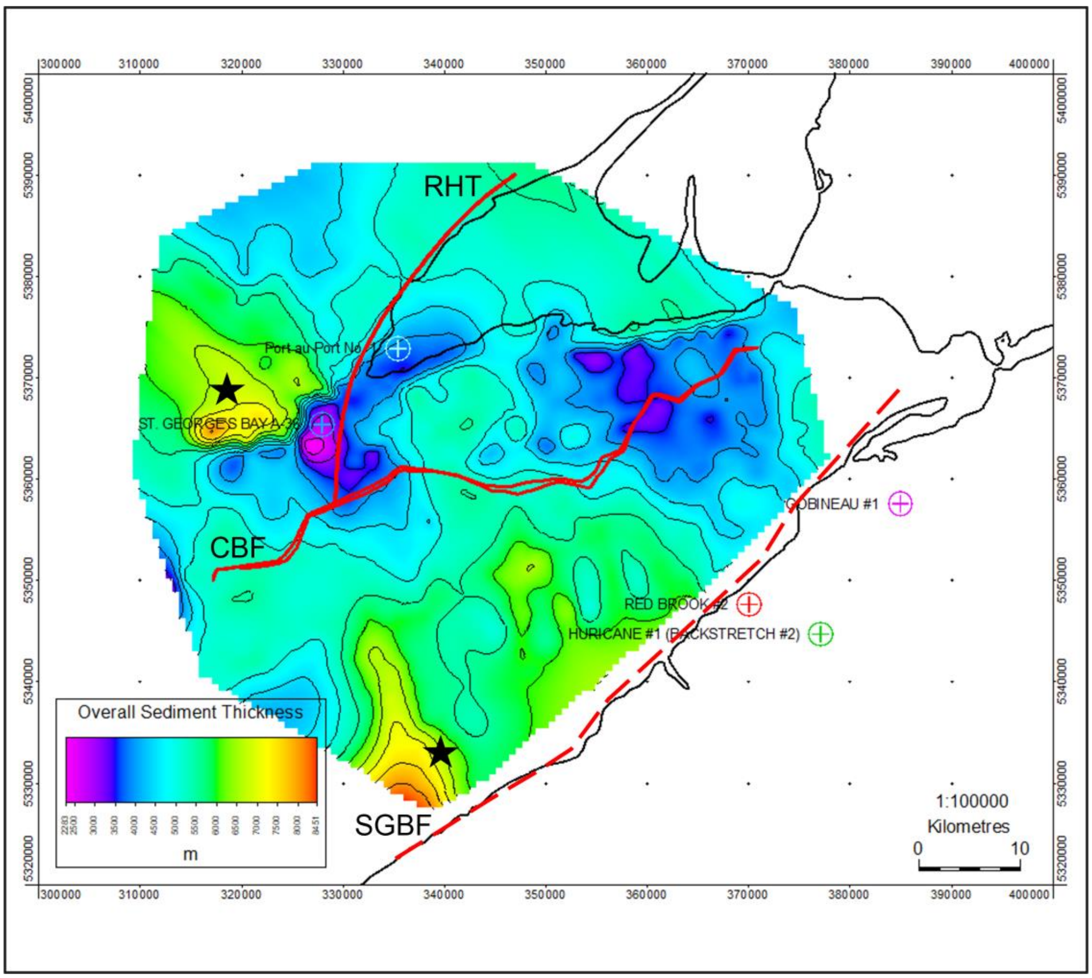

Figure 5.1: The overall sediment thickness map (isopach) calculated using the seabed and Base Carbonate Platform surfaces. This isopach map reaches maximum thicknesses up to approximately 7–8 km. The black stars indicate maximum sediment thicknesses. The regional faults are also displayed (RHT, CBF, and SGBF). Contours are plotted every 300 m.

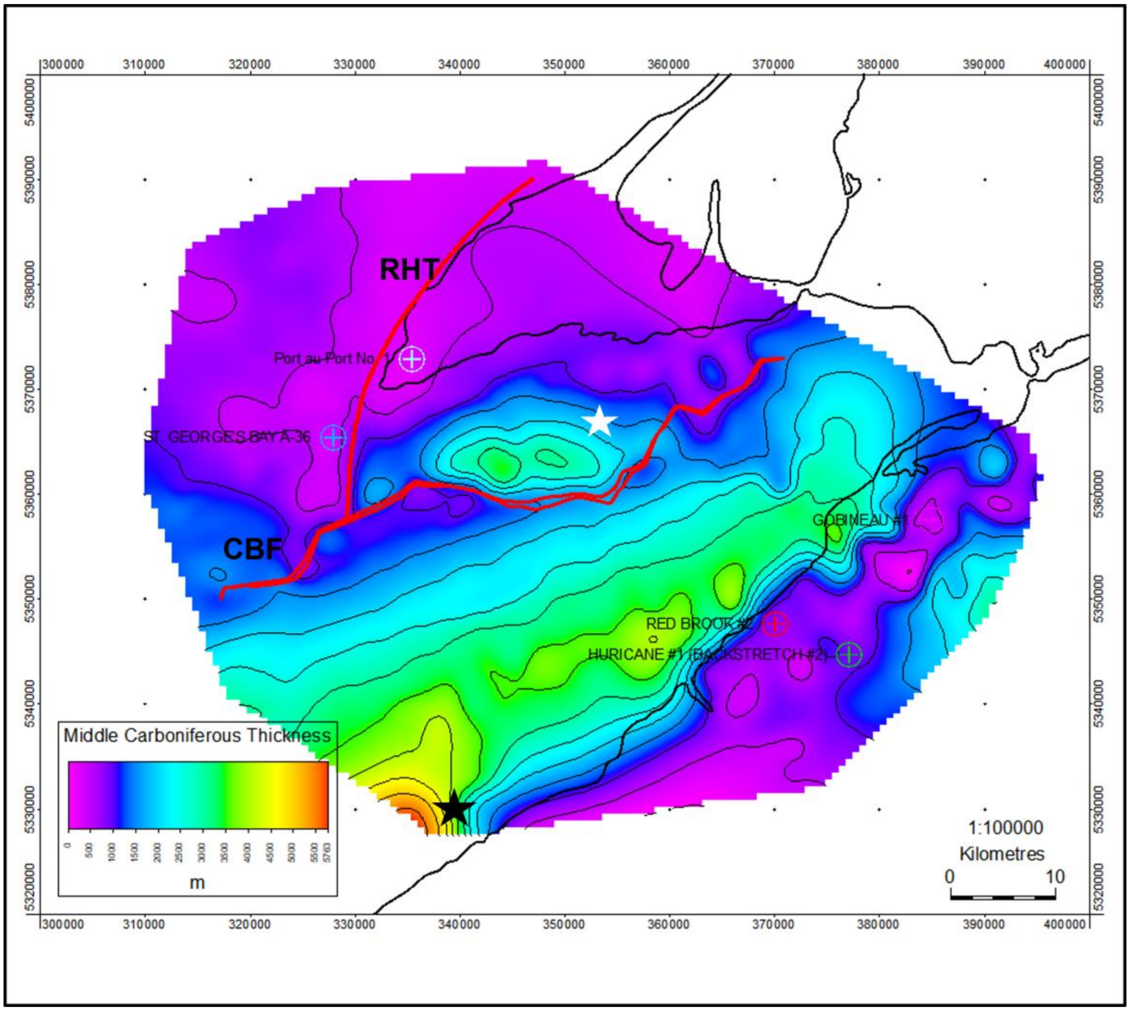

Figure 5.2: The Middle Carboniferous isopach map calculated using the seabed and Base Codroy surfaces. This isopach map reaches maximum thicknesses up to approximately 5 km (black star). The white star correlates with a small sedimentary basin associated with the CBF. The RHT is also displayed as it relates juxtaposed contrasting thicknesses. Contours are plotted every 300 m.

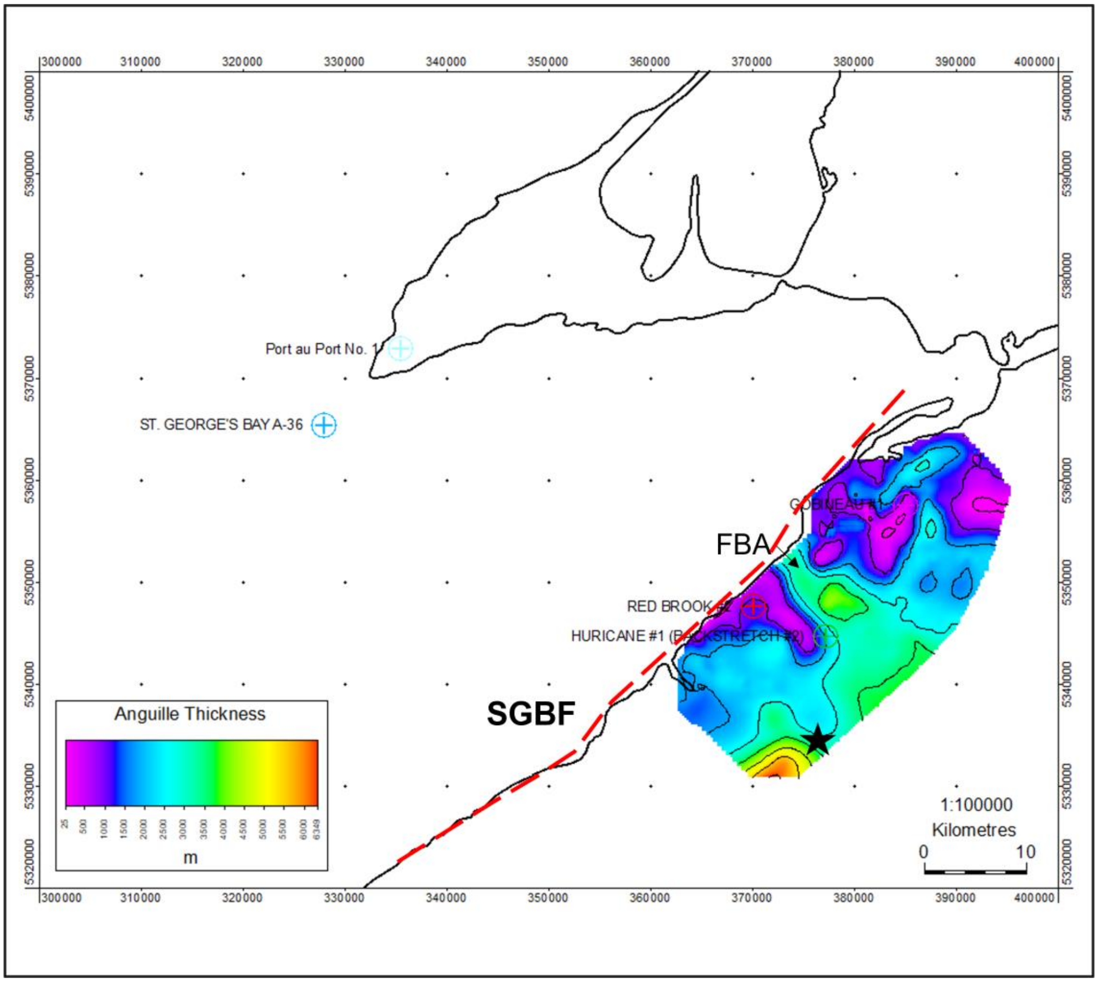

Figure 5.3: The Anguille isopach map calculated using the seismic reference datum and Base Anguille surfaces. This isopach map reaches maximum thicknesses up to approximately 4 km (black star). The localized thickening near the central part of the thickness map is associated with the Flat Bay Anticline (FBA) structure. Contours are plotted every 300 m.

Miller et al. (1990) obtained a maximum thickness of Carboniferous sediments reaching 6 km offshore and 3 km onshore. The present study found a maximum thickness of Carboniferous sediments reaching approximately 5 km offshore and 4 km onshore. Several reasons may explain the discrepancies between the maximum sediment thicknesses. Since the seismic data are interpreted in the time domain, a depth conversion is required. There are often uncertainties with converting seismic data to the depth domain, which could explain these discrepancies since a relatively simple velocity model is used in this study. Miller et al. (1990) conducted their research using older seismic data acquired in 1971 and 1973, while their gravity data were collected from 1983–1984. The depth conversion uncertainty from the present study is estimated to be approximately 500 m, while the work from Miller et al. (1990) may have a greater depth uncertainty of approximately 1 km. The results from the present study agree with Miller et al. (1990) considering these uncertainties.

Although the sediment thickness results in this study do not give the exact maximum thickness values, similarities are observed. Both studies determine considerable thicknesses near the offshore transition and relatively consistent sediment thicknesses onshore. A new finding from the seismic interpretation results in this study is a small sedimentary basin located south of the Port au Port Peninsula (white star in Figure 5.2). This small sedimentary basin has a thick sediment cover with a negative gravity anomaly near the -10 mGals contour (Figure 2.11). The gravity modeling evidence indicates this basin is underlain by a shallow depth to Moho and thin crust (Figures 4.10 and 4.11). This small sedimentary basin likely formed due to movement along the CBF as an influx of sediments deposited during a significant extension period. Figure 5.4B shows a seismic profile crossing this sedimentary basin, where the CBF creates tilted fault blocks. As the fault initiated, this created a significant offset and the present-day tilted stratigraphy. The CBF system likely demonstrates strike-slip motion as there is more offset for the shallower sediments than the deeper layers (Figure 5.4b). The sediment was likely deposited concurrently to the fault movement and influenced by the strike-slip sense from a Port au Port Peninsula source. Significant thickening of sediments is observed in the southeast near the coastline at the transition between onshore-to-offshore (black star in Figure 5.2). This significant thickening coupled with the variations in sediment thicknesses throughout the entire basin implies differential subsidence occurred as the basin formed (Dafoe et al., 2016).

5.2 Brittle Deformation

Brittle deformation occurs throughout St. George Bay as a consequence of the Newfoundland Appalachian Orogeny and the formation of the Bay St. George subbasin. The brittle deformation is captured on seismic and magnetic data as faults. The magnetic data displayed in Figure 2.14 are used to highlight fault lineations and correlated with the seismic data. Normal and reverse faults are interpreted on the seismic data and correlated with magnetic observations. There is evidence of oblique motion along fault systems related to the dextral strike-slip opening of the basin (Figure 5.4B). The oblique motion evidence includes an increased offset of shallower sediments in contrast to deeper layers represented by the CBF in Figure 5.4B. Overall, most regional faults are interpreted to strike NE–SW and E–W. Other minor faults are interpreted, such as NW–SE trending antithetic faults and NE–SW trending synthetic faults. Reactivation and inversion of older faults as thick-skinned deformation are also observed, as previously suggested by Stockmal et al. (2004) (Figure 5.4D and Figure 5.4E).

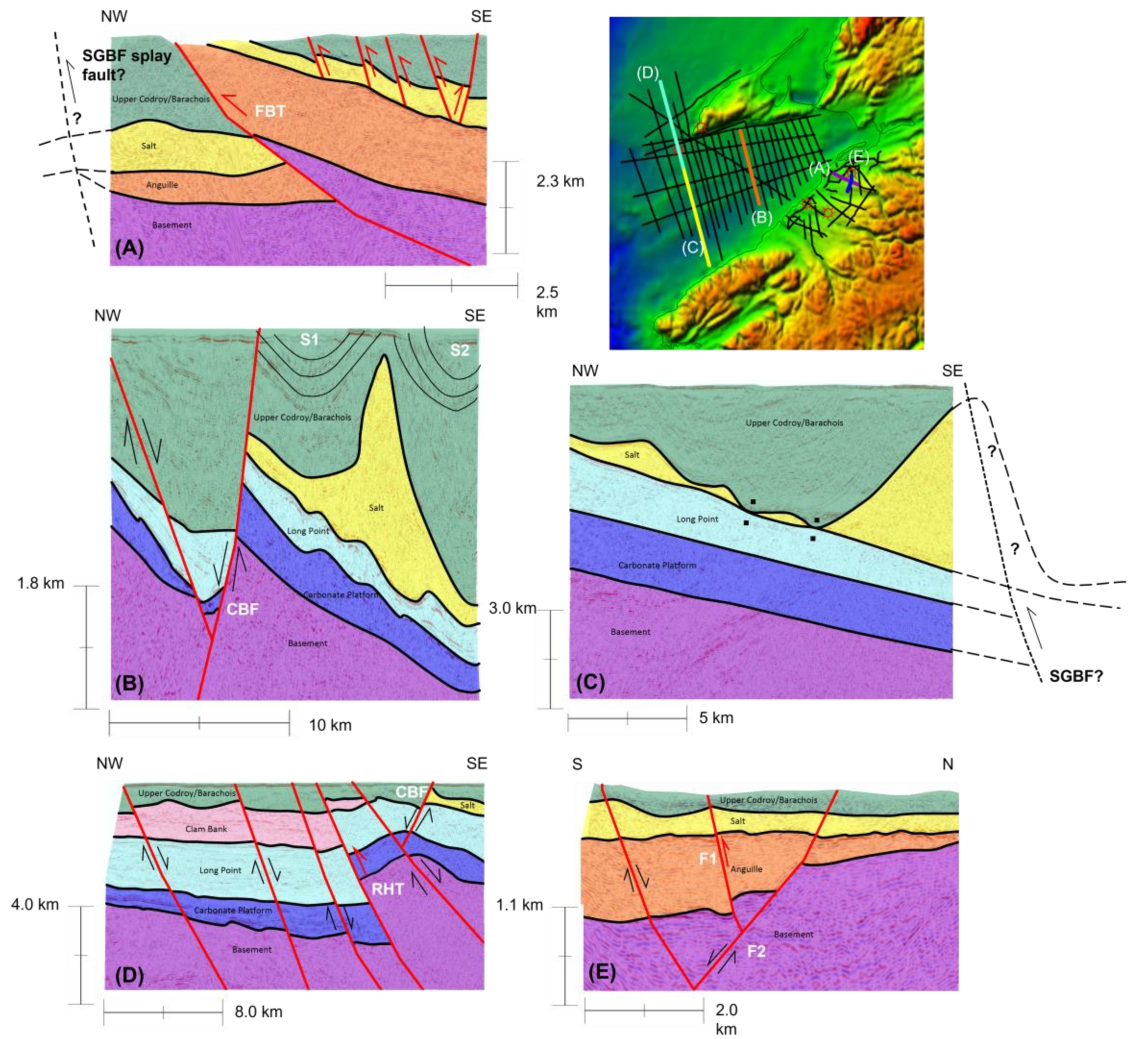

Figure 5.4: Enlargements of interpreted seismic profiles in the Bay St. George subbasin. The bathymetry map displays the location of the seismic lines shown. The interpreted seismic sections include annotated faults, where the red and black arrows correspond to reverse and normal faults, respectively. The vertical and horizontal exaggerations vary per plot based on the structures highlighted. (A) shows a highly segmented seismic profile, where the Flat Bay Thrust (FBT) displays a significant offset of Carboniferous sediments. The Anguille sediments appear to pinch out against a splay fault branching from the SGBF. (B) shows a well-defined salt-cored anticline and intervening synclines (S1 and S2), with the Central Bay Fault (CBF) truncating salt deposition to the north. The S2 synclines display progressive deformation to the south, indicating deformation continued during the deposition of overlying sediments. (C) shows two interpreted primary salt welds as annotated by the two filled circles and well-defined salt-cored anticlines. A possible scenario involving the termination of carbonate platform successions is also annotated. (D) shows a highly compartmentalized seismic section with mainly normal faults, except for the reactivated inverted Round Head Thrust (RHT). The CBF truncates the salt deposition to the north. (E) shows the thickening of sediments towards the south along a large south-dipping normal fault (F2). The F1 fault is an interpreted reactivated inverted fault.

Normal faults are observed throughout the basin as a result of divergence within an extensional environment. Most of the interpreted normal faults are striking NE–SW with minor synthetic faults striking subparallel to the main fault systems. The faults delimit significant stratigraphic and structural relationships, such as the Central Bay Fault (CBF) truncating salt deposition to the north (Figure 5.4B and Figure 5.4D). The CBF is an extension to the Romaines Brook Fault (RBF) that extends from the onshore (Figure 2.14). The CBF shows oblique motion along some seismic profiles (Figure 5.4B) as the shallower Carboniferous sediments display substantial offset while the deeper carbonate platform successions display minor offset. The CBF is suggested to have formed during the reactivation of the Romaines Brook Fault (RBF) (late Devonian) and deposition of the Codroy Group (Visean) (Dafoe et al., 2016; Stockmal et al., 2004). The CBF is also inferred to reach crustal-scale depths juxtaposing lower crustal blocks of differing properties. This is an important finding, as it provides a better constrained structural characterization of the basin. Additional analysis on the juxtaposition produced from the CBF is discussed in section 5.4. Growth faults are observed onshore (F2 fault in Figure 5.4E), indicating a syn-depositional setting. There is a thickening of sediments along these faults towards the southeast onshore. The growth faults and Carboniferous sediment thickness differences between the hanging wall and footwall imply that the faults formed during the deposition of Carboniferous sediments (Tournaisian–Pennsylvanian).

Reactivation and inversion of faults are evident in this study area and imaged on the seismic profiles (e.g., F1 fault in Figure 5.4E). The Round Head Thrust (RHT), marked on numerous seismic profiles (e.g., Figure 5.4D), is another example of a reactivated inverted fault. This fault is interpreted to have initiated as a normal fault, synthetic to adjacent normal faults, and was subsequently reactivated and inverted. The RHT was initially formed during the opening of the Iapetus Ocean. This was followed by reactivation from Taconian foreland basin subsidence, inversion in thick-skinned deformation from the Devonian Acadian Orogeny, and minor dextral strike-slip motion (Stockmal et al., 2004). The RHT is inferred to be a vital fault that juxtaposes contrasting crustal blocks. The juxtaposition of crustal-scale blocks created from the RHT indicates that this fault is of crustal-scale importance for the basin and likely the Northern Appalachian Orogeny. A more detailed analysis regarding the implications of the juxtaposed crustal blocks produced from the RHT is provided in section 5.4.

Reverse faults are also commonly observed throughout the study area. The Flat Bay Thrust (FBT) in Figure 5.4A is an onshore thrust fault creating significant displacement. The FBT displays substantial offset in Carboniferous sediments and likely formed during the later transpressional Carboniferous deformation and formation of Pangea. This fault is projected in Figure 5.5 as it crosses the Flat Bay Anticline. The St. George Bay Fault (SGBF) is interpreted to mark the southern limit of carbonate platform successions offshore (Langdon & Hall, 1994). Although Langdon & Hall (1994) identified the SGBF and determined that it corresponded to a significant stratigraphic relationship, the work from Dafoe et al. (2016) did not confirm this. Figure 5.4C shows a potential interpretation where the SGBF is situated just south of the southernmost seismic profile. This regional fault is argued to terminate carbonate platform successions offshore allowing for the presence of Anguille sediments southeast of this. These successions are suggested to potentially have been thrusted and eroded. The onshore Anguille sediments are suggested herein to have pinched out against a fault synthetic to the SGBF. Figure 5.4A displays a potentially feasible interpretation where the Base Anguille sediments pinch out against a splay fault branching from the main SGBF. This pinch out implies Aguille sediments may have been eroded or this was the edge of where they were deposited. These faults are suggested to have formed post-Ordovician, likely during the Middle–Late Carboniferous (Langdon & Hall, 1994). These faults continued to deform Carboniferous sediments and influence salt expulsion.

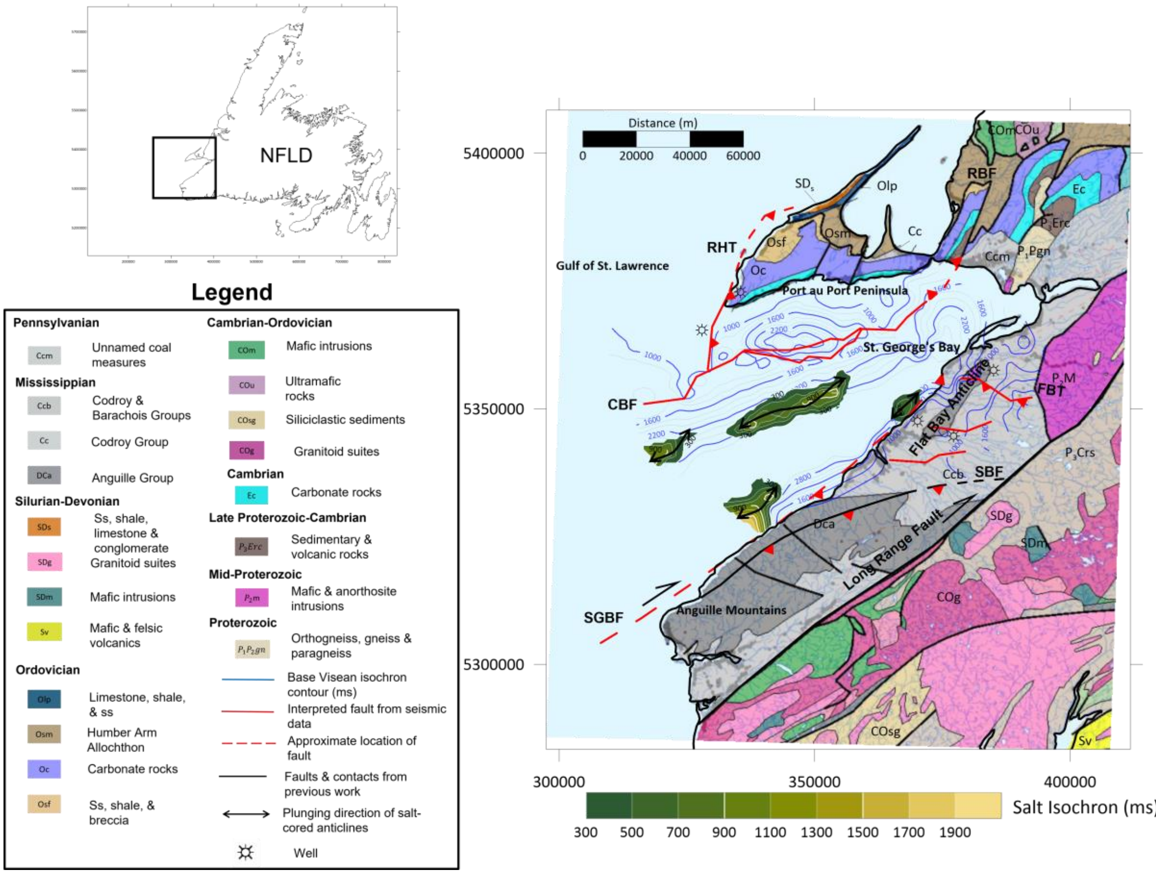

Figure 5.5: The structure map of the Bay St. George subbasin with overlying onshore geology. The faults are interpreted from the seismic data in this study (red) and derived from previous work (black). This map also displays important isochron maps. The Middle Carboniferous (blue) and salt isochron (green–yellow) contours are displayed as they correlate with major bounding faults. The black arrows indicate the doubly plunging direction of salt-cored anticlines. The onshore geology and interpolated faults are after Coleman-Sadd et al. (2000), Knight (1983), and Langdon & Hall (1994).

The reverse faults (FBT, SGBF, and SBF) are primarily located in the southern part of the basin, while the other major reactivated and inverted faults are situated in the north (CBF and RHT) (Figure 5.5). A transition from initial transtensional faults (CBF and RHT) to transpressional faults (FBT) is proposed based on the geographical location of these faults and the seismic interpretation in this study. The transpressional faults, such as the thrusts in Figure 5.4A, mostly strike in the same direction and display pure transpression, not showing any indicators of initial extension. Furthermore, there are no interpreted normal faults on this seismic section. This is important as these transpressional faults were likely not reactivated and inverted like other major faults in the basin and provide evidence for a change in tectonic environments. The change from transtension to transpression is characteristic of strike-slip basins (Waldron, 2004). This transition in tectonic environments is a new finding for the Bay St. George subbasin that improves the constraints on the tectonic evolution of the basin.

Figure 5.5 summarizes the geological and structural interpretations of the Bay St. George subbasin from this study. Figure 5.5 contains the onshore geology, isochron maps of Carboniferous strata, and the main regional faults. The faults in Figure 5.5 include the faults interpreted from the seismic data in this study (red) and faults derived from previous work (black). The (red) faults interpreted in this study in Figure 5.5 were already established structures agreeing with previous discoveries (Coleman-Sadd et al., 2000; Dafoe et al., 2016; Langdon & Hall, 1994; Snyder, 2019). The onshore geology provides context for the geological formations and primary geological contacts within the onshore part of the Bay St. George subbasin. The Carboniferous strata and salt isochron contours are included in the map since these surfaces are critical in providing the stratigraphic and structural relationships. The integrated geological and structural map of the Bay St. George subbasin provides an updated framework with newly interpreted faults. This map also verifies and improves constraints on previously uncertain structures in the basin and identifies a significant tectonic environment change.

5.3 Salt Deformation

The ductile deformation observed in the Bay St. George subbasin is primarily due to salt tectonics. The evaporite-bearing packages were deposited during the Early Visean within the Codroy Road Formation. The salt-related structures include salt welds, anticlines, synclines, and salt expulsion minibasins (e.g., Figure 5.4C).

The timing of halokinesis is critical for constraining the tectonic evolution of the Bay St. George subbasin. The salt deposition is truncated sharply to the north by the CBF, indicating that the salt movement may be concurrent with the motion along this fault (Dafoe et al., 2016). The southeast movement of salt is indicated by the synclines interpreted in the seismic data (Figure 5.4B). The S1 and S2 synclines interpreted in Figure 5.4B show different seismic characteristics. The S1 reflectors show parallelism, while the S2 reflectors show progressive deformation towards the southeast. The S1 reflectors are relatively uniform, showing consistent characteristics and structures that prove that the halokinesis occurred post-deposition (Dafoe et al., 2016). However, S2 reflectors show progressive deformation deeper in the basin towards the southeast. The characteristics of the reflectors for S2 show non-parallelism and distortion, indicating that deformation continued during the deposition of overlying sediments (Dafoe et al., 2016). Snyder (2019) traced trough points in salt-expelled minibasins to investigate salt movement (Figure 5.6). This technique involves mapping salt-expelled minibasins with the highest salt expulsion or dissolution (trough points). The movement of successive trough points upwards within salt-expelled minibasins is used to track the salt migration direction. Snyder (2019) determined a salt migration change from southeast to northwest due to the emplacement of a tectonic wedge. Figure 5.6 shows the trough surface trace migrating towards the southeast on the seismic profiles without the tectonic wedge (E and W profiles in Figure 5.6). The trough surface trace migrates towards the northwest on the seismic profile with the tectonic wedge (C profile in Figure 5.6), implying a salt migration change. The salt migration analysis was done using seismic data in TWTT by Snyder (2019), although a better understanding of salt movement can be obtained using depth-converted seismic data. Upon analyzing the same seismic profiles as Snyder (2019) in the depth-domain, it is evident that the salt initially migrates towards the southeast, as previously discussed. The change in salt migration direction towards the northwest is also observed along the same seismic profile (Figure 5.4C) as Snyder (2019). However, the present study results suggest that salt migration direction changed due to differential sediment loading and salt expulsion, not due to tectonic control as Snyder (2019) proposed. Differential sediment loading on viscous salt is a mechanism driven by the differential pressures between the ductile salt and brittle surrounding strata (Cohen & Hardy, 1996). The tectonic wedge interpreted by Snyder (2019) is herein interpreted to be a salt-cored anticline with an overlying salt-expelled minibasin created from sediment loading and salt expulsion (Figure 5.4C) rather than a tectonic wedge created from opposite verging thrust faults. The salt-cored anticline is the preferred interpretation since there is a lack of underlying reflectivity beneath the structure (Figure 5.4C) and due to the low gravity anomaly (Figure 2.11) indicating a salt related structure.

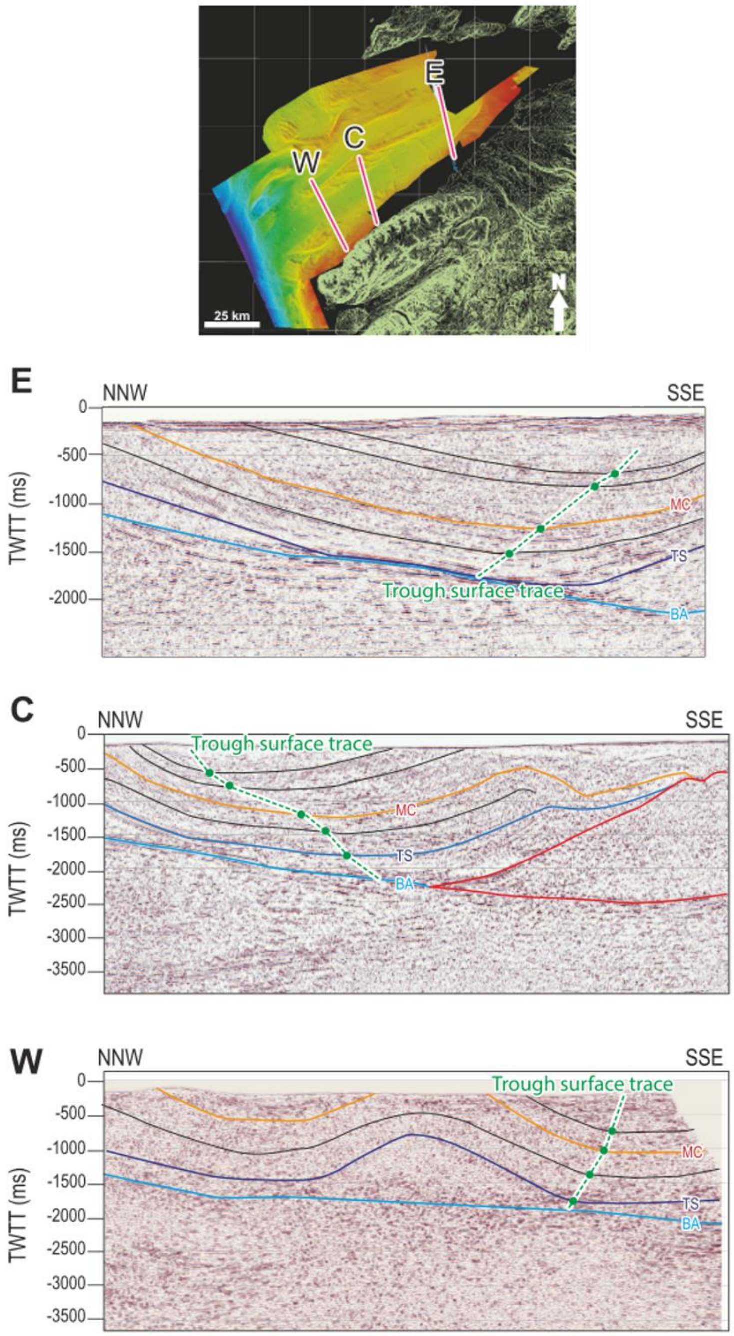

Figure 5.6: Trough surface traces interpreted on three seismic profiles corresponding to the bathymetric map location. The E and W seismic profiles indicate salt migration towards the southeast. The C seismic profile includes a tectonic wedge and shows salt migration towards the northwest. Figure from Snyder (2019).

Salt-related structures such as salt-expulsion minibasins and salt-cored anticlines provide further constraints on the basin's evolution. The doubly plunging salt-cored anticlines display *en echelon* characteristics parallel to the basin-bounding faults (Figure

5.5). These *en echelon* features indicate dextral strike-slip motion along the Bay St. George subbasin bounding regional faults (Dafoe et al., 2016; Knight, 1983). Similar observations are seen in the Cumberland subbasin, which is a part of the broader Maritimes Basin (Figure 5.7). The Cumberland subbasin shows regional faults bounded by basement highs and elongate, oval-shaped salt-expulsion minibasins surrounded by primary salt welds resulting from vertical salt expulsion similar to those seen in the Bay St. George subbasin (Figure 5.8) (Hibbard & Waldron, 2009; Waldron et al., 2013). Waldron et al. (2013) suggest that these evaporite expulsion structures and brittle deformation result from NE–SW transtensional tectonics during the opening of the Maritimes Basin. Analysis of the Cumberland subbasin may be used as an analog for the Bay St. George subbasin and supports past work suggesting the subbasin formed within a transtensional environment along the NE–SW bounding LRF. The *en echelon* salt-related structures interpreted in the present study and by Dafoe et al. (2016) provide further evidence of the correlation between the ductile and brittle deformation observed.

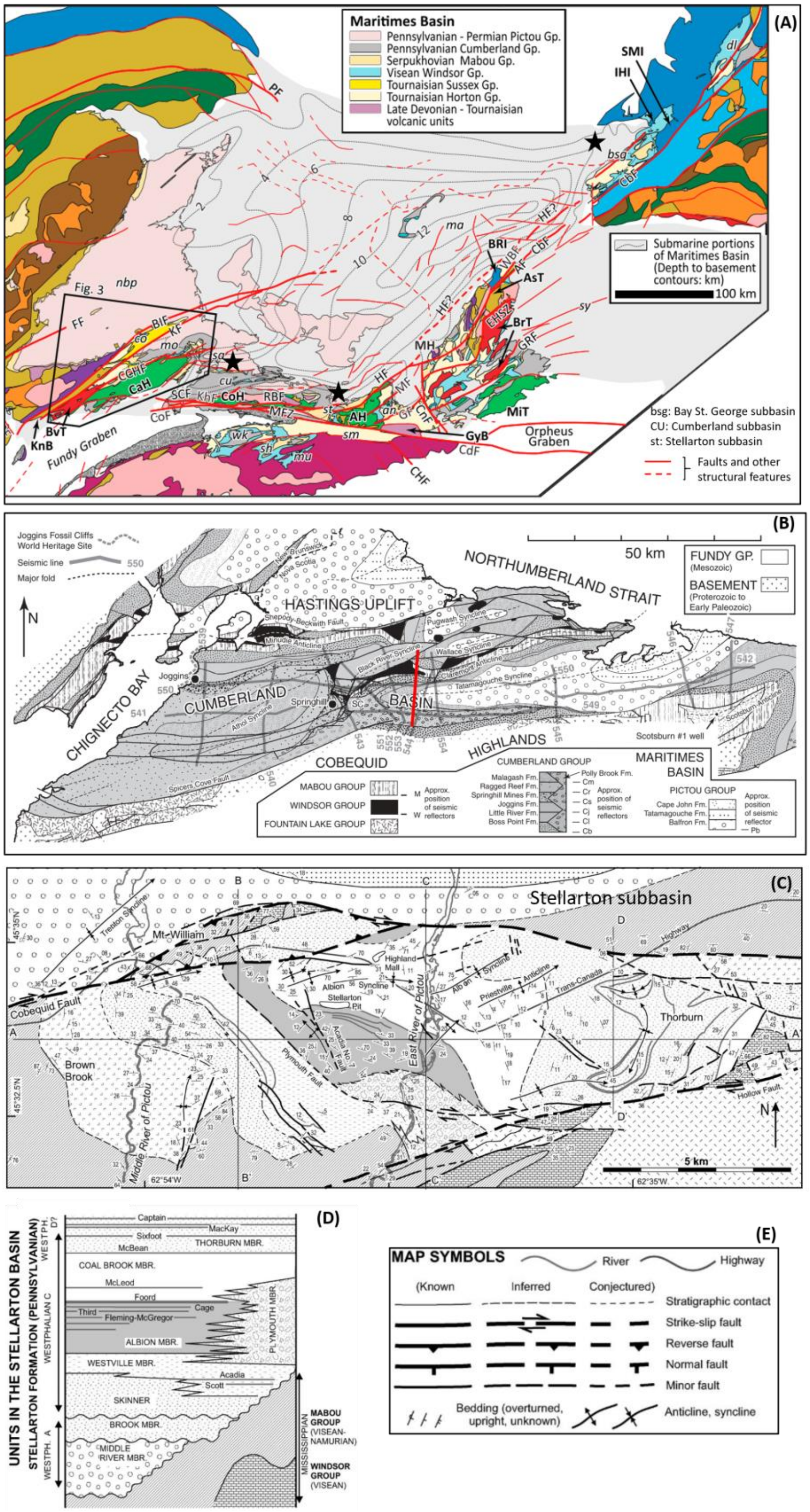
(A)
Maritimes Basin
Pennsylvanian - Permian Pictou Gp.
Pennsylvanian Cumberland Gp.
Serpukhovian Mabou Gp.
Visean Windsor Gp.
Tournaisian Sussex Gp.
Tournaisian Horton Gp.
Late Devonian - Tournaisian volcanic units
Submarine portions of Maritimes Basin (Depth to basement contours: km)
100 km
bsg: Bay St. George subbasin
CU: Cumberland subbasin
st: Stellarton subbasin
Faults and other structural features
Fig. 3
Fundy Graben
Orpheus Graben
SMI
IHI
BRI
AsT
BrT
MH
MiT
CaH
CoH
AH
GyB
BvT
KnB
(B)
Joggins Fossil Cliffs World Heritage Site
Seismic line
Major fold
50 km
FUNDY GP. (Mesozoic)
BASEMENT (Proterozoic to Early Paleozoic)
NORTHUMBERLAND STRAIT
HASTINGS UPLIFT
CHIGNECTO BAY
CUMBERLAND
BASIN
COBEQUID
HIGHLANDS
Joggins
Springhill
Scotsburn #1 well
MABOU GROUP
WINDSOR GROUP
FOUNTAIN LAKE GROUP
Approx. position of seismic reflectors
CUMBERLAND GROUP
Polly Brook Fm.
Malagash Fm.
Ragged Reef Fm.
Springhill Mines Fm.
Joggins Fm.
Little River Fm.
Boss Point Fm.
MARITIMES BASIN
PICTOU GROUP
Cape John Fm.
Tatamagouche Fm.
Balfron Fm.
(C)
Stellarton subbasin
Mt. William
Cobequid Fault
Brown Brook
Middle River of Pictou
East River of Pictou
Albion Syncline
Stellarton Pit
Highland Mall
Priestville Anticline
Trans-Canada
Thorburn
Plymouth Fault
Hollow Fault
5 km
(D)
UNITS IN THE STELLARTON BASIN
STELLARTON FORMATION (PENNSYLVANIAN)
WESTPH. D?
WESTPHALIAN C
WESTPH. A
Captain
MacKay
Sixfoot
McBean
THORBURN MBR.
COAL BROOK MBR.
McLeod
Foord
Third
Cage
Fleming-McGregor
ALBION MBR.
PLYMOUTH MBR.
WESTVILLE MBR.
Acadia
Scott
SKINNER
BROOK MBR.
MIDDLE RIVER MBR.
MISSISSIPPIAN
MABOU GROUP (VISEAN-NAMURIAN)
WINDSOR GROUP (VISEAN)
(E)
MAP SYMBOLS
River
Highway
(Known
Inferred
Conjectured)
Stratigraphic contact
Strike-slip fault
Reverse fault
Normal fault
Minor fault
Bedding (overturned, upright, unknown)
Anticline, syncline

Figure 5.7: (A): The regional geology of Atlantic Canada with the Maritimes Basin and the smaller subbasins. The significant faults and structural features are annotated as red lines. The stars represent the Bay St. George subbasin (bsg), Cumberland subbasin (CU), and Stellarton subbasin (st). (B): The enlargement of the Cumberland Basin with the major stratigraphy in the basin. The red line represents the seismic profile shown in Figure 5.8. (C): The enlargement of the Stellarton subbasin, where (D) shows the major stratigraphy and (E) is the legend for the map symbols of the Stellarton subbasin in (C). Figure modified after Waldron (2004), Waldron et al. (2013), Waldron et al. (2015).

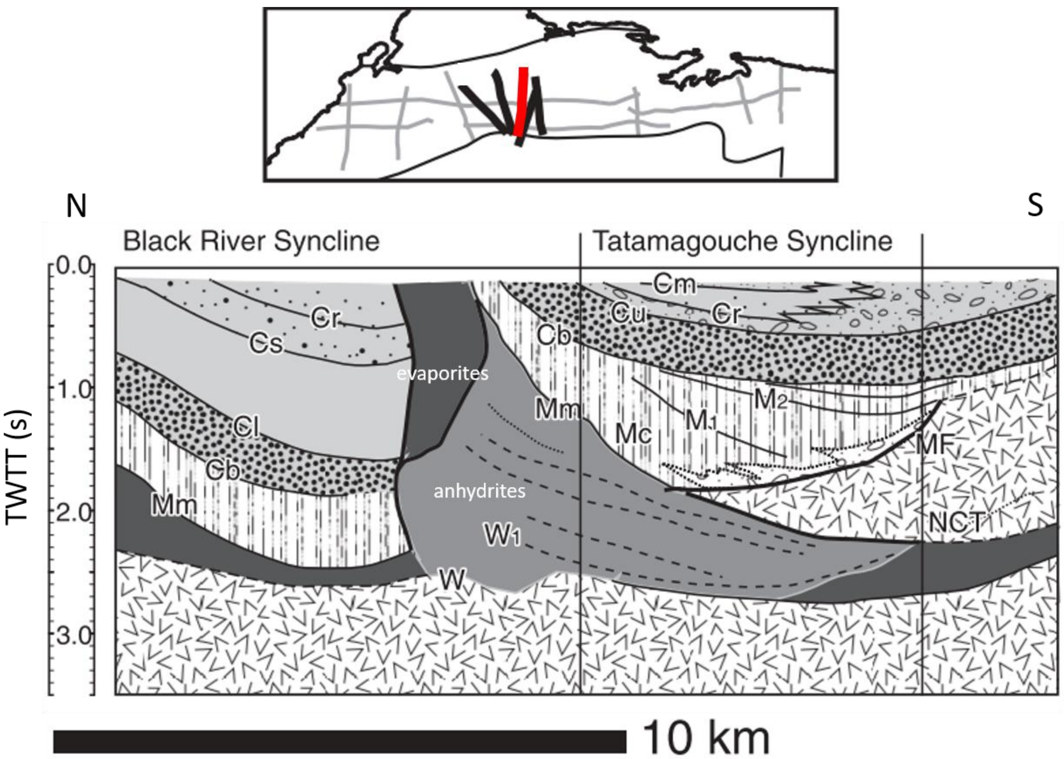

Figure 5.8: An interpreted seismic section displaying salt-related features, such as synclines and an oval-shaped salt-expelled minibasin. The map above the interpreted seismic section is a simplified version of Figure 5.7B. Figure from Waldron et al. (2013).

5.4 Moho and Crustal Variations

The Moho depth and crustal thickness variations of the Bay St. George subbasin provide the crustal framework for deciphering the basin's formation. The extracted depth to Moho from the 3-D gravity inversion is derived using a Moho proxy of 2.90 g/cm^3. The crustal thickness is determined using the depth to Moho and top basement surfaces. The depth to Moho and crustal thickness obtained from this study are compared with the Marillier & Verhoef (1989) results. They performed a gravity inversion focusing on the entire Gulf of St. Lawrence using complete Bouguer gravity data, deep seismic data, and well logs. Although Marillier & Verhoef (1989) focused their analysis on the Gulf of St.

Lawrence and the Maritimes Basin, their results still apply to the Bay St. George subbasin since it is a part of the broader Maritimes Basin.

The depth to Moho of the Bay St. George subbasin derived from the 3-D gravity inversion in this study ranges from 39–49 km with an average Moho depth of 46 km (Figure 5.9A). Overall, the shallowest Moho depth is observed in the central offshore, with the Moho depth increasing radially (Figure 5.9A). The general shape of the depth to Moho map in Figure 5.9A shows a NNE–SSW/E–W orientation corresponding to the approximate orientation of the strike-slip motion responsible for opening the Bay St. George subbasin. The NE–SW trend of the depth to Moho and the patterns described in this study are also observed by Marillier & Verhoef (1989) (Figure 5.9B). They derived a depth to Moho for the entire Gulf of St. Lawrence, with depths ranging from 34–49 km and an average depth of 43 km (Figure 5.9B). This was determined by setting an average depth to Moho of 42 km obtained from the deep seismic profiles. The gravity inversion from the present study derives a deeper depth to Moho than Marillier & Verhoef (1989). The deeper depth to Moho translates into a thicker crust, suggesting less extension may have occurred than previously interpreted. However, the density used for the Moho-proxy in the present work must be considered when comparing the two.

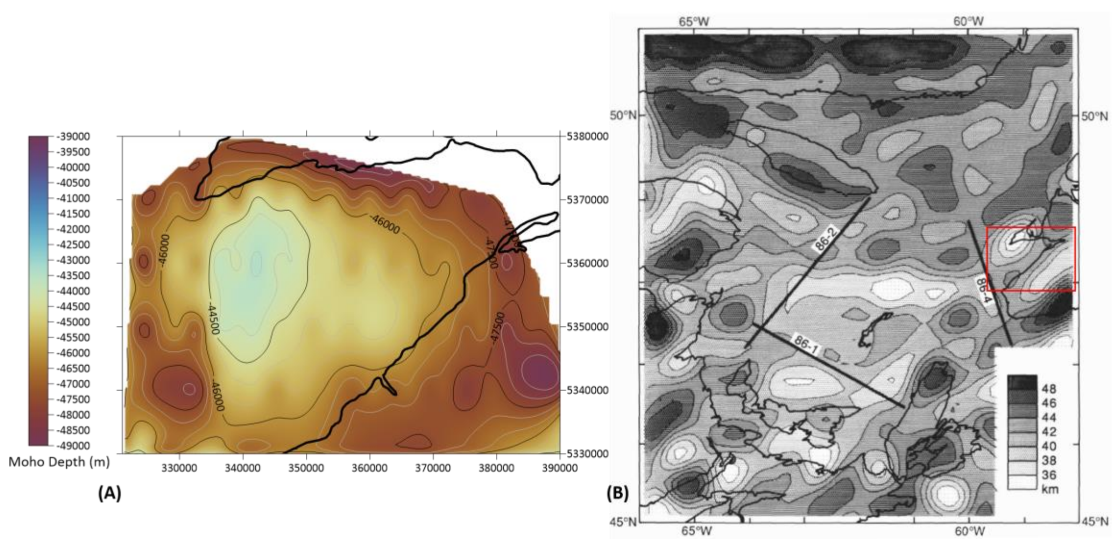

Figure 5.9: The depth to Moho maps, where (A) is derived from the gravity inversion in the present study and (B) is obtained from Marillier & Verhoef (1989). The red box is the approximate location of the Bay St. George subbasin.

The Bay St. George subbasin crust is subdivided into an upper and lower crust using a mid-crustal density proxy of 0.0 g/cm^3 (relative to 2.67 g/cm^3). Figure 5.10 displays the crustal variations of the upper and lower crustal thicknesses. The fairly high crustal thicknesses correlate with the deep Moho obtained from the gravity inversion. The regional faults are also displayed on this figure, providing potential structural boundaries within the crustal layers. Overall, a thicker upper crust is observed near the central offshore with a thinner upper crust towards the west (Figure 5.10A). The lower crustal thickness map shows a thinner lower crust near the central offshore and a thicker lower crust towards the west (Figure 5.10B). The southeastern part of the crustal thickness maps shows a thin upper crust and thick lower crust, delimited by the LRF. Variations in the upper and lower crust (Figure 5.10) may be due to crustal-scale faults.

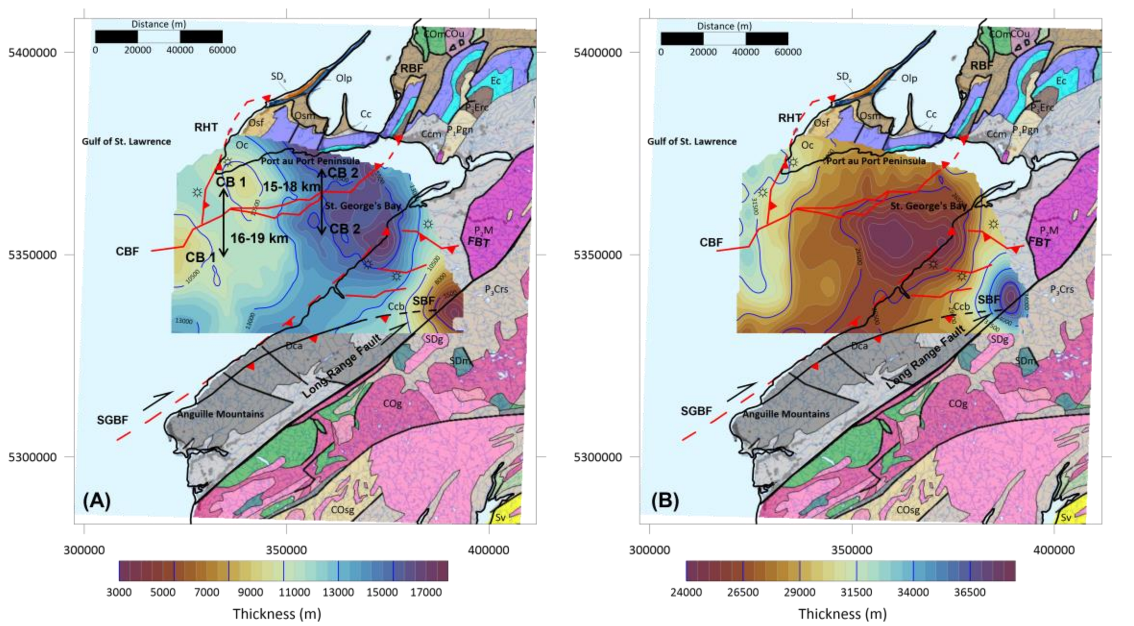

Figure 5.10: The crustal thickness maps with the regional faults displayed where (A) is the upper crustal thickness map and (B) is the lower crustal thickness map. CB1 and CB2 are annotated as crustal blocks. The vertical arrows emphasize the distance from the center of the crustal blocks. The crustal thickness maps are obtained using the depth to Moho, top basement, and mid-crustal boundary surfaces. The legend for these maps is shown in Figures 1.1, 3.18, and 5.5. The faults and onshore geology are after Coleman-Sadd et al. (2000), Knight (1983), Langdon & Hall (1994), and this study.

The regional faults displayed in Figure 5.10 reveal evidence of juxtaposed contrasting crustal blocks. Crustal blocks are described as blocks of crust separated by a deep crustal-scale fault. Crustal Block 1 (CB1) and Crustal Block 2 (CB2) are examples of crustal blocks that have been juxtaposed from crustal-scale faults (Figure 5.10A). The offset between the two parts of CB1 towards the northwest part of the basin correlates with the Round Head Thrust (RHT) (Figure 5.10A). These crustal blocks appear to have the same thickness, suggesting that they may have once been continuous. The distance between the centers of the CB1 blocks is approximately 16–19 km implying that the RHT affected shallow and deep crustal structures (Figure 5.10). The Central Bay Fault (CBF) also contributes to the offset of these crustal blocks as this fault truncates the northeast CB1 block. Based on the RHT and CBF timing, it is inferred that the RHT exerted the primary influence on offsetting the CB1 block. The CBF later truncated the crustal blocks during early reactivation of the RBF and deposition of early Carboniferous sediments (Late Devonian–Early Carboniferous). Another example of offset crustal blocks derived from a similar origin is in the eastern part of the basin (CB2), and these are associated with the CBF (Figure 5.10A). The movement of the two parts of CB2 is inferred to have occurred after the movement of the CB1 blocks. The distance between the centers of the CB2 blocks is approximately 15–18 km (Figure 5.10). The amount of distance between these crustal blocks and the timing of the CBF imply that they were likely offset shortly after the reactivation of the RHT and during the early stages of the basin formation, agreeing with the deformation history determined from the seismic profiles.

The juxtaposition of crustal blocks with contrasting thicknesses is suggested throughout the southern extent of the Bay St. George subbasin towards Nova Scotia. However, there are limited constraints to derive the amount of slip that may have produced the juxtaposition of some crustal blocks in this study. It is also challenging to determine if these crustal blocks originated together because the crustal maps only constrain the existing blocks within the basin. The amount of distance between some juxtaposed crustal blocks may not be recoverable because the gravity modeling is restricted to the Bay St. George subbasin. Nonetheless, the juxtaposition of contrasting crustal blocks is expected to persist to the southwest due to the regional-scale basin bounding faults and the overall trend of the Appalachian Orogeny. In total, 250 km of late Paleozoic strike-slip motion is inferred to have affected the Northern Appalachians in Atlantic Canada, resulting in the juxtaposition of contrasting crustal blocks (Waldron et al., 2015). This extensive fault movement likely also affected the Bay St. George subbasin. The juxtaposed contrasting crustal blocks may have moved significant distances towards the Maritimes Basin along crustal-scale faults such as the Long Range Fault (Cabot Fault) to their current position (Waldron et al., 2015).

Overall, there are slight variations in density contrasts modeled throughout the lower crust within the Bay St. George subbasin. High-density lower crustal blocks have been used to explain the density differences and shallow Moho depths beneath the Maritimes Basin (e.g., Marillier & Verhoef, 1989; Marillier et al., 1991; Michel et al., 1992). Such high-density lower crustal blocks are also inferred to exist beneath the Bay St. George subbasin, given the regional tectonic history.

There are several hypotheses regarding the origin of the contrasting densities within the lower crust. One possible origin is mafic underplating due to the opening of the Atlantic Ocean during Mesozoic rifting (Marillier et al., 1991). However, this is unlikely because there is no evidence of Mesozoic rifting within Western Newfoundland. High-density lower crustal blocks are commonly produced in convergent environments by trapping subducted oceanic crust (Marillier et al., 1991). A convergent environment for the Bay St. George subbasin is also an unlikely origin for the high-density lower crust since the active subduction zone during the closing of the Iapetus Ocean was situated further east (Stockmal et al., 1990). Movement along a shear zone may explain the juxtaposition of contrasting high-density lower crustal blocks (Marillier et al., 1991). This suggestion is based on the juxtaposition of highly reflective and relatively unreflective crust, crosscut by northwest dipping reflectors, where the northwest dipping reflectors may represent a shear zone (Marillier et al., 1991).

Based on the synthesis of the results from this study, the mafic underplating interpretation is preferred for the high lower crustal densities. The mafic underplating is suggested to occur during the Late Precambrian–Early Cambrian rifting of the Iapetus Ocean or during the reactivation of Carboniferous strike-slip motion creating the Bay St. George subbasin. Mafic underplating due to one of these tectonic events is the preferred origin of juxtaposed contrasting crustal blocks proposed by Marillier et al. (1991). The present study suggests that contrasting high-density lower crustal blocks (2.8 g/cm^3) have been juxtaposed during multiple tectonic evolutionary stages. The contrasting lower crustal blocks is inferred in the northwestern part of the basin due to the Early Carboniferous transtensional motion. The RHT, located in the northwestern part of the basin, initially formed during the rifting of the Iapetus Ocean and was subsequently reactivated during the Early Carboniferous strike-slip motion. The evidence of juxtaposed lower crustal blocks is observed along a density profile associated with the RHT (Figure 5.11B). This density profile shows higher densities for the lower crust in the north than in the south. This shows that the lower crust is thicker to the north or the upper crust is thinner. Continued strike-slip motion during the Middle Carboniferous juxtaposed high-density lower crustal blocks within the southern parts of the basin. The evidence of contrasting lower crustal blocks in the southeast is associated with the Long Range Fault (LRF) (Figure 5.11A). This density profile reveals the depth extent of the LRF by placing high-density lower crust to the southeast and low-density lower crust to the northwest. From the timing of these faults and the structural characterization, it is proposed that the Early Carboniferous strike-slip motion influenced the lower crust in the northern part of the basin. In comparison, the lower crust in the southern part of the basin was affected by the Middle–Late Carboniferous strike-slip motion. The present study suggests that the Bay St. George subbasin is broadly compartmentalized into northwest/west and southeast/east structural domains, separated by the CBF. The crustal structures in the northwest were dominantly affected by Early Carboniferous deformation, while the crustal structures in the southeast were primarily influenced by Middle–Late Carboniferous deformation. Robbins (2000) performed a similar structural characterization, where they identified northern and southern half-graben structures separated by the CBF. They mainly characterized the basin using shallow seismic data and did not consider crustal-scale structures. Therefore the work from the present study extends those insights to the crustal-scale view of the basin and greatly improves the structural characterization initially proposed by Robbins (2000).

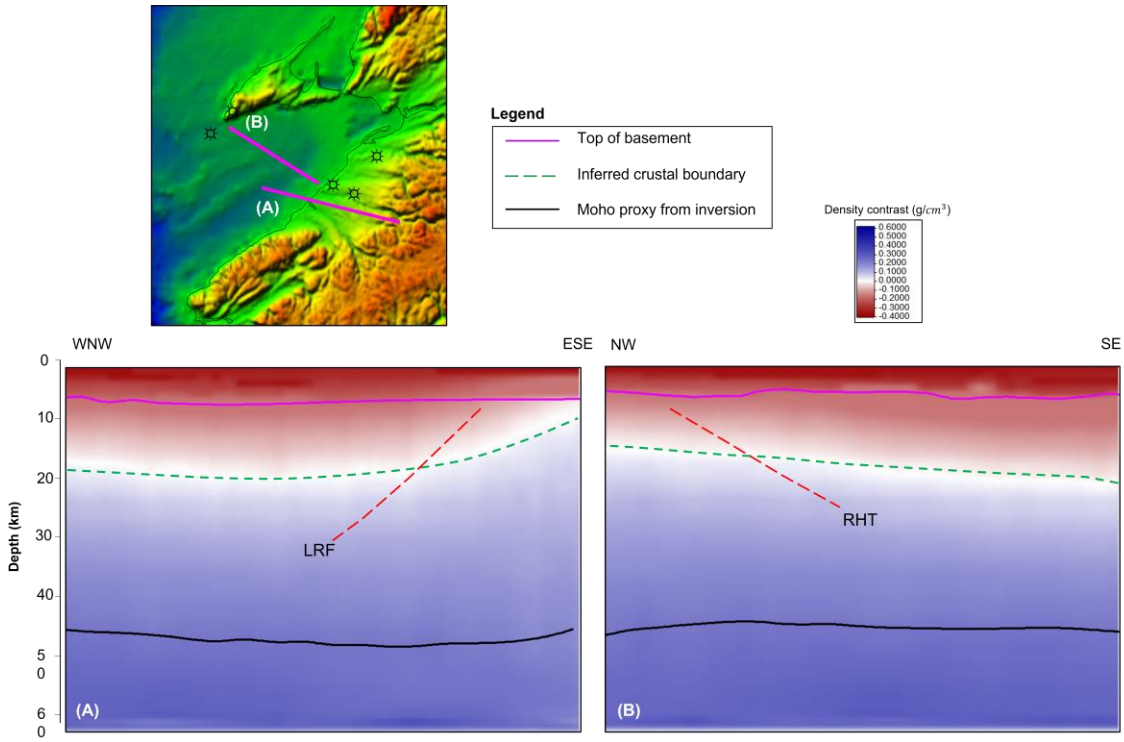

Figure 5.11: Density profiles with inferred crustal-scale faults juxtaposing lower crustal blocks with contrasting densities. (A): An example of a density profile with the interpreted LRF juxtaposing high-density lower crust in the southeast and low-density lower crust in the northwest. (B): An example of a density profile with the interpreted RHT juxtaposing high-density density lower crust in the northwest and low-density lower crust in the southeast. This implies thicker lower crust in the north or thinner upper crust.

5.5 Global Analogs

Global analogs herein are used to contrast the geometry and structure of the Bay St. George subbasin with similar basins elsewhere. Global analogs in the Bohai Basin, NE China (Figure 5.12) (Allen et al., 1998), and the Stellarton Basin, Nova Scotia (Figure 5.7) (Waldron, 2004, 2005) are compared since they have similar structural elements. These analogs represent larger (Allen et al., 1998) and smaller (Waldron, 2004, 2005) scale basins to help understand the Bay St. George subbasin better.

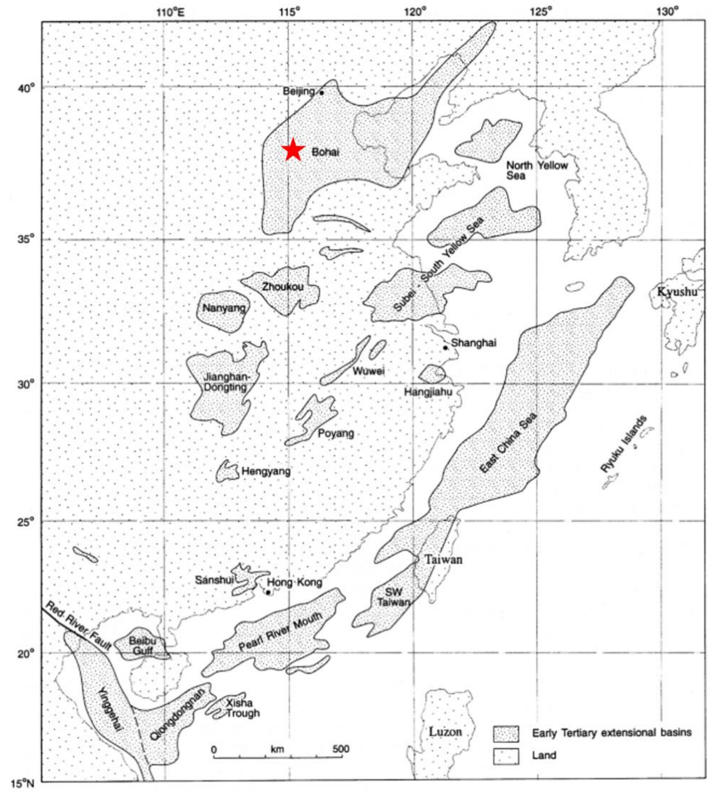

Figure 5.12: The location of Tertiary extensional basins located in eastern China. The red star is the location of the Bohai Basin. Figure from Allen et al. (1998).

The Bohai Basin, NE China (Figure 5.12), was initially characterized as either a pure dextral strike-slip basin (Klimetz, 1983) or an extensional rift basin with minor or no strike-slip deformation (Ye et al., 1985). Allen et al. (1998) proposed that the Bohai Basin is formed by dextral transtension using available 2-D and 3-D seismic data and well logs. This basin characterization also applies to the Bay St. George subbasin as similarities are observed. Transtensional basins are characterized by containing an *en echelon* array of individual normal faults oriented obliquely to the boundaries within the deformation zone (Figure 5.13) (Allen et al., 1998). One or both margins of the transtensional zone may be a normal or strike-slip fault (Figure 5.13). Alternatively, a hybrid model is possible, where the deformation zone is represented by a half-graben structure, with one margin faulted and one un-faulted (Figure 5.13) (Allen et al., 1998). The Bohai Basin is described as resulting from a transtensional regime where individual normal faults within half-grabens are striking obliquely to the basin bounding fault (Figure 5.14) (Allen et al., 1998). The array of these normal faults is defined as having an *en echelon* pattern and is oriented parallel to the basin-bounding fault as a whole (Figure 5.14) (Allen et al., 1998). The overall geometry of this basin represents dextral pull-apart, with a set of east–west trending normal faults in the central parts of the basin bounded by a dominantly northeast–southwest dextral strike-slip fault system (Figure 5.14) (Allen et al., 1998).

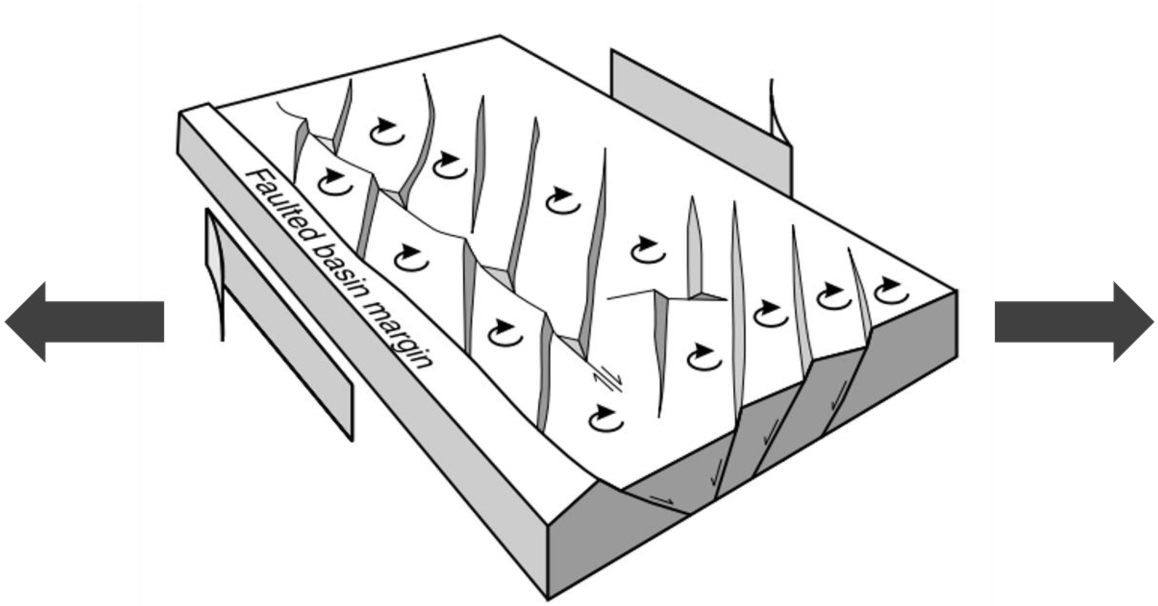

Figure 5.13 The idealized structure of a dextral transtensional basin. The grey-filled zones within the basin represent normal faults, where each fault within the deformation zone is collectively an array of *en echelon* faults oriented obliquely to the basin bounding fault. The fault blocks within the basin provide evidence of rotational deformation. The large arrows indicate an overall extensional motion. Figure from Allen et al. (1998) and Waldron (2005).

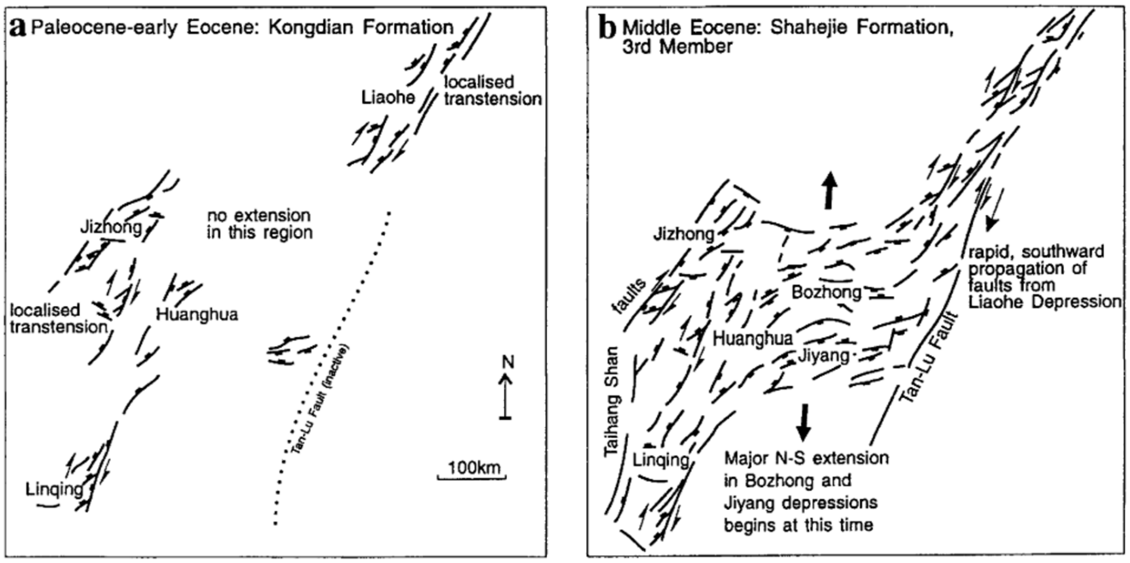

Figure 5.14: The Tertiary tectonic evolution of the Bohai Basin. (A): Initial dextral transtension primarily occurred in the western part of the basin. (B): Middle Eocene rifting propagated towards the south, creating an extensional overlap (Bozhong Depression). The dominant east–west normal faults striking obliquely to the basin bounding fault are suggested to have developed during the creation of the extensional overlap in an environment similar to classic pull-apart basins but more complex. Figure from Allen et al. (1998).

These structural descriptions identifying the Bohai Basin as a dextral transtensional basin are strikingly similar to the Bay St. George subbasin in the present study. The Bay St. George subbasin is described to have initially formed as a pull-apart basin, developed from multi-stage dextral strike-slip faults (Knight, 1983). The subsidence and deposition of sediments are suggested to have occurred from dextral strike-slip faults that also show extensional motion (Knight, 1983). Knight (1983) describes the Bay St. George subbasin as a pull-apart basin with the possibility of wrenching. In a true pull-apart basin, there is zero extension across the deformation zone (Allen et al., 1998). A better basin characterization from the present study is that of a transtensional basin, similar to the Bohai Basin. The Bay St. George subbasin has similar structural elements to transtensional basins (e.g., Bohai Basin), including an *en echelon* array of normal faults striking oblique to the boundary of the deformation zone (faulted basin margin) (Allen et al., 1998). Rotated fault-bounded crustal blocks (transrotational basins) are often defined as transtensional basins (Allen et al., 1998; Ingersoll, 1988), and this is modeled by Waldron et al. (2015) for the Maritimes Basin (Figure 5.15). Rotated fault-bounded crustal blocks provide further evidence that a transtensional basin characterization better fits the Bay St. George subbasin

(Figure 5.15). Overall, the Bay St. George subbasin represents a pull-apart structure, although the basin is much larger than typical pull-apart basins. The structure of the Bay St. George subbasin does not show pure strike-slip since transtensional deformation is present. The Bay St. George subbasin displays a dominantly dextral strike-slip fault (LRF) bounding the basin where transtensional faults with half-graben structures are striking obliquely to the faulted margin (Figure 5.17).

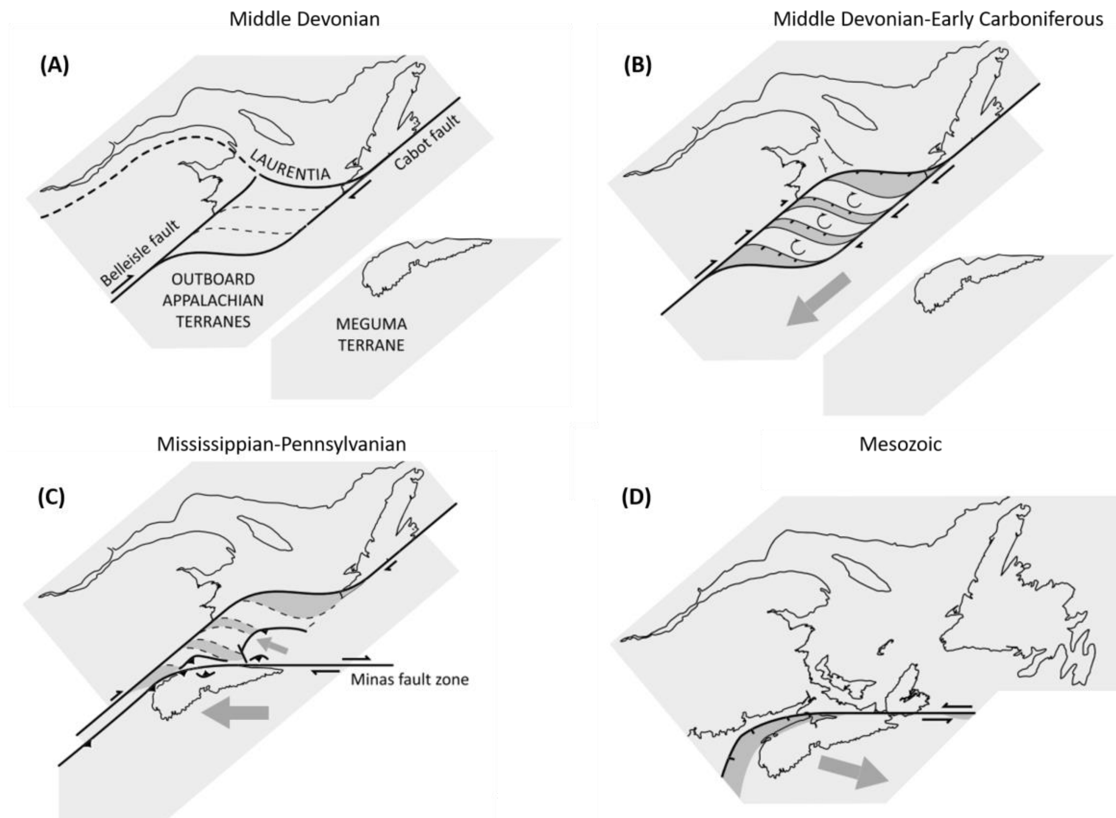

Figure 5.15: Simplified diagram of the kinematic history of the Maritimes Basin. The Cabot Fault is also often referred to as the Long Range Fault in this study. (A): Initiation of a broad zone of transtension. (B): Post transtension, where the fault blocks have subsided and rotated clockwise. The actual number of fault blocks is not represented. (C): Westward movement of Meguma on the Minas fault imposing dextral transpression. (D): The opening of the modern Atlantic Ocean. Figure from Waldron et al. (2015).

Waldron (2004; 2005) analyzed the rotational strain of faults and the overall structure of the Stellarton Basin, Nova Scotia (Figure 5.7). The rotational strain of faults is essential to consider when modeling since it can quantify transtensional deformation. This analysis is often not included since most simplified models ignore rotation. The Carboniferous Stellarton Basin is a part of the broadly distributed Maritimes Basin (Figure

5.7), and the structural evolution from Waldron (2004) may be applied to the analogous Bay St. George subbasin. Furthermore, the kinematic analysis from Waldron (2005) may also infer structural constraints on the Bay St. George subbasin because of the similar regional tectonic evolution.

The structure and geometry of the Stellarton Basin are examined by Waldron (2004) using outcrop studies and seismic data. Waldron (2004) determined that the Stellarton Basin displays dextral strike-slip motion followed by progressive strain creating rotated fault blocks (Figure 5.16B). Compressional deformation is also observed, including younger reverse faults within the basin and a positive flower structure (Figure 5.16C). The compressional deformation evidence indicates that the transition from transtension to transpression may be inevitable during the continued deformation due to strike-slip motion and is suggested to be characteristic of basins developed along major strike-slip faults (Figure 5.16D) (Waldron, 2004). This analogy likely applies to all sedimentary basins developed in similar settings, such as the Bay St. George subbasin (Waldron, 2004). Younger compressional structures in the Bay St. George subbasin, such as the Flat Bay Thrust, may be evidence of this transition to transpressional deformation. This compressional feature may indicate transpressional deformation during the late Pennsylvanian–Permian that is inferred in other areas of the Northern Appalachians (Gibling et al., 2002).

Waldron (2005) measured fault heaves and orientations using subsurface mine plans within the Stellarton Basin to derive the shear strain and divergence angle (α), which can quantify how much transtension occurred in a basin. This quantifies the basin characterization while including the importance of rotational strain, unlike simpler models. This kinematic analysis is not done in the present study for the Bay St. George subbasin due to a lack of 3-D seismic data. However, given the regional tectonic history, the Stellarton Basin results are assumed to be similar to the Bay St. George subbasin. Waldron (2005) determined that transtensional deformation occurred in the Stellarton Basin with a divergence angle of 6–8°, lower than the expected divergence angle of 24°. This is a consequence of only including a subset of the significant faults, excluding minor faults with little offset. These major faults only relate to a small part of the deformation history, and outcrop studies indicate minor faults are essential to consider when calculating the divergence angle (Waldron, 2005). The quantitative transtensional deformation results may apply to the Bay St. George subbasin providing further constraints on the basin development. The divergence angle is inferred to range from 6–24 ° in the Bay St. George subbasin and implies significant transtensional deformation occurred.

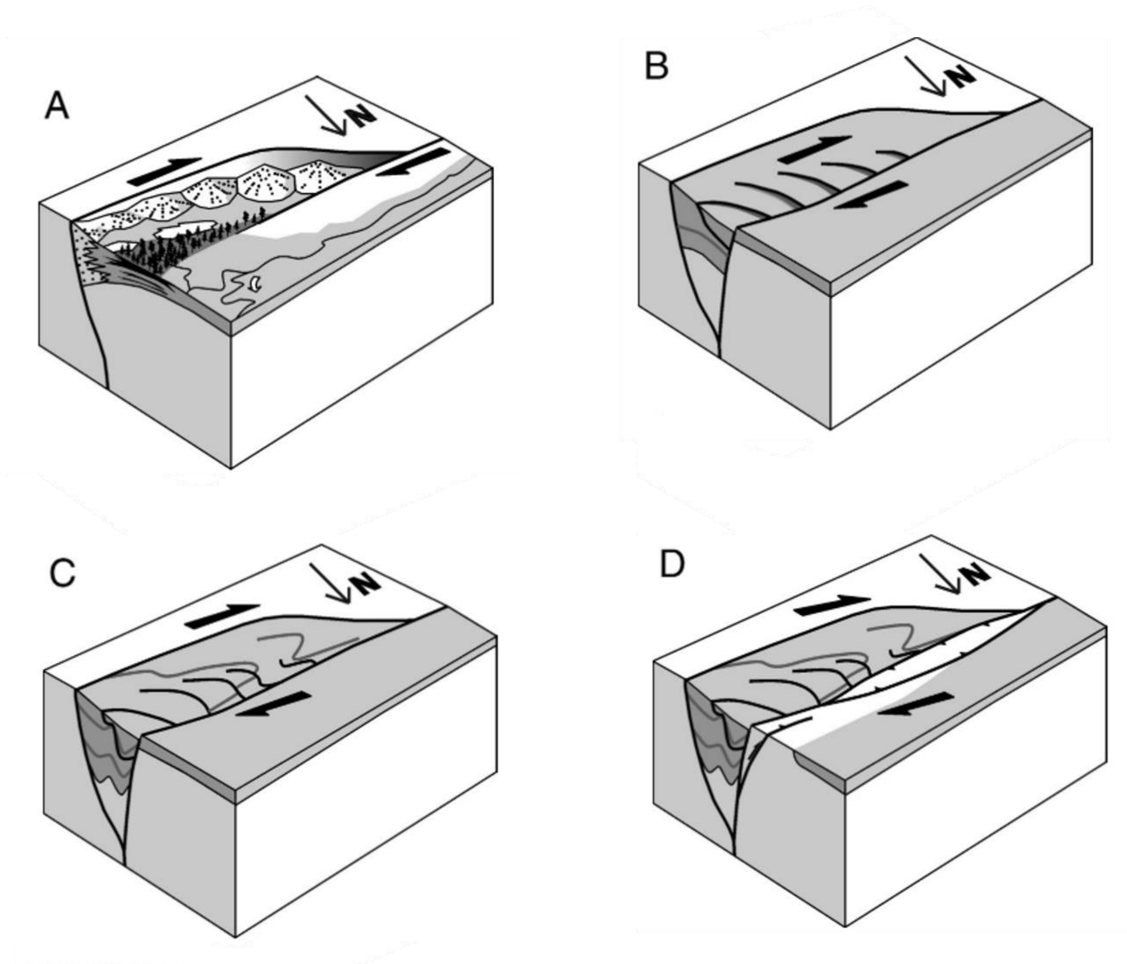

Figure 5.16: The simplified diagrams of the structural evolution of the Stellarton Basin. (A): Differential subsidence initiates throughout the basin. (B): An array of *en echelon* faults are created with rotated fault blocks. (C): Faults become folded during progressive deformation due to transtension or the transition from transtension–transpression. (D): Transpressional deformation occurs with continued folding and the generation of positive flower structures. Figure from Waldron (2004).

5.6 Tectonic Evolution of the Bay St. George Subbasin and Broader Implications

The tectonic evolution of the Bay St. George subbasin is actively discussed throughout this study. Comparisons with other basins of similar tectonic origin are contrasted to better understand the Bay St. George subbasin. The tectonic evolution of the Bay St. George subbasin has regional implications to the broader Northern Appalachians that may impact future studies. This section summarizes the tectonic evolution of the Bay St. George subbasin determined using the data in this study and previous literature. The structural evolution of the Bay St. George subbasin is displayed in Figure 5.17. Broader implications that apply to the Northern Appalachians are also inferred from the detailed geological evolution of the Bay St. George subbasin.

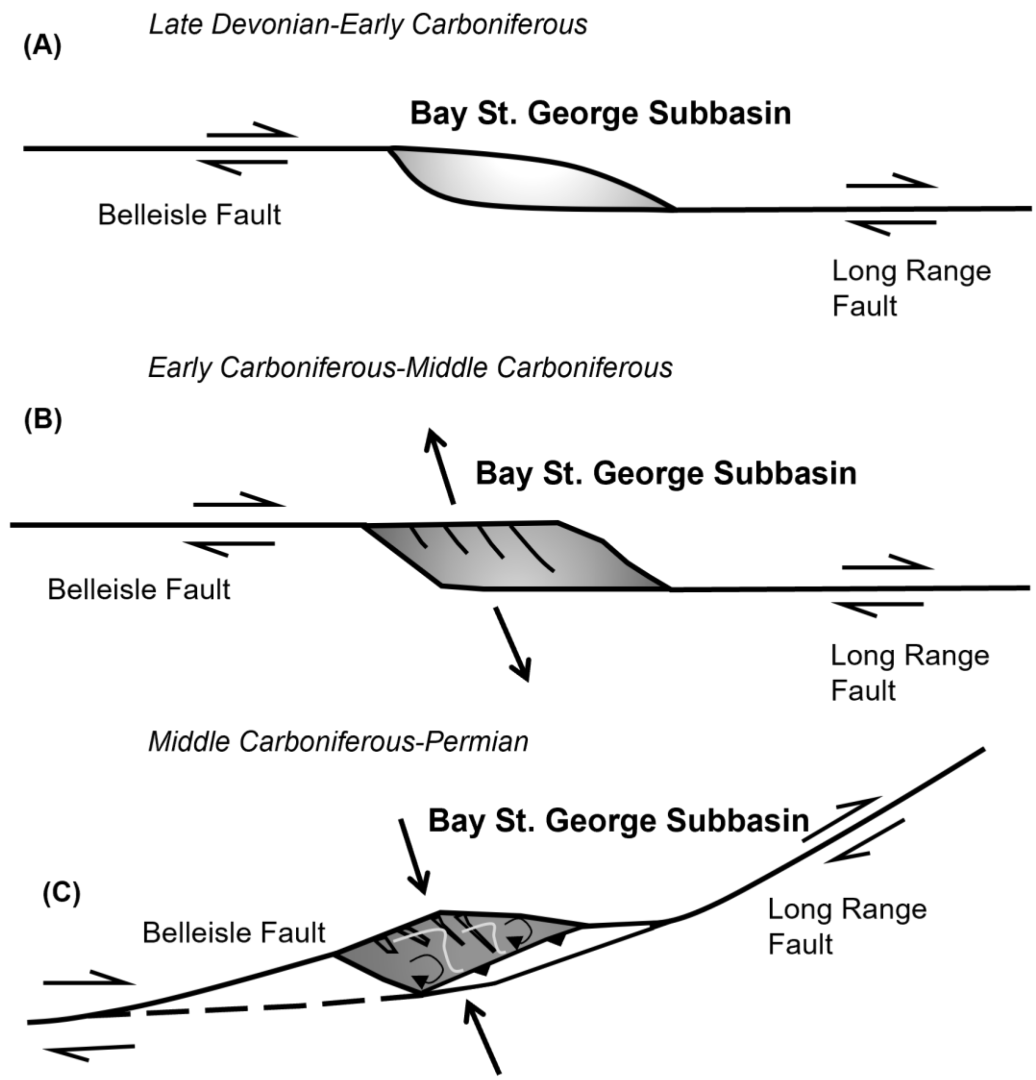

Figure 5.17: Map view diagrams showing the structural evolution of the Bay St. George subbasin. (A): Early Carboniferous dextral strike-slip faulting creating the pull-apart basin. (B): Early–Middle Carboniferous deformation along extensional faults within a transtensional environment. (C): The basin transitions to a transpressional environment during the Middle Carboniferous–Permian. Folds and rotation of fault blocks are also represented during this time. Figure modifed after Waldron (2004).

A newly constrained structural evolution of the Bay St. George subbasin is provided in the present study (Figure 5.17). The Bay St. George subbasin developed during the Late Devonian to Carboniferous due to the dextral strike-slip Long Range Fault (LRF) (Figure 5.17) (Knight, 1983). Knight (1983) notes that the basin began as a pull-apart basin primarily controlled by the LRF and formed where a splay fault developed off the LRF and trended northwest, creating the northern margin of the basin (Figure 5.17A). This splay fault is defined as the Belleisle Fault, although there is little evidence of this fault's existence in the Bay St. George subbasin (Webb, 1968). Deposition of sediments occurred from transtensional faults within the basin during the progression of basin development (Knight, 1983). The Bay St. George subbasin contains transtensional faults that strike obliquely to the faulted basin margins (Figure 5.17B). The array of these transtensional faults displays an *en echelon* pattern and strikes parallel to the basin as a whole similar to the Bohai Basin (Figure 5.17B) (Allen et al., 1998).

Reactivation and inversion of earlier transtensional faults occurred as thick-skinned deformation (Stockmal et al., 2004). Differential subsidence and sedimentation progressed as the pull-apart basin was gradually affected by fault reactivation and inversion (Figure 5.17B) (Knight, 1983). This is evident from the fault interpretation in the present study, including reactivated inverted faults like the Round Head Thrust (RHT). The RHT is suggested to have been reactivated and inverted during the early stages of basin development (Devonian–Carboniferous) (Dafoe et al., 2016; Stockmal et al., 2004). The Flat Bay Thrust (FBT) and other reverse faults annotated in Figure 5.4A demonstrate transpression with no indications of initial transtension. These faults are likely derived from progressive deformation that occurs in strike-slip basins similar to the Stellarton Basin, Nova Scotia (Waldron, 2004) (Figure 5.17C).

The transition from transtension to transpression is often inevitable during progressive deformation due to the strike-slip faulting characteristics of strike-slip basins (Waldron, 2004). Products of this transition include finite rotation and changes in basin bounding faults (Waldron, 2004). Transpression developed along the Minas Fault, as evident from the FBT and likely occurred during the convergence of Laurentia and Gondwana that resulted in the Alleghanian Orogeny (Figures 5.15 and 5.17C) (Waldron et al., 2015).

Halokinesis also occurred during the transition from transtension to transpression, further complicating the tectonic evolution of the basin. Salt-related structures reveal essential correlations with the tectonic evolution of the basin. Doubly plunging salt-cored anticlines display *en echelon* characteristics parallel to the basin bounding faults (Figure 5.17C). This suggests a relationship between the salt movement and salt-cored anticlines that correlate with the NE–SW transtensional environment of the Bay St. George subbasin (Dafoe et al., 2016; Waldron et al., 2013).

The Bay St. George subbasin is characterized as a transtensional basin based on the present study and according to the definition of transtensional basins proposed by Allen et al. (1998). The Bay St. George subbasin demonstrates an overall pull-apart structure due to the dextral LRF (Late Devonian–Early Carboniferous). The basin does not show pure strike-slip as normal faults are present within a transtensional environment. Subsidence and deposition of sediments occurred within this transtensional environment (Early Carboniferous–Middle Carboniferous). Reactivation and inversion occurred during and after sediment deposition as the basin developed. The basin evolved, corresponding with a transition from transtension to transpression inevitable during progressive deformation in strike-slip basins (Middle Carboniferous–Permian) (Waldron, 2004).

The tectonic evolution of the Bay St. George subbasin covers only a relatively small part of the broader regional tectonic evolution of the Northern Appalachian Orogeny and Maritimes Basin (Figure 5.18). The findings in the present study provide additional constraints on the tectonic evolution of the Maritimes Basin and the broader Appalachian Orogeny. Based on the synthesis of the present study results, a change from transtension to transpression is documented in parts of the basin (Figure 5.18B). The transition boundary may correspond with the northern limit of transpression occurring during the convergence of Laurentia and Gondwana. The transtension to transpression border is a key boundary as it may mark the Northern Appalachian deformation front and improve structural reconstructions of the Northern Appalachians.

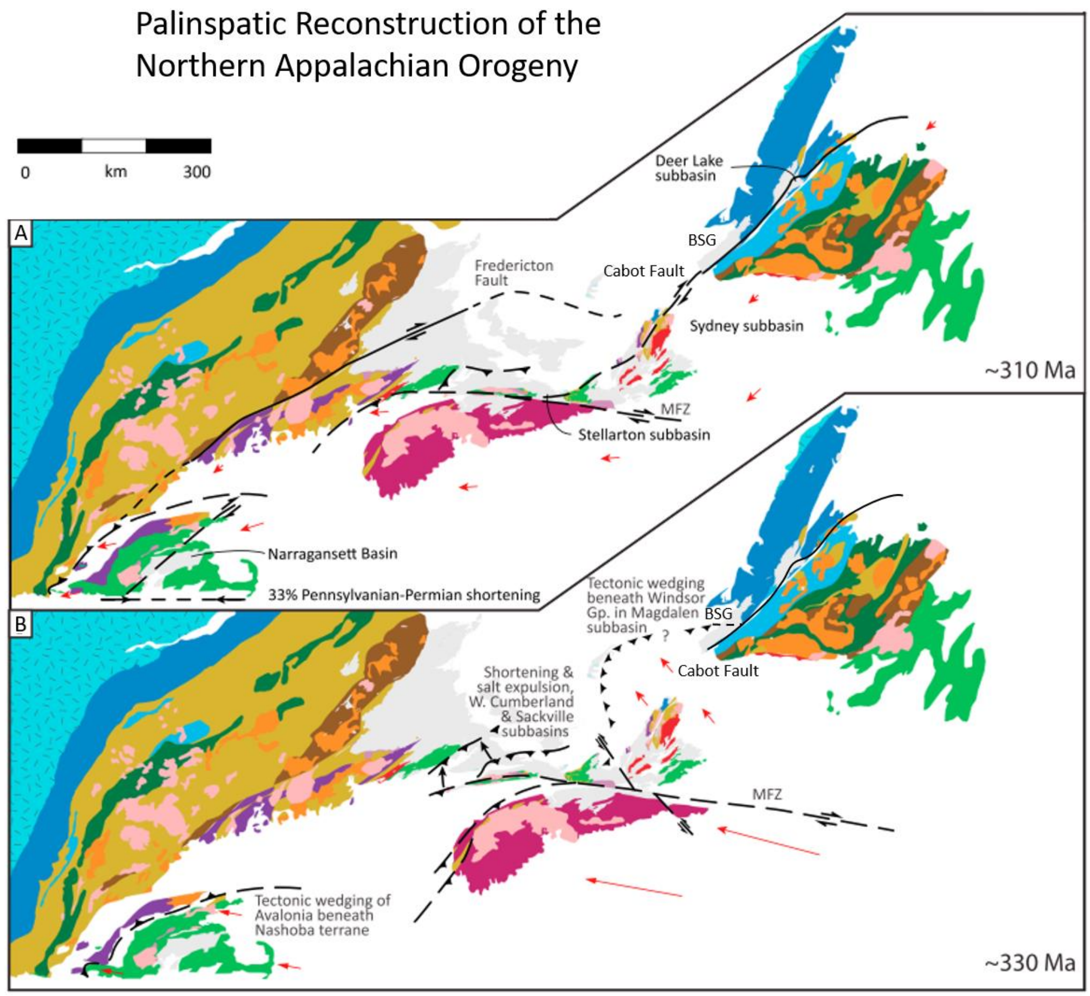

Figure 5.18: The Palinspatic reconstructions of the Northern Appalachian Orogeny from ca. 330 Ma to 310 Ma. The red arrows indicate the motion relative to Laurentia, and the black arrows indicate relative motion at the terrane boundaries. (A): This reconstruction shows most of the fault motion affecting the Stellarton subbasin. 25 km of slip is suggested to have occurred in the Stellarton subbasin and likely extended through Newfoundland. (B): This reconstruction displays compression propagated along the Minas Fault Zone (MFZ), extending to the Bay St. George subbasin (BSG). Figure from Waldron et al. (2015).

Large amounts of slip, including tens of kilometers for individual faults and a total of 250 kilometers, resulted from strike-slip motion in the Northern Appalachian Orogeny of Atlantic Canada (Waldron et al., 2015). The present study provides evidence of this slip as juxtaposed lower crustal blocks with contrasting densities are recovered from the 3-D inverted model. The juxtaposed crustal blocks likely resulted from the large regional faults related to the Northern Appalachian Orogeny (Figure 5.18). The significant amount of motion produced from regional faults in Atlantic Canada is evident in Figure 5.18. This figure provides context into the importance of the crustal-scale variations observed in the Bay St. George subbasin. Constraints from the present study involving the Bay St. George subbasin should be implemented in structural restorations.

Chapter 6 Conclusions and Future Work

This chapter provides the conclusions and major takeaways from the present study. This includes a summary of the work done, the important new findings in this study, and provides supportive evidence for previously suggested concepts. Recommendations for future work in the Bay St. George subbasin that would improve the geological understanding are suggested. The future work recommendations include investigations that involve acquiring more data and also using the currently available data.

6.1 Conclusions

Western Newfoundland, in particular the Bay St. George subbasin, is a geologically complex area that has undergone multiple significant tectonic phases. Although the onshore part of the Bay St. George subbasin is fairly well understood (Knight, 1983), the offshore geology is poorly constrained, as are the correlations between the onshore-to-offshore. Furthermore, there is a lack of crustal-scale knowledge regarding the Bay St. George subbasin. The knowledge gaps of onshore-to-offshore geology for the Bay St. George subbasin and the crustal-scale structures were addressed in the present study. A 3-D density model of the Bay St. George subbasin was generated using seismic and well log constraints to better understand the deep crustal-scale structures and correlate them with the broader Northern Appalachian Orogeny. A newly updated tectonic evolution model was constructed for the Bay St. George subbasin using the 3-D inverted density model and seismic interpretation results.

The 2-D seismic reflection data revealed variations in basin thickness throughout the basin, with significant thickening observed near the coastline. The variations in basin thickness indicated differential subsidence that likely progressed from the south towards the north. A new small offshore sedimentary basin was discovered south of the Port au Port Peninsula, related to major faults in the area that contributed to the tectonic evolution of the Bay St. George subbasin. This newly interpreted small sedimentary basin was likely related to the transtension to transpression transition inferred in the Bay St. George subbasin. The transtension to transpression change is a new concept determined from the present study regarding the tectonic evolution of the Bay St. George subbasin.

The generation of well ties was essential for a robust and improved seismic interpretation in this study since well logs give the geological ground truth to tie with the seismic data. Anguille strata were only observed onshore since the lone offshore well did not penetrate this unit. The offshore strata that underlie the Codroy Group were often thought to contain Anguille rocks, yet these units belong to the Cambrian–Ordovician carbonate platform successions. Although this was already determined, few studies have mapped surfaces below the Codroy Group (e.g., Dafoe et al., 2016). The present study mapped these deeper surfaces to better constrain the gravity inversions and improve upon the previous seismic interpretation studies.

The carbonate platform successions were correlated with the offshore well, providing a crucial structural relationship with the St. George Bay Fault (SGBF). Langdon & Hall (1994) previously interpreted these faults as truncating carbonate platform successions offshore; however, there was uncertainty about this interpretation since Dafoe et al. (2016) did not interpret this truncation. The present study supports the existence of these faults first identified by Langdon & Hall (1994), reducing this uncertainty.

Salt deformation was also widely observed in the Bay St. George subbasin, and it provides structural controls on the basin evolution. Although Snyder (2019) initially inferred the change in salt migration due to a tectonic wedge emplacement, the present study suggests it was likely due to differential loading.

Brittle deformation is prominent throughout the basin, and this study provided an updated structural framework to be used for future work in the area. The updated fault framework for the basin contains interpreted reactivated and inverted faults. These reactivated and inverted faults (e.g., Round Head Thrust) provided temporal constraints on the basin evolution, such that the Central Bay Fault (CBF) is younger than the Round Head Thrust (RHT). These regional faults are of significance as they juxtapose lower crustal blocks with contrasting densities. The 3-D density model from the present study revealed the depth of inferred regional faults based on juxtaposed densities. Juxtaposed crustal blocks were previously inferred in the Bay St. George subbasin; however, there was a lack of evidence to prove their existence (Marillier et al., 1991). Therefore, this new finding provided evidence to support the juxtaposition of lower crustal blocks within the Bay St. George subbasin.

The tectonic evolution of the Bay St. George subbasin has been updated with new concepts derived from this study. The main finding involving the tectonic evolution of the basin was the tectonic change from transtension to transpression as the basin evolved. The transtension to transpression transition was previously documented in other parts of the Maritimes Basin (e.g., Stellarton Basin) and was suggested to be present in other basins within Atlantic Canada (Gibling et al., 2002). This new finding provides evidence of the tectonic environment change in the Bay St. George subbasin and improves constraints on the broader tectonic evolution of the Maritimes Basin.

The poor petroleum exploration results in the past may be explained due to the complex tectonic history of the basin. The basin contains a highly compartmentalized subsurface with numerous faults, including reactivated and inverted faults as well as thrusts. Additionally, salt is abundant throughout the basin, creating further issues with subsurface interpretations. Predicting where hydrocarbon prospects are is a challenge due to these complex structures. This study reduces these subsurface complexities using an integrated dataset that will benefit future exploratory efforts.

6.2 Recommendations for Future Work

Future work that would improve the geological understanding of the Bay St. George subbasin includes acquiring more geophysical data. Additional deep seismic reflection and seismic refraction data would significantly improve crustal-scale investigations, supporting the proposed findings in this study. Most of the seismic reflection data within the Bay St. George subbasin are relatively shallow, and the only deep seismic data are slightly outside the basin region. The 3-D gravity inversion performed in this study used those limited seismic refraction constraints to investigate the crustal structures, and hence, deeper seismic would better support the inversion results. In particular, deep 3-D seismic reflection data would be beneficial to constrain crustal features and reduce the uncertainty and nonuniqueness of the gravity modeling work. The quantitative techniques and kinematic analysis used by Waldron (2005) may be applied for future work in the Bay St. George subbasin to constrain the tectonic evolution better and justify 3-D seismic data acquisition in the basin.

There is only one offshore drilled well in the Bay St. George subbasin located in the northwestern part of the basin. Drilling more wells offshore throughout the basin would better constrain the seismic interpretation of this study. The present study proposes that wells be drilled offshore in the newly identified small sedimentary basin south of the Port au Port Peninsula and near the southern limits of the offshore St. George Bay. These wells would provide insights into the tectonic evolution of the basin and better constrain the interpretations in this study. The carbonate platform successions are identified on one offshore well yet are believed to exist throughout the offshore part of the basin. Additional wells would confirm this and support the seismic interpretation results in this study while also reducing uncertainty about the existence of these units for the rest of the offshore.

In addition to future work that requires acquiring more geophysical data, other investigations are recommended for the Bay St. George subbasin with the currently available data. A 3-D magnetic inversion is suggested since the Department of Industry, Energy and Technology-Newfoundland and Labrador acquired new high-resolution magnetic data in the basin. This magnetic inversion would give an improved structural framework of the basin, in particular for the shallower features. Structural restorations using Petroleum Expert's MOVE software along seismic lines interpreted in this study would improve the geological knowledge in this study. Future work using the kinematic evolution modeling and fault analysis modules in MOVE would give a better understanding of the structural evolution of the basin.

References

Allen, M. B., Macdonald, D. I. M., Xun, Z., Vincent, S. J., & Brouet-Menzies, C. (1998). Transtensional deformation in the evolution of the Bohai Basin, northern China. *Geological Society Special Publication*, *135*, 215–229. https://doi.org/10.1144/GSL.SP.1998.135.01.14

Allison, C. (1996). *Final Well Report St. George's Bay A-36, Newfoundland Hunt Oil Company*.

Bell, F. G. (2005). ENGINEERING GEOLOGY | Problematic Rocks. In R. C. Selley, L. R. M. Cocks, & I. R. Plimer (Eds.), *Encyclopedia of Geology* (pp. 543–554). Elsevier. https://doi.org/https://doi.org/10.1016/B0-12-369396-9/00220-3

Callot, J. P., Salel, J. F., Letouzey, J., Daniel, J. M., & Ringenbach, J. C. (2016). Three-dimensional evolution of salt-controlled minibasins: Interactions, folding, and megaflap development. *AAPG Bulletin*, *100*(9), 1419–1442. https://doi.org/10.1306/03101614087

Cawood, P. A., McCausland, P. J. A., & Dunning, G. R. (2001). Opening Iapetus: Constraints from the Laurentian margin in Newfoundland. *Bulletin of the Geological Society of America*, *113*(4), 443–453. https://doi.org/10.1130/0016-7606(2001)113<0443:OICFTL>2.0.CO;2

Cawood, Peter A., & Suhr, G. (1992). Generation and obduction of ophiolites: Constraints from the Bay of Islands Complex, western Newfoundland. *Tectonics*, *11*(4), 884–897. https://doi.org/10.1029/92TC00471

Cawood, Peter A. (1993). Acadian orogeny in west Newfoundland: Definition, character, and significance. In D. C. Roy & J. W. Skehan (Eds.), *The Acadian Orogeny: Recent Studies in New England, Maritime Canada, and the Autochthonous Foreland* (Vol. 275, p. 0). Geological Society of America. https://doi.org/10.1130/SPE275-p135

Cohen, H. A., & Hardy, S. (1996). Numerical modelling of stratal architectures resulting from differential loading of a mobile substrate. *Geological Society, London, Special*

Publications, *100*(1), 265 LP – 273. https://doi.org/10.1144/GSL.SP.1996.100.01.17

Coleman-Sadd, S. P., Hayes, J. P., & Knight, I. (2000). Geology of the Island of Newfoundland (digital version of Map 90-01 with minor revisions). *Newfoundland Department of Mines and Energy, Geological Survey*.

Cooper, M., Weissenberger, J., Knight, I., Hostad, D., Gillespie, D., Williams, H., Burden, E., Porter-Chaudhry, J., Rae, D., & Clark, E. (2001). Basin Evolution in Western Newfoundland: New Insights from Hydrocarbon Exploration. *AAPG Bulletin*, *85*(3), 393–418. https://doi.org/10.1306/8626C901-173B-11D7-8645000102C1865D

Dafoe, L. T., Shaw, J., Jauer, C., Giles, P. S., Waldron, J. W. F., & Potter, D. P. (2016). New insights into the Bedrock and Quaternary geology of St. George's Bay from a vertical integration of marine datasets, offshore western Newfoundland. *Bulletin of Canadian Petroleum Geology*, *64*(1), 1–23. https://doi.org/10.2113/gscpgbull.64.1.1

Forcinal, A. (2013). *Investcan Energy Gobineau #1 Final Well Report*. 206.

Gardner, G. H. F., Gardner, L. W., & Gregory, A. R. (1974). Formation Velocity and Density-The Diagnostic Basics For Stratigraphic Traps. *Geophysics*, *39*(6), 770–780. https://doi.org/10.1190/1.1440465

Gibling, M. R., Langenberg, W., Kalkreuth, W. D., Waldron, J. W. F., Courtney, R., Paul, J., & Grist, A. M. (2002). Deformation of Upper Carboniferous coal measures in the Sydney Basin: evidence for late Alleghanian tectonism in Atlantic Canada. *Canadian Journal of Earth Sciences*, *39*(1), 79–93. https://doi.org/10.1139/e01-062

Hall, J., Langdon, G., Roberts, B., Hawkins, D., Fagan, A., Knight, I., & Kilfoil, G. (1992). Reflection seismic imaging of the Carboniferous Bay St. George Subbasin, onshore western Newfoundland: a reappraisal of Paleozoic stratigraphic thickness. In *Bulletin of Canadian Petroleum Geology* (Vol. 40, Issue 4).

Halley, S. (2010). *Vulcan Minerals-Investcan Redbrook #2 Final Well Report*. 318.

Hibbard, J., & Waldron, J. W. F. (2009). Truncation and translation of Appalachian promontories: Mid-Paleozoic strike-slip tectonics and basin initiation. *Geology*, *37*(6), 487–490. https://doi.org/10.1130/G25614A.1

Hogg, J. R., & Enachescu, M. E. (2015). *Petroleum Potential and Sedimentary Basins*. 1–77. http://www.nr.gov.nl.ca/nr/publications/energy/WNL_SedimentaryBasins.pdf

Ingersoll, R. V. (1988). Tectonics of sedimentary basins. *GSA Bulletin*, *100*(11), 1704–1719. https://doi.org/10.1130/0016-7606(1988)100<1704:TOSB>2.3.CO;2

Jackson, C. A. L., Rodriguez, C. R., Rotevatn, A., & Bell, R. E. (2014). Geological and geophysical expression of a primary salt weld: An example from the Santos Basin, Brazil. *Interpretation*, *2*(4), SM77–SM89. https://doi.org/10.1190/INT-2014-0066.1

Jackson, H. R., Marillier, F., & Hall, J. (1998). Seismic refraction data in the Gulf of Saint Lawrence: implications for the lower-crustal blocks. *Canadian Journal of Earth Sciences*, *35*(11), 1222–1237. https://doi.org/10.1139/cjes-35-11-1222

Jackson, M.P.A, & Talbot, C. J. (1991). *A glossary of salt tectonics: Bureau of Economic Geology, University of Texas, Austin, Texas*. 44.

Jackson, Martin P. A., & Hudec, M. R. (2017). Seismic Interpretation of Salt Structures. In *Salt Tectonics* (pp. 364–398). Cambridge University Press. https://doi.org/10.1017/9781139003988.018

Kamo, S. L., Gower, C. F., & Krogh, T. E. (1989). Birthdate for the Iapetus Ocean? A precise U-Pb zircon and baddeleyite age for the Long Range dikes, southeast Labrador. *Geology*, *17*(7), 602–605. https://doi.org/10.1130/0091-7613(1989)017<0602:BFTLOA>2.3.CO;2

Kilfoil, G. J. (1988). *An Integrated Gravity, Magnetic and Seismic Interpretation of the Carboniferous Bay St. George Subbasin, Western Newfoundland*. Memorial University of Newfoundland.

Klimetz, M. P. (1983). Speculations on the Mesozoic Plate tectonic evolution of eastern China. *Tectonics*, *2*(2), 139–166.

https://doi.org/https://doi.org/10.1029/TC002i002p00139

Knight, I. (1983). *Geology of the Carboniferous Bay St. George subbasin, western Newfoundland*. Mineral Development Division, Dept. of Mines and Energy, Government of Newfoundland and Labrador. https://books.google.ca/books?id=1ZROAQAAIAAJ

Langdon, G. S., & Hall, J. (1994). Devonian-Carboniferous tectonics and basin deformation in the Cabot Strait area, eastern Canada. *American Association of Petroleum Geologists Bulletin*, *78*(11), 1748–1774. https://doi.org/10.1306/a25ff283-171b-11d7-8645000102c1865d

Lavoie, D., Burden, E., & Lebel, D. (2003). Stratigraphic framework for the Cambrian-Ordovician rift and passive margin successions from southern Quebec to western Newfoundland. *Canadian Journal of Earth Sciences*, *40*(2), 177–205. https://doi.org/10.1139/e02-078

LeDrew, T. (2011). Seismic Processing QC Report: Robinsons River. *Triumph Atlantic*, 27.

Li, Y., & Oldenburg, D. W. (1996). 3-D inversion of magnetic data. *1996 SEG Annual Meeting*, *61*(2), 400–402. https://doi.org/10.1190/1.1822498

Li, Y., & Oldenburg, D. W. (1998). 3-D inversion of Gravity Data. *1998 SEG Annual Meeting*, *63*(1), 264–267. https://doi.org/10.1190/1.1887478

Li, Y., & Oldenburg, D. W. (2003). Fast inversion of large-scale magnetic data using wavelet transforms and a logarithmic barrier method. *Geophysical Journal International*, *152*(2), 251–265. https://doi.org/https://doi.org/10.1046/j.1365-246X.2003.01766.x

Li, Y., & Oldenburg, D. W. (2010). Rapid construction of equivalent sources using wavelets. *Geophysics*, *75*(3), L51–L59. https://doi.org/10.1190/1.3378764

Marillier, F., Hall, J., Hughes, S., Louden, K., Reid, I., Roberts, B., Clowes, R., Coté, T., Fowler, J., Guest, S., Lu, H., Luetgert, J., Quinlan, G., Spencer, C., & Wright, J. (1994). LITHOPROBE East onshore-offshore seismic refraction survey -constraints on interpretation of reflection data in the Newfoundland Appalachians. *Tectonophysics*, *232*(1–4), 43–58. https://doi.org/10.1016/0040-1951(94)90075-2

Marillier, F., & Verhoef, J. (1989). Crustal thickness under the Gulf of St. Lawrence, northern Appalachians, from gravity and deep seismic data. *Canadian Journal of Earth Sciences*, *26*(8), 1517–1532. https://doi.org/10.1139/e89-130

Marillier, François, Dentith, M., Michel, K., Reid, I., Roberts, B., Hall, J., Wright, J., Louden, K., Morel-à-l'Huissier, P., & Spencer, C. (1991). Coincident seismic-wave velocity and reflectivity properties of the lower crust beneath the Appalachian Front, west of Newfoundland. *Canadian Journal of Earth Sciences*, *28*(1), 94–101. https://doi.org/10.1139/e91-008

Michel, H. K., Louden, K. E., Marillier, F., & Reid, I. (1992). The seismic velocity structure of northern Appalachian crust around western Newfoundland. *Canadian Journal of Earth Sciences*, *29*(3), 462–478. https://doi.org/10.1139/e92-040

Miller, H. G., Kilfoil, G. J., & Peavy, S. T. (1990). An integrated geophysical interpretation of the Carboniferous Bay St. George Subbasin, western Newfoundland. *Bulletin of Canadian Petroleum Geology*, *38*(3), 320–331.

Pavlis, N.K., Holmes, S.A., Kenyon, S.C., and Factor, J. . (2008). *An Earth Gravitational Model to Degree 2160: EGM2008*.

Peavy, T. S. (1985). *A Gravity and Magnetic Interpretation of the Bay St. George Subbasin in Western Newfoundland*. MSc Thesis Memorial University of Newfoundland.

Robbins, H. J. (2000). *Geological Evolution of Carboniferous Basins in Bay St. George, Humber Zone, Western Newfoundland*. BSc (Hons) Thesis Memorial University of Newfoundland.

Smith, K. (2006). *Vulcan Minerals Hurricane #1 Final Well Report*. 200.

Snyder, M. E. (2019). *Deformation in the Maritimes Basin, Atlantic Canada*. PhD Thesis University of Alberta.

Stockmal, G. S., Slingsby, A., & Waldron, J. W. F. (1998). Deformation styles at the Appalachian structural front, western Newfoundland: Implications of new industry seismic reflection data. *Canadian Journal of Earth Sciences*, *35*(11), 1288–1306. https://doi.org/10.1139/e97-118

Stockmal, G. S., Slingsby, A., & Waldron, J. W. F. (2004). Basement-involved inversion at the Appalachian structural front, western Newfoundland: An interpretation of seismic reflection data with implications for petroleum prospectivity. *Bulletin of Canadian Petroleum Geology*, *52*(3), 215–233. https://doi.org/10.2113/52.3.215

Stockmal, Glen S, Colman-Sadd, S. P., Keen, C. E., Marillier, F., O'Brien, S. J., & Quinlan, G. M. (1990). Deep seismic structure and plate tectonic evolution of the Canadian Appalachians. *Tectonics*, *9*(1), 45–62. https://doi.org/https://doi.org/10.1029/TC009i001p00045

van Staal, C. (2005). NORTH AMERICA | Northern Appalachians. In *Encyclopedia of Geology* (Vol. 4, pp. 81–92). https://doi.org/10.1016/B0-12-369396-9/00407-X

van Staal, C. R., Ravenhurst, C. E., Winchester, J. A., Roddick, J. C., & Langton, J. P. (1990). Post-Taconic blueschist suture in the northern Appalachians of northern New Brunswick, Canada. *Geology*, *18*(11), 1073–1077. https://doi.org/10.1130/0091-7613(1990)018<1073:PTBSIT>2.3.CO;2

van Staal, Cees R., & Barr, S. M. (2012). Lithospheric architecture and tectonic evolution of the Canadian Appalachians and associated Atlantic margin. *Tectonic Styles in Canada: The LITHOPROBE Perspective*, *Special Pa*, 41–95.

van Staal, Cees R., & de Roo, J. A. (1996). Mid-Paleozoic tectonic evolution of the Appalachian central mobile belt in northern New Brunswick, Canada: collision, extensional collapse and dextral transpression. *Geological Association of Canada, Special Paper*, *41*, 367–389.

Waldron, J. W.F., Anderson, S. D., Cawood, P. A., Goodwin, L. B., Hall, J., Jamieson, R. A., Palmer, S. E., Stockmal, G. S., & Williams, P. F. (1998). Evolution of the Appalachian Laurentian margin: Lithoprobe results in western Newfoundland. *Canadian Journal of Earth Sciences*, *35*(11), 1271–1287. https://doi.org/10.1139/e98-053

Waldron, J. W.F., & Milne, J. V. (1991). Tectonic history of the central Humber Zone, western Newfoundland Appalachians: post-Taconian deformation in the Old Man's Pond area. *Canadian Journal of Earth Sciences*, *28*(3), 398–410. https://doi.org/10.1139/e91-036

Waldron, John W.F. (2004). Anatomy and evolution of a pull-apart basin, Stellarton, Nova Scotia. *Bulletin of the Geological Society of America*, *116*(1–2), 109–127. https://doi.org/10.1130/B25312.1

Waldron, John W.F. (2005). Extensional fault arrays in strike-slip and transtension. *Journal of Structural Geology*, *27*(1), 23–34. https://doi.org/10.1016/j.jsg.2004.06.015

Waldron, John W.F., & Stockmal, G. S. (1994). Structural and tectonic evolution of the Humber Zone, western Newfoundland 2. A regional model for Acadian thrust tectonics. *Tectonics*, *13*(6), 1498–1513. https://doi.org/10.1029/94TC01505

Waldron, John W F, Barr, S. M., Park, A. F., White, C. E., & Hibbard, J. (2015). Late Paleozoic strike-slip faults in Maritime Canada and their role in the reconfiguration of the northern Appalachian orogen. *Tectonics*, 1661–1684. https://doi.org/10.1002/2015TC003882

Waldron, John W F, Rygel, M. C., Gibling, M. R., & Calder, J. H. (2013). Evaporite tectonics and the late Paleozoic stratigraphic development of the Cumberland basin, Appalachians of Atlantic Canada. *GSA Bulletin*, *125*(5–6), 945–960. https://doi.org/10.1130/B30718.1

Waldron, John W F, & van Staal, C. R. (2001). Taconian orogeny and the accretion of the Dashwoods block: A peri-Laurentian microcontinent in the Iapetus Ocean. *Geology*, *29*(9), 811–814. https://doi.org/10.1130/0091-7613(2001)029<0811:TOATAO>2.0.CO;2

Webb, G. W. (1968). Palinspastic Restoration Suggesting Late Paleozoic North Atlantic Rifting. *Science*, *159*(3817), 875 LP – 878. https://doi.org/10.1126/science.159.3817.875

Welford, J. K., Shannon, P. M., O'Reilly, B. M., & Hall, J. (2010). Lithospheric density variations and Moho structure of the Irish Atlantic continental margin from constrained 3-D gravity inversion. *Geophysical Journal International*, *183*(1), 79–95. https://doi.org/10.1111/j.1365-246X.2010.04735.x

Welford, J. Kim, & Hall, J. (2007). Crustal structure of the Newfoundland rifted continental margin from constrained 3-D gravity inversion. *Geophysical Journal International*, *171*(2), 890–908. https://doi.org/10.1111/j.1365-246X.2007.03549.x

Williams, H. (1979). Appalachian Orogen in Canada. *Canadian Journal of Earth Sciences*, *16*(3), 792–807. https://doi.org/10.1139/e79-070

Wilson, J. T. (1966). Did the Atlantic Close and then Re-Open? *Nature*, *211*(5050), 676–681. https://doi.org/10.1038/211676a0

Ye, H., Shedlock, K. M., Hellinger, S. J., & Sclater, J. G. (1985). The North China Basin: An example of a Cenozoic rifted intraplate basin. *Tectonics*, *4*(2), 153–169. https://doi.org/https://doi.org/10.1029/TC004i002p00153

Appendix A Seismic Profiles

This appendix focuses on seismic profiles not shown in this thesis's main text. Only a subset of seismic sections is described in the main text, representing the Bay St. George subbasin, including onshore, offshore, and onshore-to-offshore seismic profiles. The number of seismic sections shown and the detail described in the main text is adequate for this study. However, more seismic sections are displayed in this appendix to provide further supplementary data used in this study. This appendix shows eight additional seismic profiles since the entire seismic dataset for this study involved 60 2-D seismic reflection lines. These seismic sections show the uninterpreted and interpreted data. Similar seismic horizons and structures are mapped, as seen in Chapter 3. The figures in this appendix highlight the varying quality and resolution of the seismic data interpreted. The seismic profiles in this appendix also demonstrate the complex subsurface structure imaged in the Bay St. George subbasin.

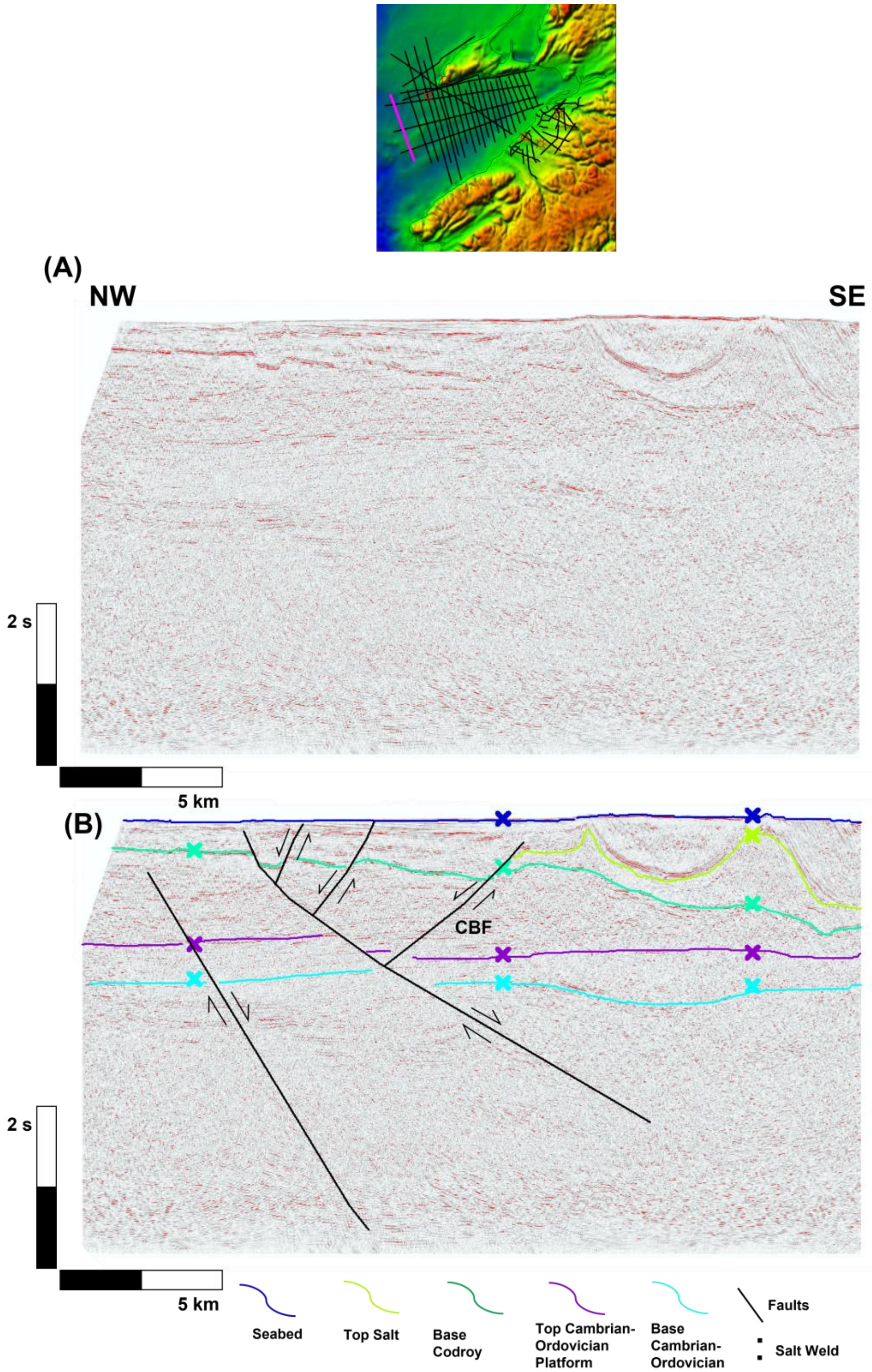

Figure A.1: Seismic section of a NW-SE offshore profile showing the different mapped features, where (A) is uninterpreted and (B) is interpreted.

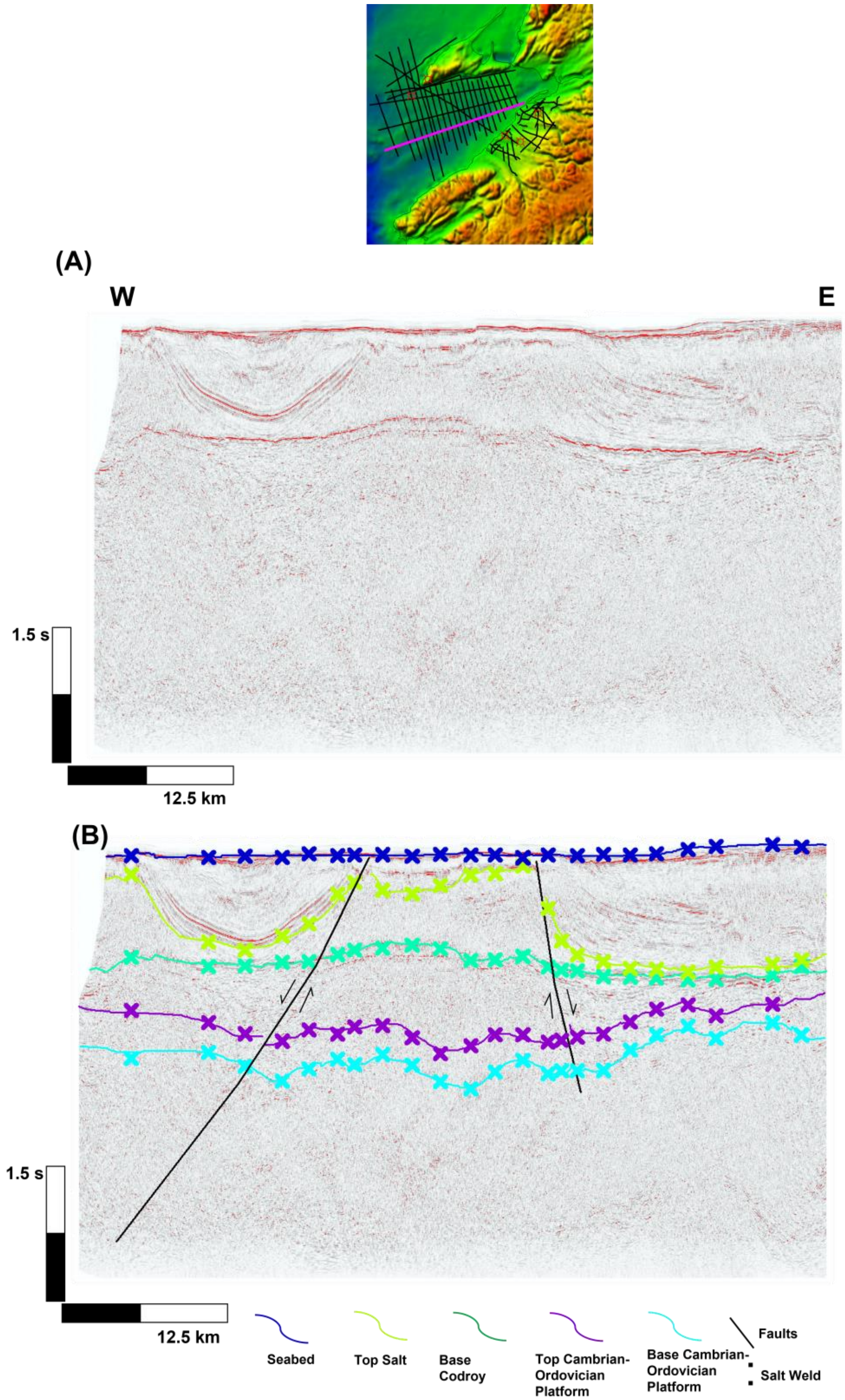

Figure A.2: Seismic section of a W–E offshore profile showing the different mapped features, where (A) is uninterpreted and (B) is interpreted.

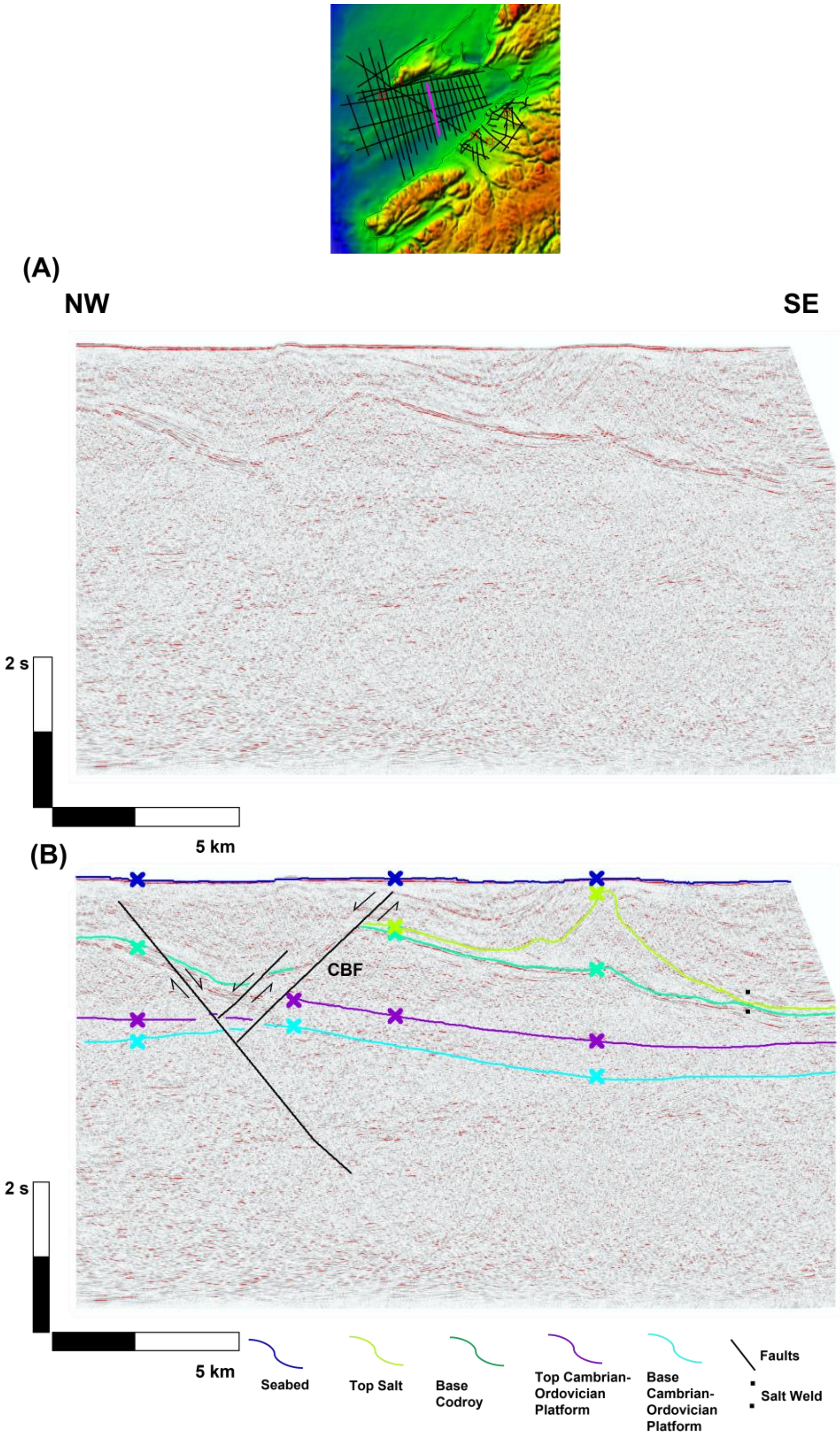

Figure A.3: Seismic section of a NW–SE offshore profile showing the different mapped features, where (A) is uninterpreted and (B) is interpreted.

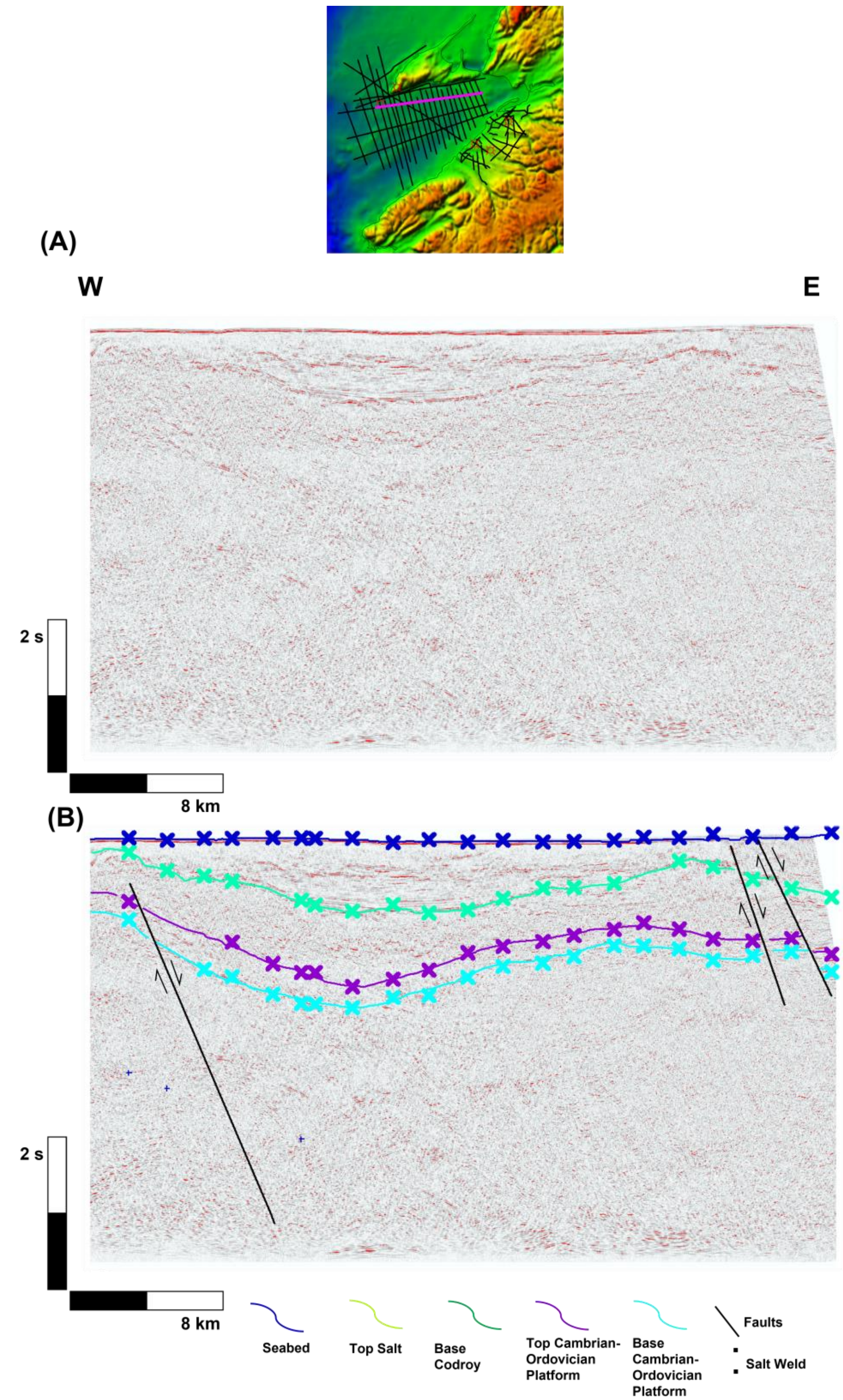

Figure A.4: Seismic section of a W–E offshore profile showing the different mapped features, where (A) is uninterpreted and (B) is interpreted.

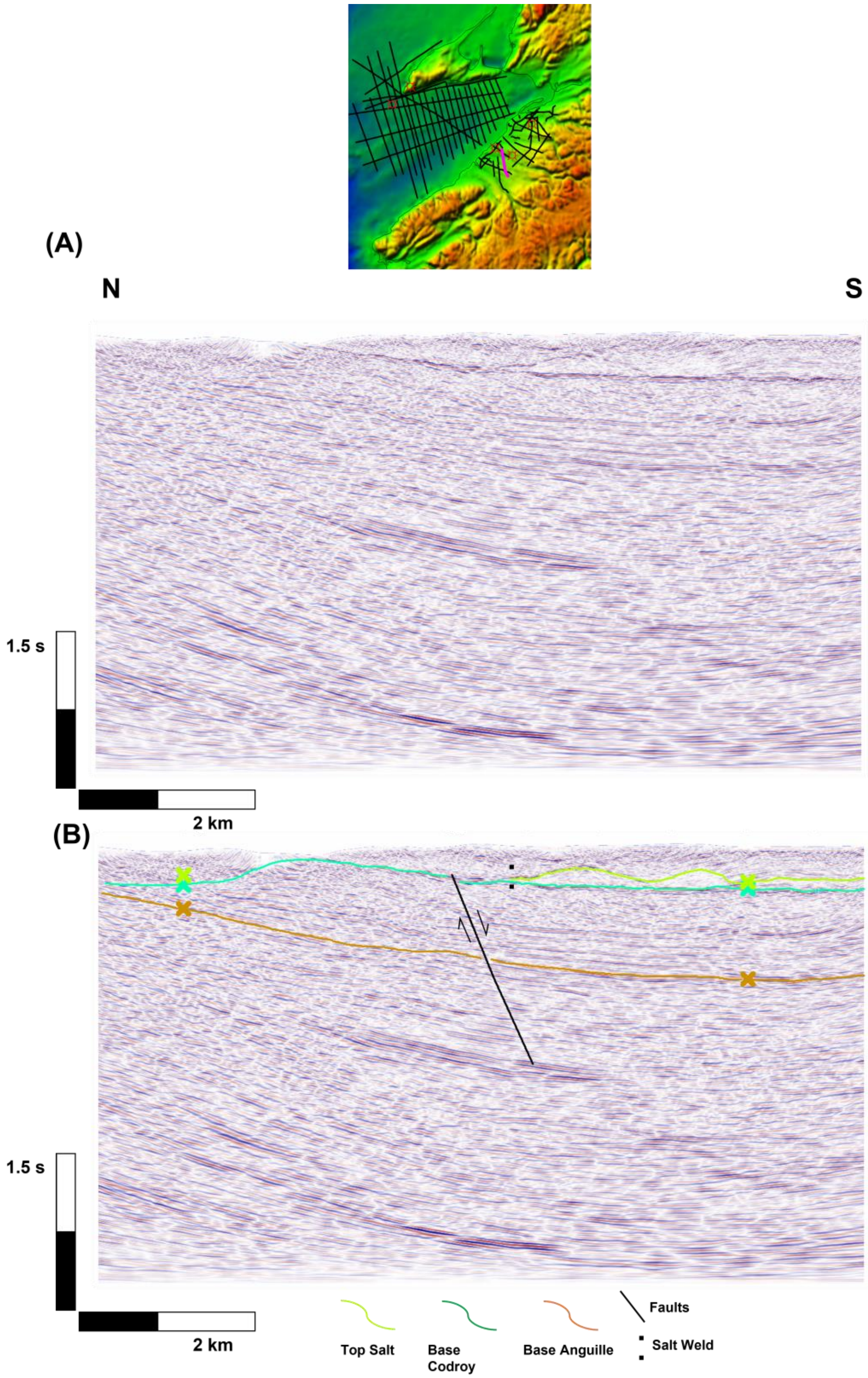

Figure A.5: Seismic section of a N–S onshore profile showing the different mapped features, where (A) is uninterpreted and (B) is interpreted.

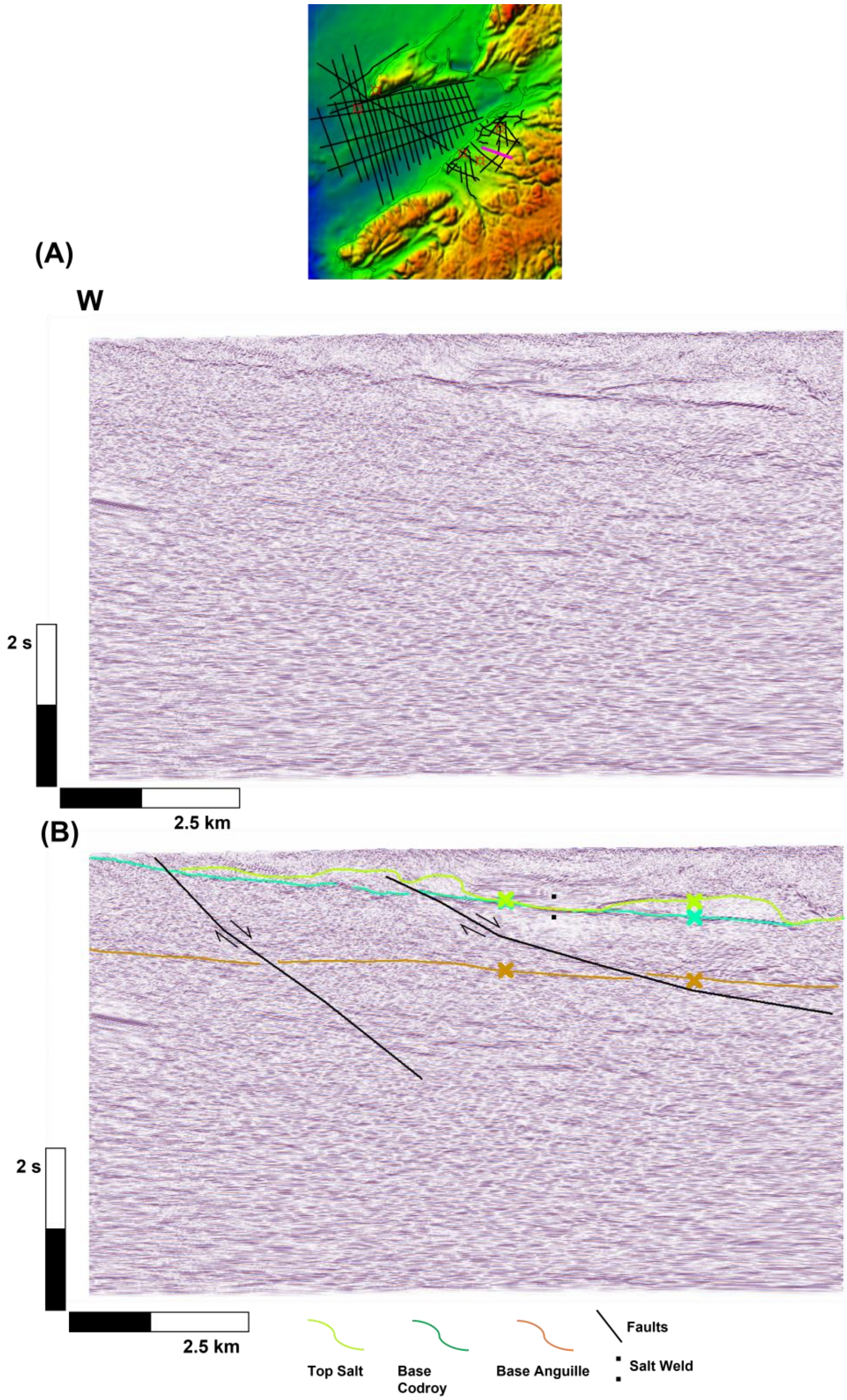

Figure A.6: Seismic section of a W–E onshore profile showing the different mapped features, where (A) is uninterpreted and (B) is interpreted.

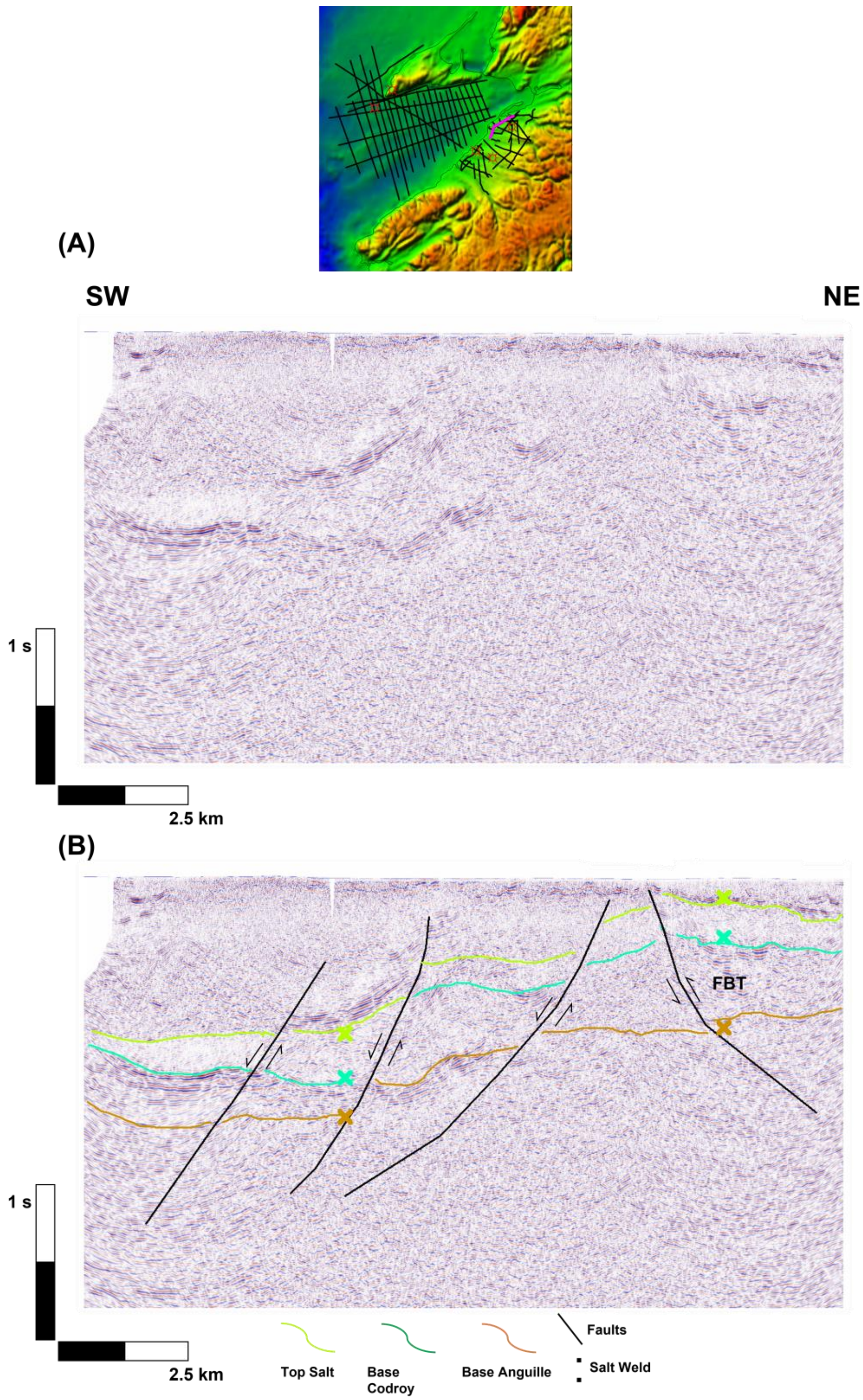

Figure A.7: Seismic section of a SW–NE onshore profile showing the different mapped features, where (A) is uninterpreted and (B) is interpreted.

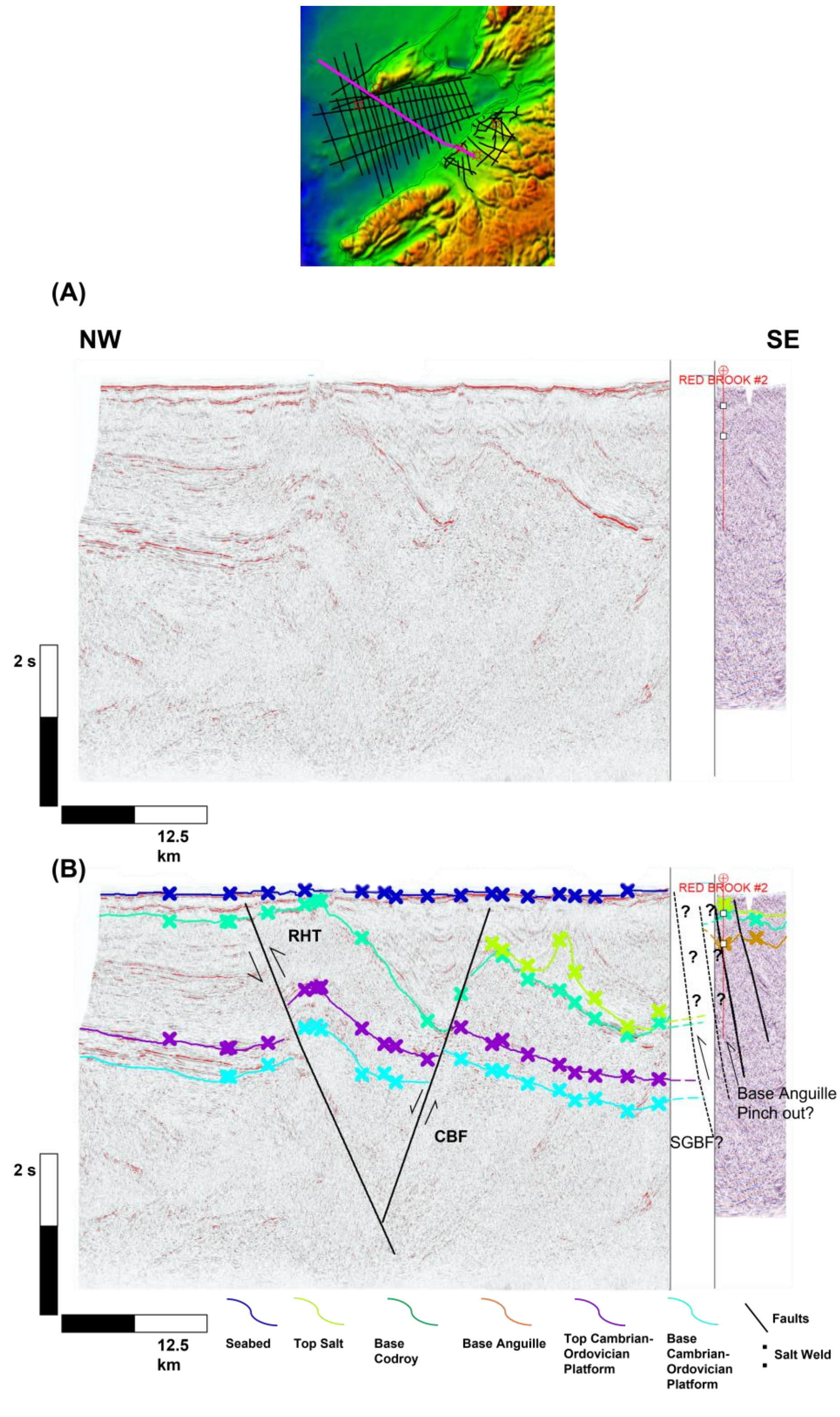

Figure A.8: Seismic section of a composite NW–SE offshore-to-onshore profile showing the different mapped features, where (A) is uninterpreted and (B) is interpreted. The Red Brook 2 synthetic seismic trace is used to correlate the seismic features with the geology from the well logs.

Appendix B Well Log Data

Five wells are used in this study to correlate the ground-truth geological information obtained from the well logs with the seismic data. Well ties are generated to match the synthetic seismogram with the real seismic data. Only two wells are displayed and described in this thesis's main text since the same process is applied for all the wells. This appendix provides the well logs and synthetics for the remaining three wells.

The Gobineau #1 well tie displayed in Figure B.1 shows the Base Codroy and Base Anguille well tops. This synthetic trace is generated using an analytical Ricker wavelet with a central frequency of 25 Hz. The synthetic trace generation for this well follows the same process as the other synthetic traces described in section 2.2.6.

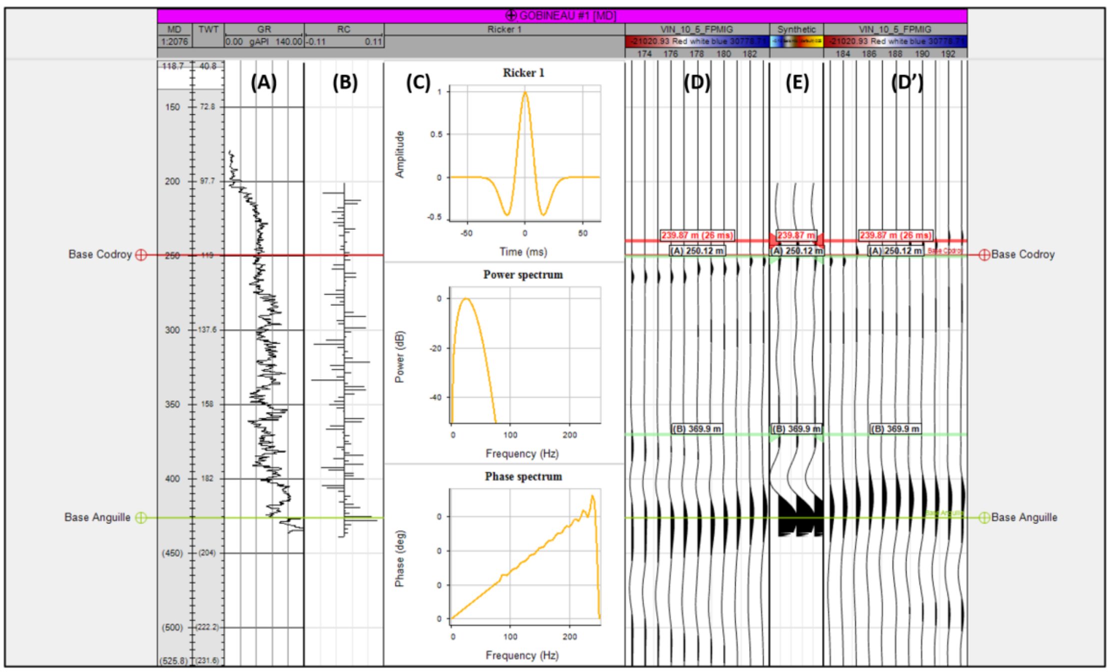

Figure B.1: The Gobineau #1 well tie. (A): Gamma Ray log (GR). (B): Reflection Coefficient (RC) series. (C): Analytical zero phase Ricker wavelet with a 25 Hz central peak. (D) and (D'): Traces from the 2-D seismic line. (E): Synthetic seismic trace.

The Hurricane #1 synthetic trace is presented in Figure B.2 with the same Base Codroy and Base Anguille well tops. Only the synthetic trace is shown since no seismic lines intersect this well.

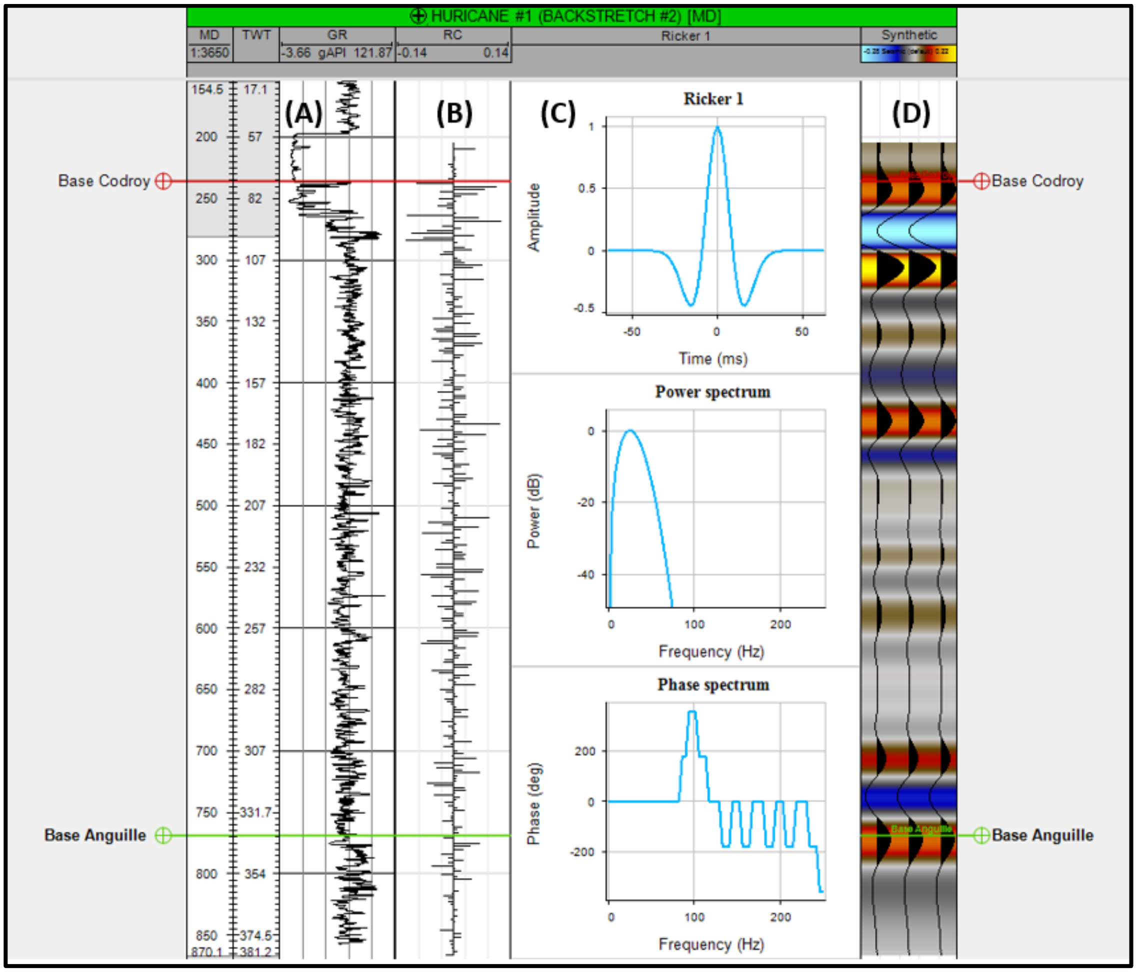

Figure B.2 The Hurricane #1 synthetic trace. (A): Gamma Ray log (GR). (B): Reflection Coefficient (RC) series. (C): Analytical zero phase Ricker wavelet with a 25 Hz central peak. (D): Synthetic seismic trace.

Figure B.3 shows the well logs for the Port au Port #1 well (Cooper et al., 2001). This well provides limited relevant information since no seismic lines in this study reach the onshore Port au Port Peninsula.

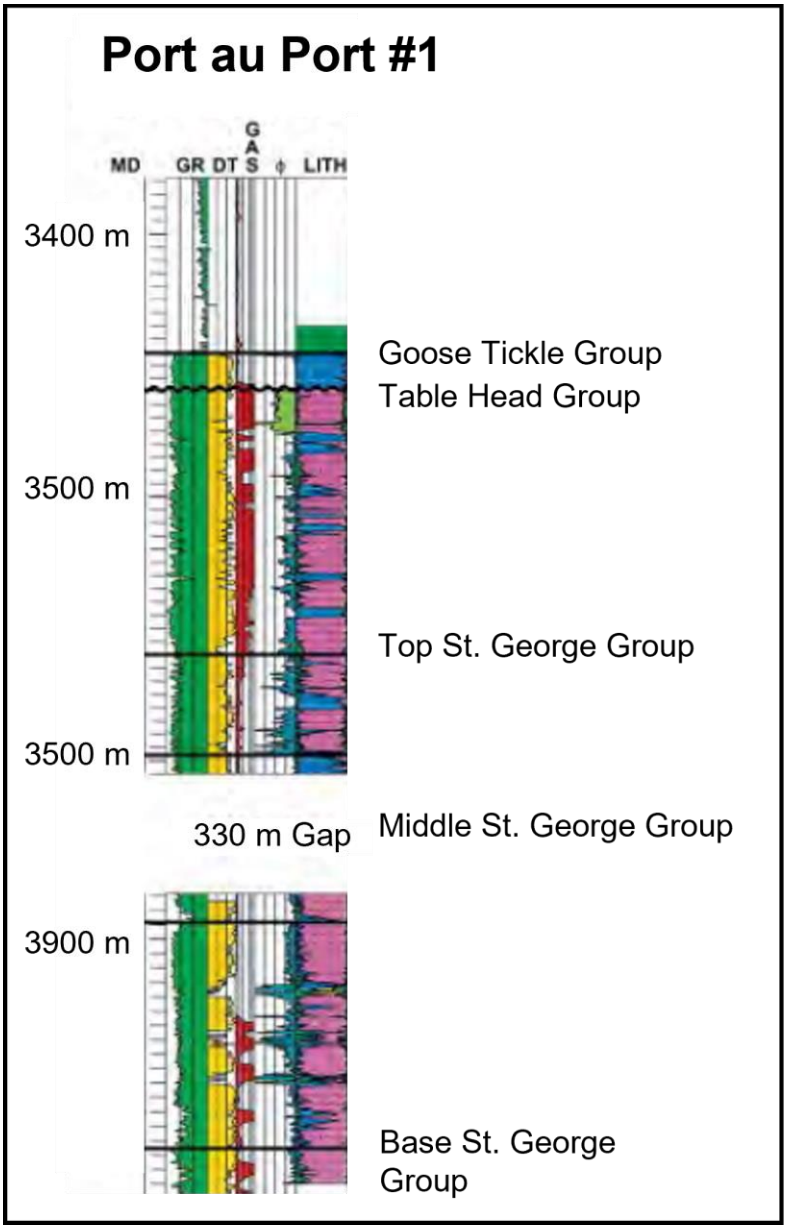

Figure B.3: Well log correlation of stratigraphic formations for the Port au Port #1 well. MD: measured depth. GR: gamma-ray. DT: Sonic velocity. Gas: total mud gas. ϕ: porosity. LITH: lithology, where green=shale, blue=limestone, and pink=dolomite. Figure after Cooper et al. (2001).

Appendix C Density Slices

This appendix contains additional density slices taken throughout the Bay St. George subbasin to provide supplementary data. All the density slices display two color bars to emphasize shallow and deep features better. The observed and predicted gravity anomaly plot is also displayed and shows how well the anomalies correlate. There are three surfaces displayed on the density slices, including the top basement, mid-crustal boundary, and Moho.

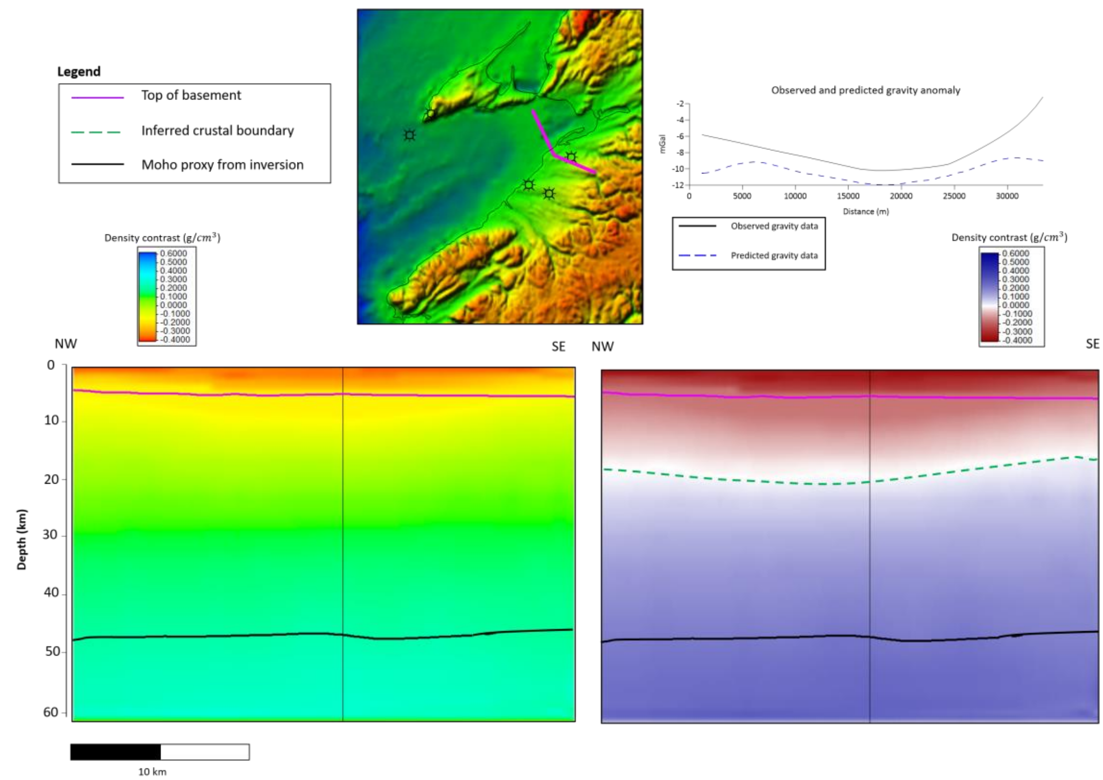

Figure C.1: A slice through the inverted density model along an onshore-to-offshore NW–SE profile. The rainbow and red-white-blue color bars are displayed to emphasize shallow and deep structures, respectively. The top basement (purple), mid-crustal boundary (dashed green), and depth to Moho (black) are displayed. The observed and predicted gravity data are also plotted to show how well correlated the gravity responses are.

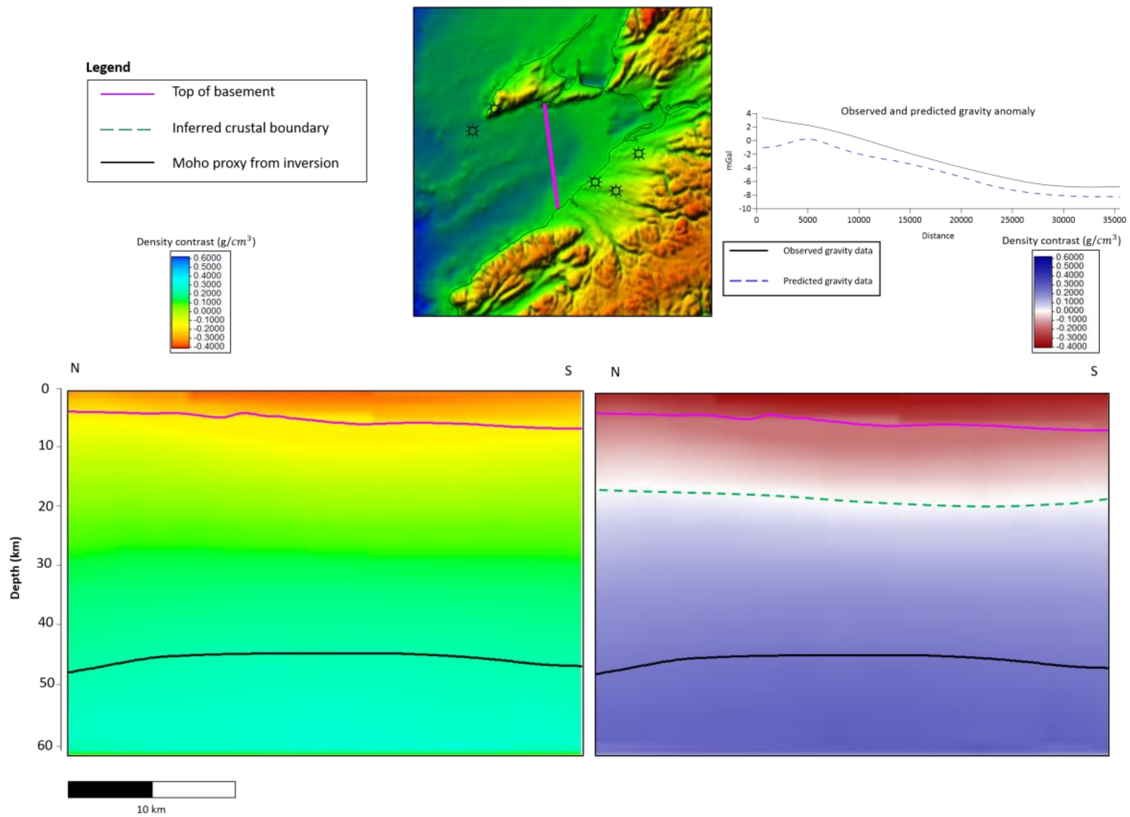

Figure C.2: A slice through the inverted density model along an offshore N–S profile. The rainbow and red-white-blue color bars are displayed to emphasize shallow and deep structures, respectively. The top basement (purple), mid-crustal boundary (dashed green), and depth to Moho (black) are displayed. The observed and predicted gravity data are also plotted to show how well correlated the gravity responses are.

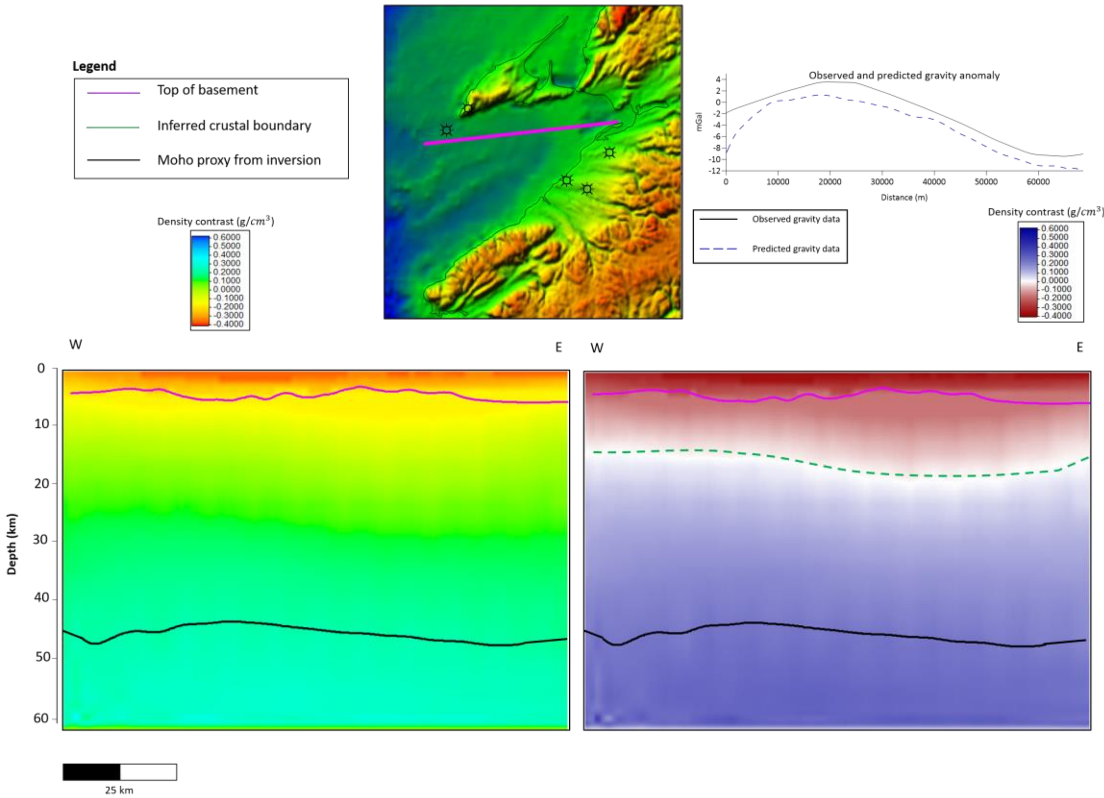

Figure C.3: A slice through the inverted density model along an offshore W–E profile. The rainbow and red-white-blue color bars are displayed to emphasize shallow and deep structures, respectively. The top basement (purple), mid-crustal boundary (dashed green), and depth to Moho (black) are displayed. The observed and predicted gravity data are also plotted to show how well correlated the gravity responses are.